M.Sc. Dissertation

# Determination of geodetic velocity field parameters for the African tectonic plate using the technique of Global Navigation Satellite Systems

by

**Cilence Munghemezulu**

Submitted in partial fulfilment of the requirements for the degree

**MASTER OF SCIENCE**

in the

**Faculty of Natural and Agricultural Sciences**

**University of Pretoria**

December 2013

# Declaration of originality

This is to declare that the research work presented here is entirely my own work, unless or otherwise explicitly acknowledged by citation of published and unpublished sources. This research has not previously been submitted for assessment in any form to the University of Pretoria or to any other institutions for any other purposes.

**Signature**…….

**Date**: December 2013

# Determination of geodetic velocity field parameters for the African tectonic plate using the technique of Global Navigation Satellite Systems

**Author** : Cilence Munghemezulu
**Supervisor** : [1,2]Prof. Ludwig Combrinck
**Co-supervisor** : [1]Dr. Joel Botai
**Department** : [1]Department of Geography, Geoinformatics and Meteorology, University of Pretoria, Pretoria 0002, South Africa
[2]Hartebeesthoek Radio Astronomy Observatory (HartRAO), P.O.Box 443, Krugersdorp 1740, South Africa
**Degree** : Master of Science

## Abstract

Space geodesy is one of the disciplines that contributes uniquely to the global society; its applications have grown to such an extent that system Earth is better understood today. The current accuracy of the Global Navigation Satellite Systems (GNSS) technique is below centimetre level and this allows very accurate determination of velocity field parameters. This study focused on utilizing GNSS to determine the inter-continental plate velocity field for Africa in support of the African Geodetic Reference Frame (AFREF). Data spanning 12.4 years were processed in the International Terrestrial Reference Frame (ITRF2008) using GAMIT/GLOBK 10.4 (developed at the Massachusetts Institute of Technology). Primarily, processing of data focused on International GNSS Service (IGS) stations with a few non-IGS stations (which are of geodetic quality) included, such as Hamburg (HAMB) and Matjiesfontein (MATJ). The same data set was analysed using the Combination and Analyses of Terrestrial Reference Frame (CATREF) software developed at Institut National de l'Information Géographique et Forestière (IGN). Validation of the results was achieved through comparison of the velocity solution from this study with a solution obtained from a core of IGS GNSS stations processed by the Jet Propulsion Laboratory (JPL). No significant differences were evident between the GAMIT/GLOBK 10.4, CATREF and JPL solutions. The results from the Matjiesfontein station indicated that the proposed

Matjiesfontein Observatory site shows no significant vertical or horizontal local motion; this information is valuable in that there is no obvious local site instability. The velocity field as derived by GNSS displays no unexpected deviations and supports current understanding of the motion of the Nubian, Somalian and Arabian plates. Furthermore, the comparison of the velocity vectors derived from the IGS station HRAO, Satellite Laser Ranging (SLR) MOBLAS-6 station and 26 m Very Long Baseline Interferometry (VLBI) telescope, which are collocated at the Hartebeesthoek Radio Astronomy Observatory (HartRAO) indicated good agreement and both techniques exhibit no significant vertical motion. This study also contributed to the first computation of the AFREF solution. It is envisaged that as more stations are added to the sparsely distributed current network, more accurate results and better tectonic models can be derived. The availability of station velocities will facilitate adjustments within the AFREF.

**Keywords:** AFREF, CATREF, GNSS, ITRF, GAMIT/GLOBK, SLR, VLBI, Tectonic plate velocities.

# Acknowledgements

I would like to express my gratitude to my supervisor Prof L. Combrinck for his support and for being patient with me during the transition period from geology to space geodesy and for his constructive comments on my idiosyncratic spelling and punctuation. I would like to thank my co-supervisor, Dr O.J Botai for his positive vision and encouragement during my academic career. Their contribution and supervision can be seen from this work. I also extend my gratitude towards the Department of Geography, Geoinformatics and Meteorology and the Hartebeesthoek Radio Astronomy Observatory (HartRAO) personnel's for their warm welcome, especially Marion West for editing this dissertation.

The financial assistance from the University of Pretoria, the National Research Foundation (NRF, project reference #: SSSS2011.06.09_1967), HartRAO and Inkaba yeAfrica towards this research is here acknowledged.

I would like to extend my gratitude towards Massachusetts Institute of Technology (MIT) for making GAMIT/GLOBK software (version 10.4) available to HartRAO and Institut National de l'Information Géographique et Forestière (IGN) for making CATREF software available including the training courses provided by the two institutes which were very helpful in processing GNSS data for this study.

Lastly, I would like to give thanks to my parents for giving me life and for nurturing it, my gratitude also go to my lovely girlfriend Zinhle Mashaba for her support.

# Conference proceedings

Different parts of this dissertation were prepared and presented at both local and international conferences in the form of posters, abstracts and oral presentations. Supervisors of this research have also co-authored the conference proceedings listed:

1. **Munghemezulu, C.,** Combrinck W. L and Botai, O.J. (2013). Velocity field parameters derived from GNSS using GAMIT/GLOBK and CATREF software. Presented at the 3nd S&T Train and Space Geodesy Observatory Workshop, 13 April 2012 to 17 April 2013, Matjiesfontein, Cape Town.

2. **Munghemezulu, C.,** Combrinck W. L and Botai, O.J. (2012). Comparison of velocity solutions from HRAO IGS station and MOBLAS-6 SLR collocated at Hartebeesthoek Radio Astronomy Observatory (HartRAO). Presented at the 9th Inkaba yeAFRICA workshop, 26 Nov-01 Dec 2012, Potsdam, Germany.

3. **Munghemezulu, C.,** Combrinck W. L and Botai, O.J. (2012). Determination of geodetic velocity field parameters for the African tectonic plate using GNSS: *A project in support of the African Geodetic Reference Frame (AFREF)*. Presented at the 9th Inkaba yeAFRICA workshop, 26 Nov-01 Dec 2012, Potsdam, Germany.

4. **Munghemezulu, C.,** Combrinck W. L and Botai, O.J. (2012). Preliminary results of GPS velocity fields for Africa derived using GAMIT/GLOBK. Presented at the 2nd S&T Train and Space Geodesy Observatory Workshop, 16 April 2012 to 20 April 2012, Matjiesfontein, Cape Town.

5. **Munghemezulu, C.,** Combrinck W. L and Botai, O.J. (2011). Preliminary results of velocity fields calculated from IGS stations in Africa using GAMIT/GLOBK to support the unified-African Geodetic Reference Frame (AFREF). Presented at the 8th Inkaba yeAfrica workshop, 28 August - 2 September 2011: CTICC, Cape Town.

6. **Munghemezulu, C** and Combrinck W. L. (2011). Determination of inter-continental plate velocity fields to support the establishment of AFREF. Presented at the First S&T Train and Space Geodesy Observatory Workshop, 28 March 2011 to 01 April 2011, Matjiesfontein, Cape Town.

7. **Munghemezulu, C** and Combrinck W. L. (2010). A proposal for the determination of intercontinental plate velocities in Africa to support the establishment of the African Geodetic Reference Frame (AFREF). Presented at the 7th Inkaba yeAFRICA workshop, 1-5 November 2010, Potsdam, Germany.

# Contents

**Contents** ..... **vii**

**List of Figures** ..... **x**

**List of Tables** ..... **xiv**

**Abbreviations** ..... **xv**

**CHAPTER 1** ..... **1**

**Introduction** ..... **1**

**1 General introduction** ..... **1**

*1.1 Problem outline* *2*
*1.2 Rationale of the project* *2*
*1.3 Aim and objectives* *4*
*1.4 Thesis structure* *4*
*1.5 Concluding remarks* *5*

**CHAPTER 2** ..... **6**

**Space geodetic techniques and applications** ..... **6**

**2 Space geodetic techniques** ..... **6**

*2.1 Introduction* *6*
*2.2 Global Navigation Satellite Systems* *8*
2.2.1 General GNSS description ..... 8
2.2.2 GNSS observables ..... 11
2.2.3 Positioning techniques ..... 14
2.2.4 GNSS limitations ..... 15
*2.3 Satellite Laser Ranging* *20*
2.3.1 Introduction ..... 20
2.3.2 Basic SLR principles ..... 22
*2.4 Very Long Baseline Interferometry* *25*
2.4.1 Introduction ..... 25
2.4.2 Basic VLBI principles ..... 28
*2.5 Modern Geodetic Reference Frames* *29*
2.5.1 Introduction ..... 29
2.5.2 Background on AFREF ..... 31
2.5.3 Contribution towards AFREF implementation ..... 38
*2.6 Concluding remarks* *39*

**CHAPTER 3** ..... **40**

**Data and analysis strategies** ..... **40**

**3 Methodology ..... 40**

*3.1 Introduction 40*
*3.2 Description of GAMIT/GLOBK (version 10.4) software 40*
*3.3 GNSS Instruments 41*
*3.4 Data acquisition and pre-processing 43*
*3.5 Data sets 45*
*3.6 Input files into GAMIT/GLOBK (version 10.4) 49*
*3.7 Strategy for processing GNSS data 50*
*3.8 Description of the CATREF software 52*
*3.9 AFREF computation 56*
*3.10 Concluding remarks 57*

**CHAPTER 4 ..... 58**

**Results and discussions ..... 58**

**4 Introduction ..... 58**

*4.1 Evaluating GNSS data 58*
4.1.1 Daily evaluation of GNSS data ..... 58
4.1.2 Multi-year data evaluation ..... 62
4.1.3 Combination of loosely constrained solutions ..... 65
4.1.4 Time-series analysis ..... 68
*4.2 GNSS velocity solution 73*
*4.3 Validating GNSS velocities 79*
4.3.1 Comparison of velocity solution from HartRAO and JPL ..... 79
4.3.2 Comparison of velocity vectors between different space geodetic techniques ..... 85
*4.4 Estimated parameters from the CATREF software 89*
*4.5 Concluding remarks 93*

**CHAPTER 5 ..... 94**

**Examples of the application of GNSS velocities to geodynamics ..... 94**

**5 Introduction ..... 94**

*5.1 Geodynamics of Africa 95*
5.2.1 Nubian-Somalian-Arabian Plates ..... 95
5.2.2 Southern Africa ..... 99
5.2.3 Proposed Matjiesfontien observatory site ..... 102
*5.2 Concluding remarks 108*

**CHAPTER 6 ..... 109**

**Conclusion and recommendations ..... 109**

*6.1 Summary 109*
*6.2 Future work and recommendations 111*

**References** ..... **114**

**Appendix A: Tables** ..... **123**

**Appendix B: Sky plots** ..... **134**

**Appendix C: Network statistics from 2000 to 2012.4.** ..... **141**

**Appendix D: List of GNSS station time-series plots.** ..... **146**

# List of Figures

Figure 1. Geodetic instruments collocated at HartRAO, South Africa. In the far distance left, the 15 m VLBI antenna, left-foreground the 26 m VLBI antenna, centre-foreground the SLR (MOBLAS-6) station, right-centre the Lunar Laser Ranging (LLR) in development and the IGS GNSS station (HRAO) antenna in the foreground. ..... 7
Figure 2. Distribution of GNSS stations around the world (sourced from: http://igscb.jpl.nasa.gov/network/complete.html; accessed: 01 March 2012)..... 10
Figure 3. Principle of pseudo-range positioning in the satellite reference system, adapted from Kahmen and Faig (1988). ..... 11
Figure 4. PRN-code generated by satellites and receivers, adapted from Kahmen and Faig (1988). ..... 12
Figure 5. Principle of double differencing between two receivers (*i* and *z*) and two satellites (*k* and *b*) (adapted from: Yang, 1995). ..... 15
Figure 6. Concept of GNSS signal propagation through different atmospheric levels (Komjathy, 1997). ..... 16
Figure 7. Map illustrating ILRS (International Laser Ranging Service) SLR network stations (source: http://ilrs.gsfc.nasa.gov/network/stations/index.html; accessed: 08 April 2012). ..... 21
Figure 8. Collocated geodetic instruments at HartRAO, South Africa. Left: LLR/SLR station under development; Right: SLR (MOBLAS-6) station, due to bad weather the telescopes are closed up. ..... 22
Figure 9. Schematic view of a Satellite Laser Ranging tracking artificial LAser GEOdynamics Satellite (LAGEOS) launched 4 May 1976 (adapted from: Degnan, 1985). ..... 24
Figure 10. The HartRAO 26 metre VLBI telescope facing north-west. ..... 25
Figure 11. Map depicting tracking network of Very Long Baseline Interferometry (VLBI) stations (source: http://cddis.nasa.gov/images/ivsmap.gif; accessed: 08 April 2012). ..... 27
Figure 12. Illustrated basic principles of Very Long Baseline Interferometry; a very stable atomic clock is required as well as a fast and high capacity storage medium..... 29
Figure 13. Illustration of global sites that are equipped with different, collocated space-based techniques i.e., SLR, GNSS-red dots, VLBI and DORIS, and these sites are used for the realization of ITRF (Altamimi *et al.* 2011). ..... 30
Figure 14. Examples of existing reference frames, Africa being under construction (adapted after: Bruyninx *et al.* 2009). ..... 32
Figure 15. Map illustrating current AFREF network of GNSS stations. There is an obvious weak station geometry in the north, the north-east and east central areas of the African continent. These gaps will have to be filled with GNSS stations to improve AFREF solutions. ..... 34
Figure 16. GNSS installation at Hamburg (HAMB), South Africa. This example station is totally self-contained. The station incorporates GPRS communication for data transfer, solar panel, wind charger, regulator and batteries for power, and a hermetically sealed box protects the equipment (picture credit: L. Combrinck, 2012, personal communication). ..... 35

Figure 17. It was proposed that Africa be sub-divided into five regions to facilitate the processing of GNSS data and the results would then be combined later to form a complete AFREF (Kamamia, 2004). The first AFREF computation (April 2013) utilised data from all the regions simultaneously. ..... 37
Figure 18. Example of a GNSS station. This particular station (MATJ) located at Matjiesfontein, Great Karoo is power and communications independent. The station was installed by HartRAO. Solar panels and metal boxes containing batteries to supply power can be seen on the ground. ..... 42
Figure 19. Satellite visibility for Hamburg (HAMB) station, South Africa, on 27 December 2010, cut off elevation: $10^{\circ}$. ..... 44
Figure 20. Polar sky plot for Hamburg, South Africa, on 27 December 2010, cut off elevation: $10^{\circ}$ ..... 45
Figure 21. Geometrical distribution of GNSS stations used in this study..... 46
Figure 22. Distribution of measurement time span of GNSS stations used in this study. ..... 49
Figure 23. Simple flow chart of GAMIT/GLOBK 10.4 software..... 51
Figure 24. Residuals of GNSS data against elevation angle for station PERT, 2001 day 001. Error model gives RMS value of 5.2 mm..... 59
Figure 25. Quality assessment of daily GNSS data for HRAO, GRAS and SUTH stations between day 1 and 100, of year 2000. Average RMS values are 7.7 mm, 5.2 mm and 6.7 mm for HRAO, GRAS and SUTH stations, respectively..... 59
Figure 26. Calculated RMS values for two best and two worst GNSS stations from the overall processed stations during 2001 of January from day 1 to 6. ..... 60
Figure 27. Quality assessment of daily GNSS data for HRAO, GRAS and SUTH stations between day 1 and 100, of year 2012. Average RMS values are 9.7 mm, 7.2 mm and 7.8 mm for HRAO, GRAS and SUTH stations, respectively. Station GRAS still maintains low RMS values while other stations are noisy. ..... 61
Figure 28. Polar sky plot of GNSS station HRAO as on January 1, 2000. Each plot covers a 4 hour period. The period 8-12 (UT) clearly contains more noise as there are several satellite tracks which exhibit larger RMS values than at other times of the day.... 62
Figure 29. Mean values of NRMS (mm) for GNSS residuals for each individual experiment before combination (each experiment has a duration of 1 year). ..... 64
Figure 30. Histogram derived from the network the year 2000. The NRMS values (mm) are calculated for East, North and Up components. ..... 64
Figure 31. Calculated $\chi^2$ for the combined solutions. Note the variations of $\chi^2$ in different H-files. ..... 66
Figure 32. Histograms of NRMS values for the combined solutions. ..... 67
Figure 33. Comparison of the NRMS (mm) values of the sub-networks and a GLOBK combined solution plotted next to the 2000 sub-network..... 67
Figure 34. Time-series plot for IGS station HRAO. Note the displacement of about 15 mm in the north component during the year 2009..... 69
Figure 35. Corrected north component of IGS station HRAO. Note the effect of correcting the north component of the velocity estimation on the other two components, especially the east component, which is most affected. ..... 71
Figure 36. The vertical (Up) component of HRAO exhibiting seasonal variations. The signal contains peaks after a period of a year with minimum values occurring at the middle of the year (winter) with pronounced increases in height during summer.

This could possibly be linked at some level to the ground water cycle. This will require careful recordkeeping of borehole water levels, rainfall and water withdrawal. ..... 72
Figure 37. The vertical component of IGS station VESL also illustrating seasonal variations. An improvement in data volume and quality can be seen after the year 2010 when HartRAO upgraded the station with a new receiver. ..... 72
Figure 38. Vertical velocities calculated in ITRF2008. These velocities are highly correlated with atmospherically introduced errors (Rodrigues, 2007). Therefore, they have a larger uncertainty than the horizontal components. ..... 74
Figure 39. Global horizontal velocities plotted at 95% confidence interval calculated in ITRF2008. Each continental plate exhibits independent plate motion and well-known major plate boundaries can be observed e.g., the mid-ocean ridge between the African and South American plates is evident since the station velocity vectors in both continental plates depict motion in different directions. ..... 75
Figure 40. East velocity component depicting variability of the velocity solution across different continents. More GNSS stations are required to improve spatial geometry and densification of points measured. A map such as this will be very informative and should graphically delineate the various intra-continental blocks. ..... 76
Figure 41. North component depicting variability of the velocity solution across different continents. ..... 77
Figure 42. Vertical component depicting variability of velocity solution across different continents. Note that vertical component is weaker, by a factor of 3, than the horizontal components. Therefore, very few definite conclusions can be derived from this plot. The Western Cape region seems to have slight vertical motion. ..... 78
Figure 43. Correlation comparison of North, East and Up components of GNSS velocities derived from this study (HartRAO) and those from JPL. ..... 80
Figure 44. Horizontal GNSS velocities derived from this study are represented by black arrows and those from JPL are represented by red arrows. No significant difference between the two solutions can be noted. Velocities from JPL are available at: (http://sideshow.jpl.nasa.gov/mbh/series.html). ..... 81
Figure 45. Differences (vectors subtracted) between JPL and HartRAO GNSS velocities. Most stations indicate good agreement. The scale of the velocity vectors was increased by a factor of 2 to magnify the small differences. ..... 82
Figure 46. Comparison of standard deviations of the velocities derived from this study (HartRAO) and those from JPL. Solutions from JPL (using GYPSY/OASIS II precise point positioning) indicate less than 0.2 mm/yr errors for the selected sites while the HartRAO solutions indicate slightly higher errors. ..... 84
Figure 47. Time series (mm) of the MOBLAS-6 SLR station (personal communication: L Combrinck, 2013). ..... 86
Figure 48. Time-series (mm) of the IGS station HRAO. ..... 87
Figure 49. Time-series (mm) of the VLBI 26 m telescope (personal communication: D Mayer, 2013). ..... 88
Figure 50. The origin and scale-consistency solution derived from the CATREF combination software. ..... 90
Figure 51. Estimated horizontal velocities expressed in ITRF2008. The velocities agree with those derived using the GLOBK software. ..... 91

Figure 52. Estimated vertical velocity field expressed in ITRF2008. Vertical velocities are associated with high errors. The red arrows indicate upwards movement and blue arrows indicate downwards movement of the GNSS stations..... 92
Figure 53. Mesozoic-Cenozoic rift-related basins, faulting and magmatism related to the break-up of Gondwana (Guiraud and Bosworth, 1997). ..... 96
Figure 54. Seismicity of sub-Saharan Africa between 1071 and 1996 (Graham and Brandt, 1999). ..... 97
Figure 55. Distribution of earthquakes, major structures and geological provinces in South Africa (Source: Nguuri *et al.* 2001 In: Singh *et al.* 2009). ..... 101
Figure 56. Vertical and horizontal velocities plotted at 95% confidence interval for the South African region. ..... 102
Figure 57. Matjiesfontein (MATJ) GNSS station located at the proposed site to host the S/LLR system, on the left is the meteorological instrument; this will be replaced by a MET4 unit in December 2013. ..... 103
Figure 58. Left: Google map of the proposed site. Right: an insert map depicting the location of Matjiesfontein in the Western Cape of South Africa. ..... 104
Figure 59. Time-series plot for MATJ GNSS station, Great Karoo, South Africa. ..... 105
Figure 60. Polar sky plots for station MATJ, South Africa, for day 90 of 2012..... 107
Figure 61. The Lunar Laser Ranger (LLR) is currently being developed at HartRAO (left) and MOBLAS-6 SLR station (right). Once the development is completed, the LLR station will be moved to Matjiesfontein. ..... 110
Figure 62.Current development of the web page to display spatial information such as GNSS stations. ..... 112
Figure 63. Web page depicting a time-series plot, this was executed by simply clicking on the station of interest. A user can also view other files such as log files sky-plots for more information about the station. The aim is to make this page as simple as possible for navigation purposes and give the user more information about the GNSS stations. ..... 113
Figure 64. Polar sky plots for IGS station HRAO, Hartebeesthoek, South Africa, from 1 to 6 January 2000. Note the effects of cloud on the sky plots on different days and the associated RMS. The red bar on the sky plot represents a scale which is equivalent to 10 mm. ..... 137
Figure 65. Polar sky plots for the MATJ station, South Africa, from days 90-95, 2012, cut off elevation: $10^{o}$. Note the effects of cloud on the sky plots on different days and the associated RMS. The red bars on the sky plot represent a scale which is equivalent to 10 mm. The sky above the proposed site remains relatively clear which is the most important criteria for observations made by geodetic instruments. ..... 140
Figure 66. Series of NRMS histograms from 2000 to 2012.4 for all GNSS stations processed. The NRMS values are calculated for East, North and Up components. ..... 145

# List of Tables

Table 1. Summary of the errors and their contribution to a single range observation equation (Seeber, 1993; *Kahmen and Faig, 1988). ..... 19
Table 2. List of countries that are participating in installing GNSS CORSs (Combrinck, 2011). ..... 37
Table 3. Summary of statistics for MP1 and MP2 for the Hamburg station, South Africa, as on 27 December 2010. ..... 44
Table 4. Availability of yearly GNSS data within the 2000 to 2012 period. ..... 47
Table 5. Proposed selection criteria for GNSS stations to define AFREF (modified from Rebischung *et al.* 2012). This was not applied to the first AFREF computation. ..... 56
Table 6. Summary of NRMS statistics for individual networks and the final GLOBK combined solution in terms of percentages. This was calculated by taking the sum of NRMS values for all the networks and determining the error contribution (%) of each individual network. ..... 68
Table 7. Velocities of MOBLAS-6 SLR station, 26 m VLBI telescope and IGS station HRAO. Vn, Ve and Vu represent velocities in North, East and Up components, respectively, and Sn, Se, Su represent standard deviation in North, East and Up components, respectively, (*Personal communication: L Combrinck, 2013, #personal communication: D Mayer, 2013). All outliers were removed (3 sigma) before velocity estimation. ..... 85
Table 8. Summary of average velocities of Nubian-Somalian-Arabian plates and their associated angular vectors. ..... 98
Table 9. A list of earthquakes in the National Database above magnitude 5 for south African regions (Singh *et al.* 2009). ..... 100
Table 10. Comparison of GNSS velocities derived at HartRAO and from the Jet Propulsion Laboratory (JPL; http://sideshow.jpl.nasa.gov/mbh/series.html). ..... 123
Table 11.Estimated station velocities from GLOBK software. ..... 125
Table 12. Estimated velocities utilising the CATREF software. ..... 128
Table 13. List of GNSS station positions computed using GLOBK. ..... 130
Table 14. List of IGS stations used in this study with their receiver and antenna types. ..... 132

# Abbreviations

| | |
|---|---|
| AFREF | African Geodetic Reference Frame |
| AGOS | African Geodetic Observing System |
| AVN | African Very Long Baseline Interferometry Network |
| APREF | Asian-Pacific Reference Frame |
| ADOS | African Doppler Survey |
| DORIS | Doppler Orbitography and Radiopositioning Integrated by Satellite |
| C/A-Code | Coarse Acquisition Code |
| CAFREF | Central African Reference Frame |
| CATREF | Combination and Analyses of Terrestrial Reference Frame |
| CGS | Council for Geosciences |
| CORS | Continuous Operating Reference Station |
| EUREF | European Reference Frame |
| EAFREF | East African Reference Frame |
| EARS | East African Rift System |
| EOP | Earth Orientation Parameters |
| GIS | Geographic Information System |
| GNSS | Global Navigation Satellite Systems |
| GPS | Global Positioning System |
| GSHAP | Global Seismic Hazard Assessment Program |
| HartRAO | Hartebeesthoek Radio Astronomy Observatory |
| IAG | International Association of Geodesy |
| IGS | International GNSS Service |
| IERS | International Earth Rotation Service |
| ITRF | International Terrestrial Reference Frame |
| JPL | Jet Propulsion Laboratory |
| LAGEOS | Laser GEOdynamics Satellite |
| LC | Linear Combination |
| LLR | Lunar Laser Ranging |
| MIT | Massachusetts Institute of Technology |
| NAREF | North American Reference Frame |
| NAFREF | North African Reference Frame |
| NAVAST | Navy Navigation Satellite System |
| NRF | National Research Foundation |
| NRMS | Normalized Root Mean Square |
| PRN | Pseudo Random Noise |
| P-Code | Precision Code |
| RINEX | Receiver Independent Exchange |

| | |
|---|---|
| RMS | Root Mean Square |
| RMSE | Root Mean Square Error |
| SAFREF | South African Reference Frame |
| SANSD | South African National Seismological Database |
| SDAS | SLR Data Analysis Software |
| SIRGAS | South American Reference Frame |
| SINEX | Solution Independent Exchange |
| SKA | Square Kilometre Array |
| SLR | Satellite Laser Ranging |
| SOPAC | Scripps Orbit and Permanent Array Center |
| TEC | Total Electron Content |
| TEQC | Translation Editing Quality Control |
| TRF | Terrestrial Reference Frame |
| TPS | Topcon Positioning Systems |
| VLBI | Very Long Baseline Interferometry |
| WAFREF | West African Reference Frame |
| WRMS | Weighted Root Mean Square |

# CHAPTER 1

## Introduction

*"Anyone who has never made a mistake has never tried anything new"- Albert Einstein, 1951.*

### 1 General introduction

Plate tectonics drives nearly all the geodynamic processes on Earth such as orogenesis, volcanic activities and earthquakes (Marshak, 2005); these shape the Earth. For many years, scientists have been studying the processes underlying the movement of continental plates to enhance their knowledge of plate tectonics (Anderle, 1986). An understanding of plate tectonics leads to a better understanding of the geophysical processes that affect the environment. It was only a few decades ago when it became possible to measure accurately the rates of plate movements through the development of space geodetic techniques (Erdogan *et al.* 2009).

Space-based techniques such as Satellite Laser Ranging (SLR), Very Long Baseline Interferometry (VLBI) and Global Navigation Satellite Systems (GNSS) have characterized and yielded valuable results about plate motions over the years (Stein, 1993). These techniques also contribute in defining reference frames (Altamimi *et al.* 2012). Other geophysical parameters are studied using these techniques; for example, Earth Orientation Parameters (EOPs) which are used to study orientation dynamics of the Earth System.

This thesis focuses on using one of the most commonly used geodetic techniques i.e., GNSS. In this specific case, the Global Positioning System (GPS) is used to determine horizontal and vertical velocities of the inter-continental plates of the African continent to support the establishment of the African Geodetic Reference Frame (AFREF). The problem statement, research rationale, aim and objectives and thesis structure are outlined in this chapter.

## 1.1 Problem outline

African countries have been using different geodetic datums for surveying and mapping purposes. For this reason, many projects that involve crossing political boundaries or those which require geo-spatial information are prone to errors due to the differences in the accuracies of the local reference frames across different countries (AFREF, 2002). Many proposals have been put forward since 2002 for the establishment of the AFREF; these proposals have received positive responses from most African countries (AFREF, 2002). Different structures of AFREF have been designed and partially implemented (scientific working group, advisory board) but other practical (implementation) issues still remain. Among these is the development of a velocity field for the African plate, based on long-term observations obtained from space geodetic techniques such as GNSS. Different maps such as gravity, geological, topographic maps etc., have been developed and are being published for different countries in Africa but velocity field maps have not yet received such attention. One of the reasons is that Africa has been lacking in technology to derive velocity field maps; in particular, a dense enough network of permanent GNSS receivers did not exist. One important application of velocity field maps is to monitor plate stress levels associated with seismic events. Seismic areas such as the East African Rift System (EARS) need to be monitored very closely for natural hazard mitigation purposes; this will require robust and dense velocity fields. This particular research is devoted to the derivation of a velocity field solution for the African continent using state of the art GNSS techniques, with the solutions determined in the current International Terrestrial Reference Frame (ITRF2008).

## 1.2 Rationale of the project

Space geodesy techniques such as GNSS provide cutting-edge technology, which has allowed many scientists to observe (in near-real time) the movement of GNSS stations (which then can be extrapolated to local plate motion). The accuracy of this geodetic technology has been reported to be at millimetre level (Yu *et al*. 1997; Bock *et al.* 2003). In order to ensure the robustness of the velocity solution, the measurements require long time series, which implies continuous and long-term observations

(Combrinck and Chin, 2001). Many scientists have taken advantage of this technology to solve geodynamic problems on a regional and global scale (Perez *et al.* 2003; Kaiser *et al.* 2005).

Several countries such as Europe, South America and Central America have utilised space geodetic techniques to develop unified geodetic reference frames based on permanently installed GNSS equipment, within the framework of the IGS, and based on non-IGS (local) stations. The realization of unified geodetic reference frames by these countries enabled the establishment of projects that require geo-spatial information which can then be executed with high precision. A successful geodetic reference frame requires monitoring of inter-continental crustal plates using permanently installed GNSS stations and other techniques in order to provide accurate velocities for maintenance and adjustments of the existing reference frames (Bruyninx, 2009).

The establishment and maintenance of a unified AFREF will contribute towards refining the African geoid, creating a 3-D reference network and will enhance the process of GNSS installations to increase the density of the current sparse network of GNSS in Africa (AFREF, 2002). The determination of velocity field maps will enable the development of datum transformation parameters for different countries on the African continent and on a global scale. Such a velocity field map, derived for Africa, will be a crucial scientific product for establishing AFREF. Once AFREF is operational, different scientific and non-scientific (e.g., civil engineering) projects will emerge. The initial computation of AFREF will not involve or require a velocity field, as it will basically be a static computation utilising 2 weeks of data to determine a reference frame at a certain epoch. However, future adjustments and accurate realizations will require careful consideration of differential velocities of GNSS sites, in particular when a local survey uses an AFREF GNSS station as a reference and high accuracy is required.

## 1.3 Aim and objectives

This study aims at deriving horizontal and vertical velocities of the inter-continental plates over the African continent using permanently installed GNSS stations (both IGS and local) to support the establishment of AFREF. Other applications such as hazard mitigation, regional and global plate tectonics will emerge from this project.

The main objective of this research is to determine robust velocity field vectors over Africa as determined through processing and analysing GNSS data provided by a network of GNSS stations located on the African continent.

Other sub-objectives of this project are to:

- Validate the velocity fields derived at HartRAO against velocity fields computed from other IGS analysis centres e.g., Jet Propulsion Laboratory (JPL).
- Compare velocity solutions from the MOBLAS-6 Satellite Laser Ranging (SLR) station with the IGS station HRAO and the 26 m Very Long Baseline Interferometry (VLBI) telescope collocated at Hartebeesthoek Radio Astronomy Observatory (HartRAO) as an independent inter-technique comparison.

## 1.4 Thesis structure

**Chapter 2: Space geodetic techniques and applications**

In this chapter, space geodesy techniques such as GNSS, SLR and VLBI and the current status of the modern geodetic reference frames are introduced and briefly described.

**Chapter 3: Data and analysis strategies**

The methodology of processing GNSS data using the GAMIT/GLOBK (version 10.4) software developed at the Massachusetts Institute of Technology (MIT) **(**King and Bock, 1995; Herring, 1997) and the Combination and Analyses of Terrestrial Reference Frame (CATREF) software developed at Institut National de l'Information Géographique et Forestière (IGN) (Altamimi, 2007) are discussed.

**Chapter 4: Results and discussions**

Velocity solution results derived from GNSS stations are presented with their associated statistics. The validation of the derived velocities was done through comparison with velocities derived by the Jet Propulsion Laboratory (JPL, NASA). Furthermore, the velocity vectors of the IGS station HRAO are compared with the velocity vectors from the SLR MOBLAS-6 station and the 26 m VLBI telescope collocated at HartRAO.

**Chapter 5: Examples of the applications GNSS velocities to geodynamics**

In this chapter, applications of GNSS velocities in geodynamics are discussed. This includes geodynamics of the Nubian-Somalian-Arabian plates and South Africa. The stability of the proposed space geodesy and geophysics observatory site in Matjiesfontein (Great Karoo, South Africa) is discussed.

**Chapter 6: Conclusion and recommendations**

In this chapter, a summary of the contents and results of the thesis are made and recommendations for future research are provided.

## 1.5 Concluding remarks

The aim of this research was to derive the horizontal and vertical velocities of inter-continental plates over the African continent using permanently installed GNSS stations (both IGS and local) to support the establishment of AFREF. It is envisaged that the derived GNSS velocities for Africa will not only contribute towards the AFREF project but also towards a better understanding of geodynamics of the African continent.

# CHAPTER 2

## Space geodetic techniques and applications

*"Look deep, deep into nature, and then you will understand everything better, Albert Einstein"- 1951.*

### 2 Space geodetic techniques

### 2.1 Introduction

Planet Earth is a complex system that is driven by both interior and exterior forces. Interior forces involve mantle interaction that drives plate movements and external forces involve forces between the Earth and extra-terrestrial bodies such as the Moon and Sun, which affect the orbit of the Earth and produce tides on Earth. These physical phenomena require accurate measuring techniques and long-period observations to understand them. Space geodetic techniques such as GPS, SLR and VLBI have been developed to study processes that affect the Earth on different scales. Pictured in Figure 1 are examples of geodetic instruments (GPS, VLBI and SLR) collocated at HartRAO, South Africa.

This unique state of the art site is the only observatory in Africa that is collocated with four different space geodetic techniques. A French Doppler Orbitography and Radiopositioning Integrated by Satellite (DORIS) system is located close-by (1.5 km), but not in the main valley of HartRAO as it produces radio frequency interference which affect observations made with the VLBI radio telescopes.

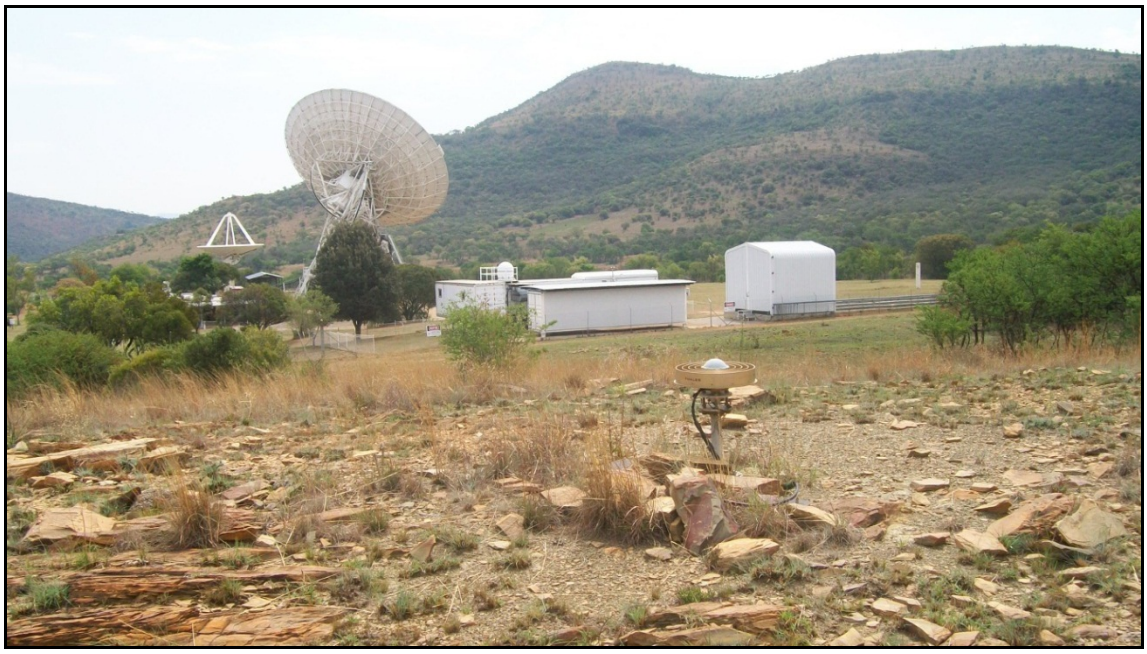

**Figure 1**. Geodetic instruments collocated at HartRAO, South Africa. In the far distance left, the 15 m VLBI antenna, left-foreground the 26 m VLBI antenna, centre-foreground the SLR (MOBLAS-6) station, right-centre the Lunar Laser Ranging (LLR) in development and the IGS GNSS station (HRAO) antenna in the foreground.

Geodesy has the capability to determine, unambiguously and with high precision, the geometric shape of the Earth, tectonic plate movement and gravity of the Earth as a global function of space and time (Plag *et al.* 2009a). Considering global plate motion, which is of the order of several millimetres to tens of millimetres per year, space geodesy techniques are able to determine the rates of plate motion with high accuracy. Additionally, as radio signals from satellites in orbit travel through non-homogeneous space, parameters describing the state of the atmosphere can be extracted and used e.g., in meteorological (water vapour) (Combrink *et al.* 2004) and ionospheric (total electron content) studies (Moeketsi *et al.* 2009). The three pillars of geodesy (gravity field, Earth rotation and reference frames) make it possible for scientists to integrate information from these pillars to produce unique products. As an example, the International Terrestrial Reference Frame (ITRF) consists of a set of selected positions and velocities of globally distributed reference points on the surface of the Earth (the physical reference points of SLR, GNSS, VLBI and DORIS instruments). In turn, the International Celestial Reference Frame is realized through positions (determined by geodetic VLBI) of radio sources such as quasars, which are selected such that they have

virtually no proper motion and very little source structure; they are therefore, used as fixed, point sources (Plag *et al.* 2009a). These points can be represented or derived from one or more space geodesy techniques. These two reference frames are connected to each other through the Earth Orientation Parameters (EOPs). The EOPs are a product of the various geodetic networks, but especially rely on geodetic VLBI. During the determination of plate tectonics on global or regional scales, for the final solution to be accurate, it must be referred to these well-known points of reference. This chapter provides a brief overview of the space geodetic techniques pictured in Figure 1.

## 2.2 Global Navigation Satellite Systems

### 2.2.1 General GNSS description

The generic name for the various navigation satellite systems is Global Navigation Satellite Systems (GNSS). Currently, the components of GNSS are the Russian Federation GLONASS system, the European Union Galileo system, and the Chinese Beidou system. These systems are similar to the USA GPS, but not exactly the same, so modern GNSS receivers must be designed and configured to receive data from the different systems, whereas older receivers typically only receive GPS data. In this work, only GPS data was processed. In general, when reference is made to GNSS, it includes GPS and specifically when reference is made to data processing it implies GPS data only.

The U.S. Department of Defense originally designed the satellite-based navigation system (GPS) for military purposes. It has a constellation of at least 24 satellites orbiting at about 20 000 km altitude, with orbital periods of 24 hours, in six different planes, with approximately four or more satellites per plane (Yu *et al.* 1997). These satellites are specially arranged to allow positioning anywhere in the world at any time. The GPS constellation also has five extra satellites for emergency purposes. The GPS technique has been applied in different fields such as geodynamics e.g., since the mid-1980s (Erdogan *et al.* 2009) to study geophysical phenomena. The principal application of GPS is the quasi-static applications, where there is appreciable relative motion among the points being measured (Wells, 1986); such applications include geodynamics and movement monitoring.

The GPS satellites transmit signals at L1 (1575.42 MHz) and L2 (1227.6 MHz) frequencies, which are equivalent to $\lambda \approx 19$ cm and $\lambda \approx 24$ cm wavelengths, respectively. The frequencies are modulated with navigation messages and two types of codes, i.e., P-Code (Precision Code) which is available in both the L1 and L2 bands and C/A Code (Coarse Acquisition Code) available only in the L1 band. The navigation message is modulated on both the L1 and L2 bands and consists of information about ephemerides of the satellites, the satellite's clock, the satellite orbit positions and various correction data (Yang, 1995). Recently, the GPS Block IIR-M SV (space vehicle) was launched in 2005 to make the L2C signal available for civil purposes. Additionally, the M-code was added for a modernized military signal centred on L1 and L2 frequencies (Bartone, 2006). In 2007, the GPS Block IIF SV was launched to add the L5 new civil signal with frequency centred on 1176.45 MHz (Bartone, 2006). In order to determine the 3-D position of the GNSS receiver on the ground, at least three satellites must be visible at a time; to determine time as well, four satellites must be visible.

The GPS receiver network has been growing consistently to meet the needs of geodetic communities such as the IGS over the last decade. One of the objectives of the IGS is to increase the density of the GNSS network in the world (http://igscb.jpl.nasa.gov/network/ complete.html). Figure 2 depicts the current GNSS network in the world; it is controlled and maintained by the IGS. The GNSS network in Africa is sparse, with higher numbers south of the equator. Geometrically the network is non-uniform, with large sections which are unoccupied. Rothacher *et al.* (2009) outlined the important multi-purpose applications of the global GNSS network:

- Monitoring of global plate tectonics and deformation phenomena.
- Monitoring of displacements during and after earthquakes to provide additional information to geodynamic communities.
- Contributions towards the reference frame realization including its monitoring and maintenance. This means that accurate crustal velocities measured using space geodesy techniques such as GNSS will be required for reference frame realization and maintenance.

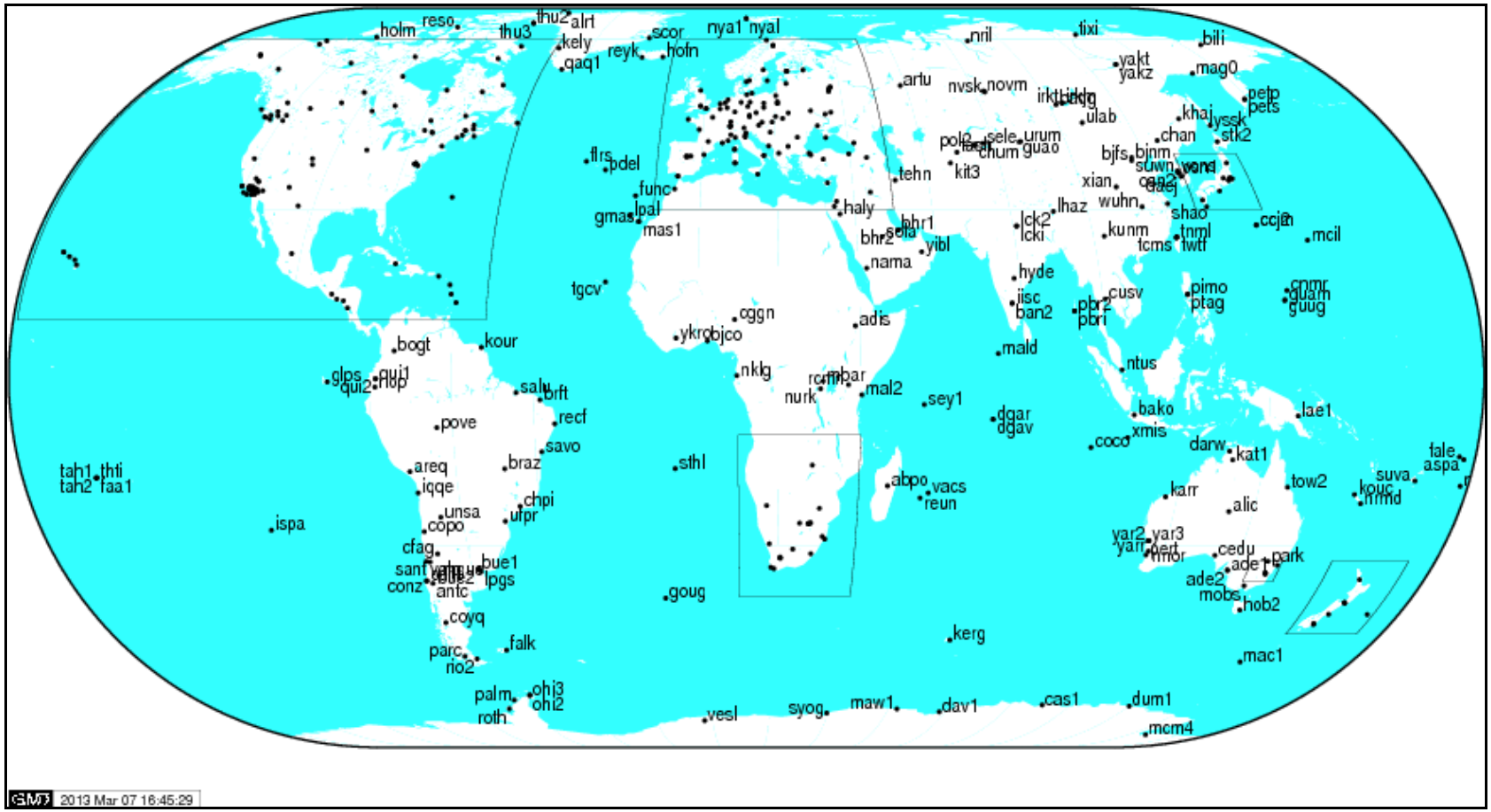


**Figure 2.** Distribution of GNSS stations around the world (sourced from: http://igscb.jpl.nasa.gov/network/complete.html; accessed: 01 March 2012).

### 2.2.2 GNSS observables

Observables of the GNSS can be described as ranges that are derived from phase differences or are time-based, based on the signal generated by the GNSS satellite and the signal received by the GNSS receiver on the ground (Hofmann-Wellenhof *et al.* 1992). The *X*, *Y* and *Z* coordinates of a point on the surface of the Earth can be accurately determined if distances from three or more fixed points are measured to that point. Similar principles apply in determining coordinates of a GNSS station on the surface of the Earth. Figure 3 illustrates point $N_i$ on the surface of the Earth with GNSS satellites $K^j$, where r1, r2, r3 and r4 represent ranges from different satellites. If the positions of the satellites $K^j$ (j=1, 2, 3, 4; $X^j$, $Y^j$, $Z^j$) are known then this information is enough to determine the (*X*, *Y*, *Z*) position of the point $N_i$.

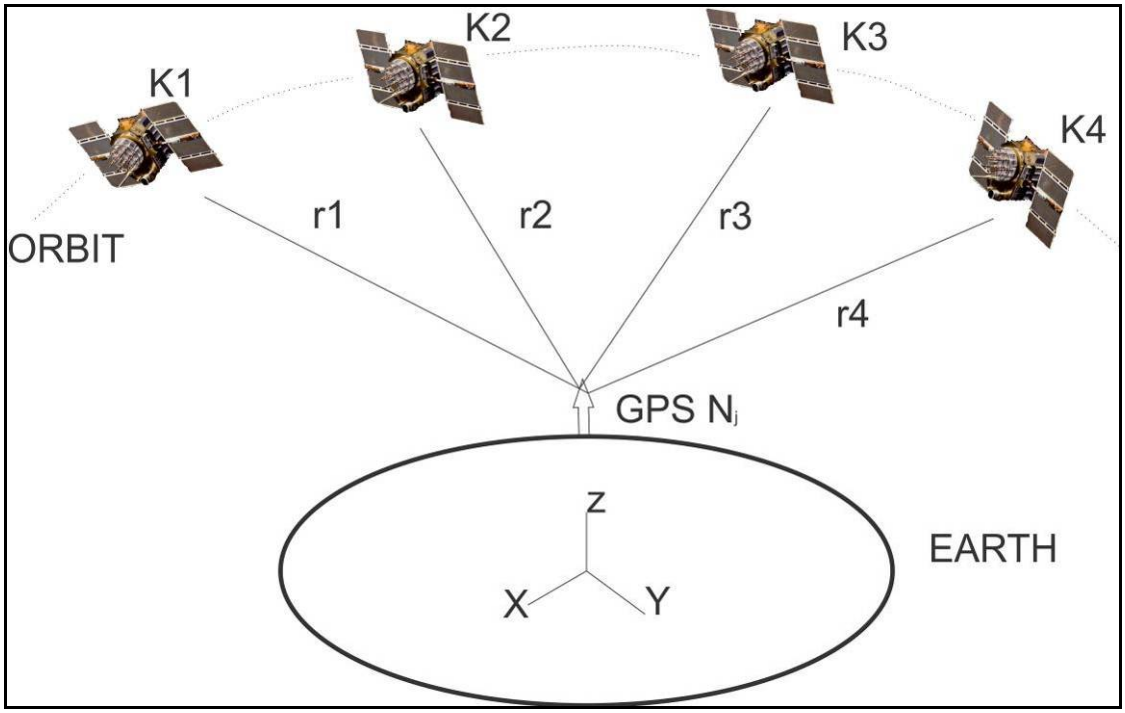


**Figure 3.** Principle of pseudo-range positioning in the satellite reference system, adapted from Kahmen and Faig (1988).

When the satellite transmits PRN-codes (Pseudo Random Noise) that are modulated onto carrier signals (Kahmen and Faig, 1988) to the receiver on the ground,

the receivers generate a reference PRN-code of a similar pattern and synchronise it with a very accurate clock. The PRN-code depicts a phase or time shift $(\Delta\varphi)$ depicted in Figure 4 that results in a signal delay.

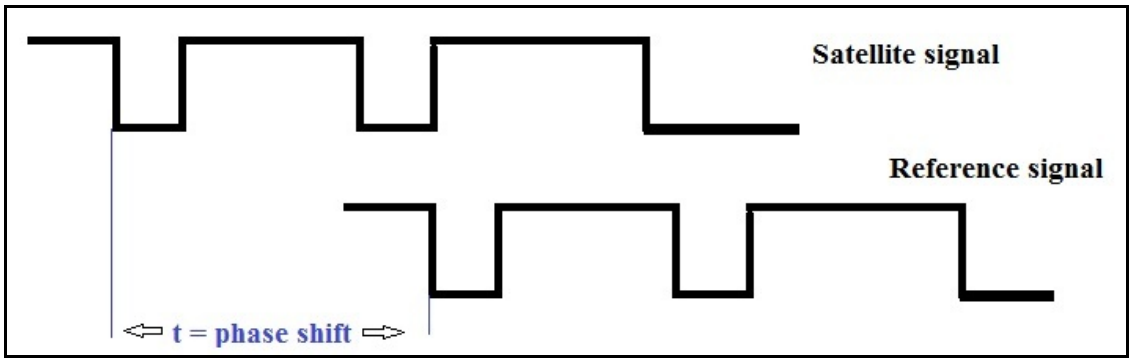


**Figure 4.** PRN-code generated by satellites and receivers, adapted from Kahmen and Faig (1988).

Having similar signals generated in the satellite and receiver, one can shift the two signals to become congruent and determine the distance $(\phi/\rho)$ between the satellite and the receiver by multiplying the time ($t$) or phase shift $(\Delta\varphi)$ by the propagation speed of light ($c$) given by:

$$[\phi/\rho] = t*c. \qquad [2.1]$$

The $(\phi/\rho)$ can be extended to form an observational equation that describes the geometric distance ( $p_i^k$ ) between satellite and receiver:

$$[\phi/\rho] = p_i^k = \left|k^j - N_i\right| = \sqrt{(x^j - x_i)^2 + (y^j - y_i)^2 + (z^j - z_i)^2}. \qquad [2.2]$$

Note that coordinates $N_i$ are unknown and can be determined only if ranges from more than four satellites are measured. Due to errors inherent in the clocks, this term $c*(dt_i - dt^k)$ is added to the observation equation to correct for clock errors:

$$[\phi/\rho] = \left|k^j - N_i\right| = \sqrt{(x^j - x_i)^2 + (y^j - y_i)^2 + (z^j - z_i)^2} + c*(dt_i - dt^k). \qquad [2.3]$$

A pseudo-range term ($\phi_i^k$) is used to describe phase ranges. Additional terms can then be added into the observation equation to compensate for other errors such as tropospheric refraction ($T_i^k$), ionospheric refraction ($I_i^k$), integer ambiguity ($N_i^k$), and multi-path effects ($\varepsilon^k$) to give Eq. [2.4] and Eq. [2.5] reported in Yang (1995) which represents phase range and code pseudo-range measured at the L1 and L2 frequencies, respectively, from satellite *k* and receiver *i*. Therefore,

$$\begin{aligned}\phi_i^k &= \rho_i^k - [I_i^k / f^2] + T_i^k + \lambda * N_i^k + c(dt_i - dt^k) \\ &+ \lambda[\varphi_i(t_0) - \varphi^k(t_0)] + \varepsilon^k,\end{aligned} \qquad [2.4]$$

$$p_i^k = \rho_i^k + [I_i^k / f^2] + T_i^k + c(dt_i - dt^k) + \varepsilon^k. \qquad [2.5]$$

$\phi_i^k$, $p_i^k$ are the phase range and code pseudo-range measured at L1 and L2 frequencies, respectively, from receiver *i* to satellite *k*. In Eq. [2.4] and [2.5]:

$\rho_i^k$ = geometric distance from satellite and receiver,

$I_i^k / f^2$ = first-order atmospheric ionosphere refraction,

$T_i^k$ = tropospheric refraction,

$\lambda * N_i^k$ = wavelength and integer ambiguity associated with L1 and L2 phases,

$c$ = vacuum speed of light,

$(dt_i - dt^k)$ = $dt_i$ clock error of receiver *i* and $dt^k$ clock error of satellite *k*,

$\lambda[\varphi_i(t_0) - \phi^k(t_0)]$ = nonzero initial fractional phase contained in the satellite generated signal and the receiver and

$\varepsilon^k$ = remaining errors.

Code pseudo-range is the measure of the distance between satellite and receiver antenna and is computed by observing the signal transmitting time from the satellite to the receiver by analysing the utmost correlation between the GNSS signal and receiver code (Stebler, 2008). Code pseudo-range is mainly used for navigation purposes and it has a low accuracy (~1 m). As geodesy requires very high accuracies, much higher than

typically required for navigation, phase pseudo-range measurements are being used instead of code pseudo-range to achieve millimetre accuracy (Torge, 1991).

### 2.2.3 Positioning techniques

Carrier beat phases are used in geodetic high precision measurements to obtain a positioning accuracy of about 1 mm or better. This is usually done by differencing the phases of simultaneously received signals at each epoch from at least two satellites and at least two receivers on the ground transmitted at both L1 and L2 frequencies (Herring *et al.* 2010). By carrying out single, double or triple differencing, atmospheric effects, instabilities within satellite clocks, ambiguities and cycle slips can be resolved (Yang, 1995). The single differencing method involves differencing GNSS signals from a satellite and between two receiver stations on the ground only. However, this technique is affected by the distance between receivers, i.e., if the baseline is large (more than 5 km) not all effects are removed using this technique. Instead, the double differencing method (Figure 5) is used to cancel out all the effects by applying a Linear Combination (LC), i.e., combining the two phases or measurements into a linear form (Herring *et al.* 2010; Yang, 1995). This is done by differencing between two receivers on the ground and between two satellites i.e., applying Eq. [2.6] and [2.7]:

$$p_{iz}^{k} = \rho_{iz}^{k} + [I_{iz}^{k} / f^{2}] + T_{iz}^{k} + c(dt_{iz} - dt^{k}) + \varepsilon^{k}, \qquad [2.6]$$

$$p_{iz}^{b} = \rho_{iz}^{b} + [I_{iz}^{b} / f^{2}] + T_{iz}^{b} + c(dt_{iz} - dt^{b}) + \varepsilon^{b}. \qquad [2.7]$$

Application of Eqs [2.6] and [2.7] creates a free ionospheric refraction model (Yang, 1995) Eq. [2.8]:

$$p_{iz} = p_{iz}^{k} - p_{iz}^{b}, \qquad [2.8]$$

where $p_{iz}$ represent the ionospheric free model derived from Eq. [2.6] and [2.7]. The satellite clock error $dt^{k}$ is removed after differencing; therefore, the term $p_{iz}$ can be described as a geometrical distance between two satellites and receivers plus the tropospheric refraction $T_{i}^{k}$. See Figure 5 for an illustration of the principle of double differencing between two receivers and two satellites.

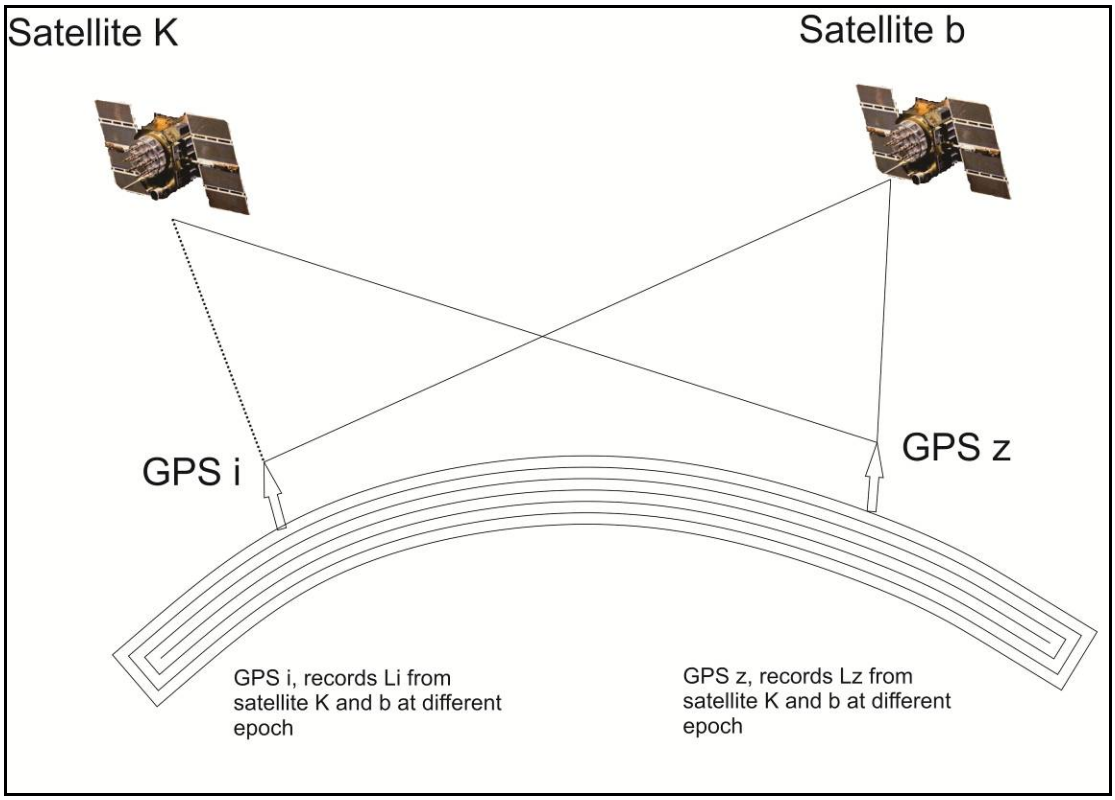


**Figure 5.** Principle of double differencing between two receivers (*i* and *z*) and two satellites (*k* and *b*) (adapted from: Yang, 1995).

### 2.2.4 GNSS limitations

The signal from a GNSS satellite does not propagate through a vacuum only, but also traverses through the atmosphere. Atmospheric effects as well as atmospheric boundaries are not static but vary with time. This has introduced a challenge in GNSS positioning due to unpredictable behaviour of the GNSS signal as it propagates through the atmospheric medium (Figure 6). Different models have been developed in an attempt to compensate for atmospheric effects. These models predict the behaviour of the GNSS signal at different levels of the atmosphere (Komjathy, 1997; Ma *et al.* 2001). Well known factors that affect the GNSS signal such as ionospheric, tropospheric and multi-path effects are discussed and the contribution of each error type is listed in Table 1.

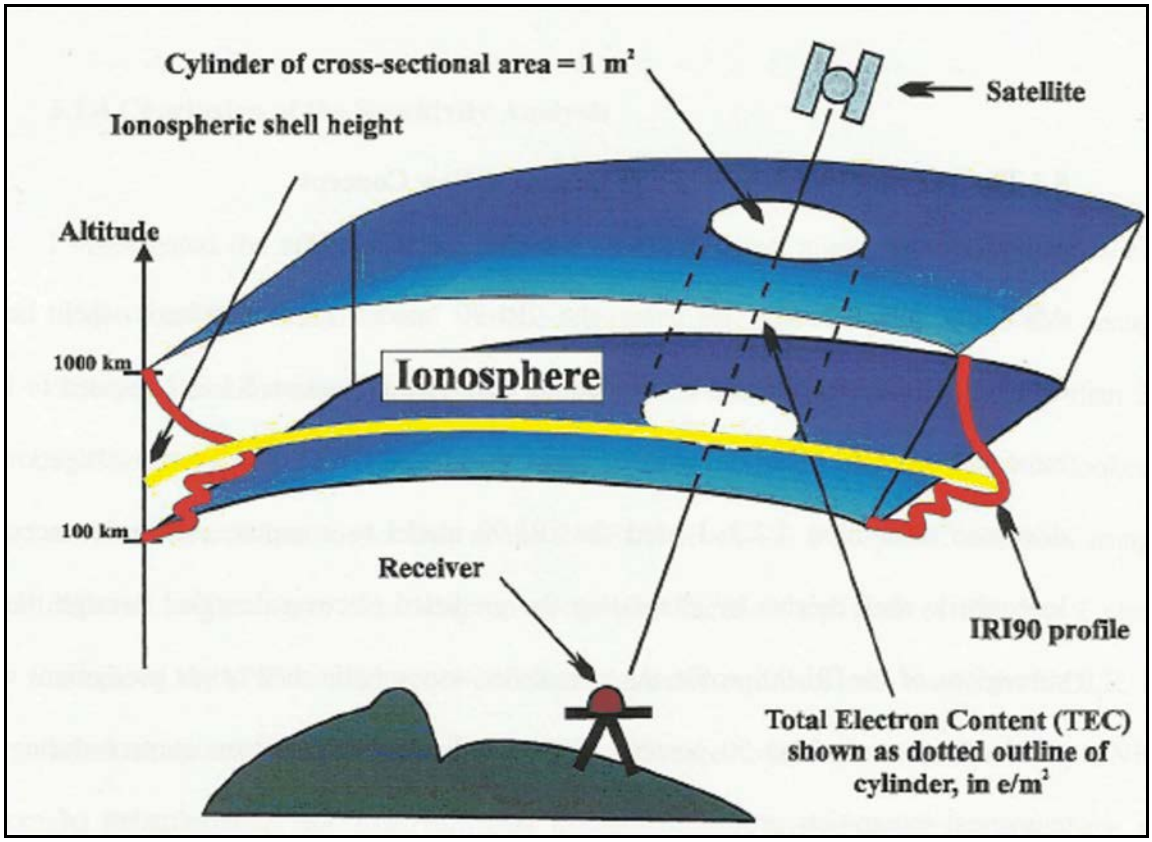


**Figure 6.** Concept of GNSS signal propagation through different atmospheric levels (Komjathy, 1997).

**Ionosphere**

The atmospheric region ranging from approximately 50 km to 1000 km above the Earth's surface is referred to as the ionosphere. The ionosphere contains free electrons which are caused by ultraviolet radiation from the Sun ionizing gas molecules and as a result, electrons are realized (Grejner-Brezezinska, 1995). Free electrons in the ionized medium cause radio signals to behave in a nonlinear fashion and cause the ionized medium to be dispersive. The delay of broadcasted GNSS signals depends on the Total Electron Content (TEC) along the propagation direction, time, geographical location and the frequency of the signal (Hofmann-Wellenhof *et al.* 1992). The range error can be anything from less than 1 m to more than 100 m. The refraction coefficient $n_p$ describing propagation of the carrier phase is given by Eq. [2.9] and Eq. [2.10]:

$$n_p = 1 + c_2 / f^2 + c_3 / f^3 + .... \quad [2.9]$$

$$n_p = 1 - 40.3 n_e / f^2. \quad [2.10]$$

Here, $f$ = frequency and $c_i$ = coefficients, which are not depend on frequency but largely depend on $n_e$, which is the number of electrons per $m^3$ along the propagation path of the signal (Hofmann-Wellenhof *et al.* 1992). For derivation of these formulas see Seeber (1993) and Hofmann-Wellenhof *et al.* (1992).

**Troposphere**

The troposphere is the lower layer of the atmosphere and its height above the Earth's surface ranges from 9 km at the poles to 16 km at the equator (Torge, 2001). It is referred to as the non-ionized region of the atmosphere and it causes tropospheric delays of the GNSS signals. This region of tropospheric refraction is not dispersive with respect to radio waves that have a frequency of less than of 15 GHz, unlike the ionospheric refraction region. Therefore, the tropospheric refractions caused by this region cannot be resolved using the LC method because the propagation path of the signal is frequency independent (Grejner-Brezezinska, 1995; Hofmann-Wellenhof *et al.* 1992). Different models have been developed to correct the effects caused by atmospheric refractions. Dodo and Idowu (2010) assessed three models i.e., the refined Saastamoinen, Neil and Hopfield models in search of an optimal model to reduce tropospheric effects in GNSS observations. They found that the refined Saastamoinen model Eq. [2.10] is a better model to mitigate the tropospheric effect with an average percentage improvement of 33.6%, while the Hopfield and Neil models have 12.5% and 13.8% improvements, respectively, (Dodo and Idowu, 2010).

The atmosphere consists of wet and dry parts. The wet component; however, largely depends on the distribution of the water vapour in the atmosphere, making it difficult to model. Therefore, to accurately model the wet component would require that regional meteorological measurements be made during the experiment to calibrate the observations (Wells, 1986). The tropospheric path delay ($\nabla^{Trop}$) is defined by:

$$\nabla^{Trop} = \int (n-1)ds. \qquad [2.11]$$

Here $n$ represents the refractive index (see Hofmann-Wellenhof *et al.* 1992 for derivation) and this can be expanded to give:

$$\nabla^{Trop} = 0.002277 / \cos(z)[\rho + (1255/T + 0.05) * e - B\tan^2 z] + R\delta. \qquad [2.12]$$

Where $z$ = Zenith angle of satellite,

$\rho$ = pressure (mbar),

$T$ = temperature (K),

$e$ = partial pressure of water vapour (mbar),

$\nabla^{Trop}$ = tropospheric path delay (m); $B$ and $R\delta$ are the corrections that depend on the height of the station and on $z$.

Hopfield (1969) expressed the tropospheric delay of the GNSS signal as the tropospheric refractivity $N^{trop}$, which is the sum of the wet ($N_w^{trop}$) and dry ($N_d^{trop}$) components that contribute towards the signal delay as follows:

$$N^{trop} = N_d^{trop} + N_w^{trop}. \qquad [2.13]$$

**Multi-path Effect**

The signals transmitted by GNSS satellites are not only prone to influence from atmospheric and ionospheric effects but are also influenced by the vicinity of the GNSS antenna. These are referred to as multi-path effects, which are usually the result of reflective objects that are located near the antenna such as reflective surfaces, buildings, trees etc., Multi-path effects affect both code and carrier measurements at different levels which can reach about 1 to 5 m in very high reflective surroundings (Seeber, 1993).

One of the best methods to eliminate multi-path effects is to wisely select the observation site in terms of GNSS stations, which should be permanently installed. The site should be free from reflective objects and the site should be regularly checked to keep reflective objects such as trees away from the GNSS antenna. Combrinck and Chin (2001) provided more details on IGS site selection. Other possible methods include

using the LC method or carefully selecting an antenna that uses a single vertical polarization since reflected GNSS signals are left-handed polarized (Hofmann-Wellenhof *et al.* 1992), this will allow reflected signals to be filtered out in the receiver. The choke ring design is widely used in different antennas to mitigate the multi-path effect. It consists of three or more concentric ring-like structures with varying radius and depth (Tranquill, 1988) that are designed to prevent reflected or surface waves from entering the antenna. Table 1 contains a summary of the average error contribution by different kinds of sources (Grejner-Brezezinska, 1995).

**Table 1.** Summary of the errors and their contribution to a single range observation equation (Seeber, 1993; *Kahmen and Faig, 1988).

| | ***P-code*** | | ***C/A-code*** | |
|---|---|---|---|---|
| **Source** | **SA off** | **SA on** | **SA off** | **SA on** |
| **Satellite** | | | | |
| -Orbit | 5 m | 10-40 m | 5 m | 10-40 m |
| -Clock | 1 m | 10-50 m | 1 m | 10-50 m |
| **Signal propagation** | | | | |
| -Relativistic propagation | ~2 cm | ~2 cm | ~2 cm | ~2 cm |
| -Multi-path effects | 1 m | 1 m | 5 m | 5 m |
| - Troposphere* | - | - | ±1-5 m | ±1-5 m |
| -Ionosphere* | - | - | ±1-3 m | ±1-3 m |
| **Receiver** | | | | |
| -Observation noise | 0.1– 1 m | 0.1– 1 m | 1-10 m | 1-10 m |
| -Hardware delays | - | mm-1 m | 1 mm-1 cm | 1 m |
| -Antenna phase centre | 1 mm-1 cm | 1 mm-1 cm | | 1 mm-1 cm |

## 2.3 Satellite Laser Ranging

### 2.3.1 Introduction

The tracking of satellites using the SLR technique was pioneered in the early 1960s (Combrinck, 2010). The first successful SLR experiment was reported on 3 December 1964 (Smith, 1964). The Explorer-22 (also known as Beacon-B) satellite was successfully tracked for ten sessions during 11 October to 13 November 1964. This experiment was led by a NASA team and a team from General Electric Co. (Valley Forge, Pennsylvania) also participated. The expected range accuracy was about 3 m (Combrinck, 2010). Since then, the SLR technique has greatly improved in accuracy (1-2 cm), and diverse applications are routine; these range from geodynamics, geophysical studies and tests of the General Theory of Relativity (Combrinck, 2011).

The distribution of SLR stations is depicted in Figure 7, it can be seen that Africa has limited station coverage, which results in poor coverage and a weaker network in the Southern Hemisphere. For this reason, many satellites have poor coverage in the Southern Hemisphere resulting in less ranging data being available. In 1993, IFAG (now BKG) operated an SLR station at HartRAO and SAAO (Sutherland) for a period of one month at each site (Combrinck, 1993). During 2000, NASA installed MOBLAS-6 (see Figure 8) at HartRAO, South Africa (Combrinck, 2009). It has been operating since then and participates on international level to provide SLR data.

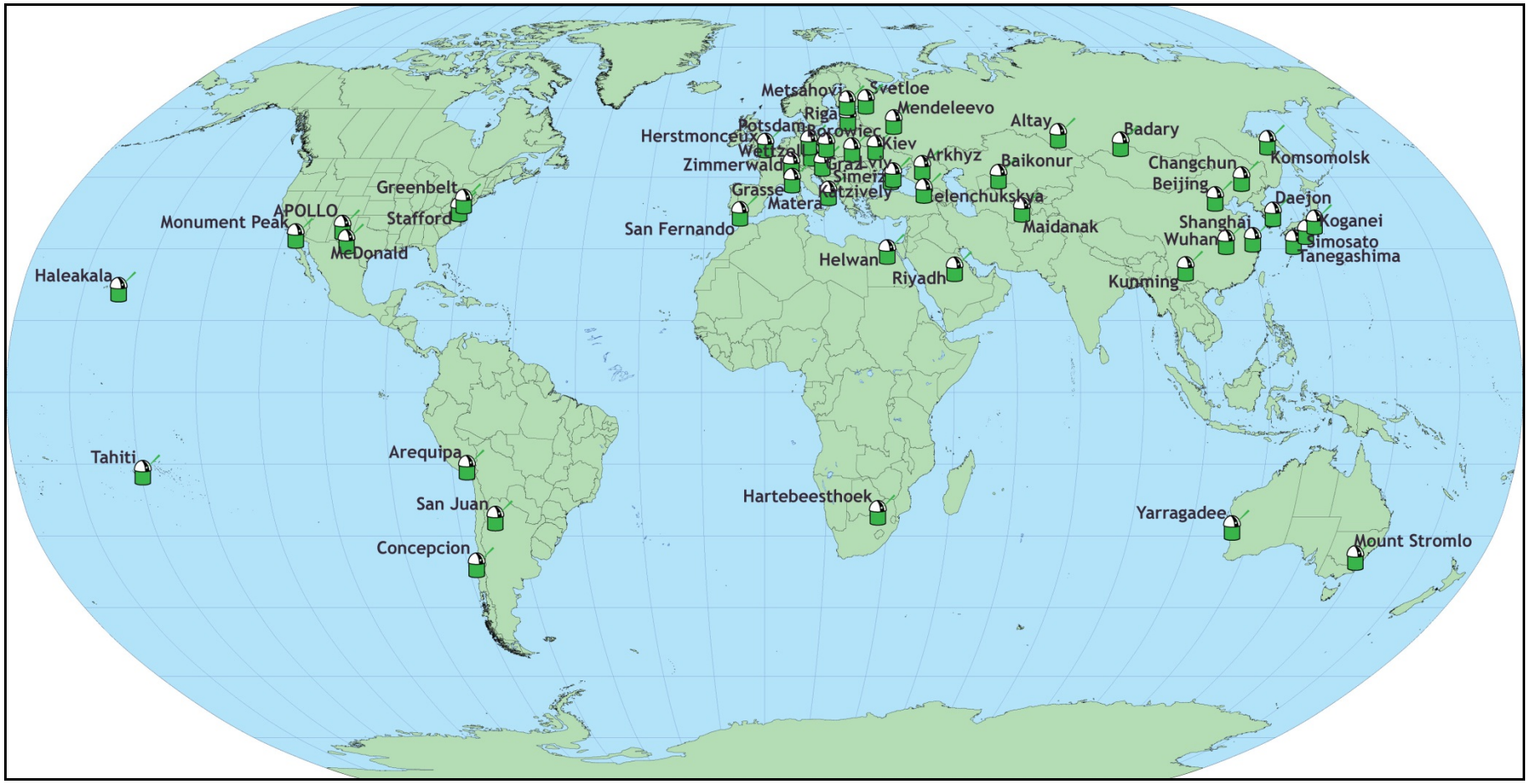


**Figure 7.** Map illustrating ILRS (International Laser Ranging Service) SLR network stations (source: http://ilrs.gsfc.nasa.gov/network/stations/index.html; accessed: 08 April 2012).

**Figure 8.** Collocated geodetic instruments at HartRAO, South Africa. Left: LLR/SLR station under development; Right: SLR (MOBLAS-6) station, due to bad weather the telescopes are closed up.

### 2.3.2 Basic SLR principles

The basics of the SLR system are illustrated in Figure 9, which depicts a base station on the surface of the Earth and a Laser GEOdynamics Satellite (LAGEOS) in orbit. The SLR system requires a Pointing Control System which controls the pointing directions of the telescope and the laser transmitter, this system is required to be accurate in order to point at the target perfectly. The laser transmitter transmits a laser pulse to the target LAGEOS in orbit, the corner-cube reflectors mounted on the surface of the LAGEOS satellite reflect the transmitted pulse back to the base station. The returned pulses are collected by the tracking telescope and the final round trip time of flight of ultra-short pulses of light to satellites are detected by special detectors (photo multiplier tube or single photon avalanche diode). Time and frequency are crucial in SLR operation, for example, MOBLAS-6 at HartRAO utilizes a rubidium clock where short-term stability and long-term drift of approximately $2*10^{-11}$ and approximately $5*10^{-11}$/month are achieved (Combrinck, 2010). The timing system allows range or time of flight to be

calculated accurately. The instantaneous range of measurements then provides a millimetre level of precision and these data can be accumulated to provide a range of applications in the science community including a contribution to crustal dynamics (Pavlis, 2010). More information about hardware specifications, range models, force and orbital models, calculated range, SLR System and logistics are described in detail in Combrinck (2010).

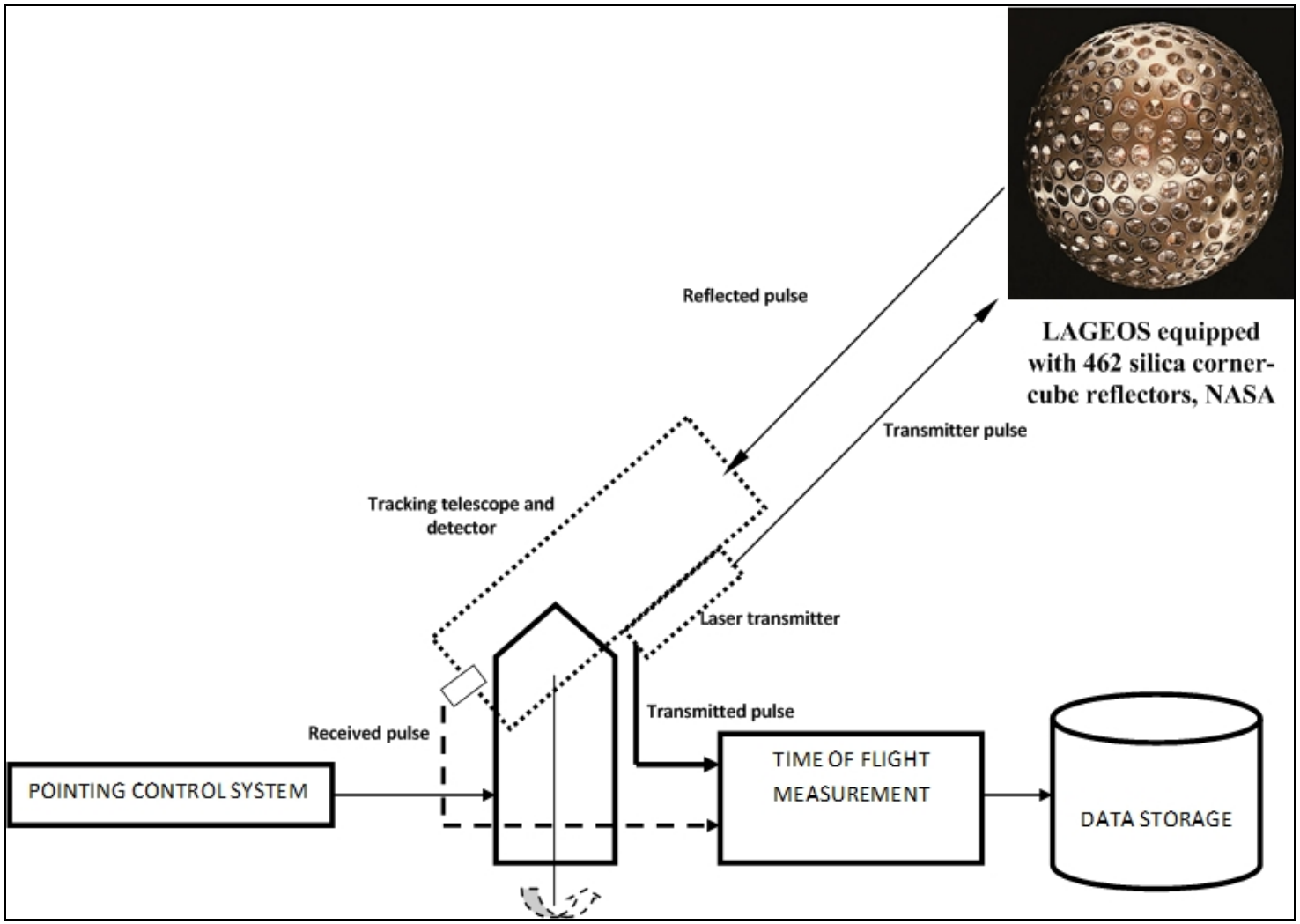


**Figure 9.** Schematic view of a Satellite Laser Ranging tracking artificial LAser GEOdynamics Satellite (LAGEOS) launched 4 May 1976 (adapted from: Degnan, 1985).

## 2.4 Very Long Baseline Interferometry

### 2.4.1 Introduction

The Very Long Baseline Interferometry (VLBI) technique is an important space geodetic technique that was developed during the 1970s. Figure 10 depicts the 26 m VLBI antenna at HartRAO and Figure 11 depicts the global VLBI tracking network. The VLBI technique was developed by radio astronomers as a tool to study extragalactic radio sources such as quasars. Soon after, this technique was applied in many different areas to derive geodynamic parameters such as polar motion, changes in the Earth's rotation, Universal Time, Earth tide parameters, study of the General Theory of Relativity and reference frame definition (Robaudo and Harrison, 1993).

**Figure 10.** The HartRAO 26 metre VLBI telescope facing north-west.

Quasars are so far from the Earth that they can be seen as motionless in the sky; this characteristic of quasars allows the implementation and maintenance of a stable reference frame which is required to provide millimetre accuracy in determination of plate motions on the surface of the Earth (Combrinck, 1993).

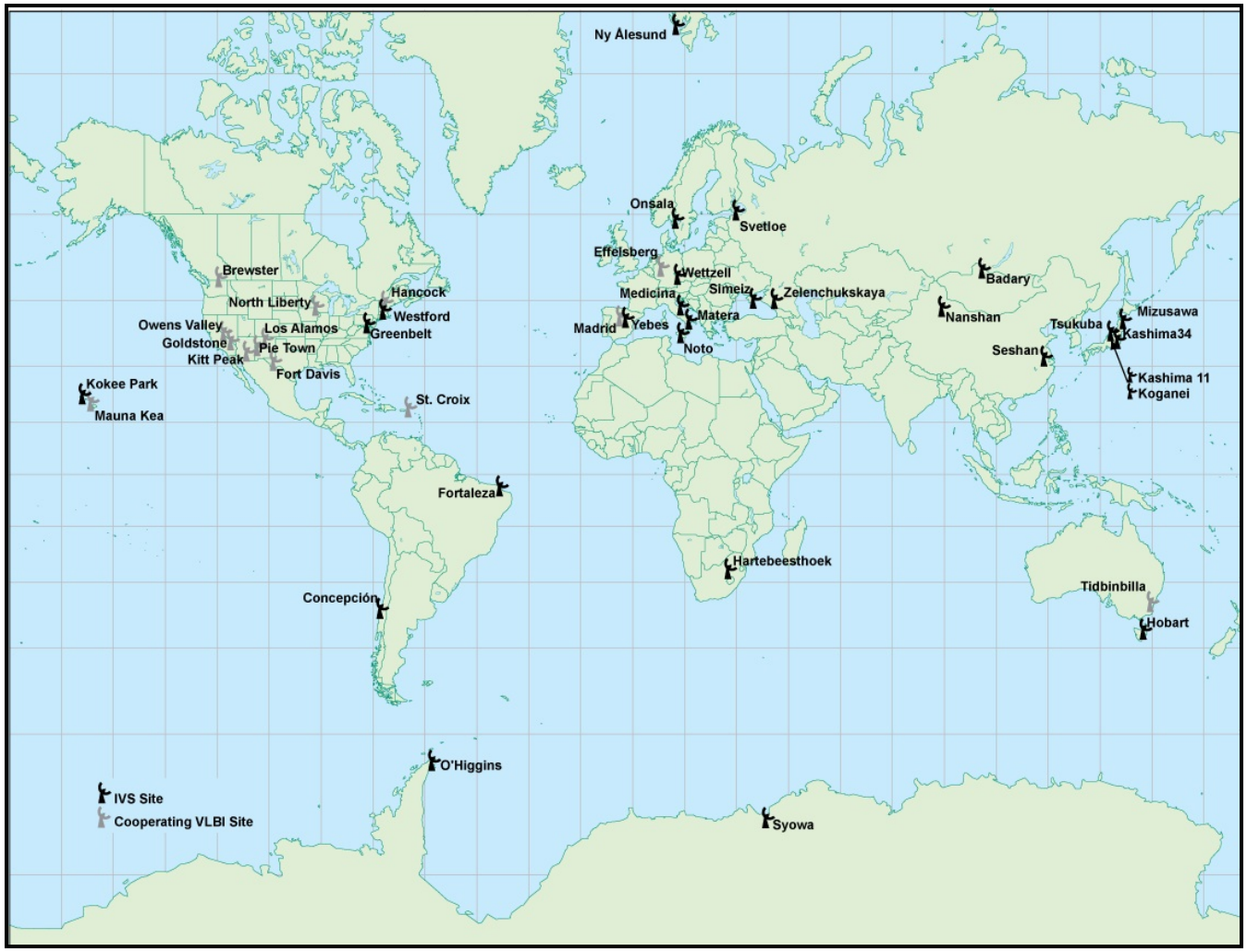


**Figure 11.** Map depicting tracking network of Very Long Baseline Interferometry (VLBI) stations (source: http://cddis.nasa.gov/images/ivsmap.gif; accessed: 08 April 2012).

### 2.4.2 Basic VLBI principles

The principles of VLBI are simple; a radio frequency bandwidth is selected from two or more radio telescopes (see Figure 10 and Figure 12) with long baselines to observe radio signals from a target that emits radio signals such as quasars. The observing stations can be separated by thousands of kilometres. If the stations are relatively close to each other, phase-synchronized local oscillators can be utilized and the signals from the antennas can feed a correlator directly. If the antennas are far apart such as the South African SKA and Australian SKA projects, this usually requires highly accurate timing systems (hydrogen MASER atomic clocks) to allow determination of "phase delay" or "time-delay" at later stages and data can be stored on high density magnetic tapes or disks (Combrinck, 1993). The radio signal being observed by two antennas located far apart will arrive at the two antennas at different times. That is, one antenna will observe a signal with additional distance defined by $\tau * c$, where $\tau$ is the time difference of the signal arriving at the two stations obtained by cross correlating the signal from two stations and $c$ is the speed of light (Plag *et al.* 2009b). The total time-delay between two antennas is the sum of geometric delay, the instrumental delay and transmission-media delay (Thomas *et al.* 1976). For crustal deformation monitoring purposes, it is necessary to measure the total delay for many different radio sources and on several baselines (Robaudo and Harrison, 1993). The parameter $\tau$ and other delays allow one to solve for astronomical and geophysical quantities (Sovers *et al.* 1984).

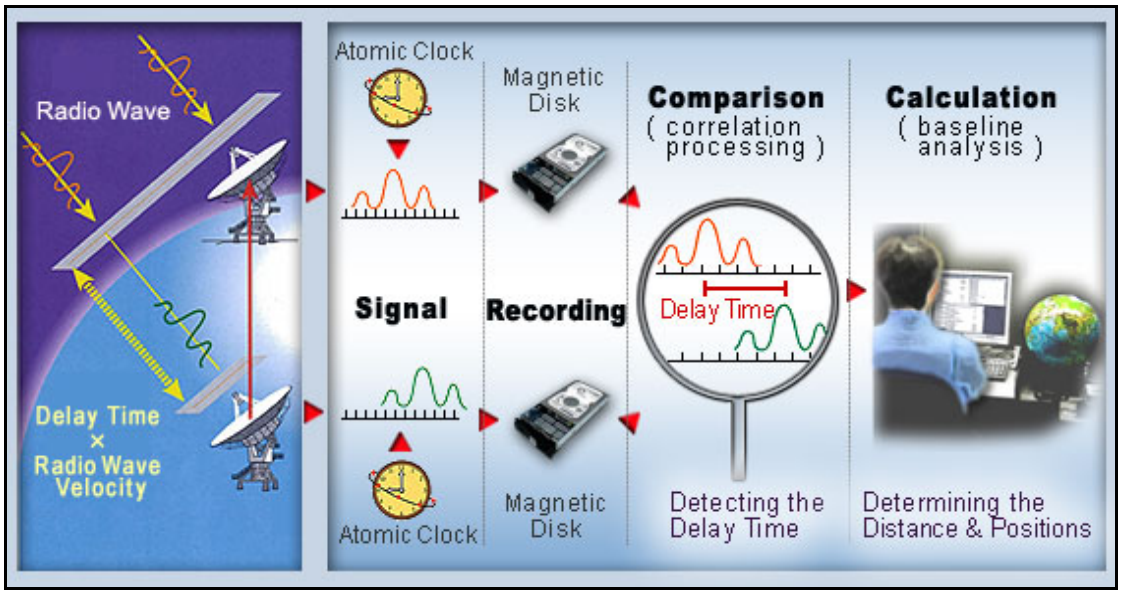


**Figure 12.** Illustrated basic principles of Very Long Baseline Interferometry; a very stable atomic clock is required as well as a fast and high capacity storage medium. (source: http://www.spacegeodesy.go.jp/vlbi; accessed: 01 October 2012).

## 2.5 Modern Geodetic Reference Frames

### 2.5.1 Introduction

Modern society is faced with complicated natural processes that tend to affect our daily lives. Some of these processes require advanced science, long periods of observation and the observation of different processes to provide a deeper understanding of system Earth and its environment. This better understanding then leads to better solutions, applications and enhanced benefits to society. Space geodesy plays a crucial role in this regard. This section discusses the role of space geodesy in the development of modern reference frames, particularly for Africa.

The Earth and its dynamic processes are not static and the celestial bodies in the universe are also not static, they change positions with time. Some of the dynamic processes that affect the geodetic reference points are polar motion, Earth's rotation, plate tectonics, loading effects on the Earth's crust, dynamics of the stars etc., For this reason, it is impossible to have a reference frame that is time independent (Iliffe, 2000) hence, the geodetic reference frames need to be updated and maintained. Different epochs of the International Terrestrial Reference Frame (ITRF) exist which include

ITRF1992, ITRF1993, ITRF1996, ITRF2000 and ITRF2005. They were created to account for dynamic processes.

The current accurate geocentric reference frame is ITRF2008 which can be described as a highly accurate geocentric reference framework, with the accuracy of the coordinates of the reference stations defined at a millimetre level. The ITRF includes the velocities of the stations and a set of coordinates that can be used to monitor dynamic processes on Earth's surface (http://itrf.ensg.ign.fr/general.php). It is maintained by the International Earth Rotation Service (IERS), this is done using geodetic techniques such as GNSS, SLR, VLBI and DORIS (Doppler Orbitography and Radiopositioning Integrated by Satellite) (Kovalevsky *et al.* 1989; Figure 13).

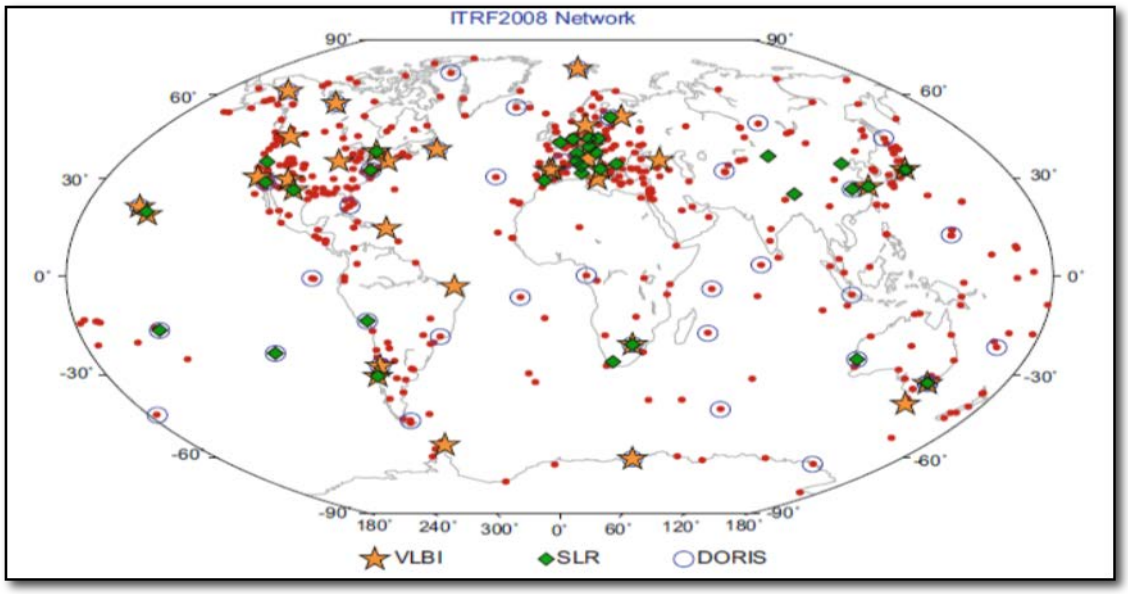


**Figure 13.** Illustration of global sites that are equipped with different, collocated space-based techniques i.e., SLR, GNSS-red dots, VLBI and DORIS, and these sites are used for the realization of ITRF (Altamimi *et al.* 2011).

The International GNSS Service (IGS) has contributed towards the establishment of the ITRF since 1991 by providing high quality GNSS data (Altamimi and Collilieux, 2009) and the spatial resolution of GNSS stations has since increased. In addition to other geodetic techniques (i.e., VLBI, SLR and DORIS), GNSS technique contributes towards the realization of ITRF. The ITRF is important in deriving unified

reference frames such as AFREF, as the derived velocity fields and other geophysical measurements need to be tied to an accurate global reference frame.

### 2.5.2 Background on AFREF

A datum can be defined as a geometrical quantity that serves as a reference for other measured quantities (e.g., during cadastral surveying) (Iliffe, 2000). It is realized by an accurately determined shape and size as given by the spheroid and sets of selected geodetic positions (e.g., latitude, longitude and height) that are fixed at the origin, an azimuth of a line to another geodetic control point and the geoid separation at the origin point of the ellipsoid (Iliffe, 2000; DMA, 1983). Due to continental plate motion, the reference positions need to be updated at specific epochs, hence, ITRF exists. The knowledge of the datum was generally confined to a small community of scientists and geodesists only, until recent years, where the development of geographic information system (GIS) and satellite remote sensing have greatly influenced the knowledge of datums.

African countries currently use different datums such as WGS 1984, Clarke 1866, Clarke 1880, Bessel 1841 (AFREF, 2002; Wonnacott *et al.* 2010). A typical problem arises e.g., when combining digital map data from two different survey campaigns, e.g., as part of a cross-border collaboration between neighbouring countries (Iliffe, 2000). The results from such a combination (if different datums are used) tend not to align and the coordinates might be off-line by several metres. For this reason, many projects which include remote sensing, mapping, land management, Geographic Information System (GIS) and hazard mitigation that involve crossing country boundaries are prone to errors. The lack of a unified African Geodetic Reference Frame (AFREF) remains a barrier for many geo-spatial projects in Africa.

Different geodetic reference frames have been established and maintained elsewhere in the world. Such reference frames include: European Reference Frame (EUREF) which was founded in 1987 and the South, Central American (SIRGAS) (Bruyninx *et al.* 2009) reference frame which was established in 1993 (Wonnacott, 2005; Figure 14). The foundation has been laid for Africa and many of the African

countries are preparing to change their old out-dated reference frames into a new modern geodetic reference frame.

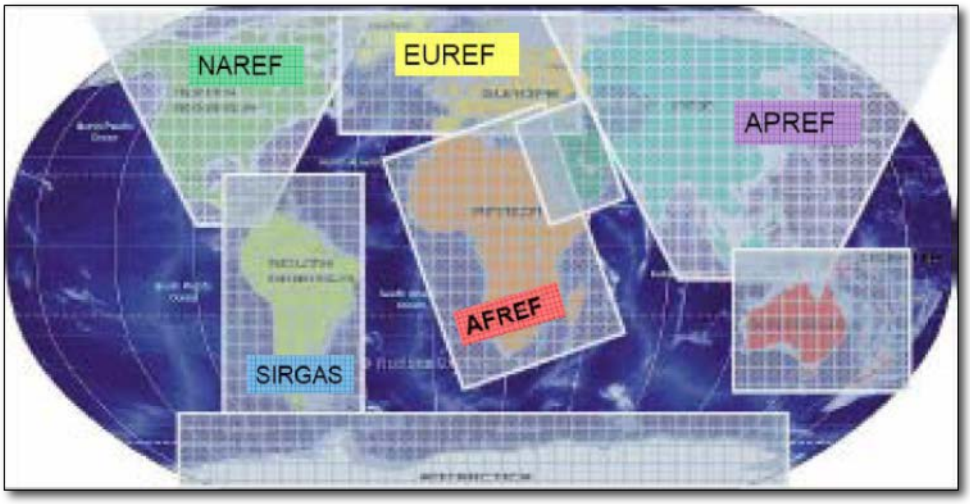


**Figure 14.** Examples of existing reference frames, Africa being under construction (adapted after: Bruyninx *et al.* 2009).

The Doppler effect technique has been used by Doppler satellites to strengthen and extend terrestrial networks and connect them to an Earth-centred coordinate system, to provide geophysical parameters such as the Earth's gravity field and polar motion data, and to determine satellite orbits (Anderle, 1986). During the 1980s, Africa, in collaboration with other international partners, attempted to establish a system that was going to provide a unified reference frame i.e., the African Doppler Survey (ADOS) project. It was conceived with the aim of providing a unified African reference frame for Africa. Anderle (1986) reported that 52 countries were involved in the programme. But the project came to a halt in 1986, due to a lack of ability to do simultaneous observations required by the Doppler Satellite system (AFREF, 2002). Most of the systems that use the Doppler effect are based on the measurement of the Doppler effect on frequencies transmitted by satellites. Such systems include NAVSAT (the U.S. Navy Navigation Satellite System); it was designed to allow navigators aboard ships to determine their position within 100 m accuracy (Anderle, 1986). In addition, the project suffered from a lack of participation by most of the African countries and the resulting accuracy of the Doppler system was not good enough to be used in geodynamic studies.

During the 1980s, scientists knew about the capabilities of GNSS and they hoped (Anderle, 1986) that if GNSS could grow rapidly, it was going to replace NAVSAT. Today, GNSS is a reliable technique and accurate enough to be used in multi-disciplinary applications.

The implementation of the GNSS technique under the auspices of AFREF was initiated in 2002. Effort included the establishment of a formal structure and government level support, but a number of scientific, technological and human capacity challenges need to be addressed before full implementation can be achieved. Nevertheless, some specific research tasks under the auspices of AFREF are envisioned. Amongst these research frontiers is the development of a velocity field for the African plate, based on long-term measurements obtained from GNSS equipment, in particular GPS. Some of the processes involved in establishing and maintaining such a reference frame are described in AFREF (2002):

- Defining and establishing a geocentric datum.
- Defining a reference system.
- Establishing and maintaining the reference network.

The reference frame will be derived from the analysis of geodetic data measured by permanently installed GNSS stations (pictured in Figure 15) and other geodetic techniques that are linked to the global network of the IGS (AFREF, 2002). Africa currently has a poor geographic distribution of GNSS stations and this creates problems in deriving a robust velocity field for AFREF. In addition it adversely affects the study of plate motions on a regional scale because different sub-plates move at different rates and station coverage is too poor to provide detailed velocity solutions on a regional or global scale.

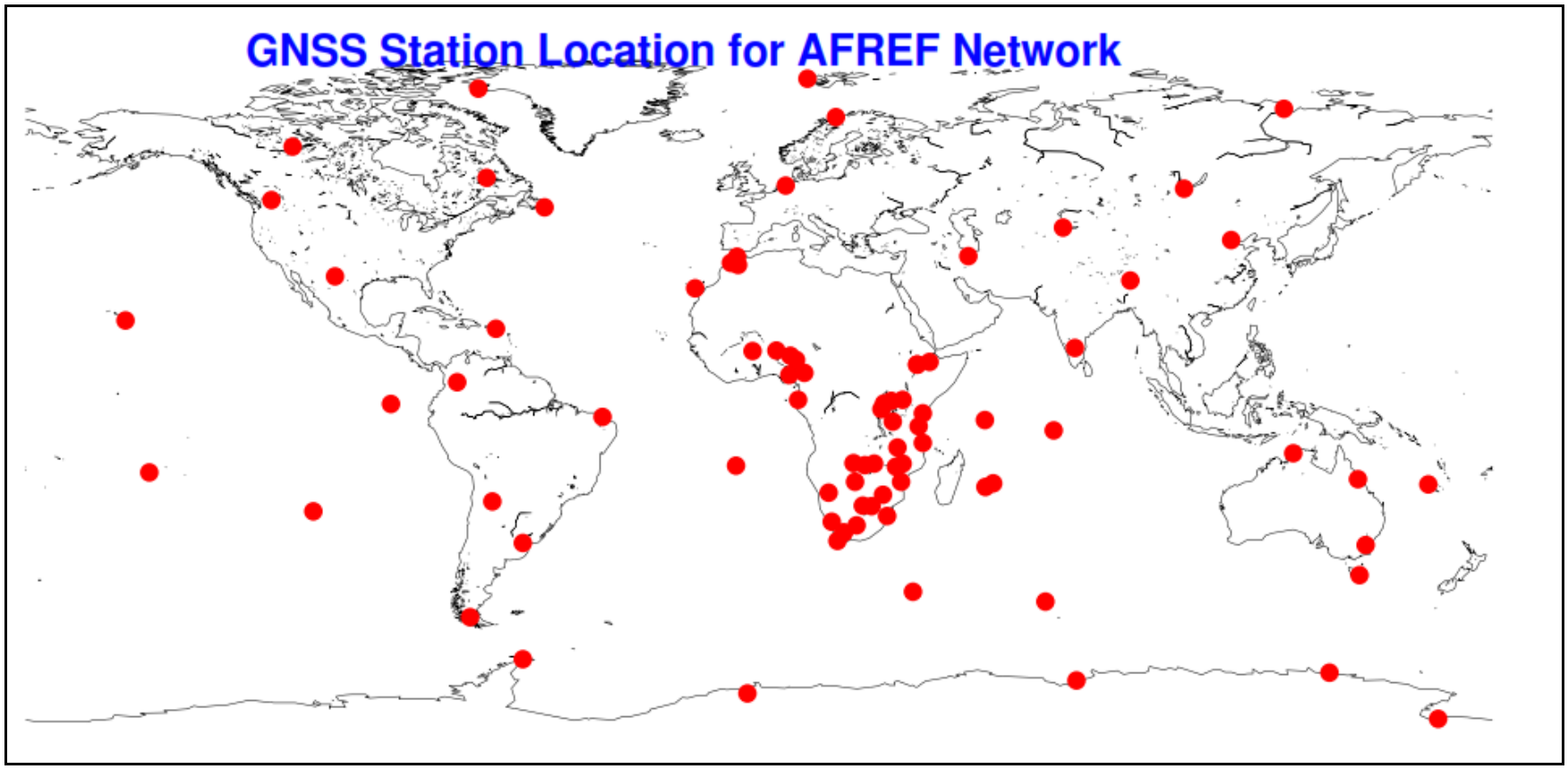


**Figure 15.** Map illustrating current AFREF network of GNSS stations. There is an obvious weak station geometry in the north, the north-east and east central areas of the African continent. These gaps will have to be filled with GNSS stations to improve AFREF solutions.

One of the long-term objectives of HartRAO is to increase the network density of GNSS stations in Africa in collaboration with local and international partners (Combrinck, 2000). A typical GNSS station is pictured in Figure 16. There is a need to continuously install additional GNSS stations thereby increase the density of the GNSS network throughout African countries. This will ultimately improve the geometry of the network, and as a result lead to long-term, stable and precise monitoring of geodetic observables vital for the determination and maintenance of the AFREF project.

**Figure 16.** GNSS installation at Hamburg (HAMB), South Africa. This example station is totally self-contained. The station incorporates GPRS communication for data transfer, solar panel, wind charger, regulator and batteries for power, and a hermetically

sealed box protects the equipment (picture credit: L. Combrinck, 2012, personal communication).

The establishment of an accurate and well maintained AFREF will contribute towards surveying and mapping, construction, mining, transport and navigation; all of which influence many activities in our modern society. In order to obtain reliable positions for AFREF in the ITRF, estimated positions ought to be tied to a particular epoch; subsequent measurements at different points in time need to be referred to the AFREF epoch. Adjustments between the AFREF epoch, and the global reference frame and later measurements will require velocity field data as an adjustment (Herring *et al.* 2009).

It has been proposed that Africa be sub-divided into five regions (NAFREF, SAFREF, CAFREF, WAFREF and EAFREF i.e., North-, South-, Central-, West- and East African Reference Frames, respectively) (depicted in Figure 17) to facilitate processing of GNSS data. The results from each region will be then be combined to form a unified reference frame for Africa i.e., AFREF (Kamamia, 2004). This is clearly impractical due to the lack of GNSS stations available and, in any event would have complicated the process.

It has been reported by Wonnacott *et al.* (2010) that over 22 countries are in the process of changing their old reference frame systems into and more modern reference frames. Installation of GNSS Continuous Operating Reference Stations (CORSs) in NAFREF and CAFREF regions will ensure that there is a station in Africa for approximately every 1000 km. This will meet one of the objectives of AFREF (Combrinck, 2011), will increase the GNSS stations network in Africa and ensure a robust AFREF. Table 2 lists the currently active countries that are participating in the establishment of AFREF and that are willing to install GNSS CORS in the near future.

The African Geodetic Observing System (AGOS) project is set to enhance space geodetic observations in Africa. It incorporates AFREF and the African Very Long Baseline Interferometry Network (AVN), in which Kenya, Ghana and Nigeria have shown great interest (Botai *et al.* 2013). It is clear that AFREF is being supported and that many countries are making an effort to grow space geodesy in Africa.

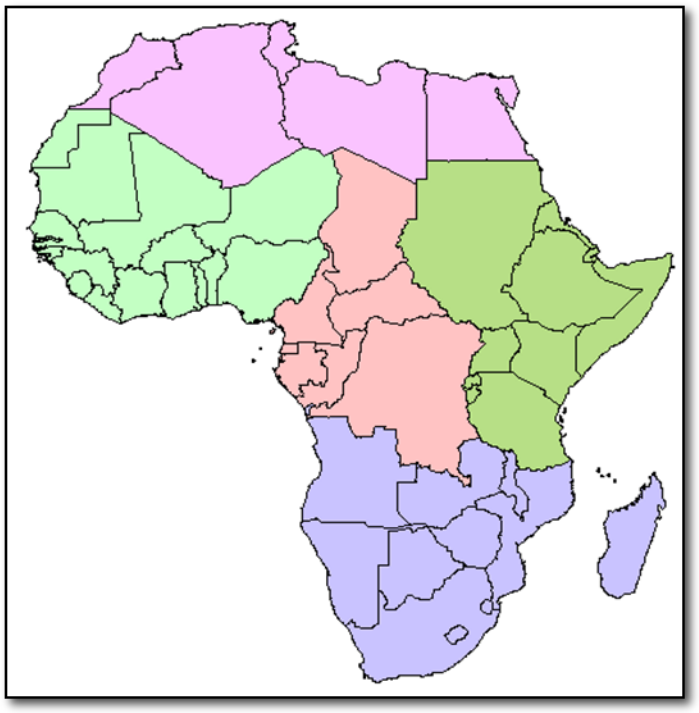

**Figure 17.** It was proposed that Africa be sub-divided into five regions to facilitate the processing of GNSS data and the results would then be combined later to form a complete AFREF (Kamamia, 2004). The first AFREF computation (April 2013) utilised data from all the regions simultaneously.

**Table 2.** List of countries that are participating in installing GNSS CORSs (Combrinck, 2011).

| | | | |
|---|---|---|---|
| Algeria | Nigeria | Ghana | Zambia |
| Benin | South Africa | Lesotho | |
| Cameroon | Tanzania | Morocco | |
| Ethiopia | Uganda | Namibia | |
| Kenya | Angola | Rwanda | |
| Malawi | Botswana | Swaziland | |
| Mozambique | Egypt | Tunisia | |

### 2.5.3 Contribution towards AFREF implementation

In 2007, the Working Group on Regional Dense Velocity Fields became part of Sub-Commission 1.3 'Regional Reference Frames', which is embedded in the International Association of Geodesy (IAG) Commission 1 on reference frames (http://epncb.oma.be/IAG/). The long-term goal of the IAG Working Group on Regional Dense Velocity Fields is to provide globally referenced dense velocity fields primarily based on GNSS observations, to be used as a densification of the multi-technique global conventional reference frame (Bruyninx *et al.* 2010). The Working Group co-exists with the six regional reference frame sub-commissions for Africa, South-East Asia and the Pacific, Antarctica, Europe, North America and South- and Central America (Drewes *et al.* 2008). Sub-Commission 1.3 is involved in establishing and coordinating regional reference frames in different countries (mentioned above). Other regions have made good progress, except Africa (AFREF), which is the focus of the Sub-commission 1.3 (Drewes and Hornik, 2005).

This study intends to participate in AFREF by deriving GNSS velocities and positions in a Solution Independent Exchange (SINEX) file format and combining these using the Combination and Analyses of Terrestrial Reference Frame (CATREF) software developed by Altamimi *et al.* (2007).

The first submission of combined SINEX solutions to the Working Group was made in 2009. During the combination process done by Bruyninx *et al.* (2012), the solutions indicated disagreement between regional and global solutions. The disagreement was due to:

- inconsistent discontinuity (missing data period) epochs,
- inconsistent station naming and DOMES numbering and
- numerical instabilities caused by velocity constraints at sites with coordinate offsets and also due to a network effect (Bruyninx *et al.* 2010).

A call for new re-submissions was made in 2010. The criteria for the new solutions include that ITRF2008 discontinuities should be applied during stacking with CATREF

or other software packages to increase the agreement level with the ITRF2008 solution and the solution should be reprocessed using absolute antenna models (Bruyninx *et al.* 2010).

## 2.6 Concluding remarks

Space geodesy is one of the disciplines that contributes to a global society; its applications and products have been utilised to such an extent that system Earth is better understood today. This chapter has reviewed three space geodetic techniques i.e., GNSS, VLBI and SLR. The accuracy that space geodesy has reached has allowed the determination of geophysical parameters such as plate velocities, polar motion and the implementation and maintenance of reference frames. Good progress has been made with the AFREF project. However, implementation issues still remain which will have to be addressed before AFREF will be at fully operational and near-optimal status.

# CHAPTER 3

## Data and analysis strategies

*"A new idea comes suddenly and in a rather intuitive way, but intuition is nothing but the outcome of earlier intellectual experience"- Albert Einstein, 1949.*

### 3 Methodology

### 3.1 Introduction

Two scientific software packages are described in this chapter; i.e., GAMIT/GLOBK (version 10.4) developed at MIT (King and Bock, 1995; Herring, 1997) and the CATREF software developed at Institut National de l'Information Géographique et Forestière (IGN) by Altamimi *et al*. (2007). These software packages were used to process phase observations of GNSS data and to accurately estimate station coordinates and velocities over the African continent in support of the establishment of AFREF.

The development and maintenance a modern reference frame requires velocities to be consistent with a recent ITRF (currently ITRF2008). Consequent measurements (e.g., for cadastral surveying) at different epochs will need to be referred to the AFREF epoch. Since inter-continental blocks may exhibit differential motion with respect to that of the African plate, continuous measurements will be required (i.e., permanent and fixed stations are required) to update velocity fields which will then be used to update AFREF. Velocity maps will result from the research described in this thesis, which will contribute towards monitoring of sub-continental and local motions.

### 3.2 Description of GAMIT/GLOBK (version 10.4) software

The long baseline solutions and highly accurate velocities resulting in the ITRF require the use of scientific quality processing software (King and Bock, 1995; Herring, 1997). The software GAMIT/GLOBK is a collection of FORTRAN subroutines and *C-shell* scripts designed to run in the Unix/Linux OS environment. This software has been used for scientific research purposes (Nilforoushan *et al.* 2003; Yu *et al.* 1997; Feigl *et al.* 1993; Kendrick *et al.* 2001; McClusky *et al.* 2003) to process GNSS phase data and

combine quasi-observations to estimate geophysical parameters, meteorological parameters etc., with high accuracy. Other scientific software used to process GNSS data includes GYPSY-OASIS ll (JPL) and the Bernese GNSS Software (University of Bern). The solutions resulting from these different software packages indicated differences in the order of a millimetre (Andrzej *et al.* 2010), for this reason it makes no significant difference which software package is used.

The GAMIT module integrates a weighted least squares algorithm to estimate station coordinates and velocities, atmospheric delay parameters, satellite orbits, Earth Orientation Parameters (EOPs) and functional representations of post-seismic deformation. It produces the associated covariance matrix, EOPs and orbital parameters (King and Bock, 1995) to be fed into the GLOBK processing engine.

The GLOBK module was originally developed to combine quasi-observations from VLBI data and was later modified at MIT to incorporate GNSS data sets (Herring *et al.* 2010). It combines loosely constrained solutions from the GAMIT module to estimate station coordinates and velocities. In order to quantify any movement observed by GNSS stations, it is necessary that a long time-series be obtained and analysed by using scientific software packages such as GAMIT/GLOBK.

### 3.3 GNSS Instruments

The geodetic observations were performed using GNSS instruments of geodetic quality such as the one pictured in Figure 18, which was installed by HartRAO at Matjiesfontein, Great Karoo, South Africa. Other stations that were used in this research might be different from the one pictured here. These instruments that are located far from any infrastructure are typically totally self-contained. GPRS communication for data transfer, a solar panel, regulator and batteries for power and a hermetically sealed box that protects the equipment are implemented. During installation, the antenna mount is mounted on bedrock to ensure that the movements measured by the stations are only due to tectonics or earthquake activities but not due to thermal expansion of soils or other unrelated tectonic forces or stresses. Specifications for installing GNSS stations are outlined in Combrinck and Chin (2001), Kouba, (2009) and Gurtner and

Neil, (1994). Different antennas and receivers have been used in most GNSS stations (see Appendix A: Table 14). The GNSS technique, particularly GPS, remains the only geodetic technique suitable to study regional or global plate tectonics due to its relative cost-effective advantages (Weston and Schwieger, 2010) as compared to other geodetic techniques such as VLBI, DORIS and SLR.

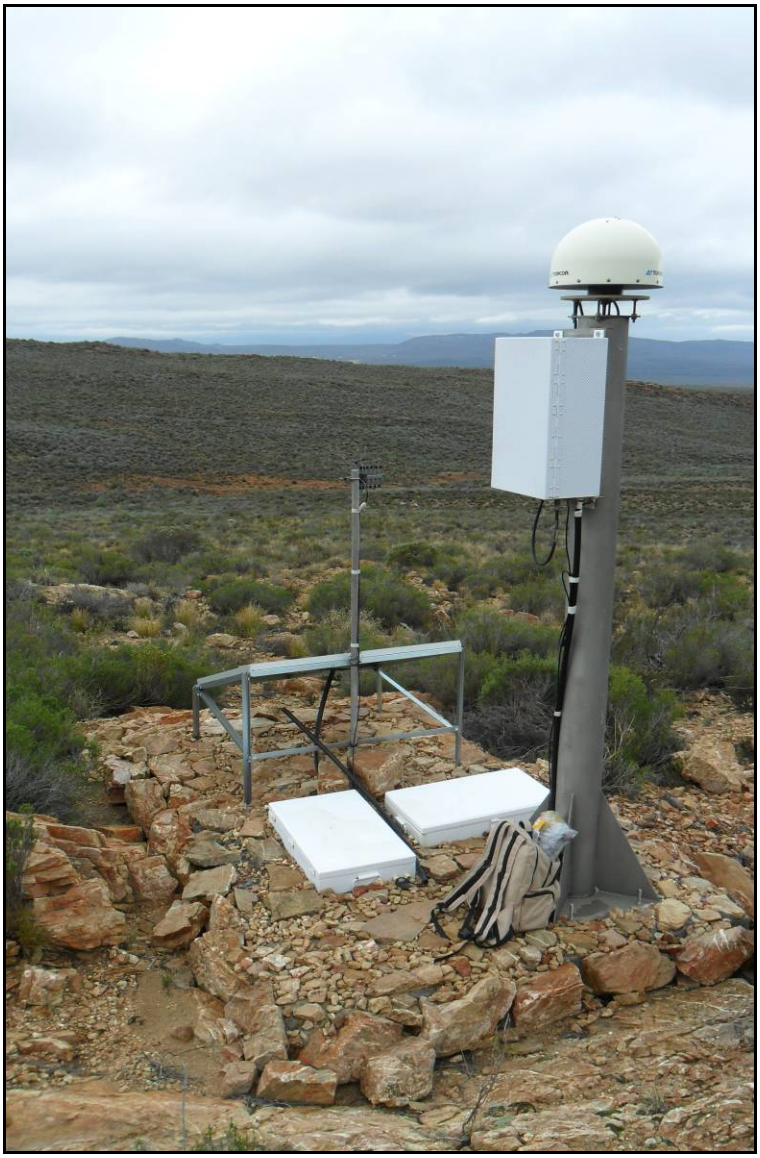

**Figure 18.** Example of a GNSS station. This particular station (MATJ) located at Matjiesfontein, Great Karoo is power and communications independent. The station was installed by HartRAO. Solar panels and metal boxes containing batteries to supply power can be seen on the ground.

### 3.4 Data acquisition and pre-processing

Receiver Independent Exchange (RINEX) data (sampled at a 30 second rate) are automatically downloaded in twenty-four hour (24 hr) session from data archieves such as geoid (ftp://geoid.hartrao.ac.za/), Scripts Orbital Permanent Array Center (SOPAC), Crustal Dynamic Data Information System (cddis), University NAVstar Consortium (UNAVCO), TrigNet (ftp://ftp.trignet.co.za/) etc., using automated specialized scripts incorporated in GAMIT/GLOBK software. The IGS stations from the African and other continents were included to improve the geometry of the network. A few non-IGS stations but of geodetic quality (HAMB-Hamburg and MATJ-Matjiesfontien) were included in the processing. Raw data in Topcon Positioning Systems (TPS) format from the HAMB and MATJ stations were transformed to RINEX format and large files were disseminated into 24 hrs session RINEX files using the Translation Editing Quality Control (TEQC) software provided by UNAVCO (Estey, 2011).

The quality of RINEX files from the surveying stations were checked using the TEQC software. In Table 3, MP1 and MP2 represent a linear combination of C1, L1 and L2 and C2, L1 and L2 frequencies, respectively, and provide an estimate of a pseudo-range multi-path. The acceptable MP1 and MP2 values must be below 0.35. For this particular example, the values indicate good data with acceptable multi-path effects.

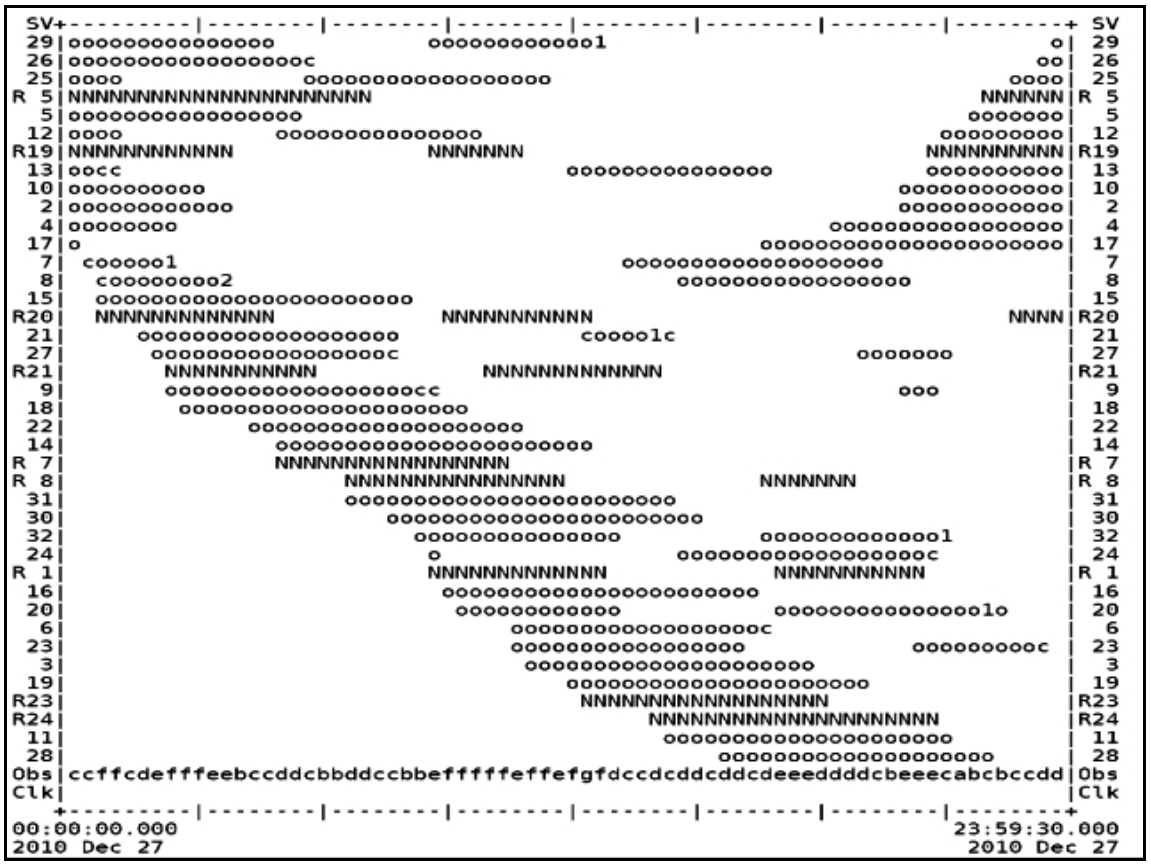


**Figure 19.** Satellite visibility for Hamburg (HAMB) station, South Africa, on 27 December 2010, cut off elevation:10°.

**Table 3**. Summary of statistics for MP1 and MP2 for the Hamburg station, South Africa, as on 27 December 2010.

| ***Statistics*** | ***MP1*** | ***MP2*** |
|---|---|---|
| **Mean rms (mm)** | 0.24322 | 0.27888 |
| **Observations** | 36121 | 36121 |
| **Slips** | 6 | 1 |

The MP1 combination frequencies indicate a lower mean RMS value and six slips while the MP2 combination frequencies indicate a higher mean RMS value with only one slip. The slips are also depicted in Figure 19, where symbols *1* and *2* represent

MP1 and MP2 slips, respectively, and symbol *c* represents clock slips for both MP1 and MP2 that occurred for all satellites being observed. Figure 19 is a graphical representation of a complete elevation-azimuth list, based on an elevation cut off angle of $10^{\circ}$, illustrating the satellite in view for a certain epoch. Shown on the vertical coordinate system is the satellite with corresponding PNR number. An improved representation of satellite visibility is depicted by the sky plot in Figure 20. The sky plot represents phase vs. time residuals projected onto the sky.

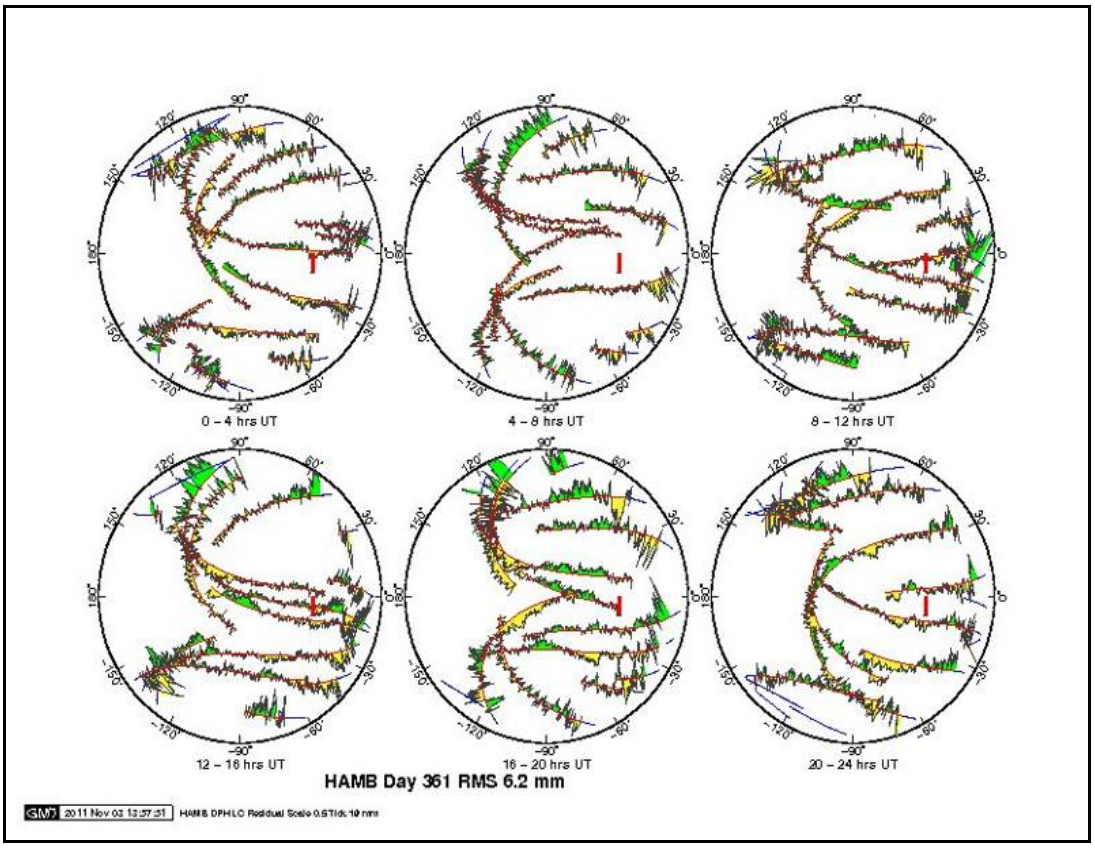


**Figure 20**. Polar sky plot for Hamburg, South Africa, on 27 December 2010, cut off elevation: $10^{\circ}$.

### 3.5 Data sets

In Table 4, a list of the GNSS stations and years in which they were operating between the 2000 and 2012.4 periods are given. Note that this table only indicates data availability in terms of years but not in terms of day numbers. Data for certain dates

might not be available; this can be seen in the time series analyses in the following chapters. The geometric distribution of the GNSS stations used in this study to derive velocities for Africa are depicted in Figure 21. A gradual increase in the number of GNSS stations with time can be seen from Table 4 and Figure 22. This shows that stations are constantly added into the IGS network. This indicates an effort made by participants in the IGS to increase the density of the GNSS stations around the world (Kouba, 2009).

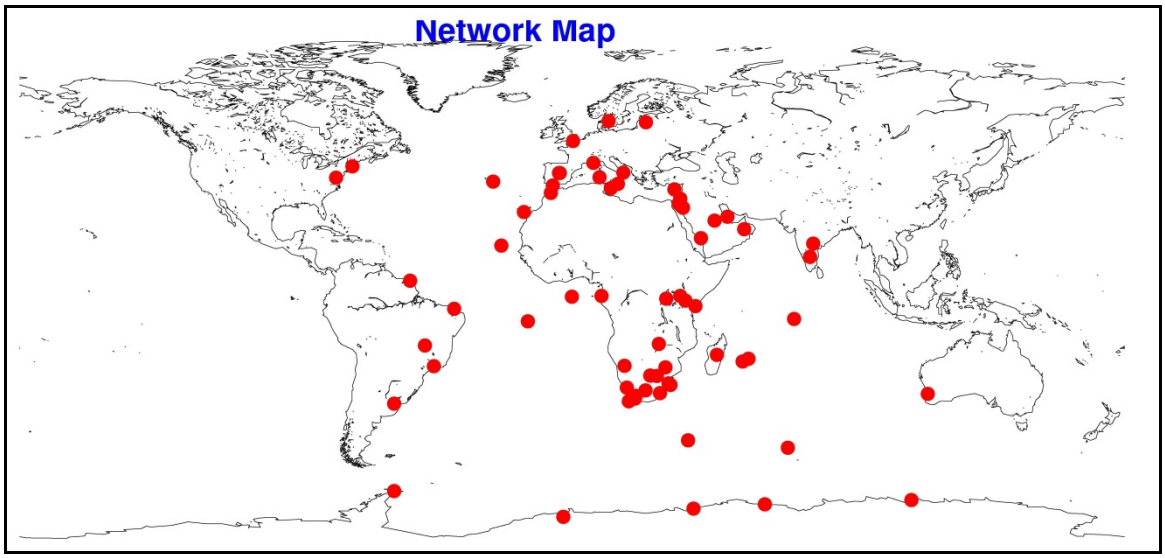


**Figure 21.** Geometrical distribution of GNSS stations used in this study.

Tectonic movement occurs on a very small scale i.e., at millimetre level over a long period of time (~21 mm per year for HartRAO) and to measure and quantify such movement requires relatively long time periods of observation using space geodesy techniques such as GNSS. This research utilised a long enough time series of observations (i.e., twelve years of GNSS observations) to produce reliable results from which concrete conclusions can be derived.

**Table 4.** Availability of yearly GNSS data within the 2000 to 2012 period.

| Station ID | 2000 | 2001 | 2002 | 2003 | 2004 | 2005 | 2006 | 2007 | 2008 | 2009 | 2010 | 2011 | 2012 |
|---|---|---|---|---|---|---|---|---|---|---|---|---|---|
| **ADIS** | | | | | | | | x | x | x | x | x | x |
| **ABPO** | | | | | | | | | | x | x | x | x |
| **BAN2** | | | | x | x | x | | x | x | x | | x | x |
| **BRFT** | | | | | | | | | x | x | x | x | x |
| **BRAZ** | x | x | x | x | x | x | x | x | x | x | x | x | x |
| **BJCO** | | | | | | | | | | x | x | x | x |
| **CHPI** | | | | x | x | x | x | x | x | x | x | x | x |
| **CAGL** | | | | | | | | x | x | x | x | x | x |
| **CAS1** | x | x | x | x | x | x | x | x | x | x | x | x | x |
| **DAV1** | x | x | x | x | x | x | x | x | x | x | x | x | x |
| **DEAR** | | | | | | | | | | | x | x | x |
| **DGAR** | x | x | x | x | x | x | x | x | x | x | x | x | x |
| **GOUG** | x | x | x | x | x | x | x | x | x | x | x | x | x |
| **GMAS** | | | | x | x | x | x | x | x | x | x | x | x |
| **GRAS** | x | x | x | x | x | x | x | x | x | x | x | x | x |
| **HAMB** | | | | | | | | | | | x | x | x |
| **HRAO** | x | x | x | x | x | x | x | x | x | x | x | x | x |
| **HARB** | x | x | x | x | x | x | x | x | x | x | x | x | x |
| **HYDE** | | | | | | | | | x | x | x | x | x |
| **HNUS** | x | x | x | x | x | x | x | x | x | x | x | x | x |
| **HERS** | x | x | x | x | x | x | x | x | x | x | x | x | x |
| **KERG** | x | x | x | x | x | x | x | x | x | x | x | x | x |
| **LPGS** | x | x | x | x | x | x | x | x | x | x | x | x | x |
| **MATE** | x | x | x | x | x | x | x | x | x | x | x | x | x |
| **MATJ** | | | | | | | | | | | | x | x |
| **MAL2** | | | | | | | | | | x | x | x | x |
| **MAS1** | x | x | x | x | x | x | x | x | x | x | x | x | x |
| **MALI** | x | x | x | x | x | x | x | x | x | | | | |
| **MAW1** | x | x | x | x | x | x | x | x | x | x | x | x | x |

**Table 4.** (Continued).

| Station ID | 2000 | 2001 | 2002 | 2003 | 2004 | 2005 | 2006 | 2007 | 2008 | 2009 | 2010 | 2011 | 2012 |
|---|---|---|---|---|---|---|---|---|---|---|---|---|---|
| **MBAR** | | | | | | x | x | x | x | x | x | x | x |
| **NICO** | x | x | x | x | x | x | x | x | x | x | x | x | x |
| **NKLG** | x | x | x | x | x | x | x | x | x | x | x | x | x |
| **NOT1** | x | x | x | x | x | x | x | x | x | x | x | x | x |
| **OHI2** | | | x | x | x | x | x | x | x | x | x | x | x |
| **OHI3** | | | | x | x | x | x | x | x | x | x | x | x |
| **ONSA** | x | x | x | | x | x | x | x | x | x | x | x | x |
| **PDEL** | | | | x | x | x | x | x | x | x | x | x | x |
| **PERT** | x | x | x | x | x | x | x | x | x | x | x | x | x |
| **RABT** | x | x | x | x | x | x | x | x | x | x | x | x | x |
| **RAMO** | x | x | x | x | x | x | x | x | x | x | x | x | x |
| **RIGA** | x | x | x | x | x | x | x | x | x | x | x | x | x |
| **REUN** | | | | x | x | x | x | x | x | x | x | x | x |
| **RCMN** | | | | | | | | x | x | x | x | x | x |
| **RBAY** | x | x | x | x | x | x | x | x | x | x | x | x | x |
| **SUTM** | | | x | x | x | x | x | x | x | x | x | x | x |
| **SUTH** | x | x | x | x | x | x | x | x | x | x | x | x | x |
| **SEY1** | x | x | x | x | x | x | x | x | x | x | x | x | x |
| **SFER** | | | | | x | x | x | x | x | x | x | x | x |
| **SBOK** | | | | | | | | | | | x | x | x |
| **SIMO** | x | x | x | x | x | | x | x | x | | | | |
| **SYOG** | x | x | x | x | x | x | x | x | x | x | x | x | x |
| **UMTA** | | | | | | | | | | | x | x | x |
| **ULDI** | | | | | | | | | | | x | x | x |
| **VES1** | x | x | x | x | x | x | x | x | x | x | x | x | x |
| **VILL** | | | | | | | | | x | x | x | x | x |
| **VASC** | | | | | | | | | | x | x | x | x |
| **WES2** | | | | | | | | | x | x | x | x | x |
| **WIND** | | | | | | | | x | x | x | x | x | x |
| **ZAMB** | | | x | x | x | x | x | x | x | x | x | x | x |

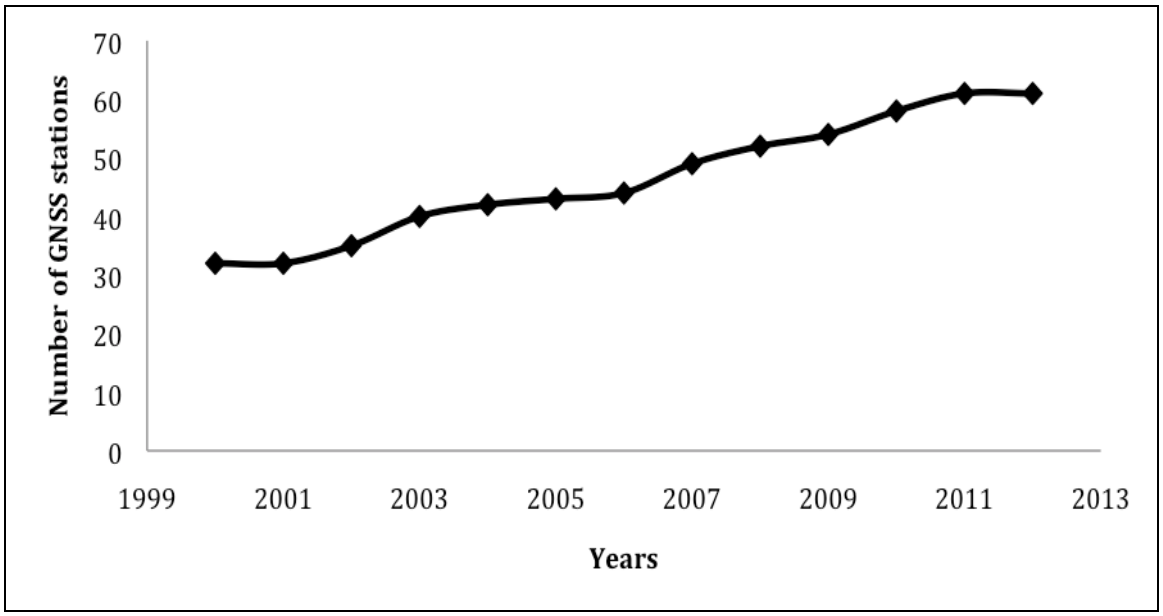


**Figure 22.** Distribution of measurement time span of GNSS stations used in this study.

### 3.6 Input files into GAMIT/GLOBK (version 10.4)

A brief description of setting up files to run the GAMIT/GLOBK software is outlined in this section. The scripts that are mentioned in this section are not described in detail; however, more detail can be found in King and Bock (1995) and Herring (1997). It is necessary to create an experimental directory (e.g., *scal* with two sub-directories: /*rinex* and /*tables*). The setup files should be edited prior to processing to suit processing requirements. All necessary RINEX files can be downloaded (using the *sh_get_rinex* script) into the /*rinex* directory, the *sh_setup* and *sh_links.tables* scripts can be invoked to link and copy all the control files described in this section into the /*tables* directory. Other files such as station coordinates in the form of an L-file, satellite list and scenario file i.e., *session.info*, satellite and station clock values (i.e., I-, J- and K-files) that are required prior to processing usually do not require editing. Selected files that usually require editing are outlined below.

- *process.default*: this file contains variables such as computational environment, sampling interval and number of epochs.

- *site.default*: specifies all sites to be downloaded automatically from a remote archive.
- *station.info*: for a site to be processed by *sh_gamit*, the header of the RINEX file needs to be included in this file. To do this, run *sh_upd_stnfo*, which will invoke the *mstinf* program to update the *station.info* file.
- *sestbl* and *sittbl*: optionally, these files can be edited to adjust analysis strategy, for instance, setting tight constraints on specific sites.
- *autcln.cmd*: this file does not require any editing unless the data contain unusual errors.

### 3.7 Strategy for processing GNSS data

Data from GNSS stations were processed for the 2000 to 2012.4 period using the GAMIT/GLOBK software (King and Bock, 1995; Herring, 1997). Data analysis was carried out at HartRAO at the Space Geodesy Laboratory (SGL). A cut-off elevation angle of $10^{\circ}$ was used, i.e., all data sampled below $10^{\circ}$ elevation were discarded due to the adverse effect of the atmosphere (increased wet component) and the possibility of increased multi-path effect on the data at low elevations. The software TEQC was used to quality check the data for possible errors using least squares adjustment and for transforming raw data into RINEX format (for HAMB and MATJ stations). Processing was done in two steps as illustrated in the GAMIT/GLOBK flow chart (Figure 23) and described as follows:

1. Processing of single-day GNSS phase observations for each year was carried out using the GAMIT module. Analysis of carrier beat phase observations and estimation of daily station coordinates, EOPs, orbital parameters and their associated covariance matrices using a least squares method were done. Different models are incorporated to correct for ocean loading. Resolved integer ambiguities, data sets and control tables are linked into the GAMIT module as depicted in Figure 23.
2. The loosely constrained solutions from the GAMIT module are then fed into the GLOBK processing engine as quasi-observations (H-files) to

combine and estimate long time-series of station velocities and station coordinates using a Kalman filter approach. This procedure of processing GNSS data has been described and adapted by Feigl *et al.* (1993), Kendrick *et al.* (2001), Nilforoushan *et al.* (2003), McClusky *et al.* (2003), King and Bock, (1995) and Herring *et al.* (2010).

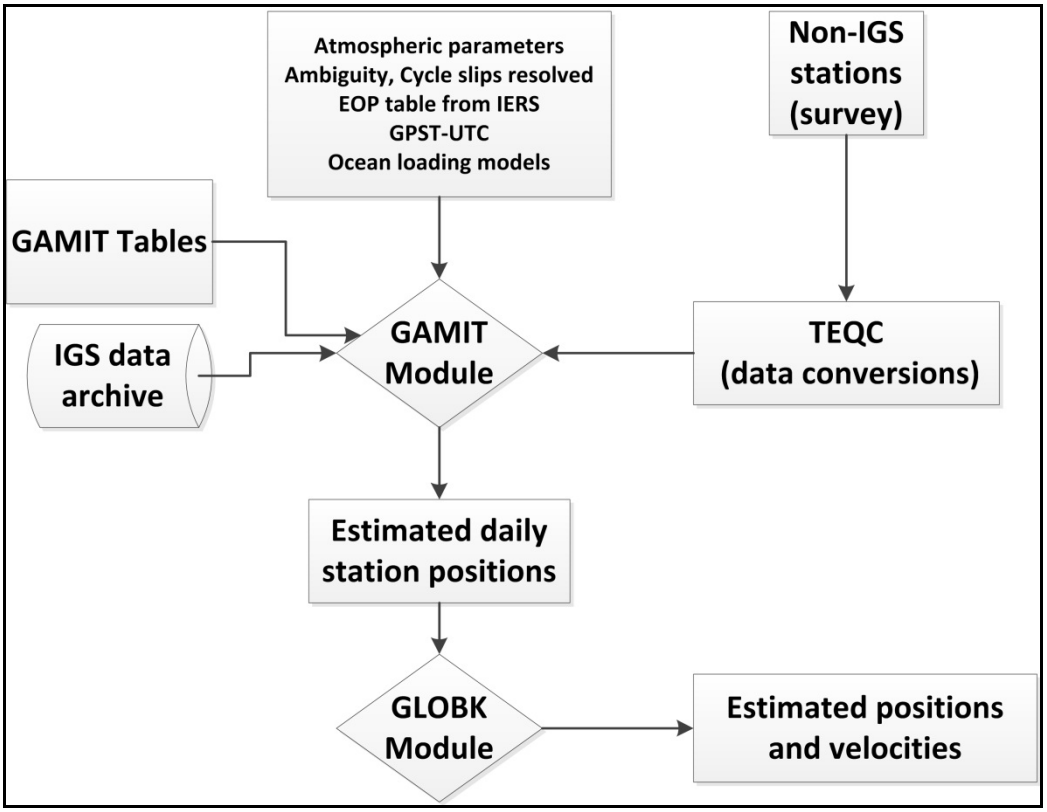


**Figure 23.** Simple flow chart of GAMIT/GLOBK 10.4 software.

In step 1, the GAMIT module calculates theoretical values for the carrier phase observations at both L1 and L2 frequencies for each satellite-station combination. The results are then subtracted from observed values to produce phase residuals. Results are also combined through a double differencing method in a least squares approach to estimate parameters such as ambiguity (Feigl *et al.* 1993). Common errors that are attached to or contained in the GNSS signal such as multi-path effects, cycle slip and atmospheric refractions (tropospheric and ionospheric effects) are minimized by using the *autcln*, *model* and *solve* programs (incorporated in GAMIT). These programs are

executed automatically during the processing stages and errors are resolved automatically. The remaining errors are investigated by examining time series plots, sky plots and RMSE (Root Mean Square Error) values of each station for each particular observation.

Criteria for selection of stations were the inclusion of long-term operating stations i.e., those that have least two to three years' data should be included (with the exception of local stations) and GNSS data should be of high quality. Due to poor geometric distribution of the GNSS stations in Africa, selected IGS stations outside the African continent were included in the processing stage to improve and strengthen the geometry of the network and to tie the network into the ITRF. Well-known GNSS stations i.e., stations with well-constrained positions, were used to stabilize the network and to reduce geometric errors that might propagate into the final solution. This was achieved by defining well constrained stations as stabilization stations. Stations in the ITRF2008 reference frame were constrained to 5 mm in the horizontal components and 10 mm in the vertical component. Local stations were kept loosely constrained to allow free determination of their coordinates, since they are not well known. The final solution is an estimate of a polyhedron consisting of global and regional stations. According to Kendrick *et al.* (2001), this approach places weak constraints on the coordinates of the local stations.

### 3.8 Description of the CATREF software

Development of CATREF started in 1995 and currently it is capable of reading and writing SINEX files with full variance matrices, combining station positions and velocities, estimating EOPs, datum definition, time series combination, quality evaluation and can handle constraints before combination (Altamimi *et al.* 2007). The model implemented by CATREF allows simultaneous combination of velocities and station positions. Basic transformation equations utilized by CATREF are given in (Altamimi *et al.* 2012); it is based on 7 (14)-parameter similarity given by [Eq. 3.1]:

$$X_2 = T + \lambda \Re X_1,$$

$$\text{with translation vector: } T = (T_x T_y T_z)^T,$$
$$\text{scale factor: } \lambda \text{ and} \qquad [3.1]$$
$$\text{rotation Matrix: } \Re = R_x R_y R_z.$$

Here:

$$R_x = \begin{pmatrix} 1 & 0 & 0 \\ 0 & \cos R1 & \sin R1 \\ 0 & -\sin R1 & \cos R1 \end{pmatrix}, \quad R_y = \begin{pmatrix} \cos R2 & 0 & -\sin R2 \\ 0 & 1 & 0 \\ \sin R2 & 0 & \cos R2 \end{pmatrix}, \quad R_z = \begin{pmatrix} \cos R3 & \sin R3 & 0 \\ -\sin R3 & \cos R3 & 0 \\ 0 & 0 & 1 \end{pmatrix}.$$

In space geodesy, the linearized formula is used:

$$X_2 = X_1 + T + DX_1 + RX_1; \quad \lambda = (1 + D), \qquad [3.2]$$
$$\Re = (1 + R),$$

where
$$R = \begin{pmatrix} 0 & -R3 & R2 \\ R3 & 0 & -R \\ -R2 & R1 & 0 \end{pmatrix}.$$

Since $T$ is less than 100 metres, $D$ and $R$ are less than $10^{-5}$ in magnitude. The second order terms are neglected since they are less than $10^{-10} \approx 0.6$ mm. If Eq. 3.2 is differentiated with respect to time, then $DX_1 \approx 0$ and $RX_1 \approx 0$ in Eq. 3.2.

A general combination model is given in [Eq. 3.3 and 3.4] assuming that for each individual solution *s*, and each point *i*, there is a position $X_s^i$ at epoch $t_s^i$ and velocity $\dot{X}_s^i$ expressed in a given Terrestrial Reference Frame (TRF) *k*.

- Different parameters are estimated: Positions $X_c^i$ at a given epoch $t_o$ and velocities $\dot{X}_c^i$, expressed in the combined TRF *c*.
- Including transformation parameters $T_k$ at an epoch $t_k$ and their rates $\dot{T}_k$ from the combined TRF *c* to each individual frame *k*.

Therefore, the combination model that is implemented by CATREF can be generalized as follows:

$$X_s^i = X_c^i + (t_s^i - t_0)\dot{X}_c^i + T_k + D_k X_c^i + R_k X_c^i + (t_s^i - t_k)[\dot{T}_k + \dot{D}_k X_c^i + \dot{R}_k X_c^i], \quad [3.3]$$

$$\dot{X}_s^i = \dot{X}_c^i + \dot{T}_k + \dot{D}_k X_c^i + \dot{R}_k X_c^i. \quad [3.4]$$

Where $k$ = individual frame, $D_k$ = scale factor, $T_k$ = translation vector and $R_k$ = rotation matrix (Altamimi and Boucher, 2003).

The CATREF software currently reads and writes only SINEX files, for this reason the program *glbtosnx* which is embedded in GAMIT was used to generate weekly SINEX files by processing RINEX files. The network used in this case is the same as used in Figure 21. The following summary is the combination strategy as described in Altamimi *et al.* (2012) which was used in work reported in this dissertation:

- Remove initial constraints from individual SINEX files
- Apply minimum/internal constraints equally to all individual SINEX files
- Combine all SINEX files
- Handle outliers and locate discontinuities
- Iterate and scale the variance-covariance matrices by the estimated variance factors
- Re-iterate until variance of unit weight ($\sigma_0^2$) is close to unity i.e., $\sigma_0^2 \approx 1$

The combination model implemented in CATREF assumes input variables as a network of $N$ points: $x_0^i, y_0^i, z_0^i, \dot{x}_0^i, \dot{y}_0^i, \dot{z}_0^i \ldots\ldots i = 1, \ldots, N$; $K$ being TRF (Terrestrial Reference Frame) and a set of $S$ solutions i.e., SINEX files with station positions and or velocities: $x_s^i, y_s^i, z_s^i, \dot{x}_s^i, \dot{y}_s^i, \dot{z}_s^i \ldots . t_s^i \ldots s = 1, \ldots, S$. Polar motion: $x_s^p, y_s^p, UT_s$ and their daily rates: $\dot{x}_s^p, \dot{y}_s^p, LOD_s$ (Length of the Day) with full variance covariance matrix: $\sum_s$ (Altamimi *et al.* 2012).

Given the inputs above, the software is currently able to estimate:

- positions at $t_0$ and velocities of the $N$ points $x_0^i, y_0^i, z_0^i, \dot{x}_0^i, \dot{y}_0^i, \dot{z}_0^i$ that are expressed in a combined frame.
- the 7 (14) transformation parameters at $t_k$ and their time derivatives including EOP parameters (Altamimi *et al.* 2012).

During the iteration process to archive $\sigma_0^2 \approx 1$, the matrix scaling factors for individual solutions are multiplied by the estimated variance factor (Altamimi *et al.* 2012) using [Eq. 3.5]:

$$\sigma_{0\,s}^2 = \frac{v_s^T P_s v_s}{6n_{ps} + n_{eops} - \frac{6n_{ps} + n_{eops}}{n_{obs}} * n_{unk}}, \qquad [3.5]$$

which is referred to as a Classical Estimator (after: Altamimi *et al.* 2012). Where: $v_s$ = residual vector; $n_{ps}$ = number of points of solution *s*; $n_{eops}$ = number of EOPs of solution *s*; $n_{obs}$ = number of observations; $n_{unk}$ = number of unknowns and $P_s$ = inverse of variance matrix of solution s ($P_s = \sum_s^{-1}$).

The concept of 'minimum constraints' was used to define the datum of the combined frame with respect to ITRF2008. Altamimi (2002) pointed out that the normal equations constructed using (Eq. 3.3 and 3.4) are singular with a rank deficiency of 14 that relates to the datum definition parameters, hence, it is efficient to use an equation of minimum constraints given by:

$$(A^T A)^{-1} A^T (X_R - X_C) = 0, \qquad [3.6]$$

which is included in CATREF. Here $X_c$ is the vector of estimated station positions and velocities, $X_R$ is the reference solution containing a selected set of stations and $A$ is the design matrix of partial derivatives (Altamimi, 2002). This method best defines a TRF datum, no distortions introduced in the TRF and the actual quality of space geodesy observations are preserved (Altamimi *et al.* 2012).

### 3.9 AFREF computation

No formal computational procedure was suggested for the AFREF solution, all the participating analysis centres used their own strategies. Each individual analysis centre utilised different software packages such as Bernese, GAMIT/GLOBK and GIPSY OASIS II. The first computation used data spanning two weeks (day 340 to 360 of year 2012), to produce a static coordinate solution. It was recommended by the AFREF committee that only loosely constrained solutions be submitted to the IGN for combination by Zuheir Altamimi (IGN) using the CATREF software.

As part of the contribution towards AFREF, HartRAO (as part of this study) processed the data using GAMIT/GLOBK, following a similar processing strategy to that described in this chapter. The GNSS station network in Figure 15, Chapter 2 was used. The first submission call was in April, 2013 and the loosely constrained solutions in the SINEX format were submitted to IGN for combination analysis.

At some stage, the AFREF committee will have to decide which stations are optimal to use. Not all stations are of geodetic quality, some stations might have wrong *a-priori* coordinates or others might have high levels of noise. To ensure that the AFREF solution is the optimal solution, Table 5 lists the proposed selection criteria for GNSS stations to be included in the AFREF solution.

**Table 5.** Proposed selection criteria for GNSS stations to define AFREF (modified from Rebischung *et al.* 2012). This was not applied to the first AFREF computation.

| ***Data span*** | ***Threshold*** |
|---|---|
| Minimum time span | 3 years |
| Number of Discontinuities | < 2 years |
| Residual time series | 3D RMS < 10 mm, visual inspection from time-series |
| 3D formal error of latest velocity estimate | < 0.3 mm/yr |

## 3.10 Concluding remarks

This chapter described the strategy of processing GNSS data using the GAMIT/GLOBK (version 10.4) and CATREF software packages. Processing of GNSS data was done in two steps; in the first step, the GAMIT module was executed to process phase observations. In the second step, the loosely constrained solutions including H-files from the GAMIT modules were used as input files to the GLOBK module that then estimated station position and velocities. Since CATREF reads and writes SINEX files, H-files from GAMIT module were transformed into SINEX files and fed into the CATREF software to also estimate position, velocities and transformation parameters. As global terrestrial reference frame, ITRF2008 was used during processing of GNSS observations. The resulting contribution to the AFREF computation was completed and the solution was submitted to IGN.

# CHAPTER 4

## Results and discussions

*"All of science is nothing more than the refinement of everyday thinking"- Albert Einstein, 1936.*

### 4 Introduction

Results from the GAMIT/GLOBK and CATREF processing sessions are presented in this section. Validation of these results was carried out through a comparison between GNSS velocities derived from this study and those derived by the Jet Propulsion Laboratory (JPL). Furthermore, velocity vectors derived from the collocated SLR MOBLAS-6, 26 m VLBI telescope and IGS station HRAO are compared.

### 4.1 Evaluating GNSS data

#### 4.1.1 Daily evaluation of GNSS data

To assess the quality of geodetic data and the accuracy of the derived velocities, statistics were used to try to understand the errors in GNSS positioning. In most cases, the error spectrum in GNSS positioning is very complicated and the sources of errors are difficult to locate and resolve (Hofmann-Wellenhof *et al.* 1992). However, errors can be observed and it usually requires a long observation period to understand the behaviour and source of the error spectrum. This is due to the fact that some of the "errors" are remnants of incomplete modelling. The imperfect modelling of, for instance, Earth-tide, will lead to seasonal, diurnal and semi-diurnal signals embedded in the positional signal. Statistics presented here are computed using the entire network depicted in Figure 21.

Computed geodetic data sets were assessed by plotting GNSS residuals against elevation angle and fitting with a polynomial (see Figure 24 as an example). The station Root Mean Square (RMS) values were calculated (by taking the square root of the computed arithmetic mean of the observations) for each observation for all the stations in the network (see Figure 25 and Figure 26). The best sites would typically have RMS values of 3-5 mm and the worst sites would be about 5-9 mm, RMS values of more than

15 mm suggest a poor tracking receiver, a multi-path environment or severe weather conditions (Herring *et al.* 2010).

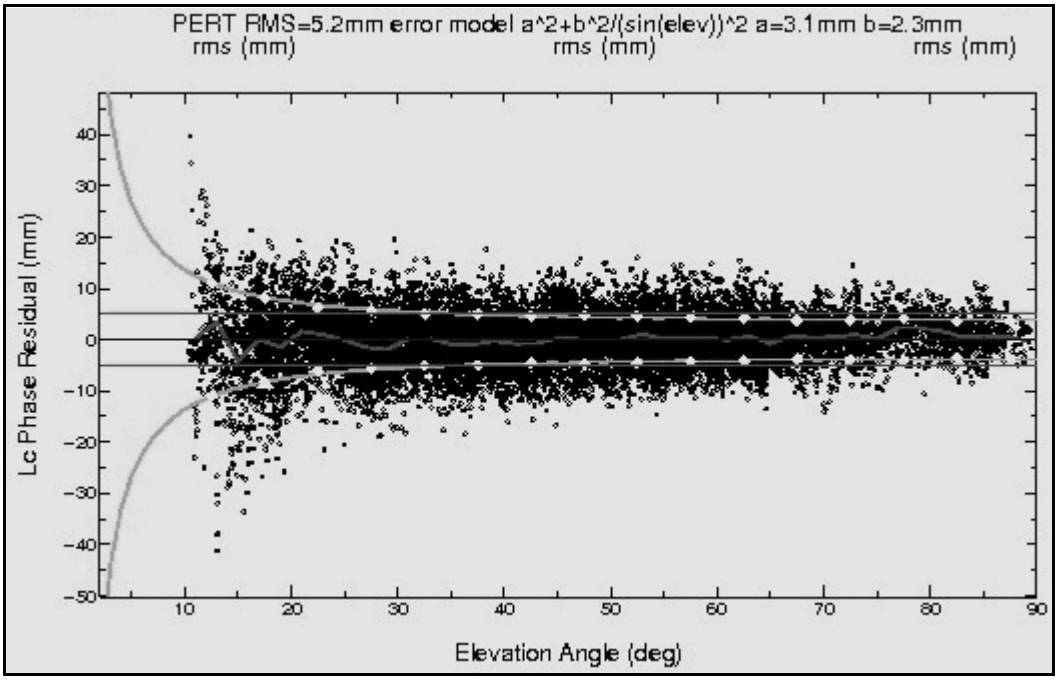


**Figure 24.** Residuals of GNSS data against elevation angle for station PERT, 2001 day 001. Error model gives RMS value of 5.2 mm.

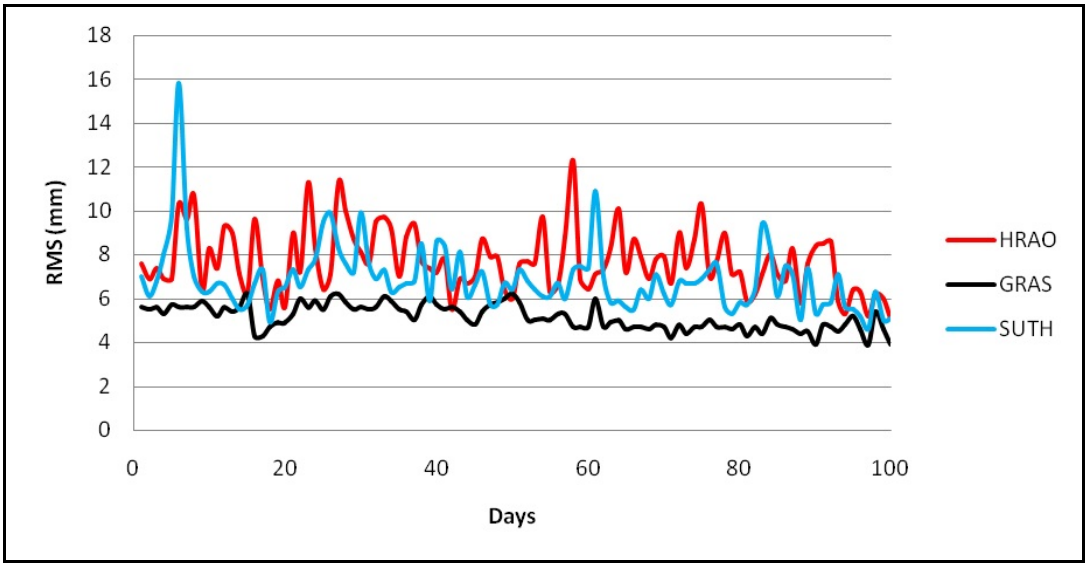


**Figure 25.** Quality assessment of daily GNSS data for HRAO, GRAS and SUTH stations between day 1 and 100, of year 2000. Average RMS values are 7.7 mm, 5.2 mm and 6.7 mm for HRAO, GRAS and SUTH stations, respectively.

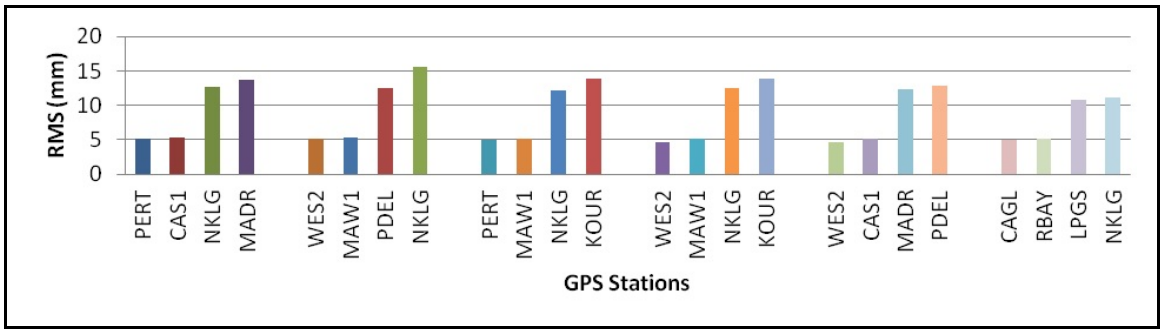


**Figure 26**. Calculated RMS values for two best and two worst GNSS stations from the overall processed stations during 2001 of January from day 1 to 6.

Two best stations and two worst stations from daily processed data were extracted to analyse the maximum and minimum RMS values for the entire network for a specific processed period. Figure 26 depicts best and worst performing stations from the network during January of 2001 from day 1 to 6.

Figure 25 illustrates the example of calculated RMS values for SUTH, HRAO and GRAS IGS stations. The IGS station GRAS depicts a very low consistent RMS value for the period of 100 days of the year 2000 while both HRAO and SUTH stations depicts higher variability of RMS values. The same analysis was done for the same stations for the period of 100 days of the year 2012 (Figure 27), the results indicate similar trends to those in Figure 25. The noise levels are not largely dependent on the type of instrumentation used, these stations have had both antennas and receivers upgraded since they were installed and currently the stations are using Ashtech choke ring antennas (ASH701945G_M, ASH701945E_M, ASH701945E_M) for the SUTH, GRAS and HRAO stations, respectively (log files see: http://sopac.ucsd.edu/cgi-bin/dbAllLogs.cgi). This suggests local noise instead, as the GRAS station maintains low RMS values while other stations are still noisy. The local noise might be due to weather conditions or a multi-path effect on site. In the case of HRAO, the current coaxial cable is very long, leading to a low signal-to-noise (SNR) ratio. This is due to change, as the receiver will be moved during July 2013 to a seismic vault being constructed about 30 m from the GNSS antenna.

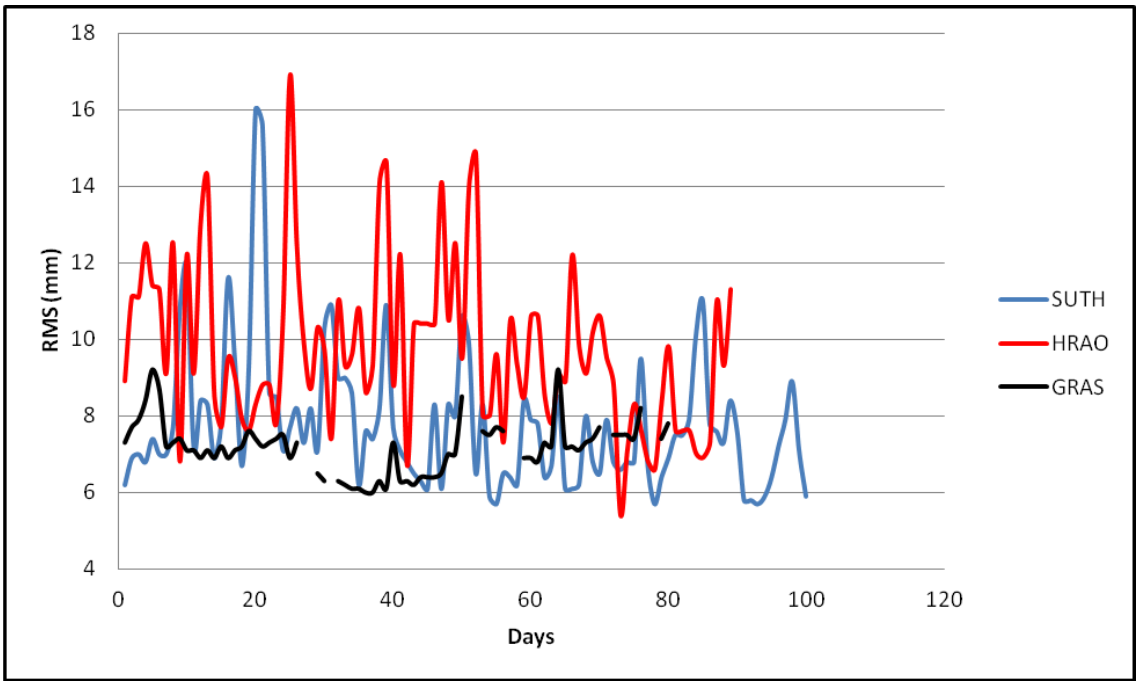


**Figure 27.** Quality assessment of daily GNSS data for HRAO, GRAS and SUTH stations between day 1 and 100, of year 2012. Average RMS values are 9.7 mm, 7.2 mm and 7.8 mm for HRAO, GRAS and SUTH stations, respectively. Station GRAS still maintains low RMS values while other stations are noisy.

The common factors that can be observed that affect GNSS data quality are mainly multi-path and water vapour content. These effects can be studied by plotting a time-series of polar sky plots as depicted in Figure 28 (see Figure 64 of Appendix B; these are computed daily; therefore, the contents of Appendix B is for illustration purposes). This provides ways in which temporal effects can be examined and a possible source of such effects can be sought. Moreover, the potential application of GNSS to meteorological studies is highlighted by making use of these polar sky plots. Figure 64 illustrates a series of polar sky plots of IGS station HRAO for only six days. The effect of water vapour can be clearly seen from the series of polar sky plots. Changes in the spontaneous spikes along the satellite tracks as a function of time indicates water vapour effects resulting in higher RMS values e.g., day 5 and 6. Multi-path effects would be represented by the consistent spikes along the satellite track for a given observation period. However, it must be noted that some meteorological measurements are required to quantify water vapour content. Sky plots can only infer the presence of water vapour or the presence of a multi-path effect.

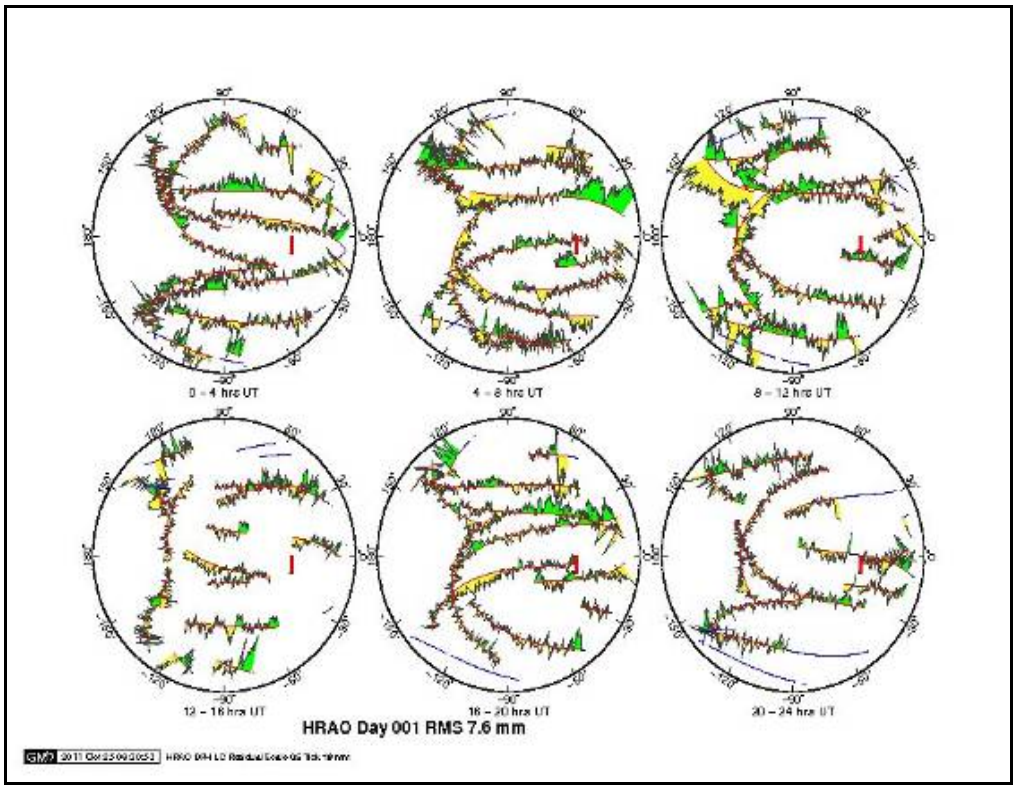


**Figure 28.** Polar sky plot of GNSS station HRAO as on January 1, 2000. Each plot covers a 4 hour period. The period 8-12 (UT) clearly contains more noise as there are several satellite tracks which exhibit larger RMS values than at other times of the day.

### 4.1.2 Multi-year data evaluation

As errors in GNSS are difficult to pinpoint, GNSS residuals are plotted as time series for each processed year and outliers are manually deleted or excluded before the final combination. The network geometry is affected by two components of the error spectrum; i.e., the temporal scale, which is comparable to the duration of the data processed, and spatial scales, which can be linked to the baseline length or distance between GNSS stations, affects the network geometry (Feigl *et al.* 1993). One can assume that the noise is stationary (Gaussian) but to justify this assumption is difficult due to the continuous upgrades of GNSS receivers in the network (i.e., changing hardware), addition of new satellites (and decommissioning of others) in orbit, as well as other bias introducing events during the time span of the data set processed for this study. These non-fixed network and technology variations could introduce equipment and network dependent biases. These biases should be of a relatively long period

compared to diurnal and sub-diurnal noise biases. As an example, water in a (damaged) coaxial cable at HartRAO has been seen to drastically reduce the signal-to-noise ratio of GNSS signals. This would increase RMS noise, especially for low elevation satellites, as SNR is lower at low elevations (this is antenna dependent). It is important to note that the statistics presented in this section are of a slightly different network, before combination in GLOBK. From Table 4 and Figure 22; it can be seen that more stations are being added and others ceased functioning and came on line again, causing data gaps during the 2000 to 2012.4 study period. This introduces a greater baseline effect and intensifies the spatial error component. For temporal effects, most stations are active for a long period (large percentage of study period) and others only for a short period and we assume that this would have similar effects to those of the spatial error component. Therefore, each 24 hour session should be evaluated separately and this should indicate the best and worst network over the given time period before combination in GLOBK.

This section presents the Normalized Root Mean Square (NRMS) statistics for the processed yearly data before data are combined to compute a velocity solution. The NRMS is based on Eq. [4.1]:

$$NRMS = \sqrt{\frac{x^2}{f}}, \qquad [4.1]$$

where $\chi^2$ = chi-squared and $f$ = degree of freedom (Feigl *et al.* 1993). The mean NRMS values for each individual experiment are presented in Figure 29 and the plots of each individual experiment (network) are presented in Figure 30 (a series of other networks are presented in Figure 66 of Appendix C). Each individual experiment indicates different NRMS values (Figure 29) for all the components. Data processed during 2003 and 2010 indicate a mean NRMS value of more than 2.5 in this North and East components while other experiments maintain average NRMS values of less than 2.5.

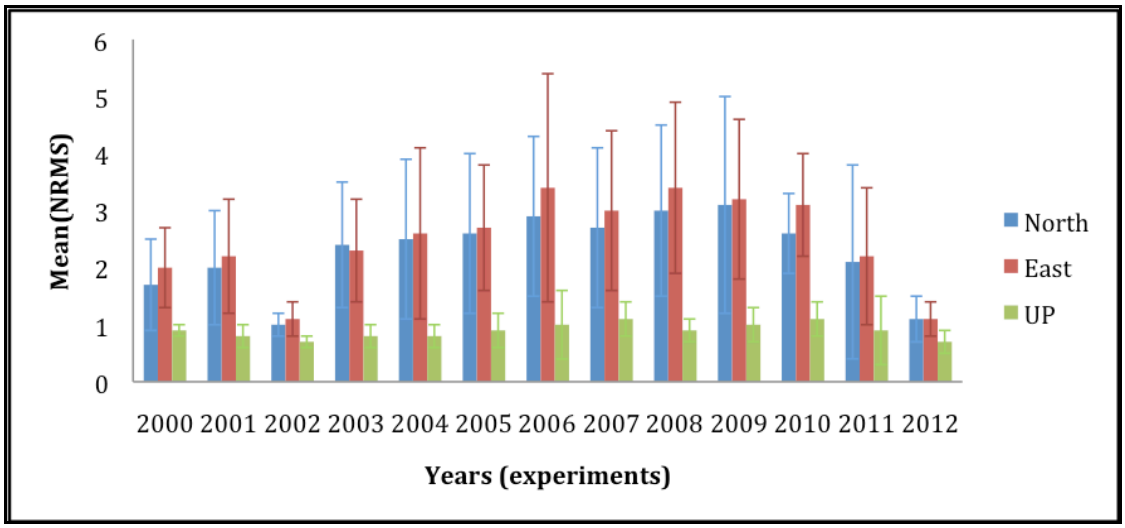


**Figure 29.** Mean values of NRMS (mm) for GNSS residuals for each individual experiment before combination (each experiment has a duration of 1 year).

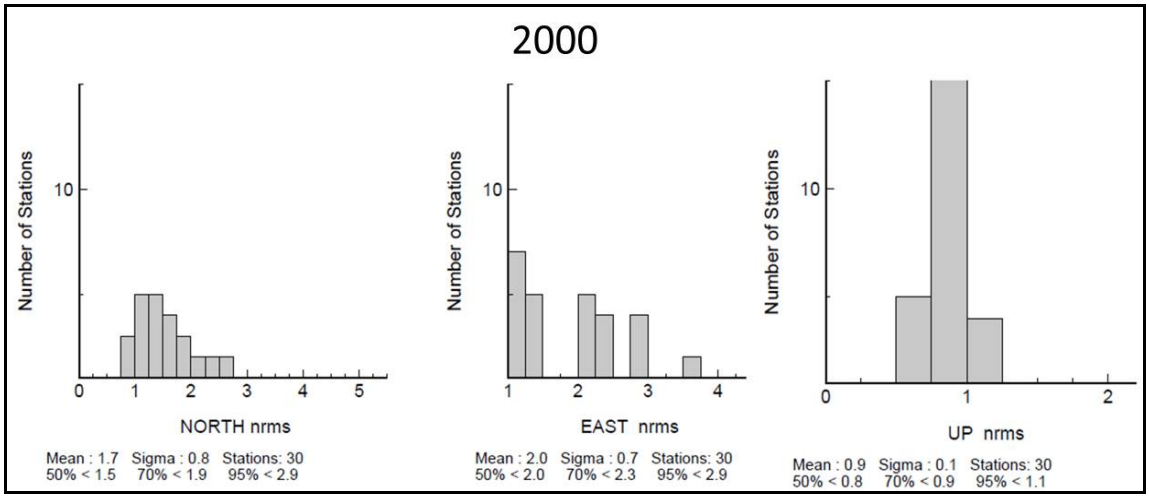


**Figure 30.** Histogram derived from the network the year 2000. The NRMS values (mm) are calculated for East, North and Up components.

### 4.1.3 Combination of loosely constrained solutions

Loosely constrained solutions from individual experiments were combined to form a daily-unconstrained network using the GLOBK software (Herring, 1997). The sub-networks were tied into a reference frame i.e., ITRF2008 to reduce spatial correlation errors. The loosely constrained solutions were combined in GLOBK by solving a system of equations as described in detail by Dong *et al.* (1998). Here, a summary of this approach is given, this approach is based on the Kalman filter of which sequential least squares is a special case. Let

$$\delta I_k = I_k - I_{0k} \qquad [4.2]$$

be the vector of linearized quasi-observations at epoch $t_k$, where the term $I_{0k}$ represents *a-priori* values and $I_k$ is the estimation of the quasi-observations from the analysis of the original observations. The observation equation is given by Eq. [4.3]:

$$\delta I_k = A_k \delta X_k + \varepsilon_k . \qquad [4.3]$$

Where $X_k$ represents the parameters to be estimated, $A_k$ is the design matrix, $\varepsilon_k$ represents the errors in the estimates $I_k$ such that $E\{\varepsilon_k\} = 0$, $E\{\varepsilon_{k+1}\varepsilon_k^T\} = 0$, where $E$ is the mathematical probability operator (Dong *et al.* 1998).

The $\chi^2$ was calculated from each H-file derived from GAMIT, which measures the goodness of fit of observed data sets and the computed data sets. Data with high $\chi^2$ increments were rejected by setting a maximum chi-square value of 100.0 (this is a default setting in the GLOBK software) and data with reasonable $\chi^2$ increments are allowed in the final combination. Figure 31 depicts the daily combinations and their associated $\chi^2$ values. Fluctuation of $\chi^2$ values from multiple networks can be seen as illustrating the differences across the networks. Herring *et al.* (2010) reported on the effect of using H-files from multiple analyses with the same parameters during the combination. The reported result is that the estimates of common parameters will clash causing $\chi^2$ to increase and this is depicted in Figure 31.

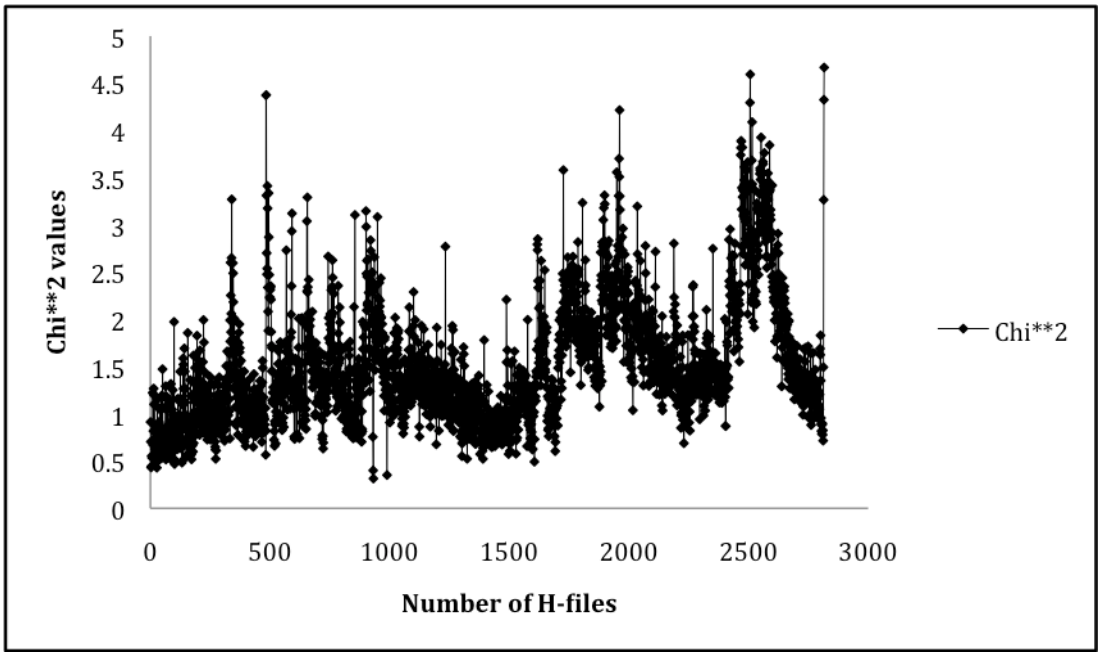


**Figure 31.** Calculated $\chi^2$ for the combined solutions. Note the variations of $\chi^2$ in different H-files.

The combined solution indicates an improvement of NRMS values from the individual sub-networks (Figure 32, Figure 33 and Table 6). Systematic errors, spatial and temporal errors as well as the geometry of the network used, contribute towards the final solution; however, the final solution shows an improvement over that of the individual network before combination. Bastos *et al.* (2010) pointed out that the standard method used to process GNSS data and estimate parameters is the ordinary least squares method. This method gives optimal results if observations are independent and normally distributed (Agnew, 1992; Bastos *et al.* 2010). Therefore, one expects deviations and slightly higher statistical errors due to the non-continuity of some GNSS stations in Africa, which will cause non-homogeneous data sampling as well as network geometry variations.

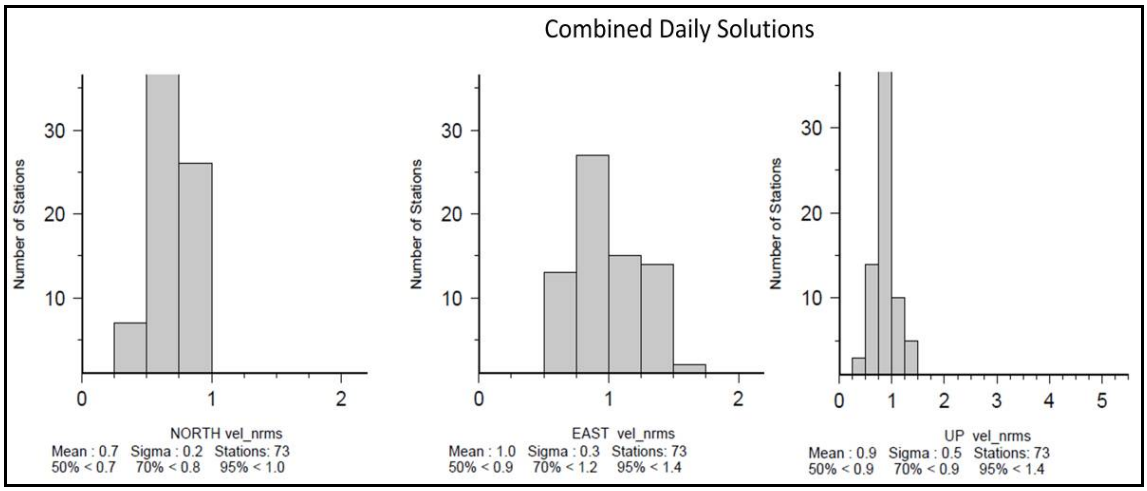


**Figure 32.** Histograms of NRMS values for the combined solutions.

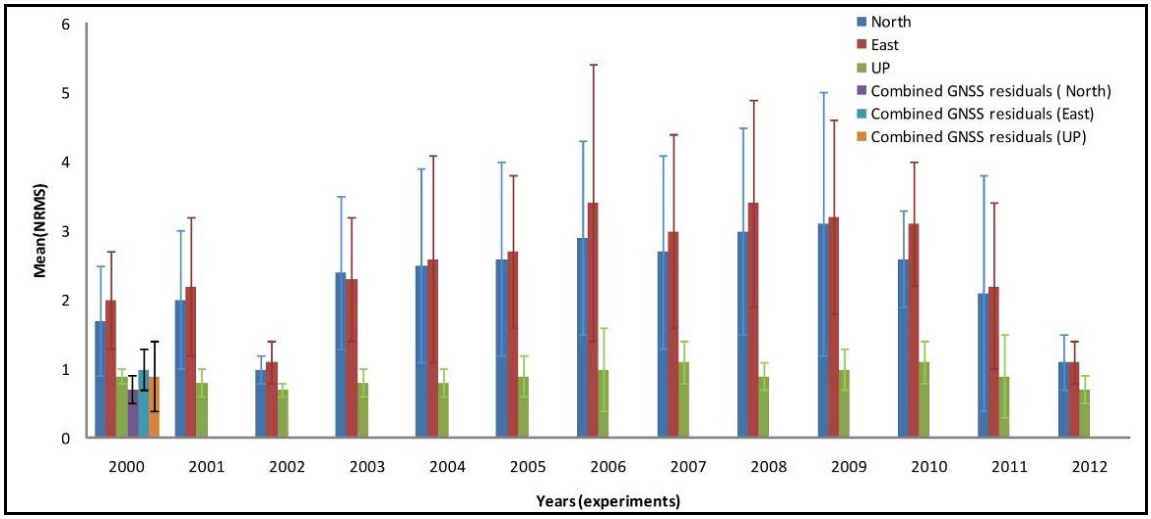


**Figure 33.** Comparison of the NRMS (mm) values of the sub-networks and a GLOBK combined solution plotted next to the 2000 sub-network.

**Table 6.** Summary of NRMS statistics for individual networks and the final GLOBK combined solution in terms of percentages. This was calculated by taking the sum of NRMS values for all the networks and determining the error contribution (%) of each individual network.

| *Year* | *North* | *East* | *Vertical (Up)* |
|---|---|---|---|
| | NRMS % | | |
| 2000 | 5.59 | 6.13 | 7.20 |
| 2001 | 6.58 | 6.75 | 6.40 |
| 2002 | 3.29 | 3.37 | 5.60 |
| 2003 | 7.89 | 7.06 | 6.40 |
| 2004 | 8.22 | 7.98 | 6.40 |
| 2005 | 8.55 | 8.28 | 7.20 |
| 2006 | 9.54 | 10.43 | 8.00 |
| 2007 | 8.88 | 9.20 | 8.80 |
| 2008 | 9.87 | 10.43 | 7.20 |
| 2009 | 10.20 | 9.82 | 8.00 |
| 2010 | 8.55 | 9.51 | 8.80 |
| 2011 | 6.91 | 6.75 | 7.20 |
| 2012 | 3.62 | 3.37 | 5.60 |
| Final Solution | 2.30 | 0.92 | 7.20 |

### 4.1.4 Time-series analysis

Time-series plots represent mean daily positions derived from GNSS measurements. The velocity of a GNSS station can then be estimated from the GNSS data over a certain period. Since GNSS stations are attached to the bedrock, any motion or position change in the time series plot is thus assumed to be equal to tectonic plate motion or local motion (Bastos *et al.* 2010). Figure 34 illustrates a variation of estimated GNSS positions over a period of 10 years. The north component of station HRAO has a shift of about 15 mm upwards during 2009. This shift was not due to tectonic movement but the result of a mechanical misalignment that occurred during antenna maintenance, as the antenna was not repositioned correctly (screwed back to its locking point) onto the pillar. After the antenna was correctly positioned, the coordinates of the station moved back to its normal position.

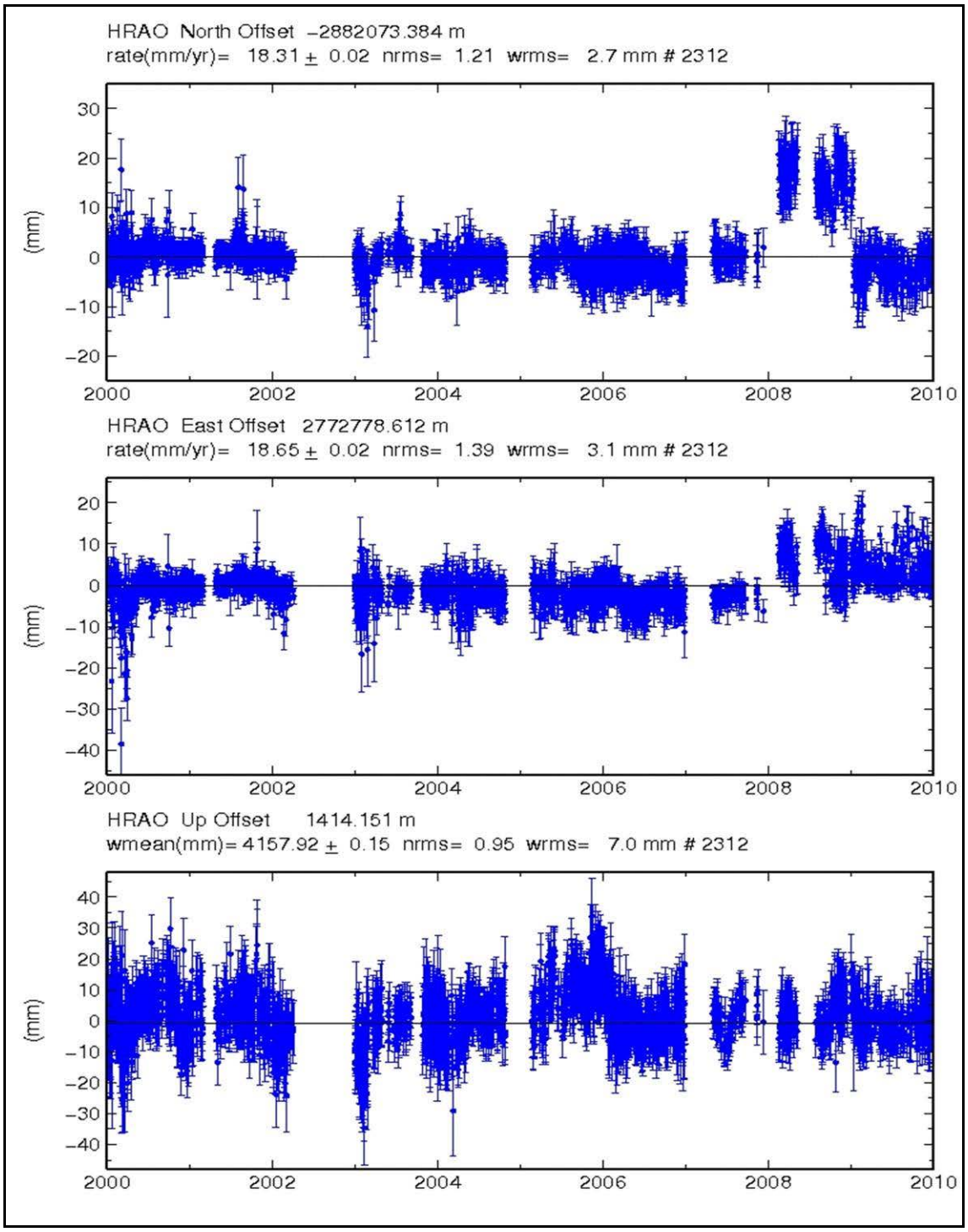


**Figure 34.** Time-series plot for IGS station HRAO. Note the displacement of about 15 mm in the north component during the year 2009.

In Figure 35 a time-series of the same station, after corrections were made is illustrated. This is a good example showing the sensitivity of this technique in estimating daily positioning. However, it also points out the importance of external validation methods to confirm conclusions about any movements depicted from the position time-series plots. In this example, a technical error might have appeared to be a displacement due to tectonics.

Station motions depicted in time-series plots are non-linear motions. Figure 36 and Figure 37 illustrate vertical components of the HRAO and VESL IGS stations, respectively. The vertical components indicate seasonal variations (with peaks during mid-summer for HRAO), which can be linked to many geophysical processes such as the ground water recharge and discharge cycle, varying atmospheric processes (ionospheric cycles) and changing multi-path effects. Even though the fluctuations are in the order of millimetres, a decreasing trend is evident over the processed data interval at a rate of -0.9 ±0.02 mm/yr for the HRAO IGS station. This is a very small signal and cannot correctly be ascribed to any particular process. In addition, some data gaps exist, which within the context of the small *negative* vertical "signal"' can be considered to be well within the true error bars (even though the statistical error is much smaller) and are; therefore, not significant. The VESL station can be linked to the same processes but at a rate of 0.3±0.05 mm/yr. Lambeck, (1988) discussed the underlying processes that might result in subsidence-uplift mode in the continental interior. They can be linked to lateral variations in the thermal system, response of the crust to the variations in surface loading caused by deposition of sediments and erosion of the elevated regions or the response of the crust to horizontal forces. In addition, there will be remnants of mismodelling due to imperfect solid Earth tides and ocean loading global models. Selected time series plots are given in Appendix D.

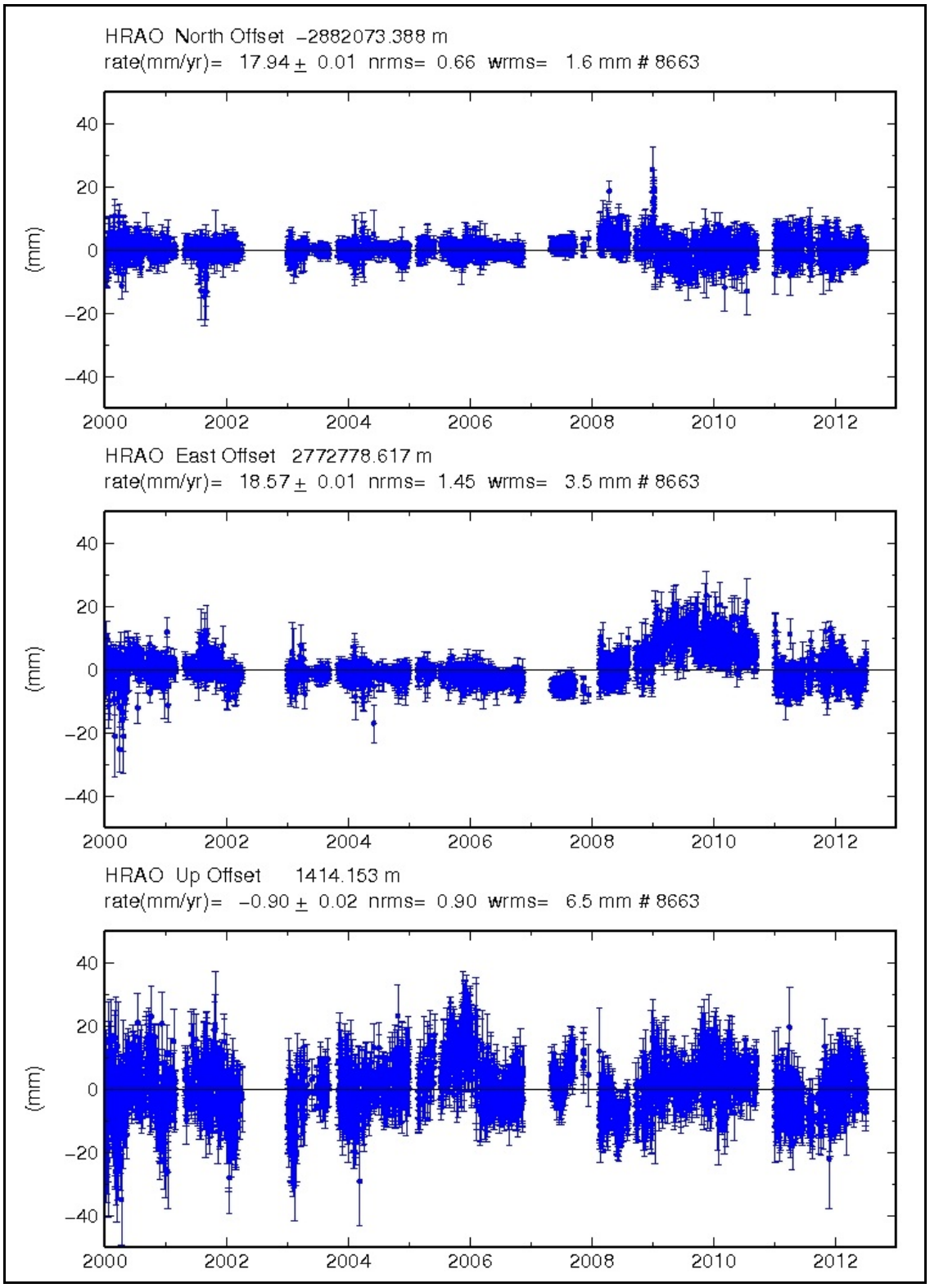


**Figure 35.** Corrected north component of IGS station HRAO. Note the effect of correcting the north component of the velocity estimation on the other two components, especially the east component, which is most affected.

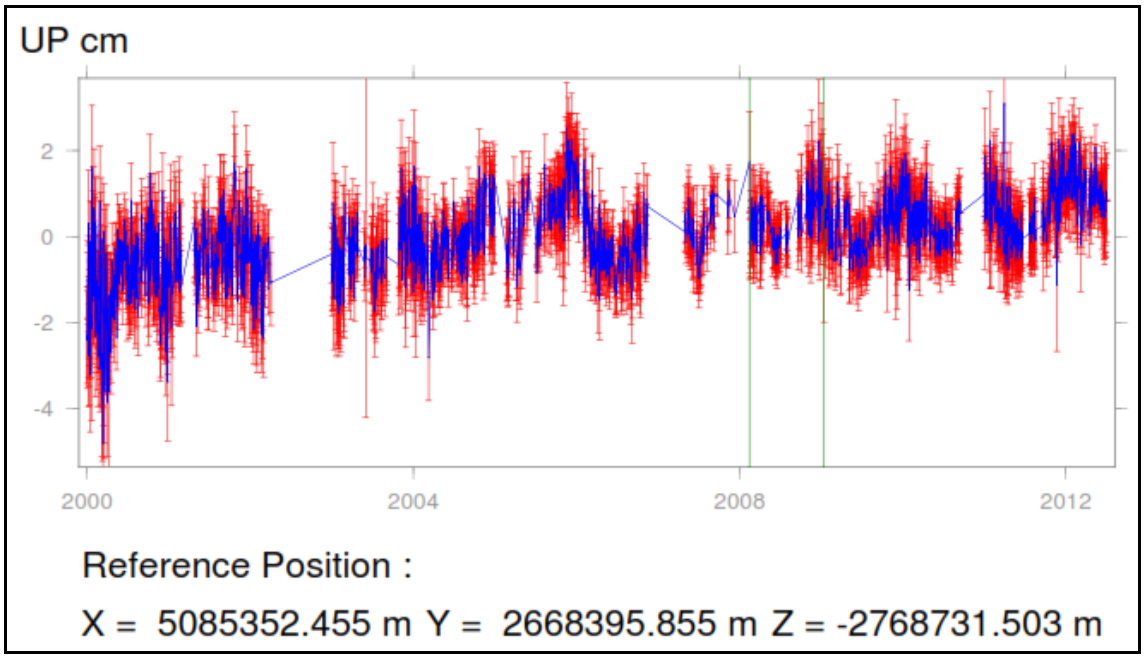


**Figure 36.** The vertical (Up) component of HRAO exhibiting seasonal variations. The signal contains peaks after a period of a year with minimum values occurring at the middle of the year (winter) with pronounced increases in height during summer. This could possibly be linked at some level to the ground water cycle. This will require careful recordkeeping of borehole water levels, rainfall and water withdrawal.

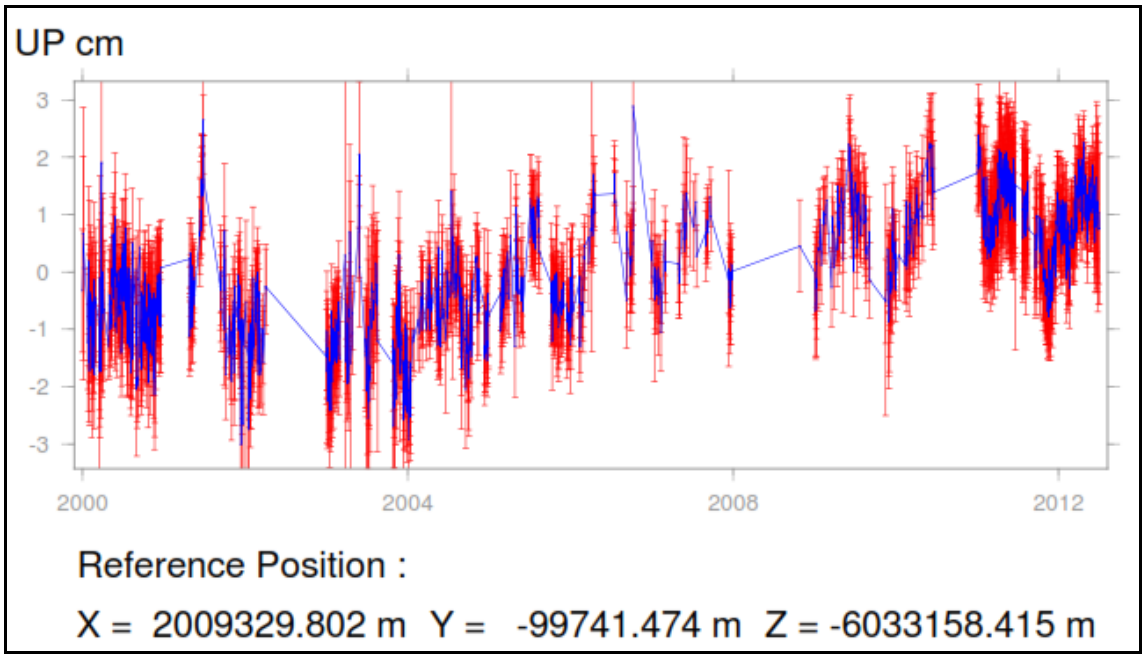


**Figure 37.** The vertical component of IGS station VESL also illustrating seasonal variations. An improvement in data volume and quality can be seen after the year 2010 when HartRAO upgraded the station with a new receiver.

## 4.2 GNSS velocity solution

The estimated velocities in ITRF2008 are listed in Table 11 of Appendix A and the calculated average station positions are listed in Table 13 of Appendix A. A few stations indicate unreliable velocities (SOLA and TGCV), due to limited data processed for these stations. More accurate results will be achieved as more data for these stations becomes available. Figure 38 depicts vertical velocities derived from GLOBK. The velocities indicate variable velocities across the network. Since these velocities are highly correlated with atmospheric effects (Rodrigues, 2007) and the vertical component is loosely constrained due to poor geometry of the visible satellites in the vertical component, this increases the level of the uncertainties associated with this component.

Distinct inter-continental plates can be clearly distinguished in Figure 39 where stations from the Somalian and Arabian plates exhibit different motions to that of the Nubian plate. The calculated average angular vectors of the stations using a dot product approach i.e., each vector is pictured as a Euclidean vector. The vectors between the Nubian-Somalian plates, the Nubian-Arabian plates and the Somalian-Arabian plates are $13.23^{\circ}$, $6.92^{\circ}$ and $10.07^{\circ}$, respectively. If this angle was equal to zero between two plates, it would imply that the two plates are moving in the same direction but this is not the case. Station velocities clearly indicate that the Nubian, Arabian and Somalian plates move independently from each other.

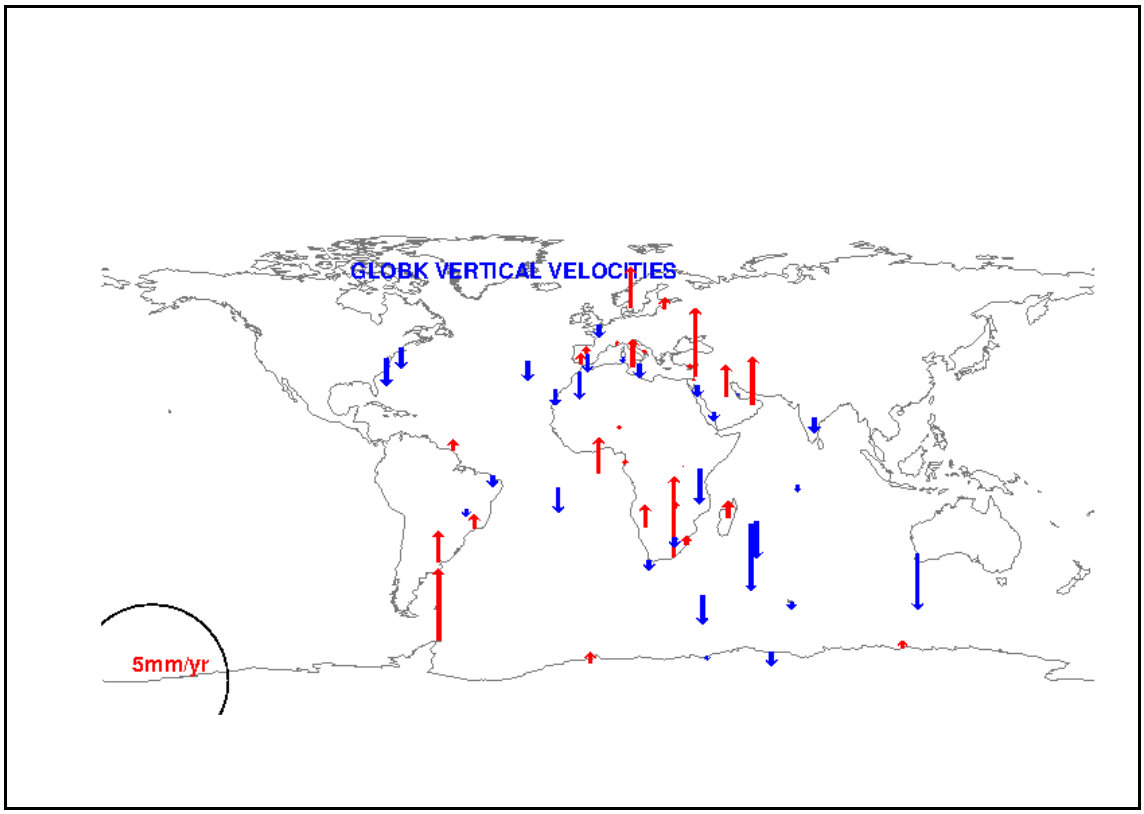


**Figure 38.** Vertical velocities calculated in ITRF2008. These velocities are highly correlated with atmospherically introduced errors (Rodrigues, 2007). Therefore, they have a larger uncertainty than the horizontal components.

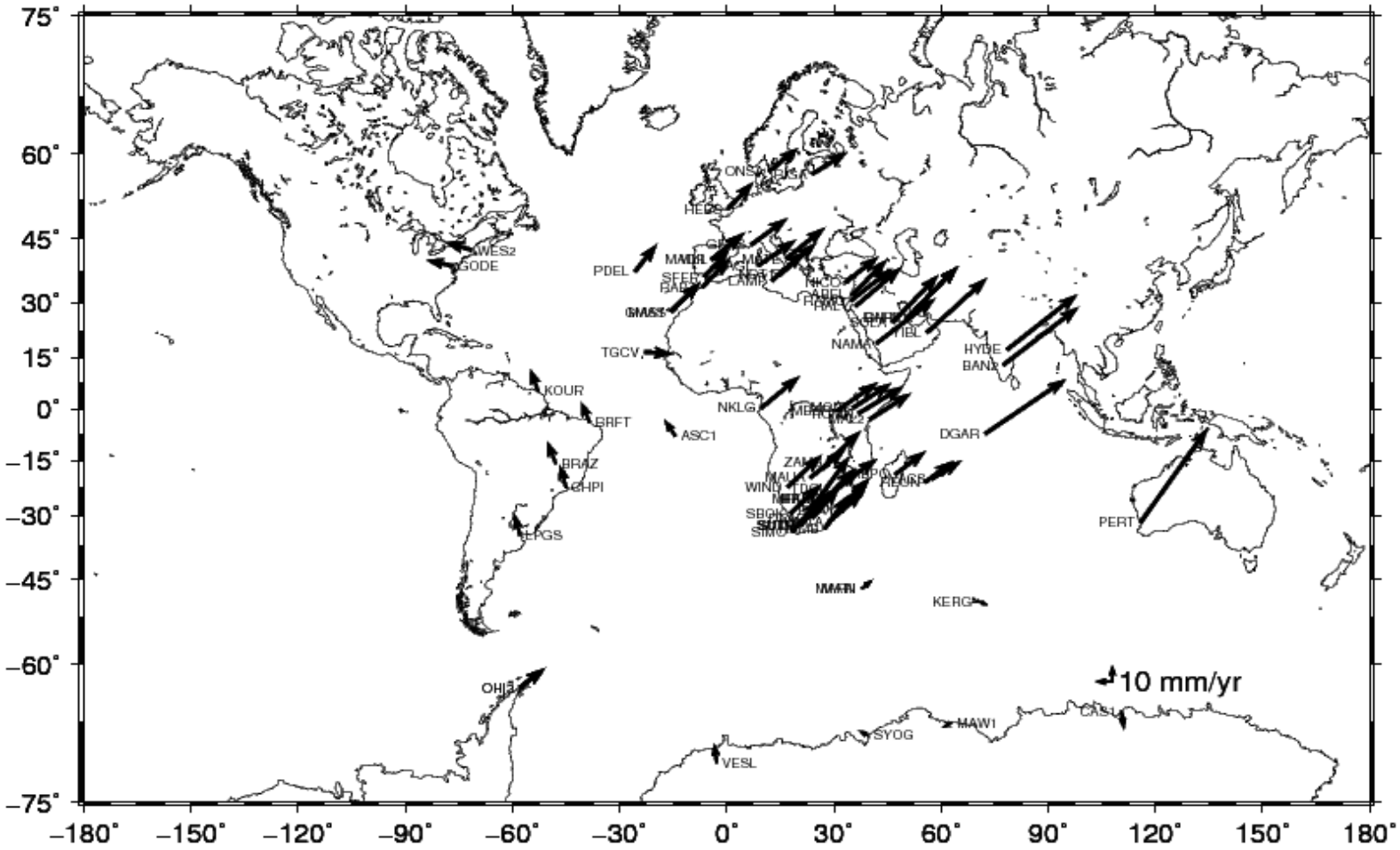


**Figure 39.** Global horizontal velocities plotted at 95% confidence interval calculated in ITRF2008. Each continental plate exhibits independent plate motion and well-known major plate boundaries can be observed e.g., the mid-ocean ridge between the African and South American plates is evident since the station velocity vectors in both continental plates depict motion in different directions.

As is well known, stations on the African plate move faster than those from the South American plate (DeMets *et al.* 1990) and in different directions. This is shown by the magnitude of the velocity vectors in Figure 39. Figure 40, Figure 41 and Figure 42 display colour enhanced velocity gradients (these are enhanced interpolated velocity maps without a particular direction; they depict variations between GNSS stations). It can be seen that stations on the Arabian plate move faster than the Nubian plate. The vertical velocities are pictured in Figure 42. This is the weaker component and the results are inconclusive, as most stations are within the error margins.

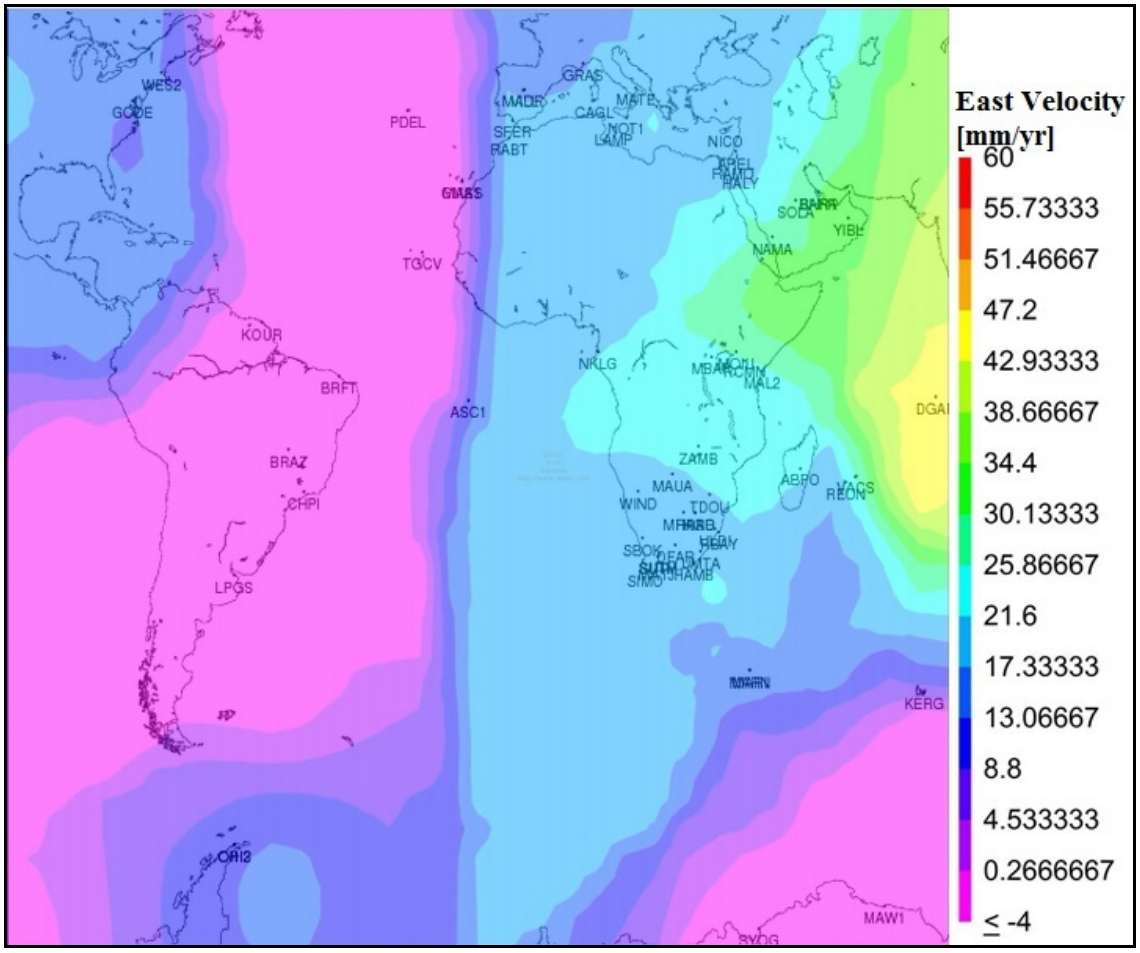


**Figure 40.** East velocity component depicting variability of the velocity solution across different continents. More GNSS stations are required to improve spatial geometry and densification of points measured. A map such as this will be very informative and should graphically delineate the various intra-continental blocks.

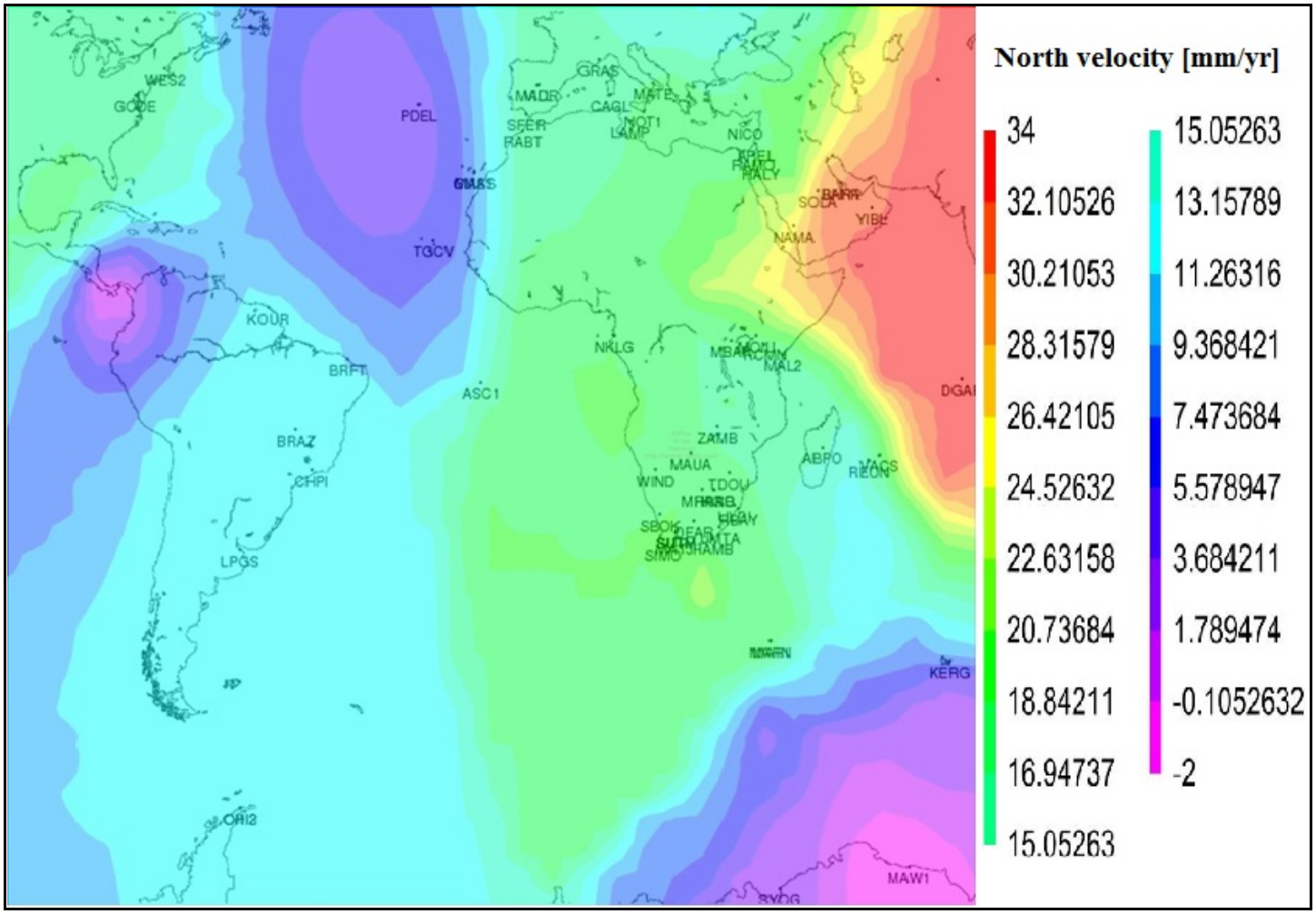


**Figure 41.** North component depicting variability of the velocity solution across different continents.

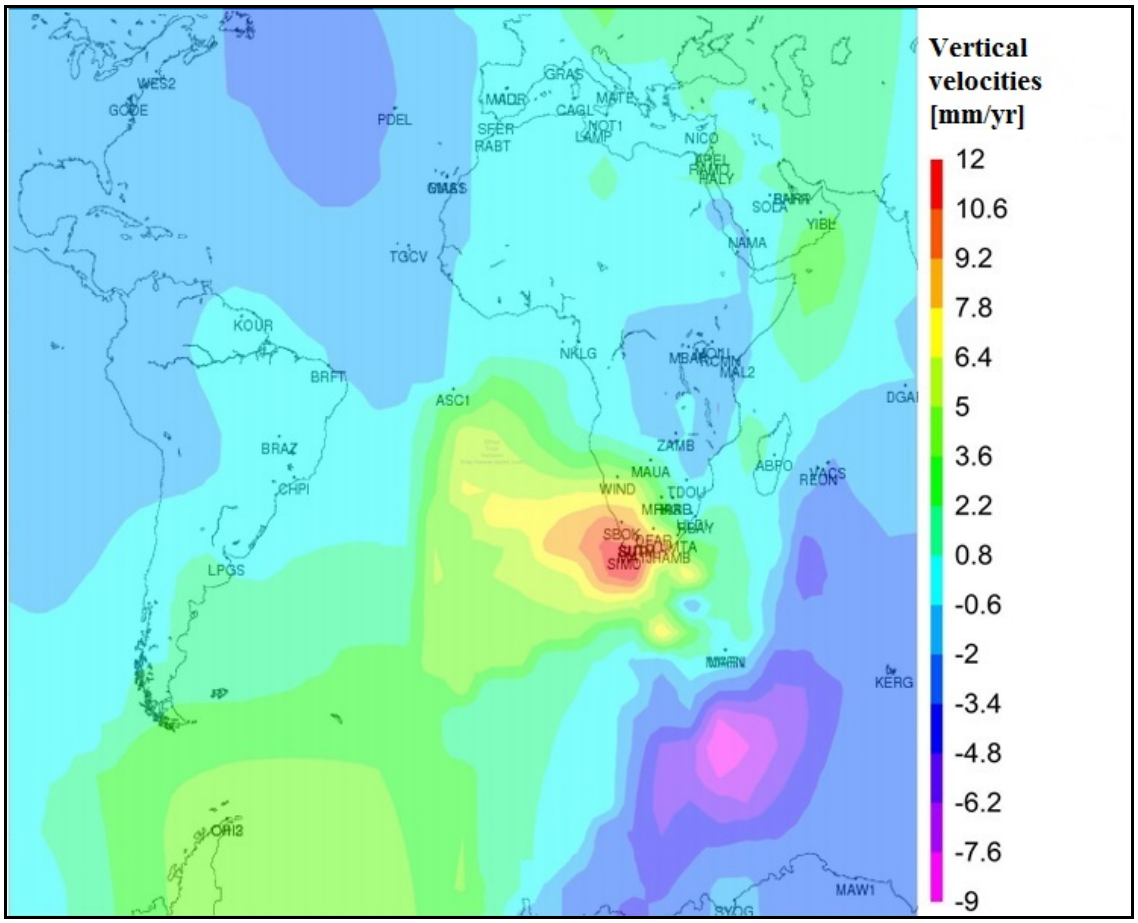


**Figure 42.** Vertical component depicting variability of velocity solution across different continents. Note that vertical component is weaker, by a factor of 3, than the horizontal components. Therefore, very few definite conclusions can be derived from this plot. The Western Cape region seems to have slight vertical motion.

If more stations were available, especially on islands in the Atlantic Ocean, it would have made the colour visualizations more instructive as the Atlantic Ridge margin would have been visible. Future analysis could include new stations installed on Gough Island and Tristan da Cunha. The derived velocities are consistent with the NUVEL-1 model (DeMets *et al.* 1990; which is based on geological models or observations) in terms of the direction of velocities. Nilforoushan *et al.* (2003) analysed the Arabian-Eurasian plate collision using GNSS stations. The BAHR GNSS station was included in the analysis, where 31.1 mm/yr east and 27.7 mm/yr North velocities were obtained. Velocities derived from this study (i.e., 31.01 ± 0.05 mm/yr East and 29.36 ± 0.12 mm/yr North) were comparable to velocities from Nilforoushan *et al.* (2003) and obtained.

## 4.3 Validating GNSS velocities

One way to validate or evaluate the accuracy of the derived GNSS velocities is to compare the results with the results from other analysis centres such as the Jet Propulsion Laboratory (JPL; http://sideshow.jpl.nasa.gov/mbh/series.html) and other space geodetic techniques. Due to the lack of other space geodesy techniques in Africa (apart fron GNSS), only IGS station HRAO will be compared against SLR station MOBLAS-6 and the 26 m VLBI telescope collocated at HartRAO.

### 4.3.1 Comparison of velocity solution from HartRAO and JPL

Velocity residuals for selected sites from JPL and HartRAO are listed in Table 10 of Appendix A. The results indicate no significant difference between the two solutions. A linear regression line fitted to the North, East and Up components between the solutions from JPL and HartRAO (Figure 43) revealed good agreement. The squares of the correlation coefficients ($R^2$ values) were 0.991, 0.993 and 0.578 in the North, East and Up components, respectively. The correlations were derived from selected common stations at JPL and HartRAO as illustrated in Table 10 of Appendix A). Accuracy range of of approximately 0.5 to 2 ± 0.5 mm/yr in both East and North components and 0.5 to 3 ± 0.5 mm/yr in the vertical component were achieved. The two solutions are plotted together in Figure 44 and Figure 45 and no significant difference between the two solutions can be noted. Jin (2003) showed that the vertical component varies with the amount of data being processed. Jin (2003) found that Shanghai GNSS station data from 1998 to 2003 indicated a *negative* vertical velocity of -1.9 ± 0.6 mm/yr, but including data from 1995 to 1998, resulted in a *positive* vertical velocity of 1.5 ± 0.4 mm/yr.

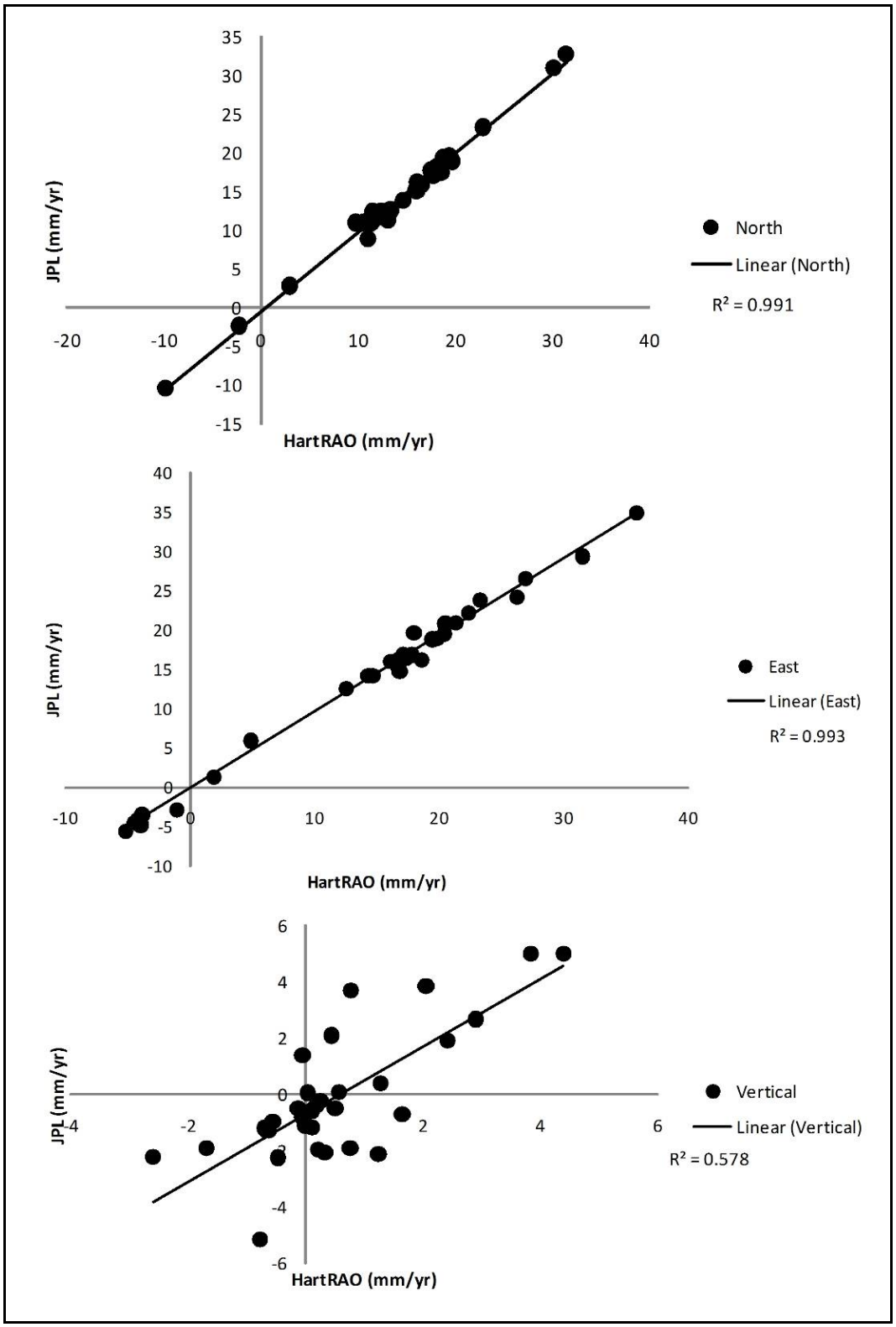


**Figure 43.** Correlation comparison of North, East and Up components of GNSS velocities derived from this study (HartRAO) and those from JPL.

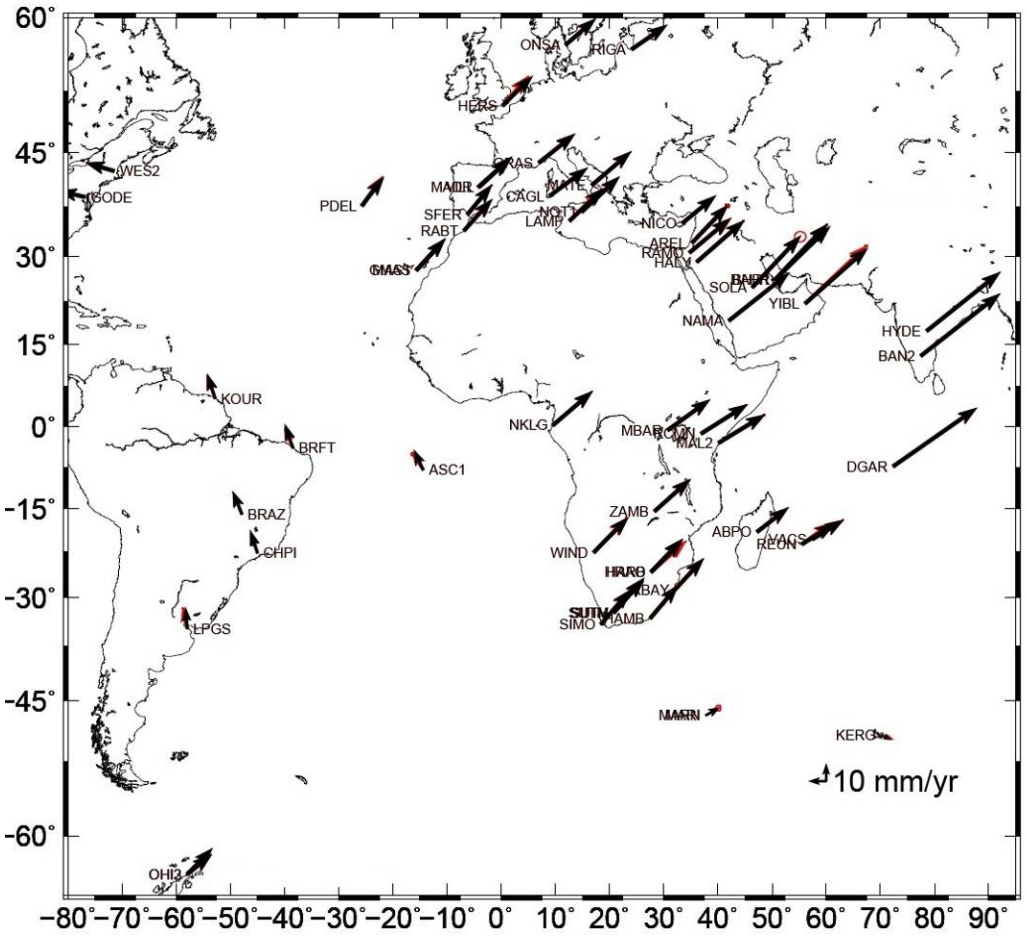


**Figure 44.** Horizontal GNSS velocities derived from this study are represented by black arrows and those from JPL are represented by red arrows. No significant difference between the two solutions can be noted. Velocities from JPL are available at: (http://sideshow.jpl.nasa.gov/mbh/series.html).

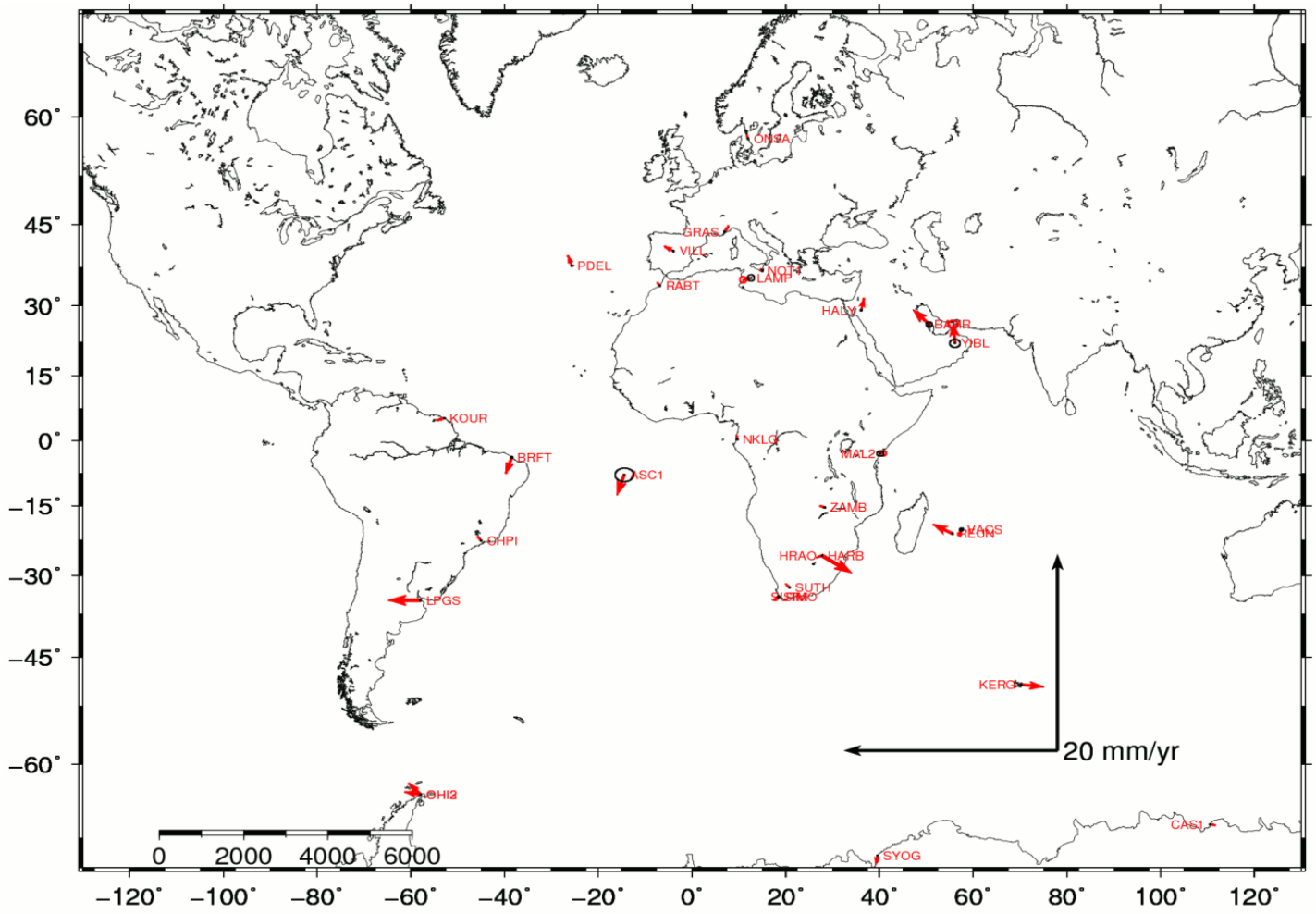


**Figure 45.** Differences (vectors subtracted) between JPL and HartRAO GNSS velocities. Most stations indicate good agreement. The scale of the velocity vectors was increased by a factor of 2 to magnify the small differences.

Uncertainties or standard deviations for the selected sites are plotted in Figure 46. Solutions from this study exhibit slightly higher errors compared to solutions from JPL. Stations that are located at the plate boundaries or at mid-ocean ridges such as MAL2, BABR, VASC, YIBL and ASC1, respectively, indicate higher discrepancies i.e., they have standard deviations greater than 0.2 mm/yr. Stations that are located close to each other and within inter-continental plates indicate good agreement i.e., standard deviation less than 0.2 mm/yr. Weaker stations could be affected by multi-path, equipment problems, noisy (radio frequency) environments, limited horizons (restricting access to satellites) and atmospheric effects. Different processing strategies are another explanation for inconsistency. Bruyninx *et al.* (2010) further explains that a solution derived on a global scale (JPL solution) will be different to some degree from a solution derived on a regional scale (solution from this study). The reason for this lies in the fact that the least squares method is mainly affected by the spatial distribution of data points, whereas transformation parameters are sensitive to the reference stations used.

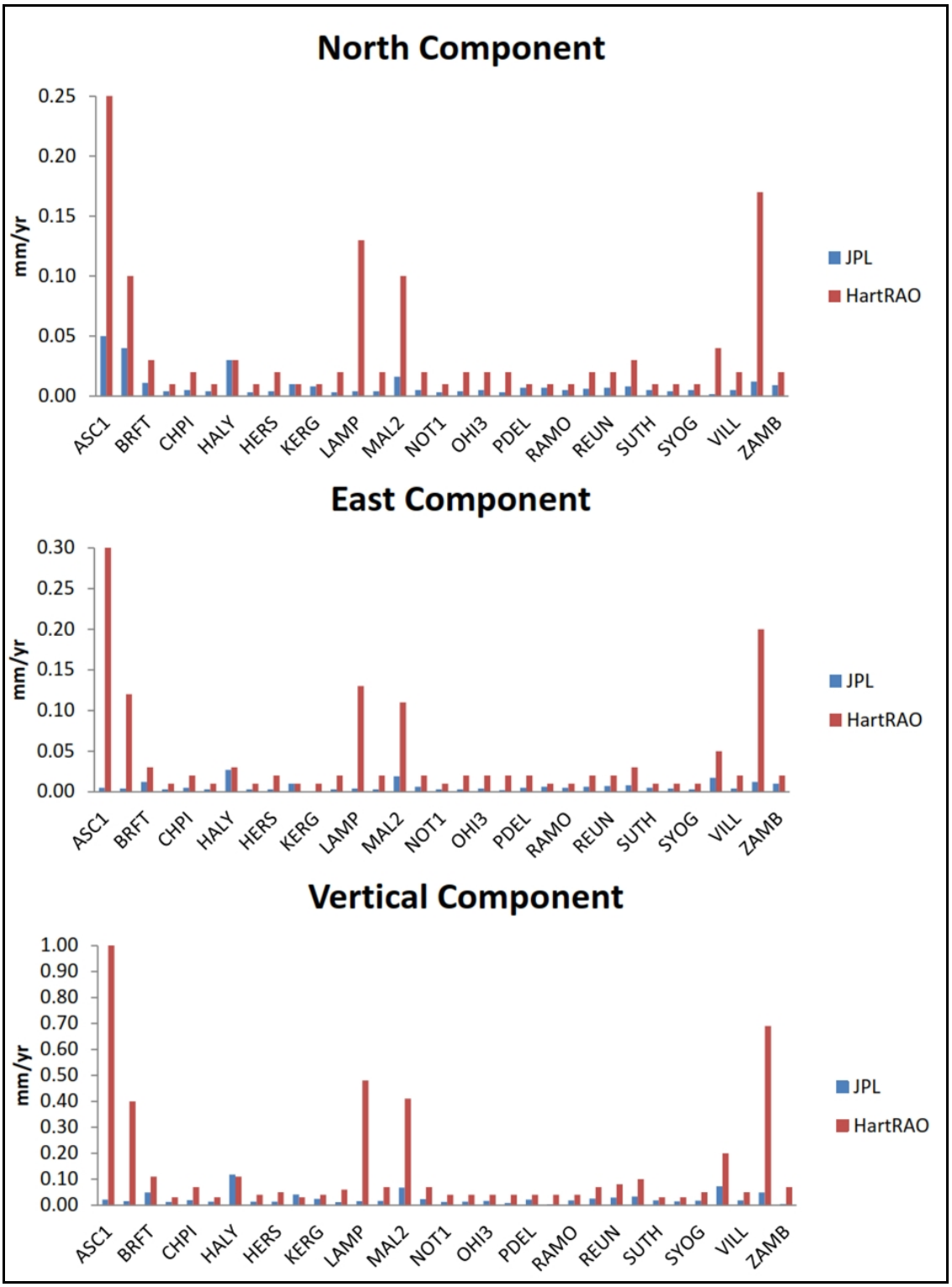


**Figure 46.** Comparison of standard deviations of the velocities derived from this study (HartRAO) and those from JPL. Solutions from JPL (using GYPSY/OASIS II precise point positioning) indicate less than 0.2 mm/yr errors for the selected sites while the HartRAO solutions indicate slightly higher errors.

### 4.3.2 Comparison of velocity vectors between different space geodetic techniques

This section contains results from a manuscript listed in the peer reviewed article section (page VI). The VLBI, SLR MOBLAS-6 and HRAO station time-series are compared in this section. These geodetic techniques are collocated at HartRAO (Figure 1 in chapter 2), where they are attached to the same bedrock. Therefore, these techniques should exhibit similar velocity vectors in all directions. If any deviations are observed, then this will indicate site instabilities or technique dependent solution errors.

Different software packages were used to process data sets from the three techniques. Data sets from SLR were processed using the SLR Data Analysis Software (SDAS) developed at HartRAO by Combrinck and Suberlak (2007) and data from the 26 m VLBI telescope were processed using the VieVS software written by the Institute of Geodesy and Geophysics (IGG), Vienna University of Technology.

The summary of the results are listed in Table 7 and time-series plots for each technique are contained in Figure 47, Figure 48 and Figure 49, where good agreement between the three techniques can be seen. A maximum deviation of 1.7 mm/yr, 0.7 mm/yr and 1.3 mm/yr between the North, East and Up velocity components, respectively, were achieved.

**Table 7.** Velocities of MOBLAS-6 SLR station, 26 m VLBI telescope and IGS station HRAO. Vn, Ve and Vu represent velocities in North, East and Up components, respectively, and Sn, Se, Su represent standard deviation in North, East and Up components, respectively, ([*]Personal communication: L Combrinck, 2013, [#]personal communication: D Mayer, 2013). All outliers were removed (3 sigma) before velocity estimation.

| Technique | $V_n$ [mm/yr] | $S_n$ [mm/yr] | $V_e$ [mm/yr] | $S_e$ [mm/yr] | $V_u$ [mm/yr] | $S_u$ [mm/yr] |
|---|---|---|---|---|---|---|
| [#]**VLBI** | 18.6 | 7.6 | 18.1 | 6.8 | 0.3 | 16.3 |
| [*]**SLR** | 19.7 | 0.6 | 18.1 | 0.8 | 1.6 | 1.1 |
| **GPS** | 18 | 1.9 | 18.8 | 4.3 | -0.9 | 6.8 |
| **VLBI-SLR** | 1.1 | | 0 | | 1.3 | |
| **VLBI-GPS** | 0.6 | | 0.7 | | 0.6 | |
| **GPS-SLR** | 1.7 | | 0.7 | | 0.7 | |

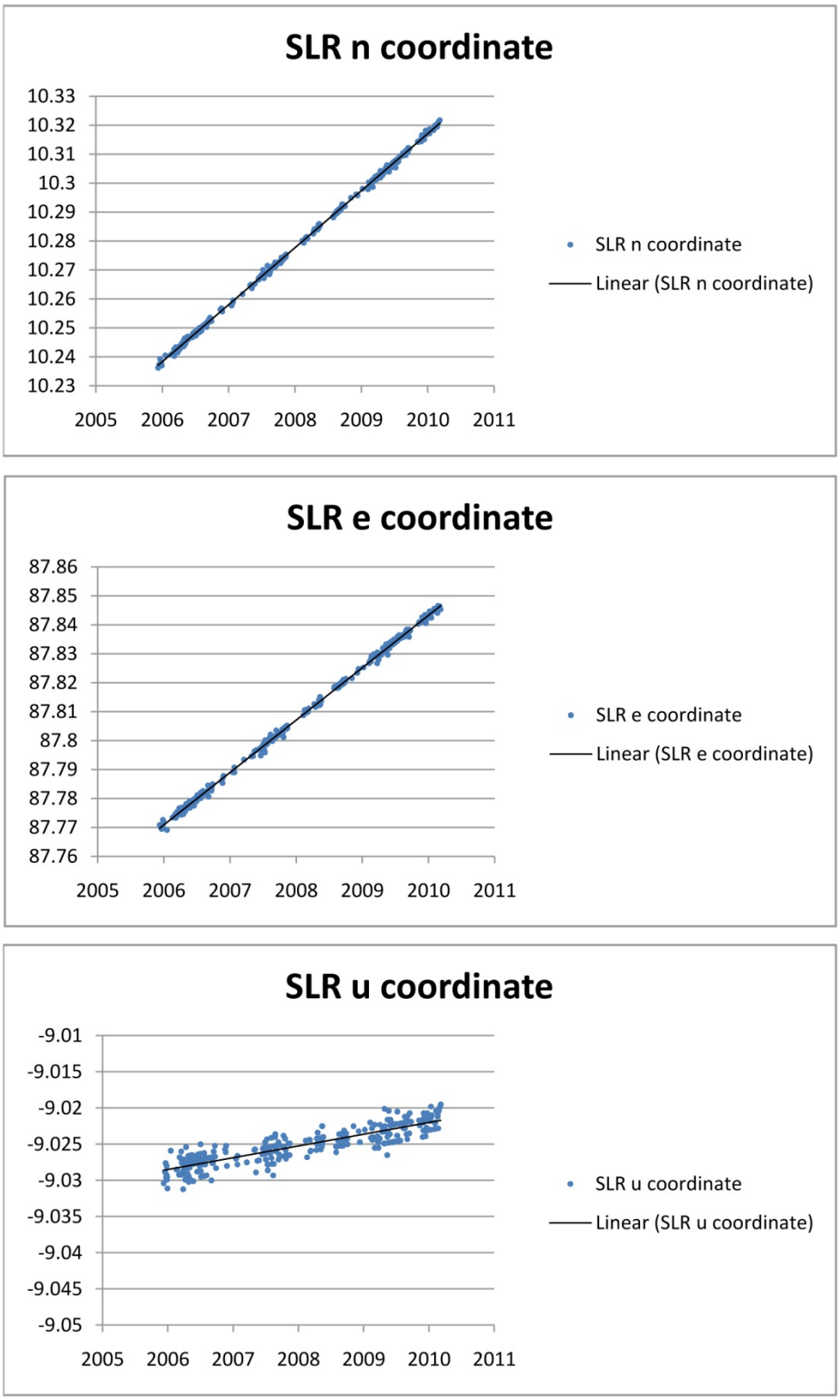


**Figure 47.** Time series (mm) of the MOBLAS-6 SLR station (personal communication: L Combrinck, 2013).

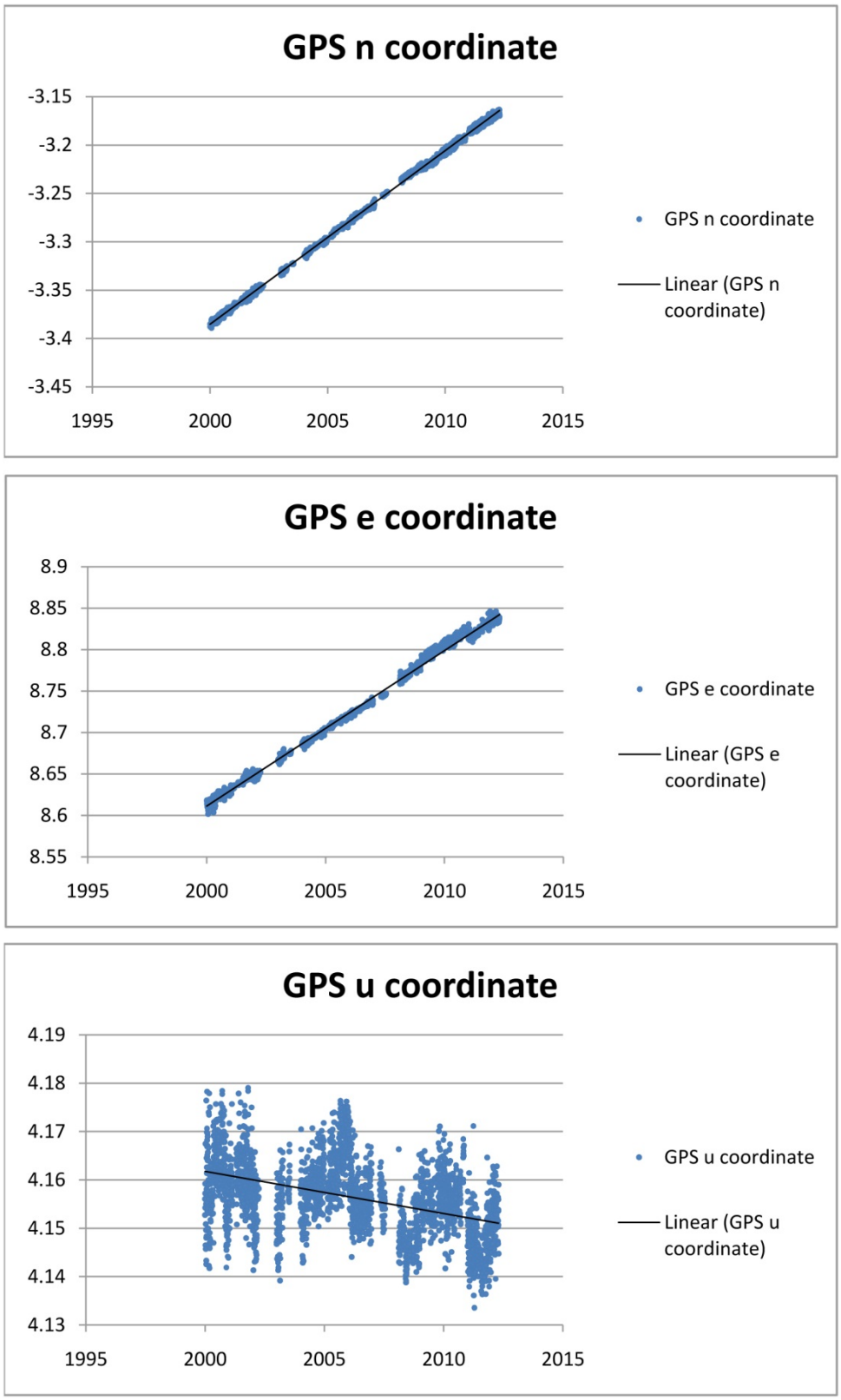


**Figure 48.** Time-series (mm) of the IGS station HRAO.

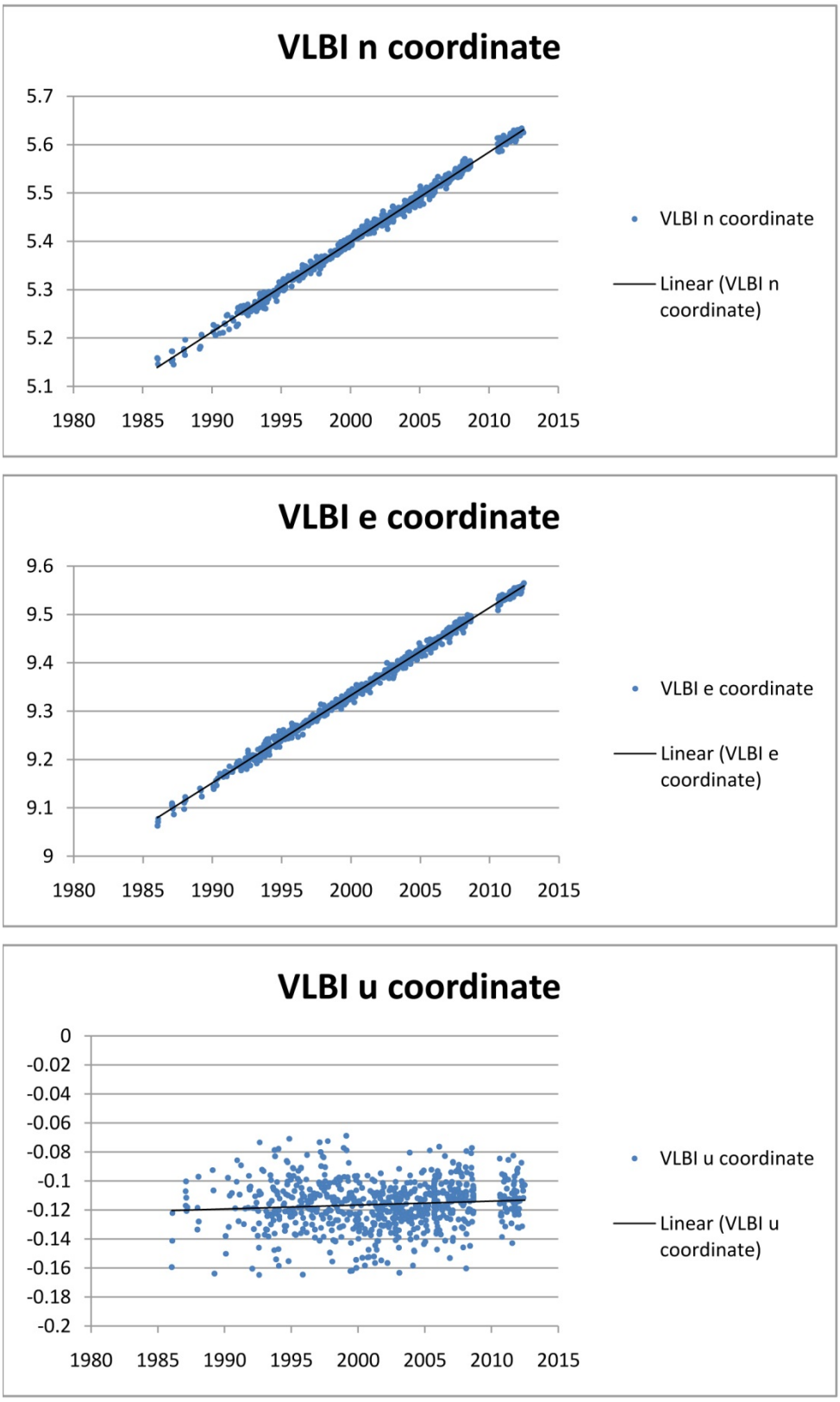


**Figure 49**. Time-series (mm) of the VLBI 26 m telescope (personal communication: D Mayer, 2013).

The techniques exhibit a high level of agreement; however, small differences in standard deviations and velocity vectors are evident. The VLBI technique exhibits high standard deviations compared with the other two techniques utilized; this is due to the statistically smaller number of observations and limited data sessions, while the SLR and GNSS observations are available nearly on a daily basis.

The close agreement achieved here validates the GNSS processing strategy used in this study and the solution provided compares favourably with the other techniques (SLR and VLBI). The HartRAO developed SDAS software proves to give reliable results that agree very well with other software packages and different processing strategies used. Since all the techniques compared here give similar results, we can conclude that the inter-technique comparison indicates no technique-dependent biases. Collocation of space geodetic techniques is crucial in the estimation of technique-dependent biases and scale differences. Fundamental sites such as HartRAO are used in the combination of techniques for the purpose of ITRF final solutions. The site vector ties between the various techniques are utilized to provide fixed parameters. That is, the technique position offsets are taken as known, and are therefore tightly constrained in ITRF global solutions.

## 4.4 Estimated parameters from the CATREF software

The estimated $\sigma_0^2$ using [Eq.3.7] in Chapter 3 for the final solution was found to be 0.99963 which is close to unity. Estimated transformation parameters for the network used are plotted in Figure 50. The zero line on the plots represents ITRF2008 and the stability of the network is illustrated, as well as how it varies with time. Seasonal variations are evident; this could be linked to non-tidal loading phenomena such as variation in ocean loading, atmospheric loading and hydrological cycles. Tidal effects caused by the moon and the Sun are corrected in GNSS and the models for such effects are accurately derived from the SLR technique; therefore, these parameters are corrected in GNSS processing.

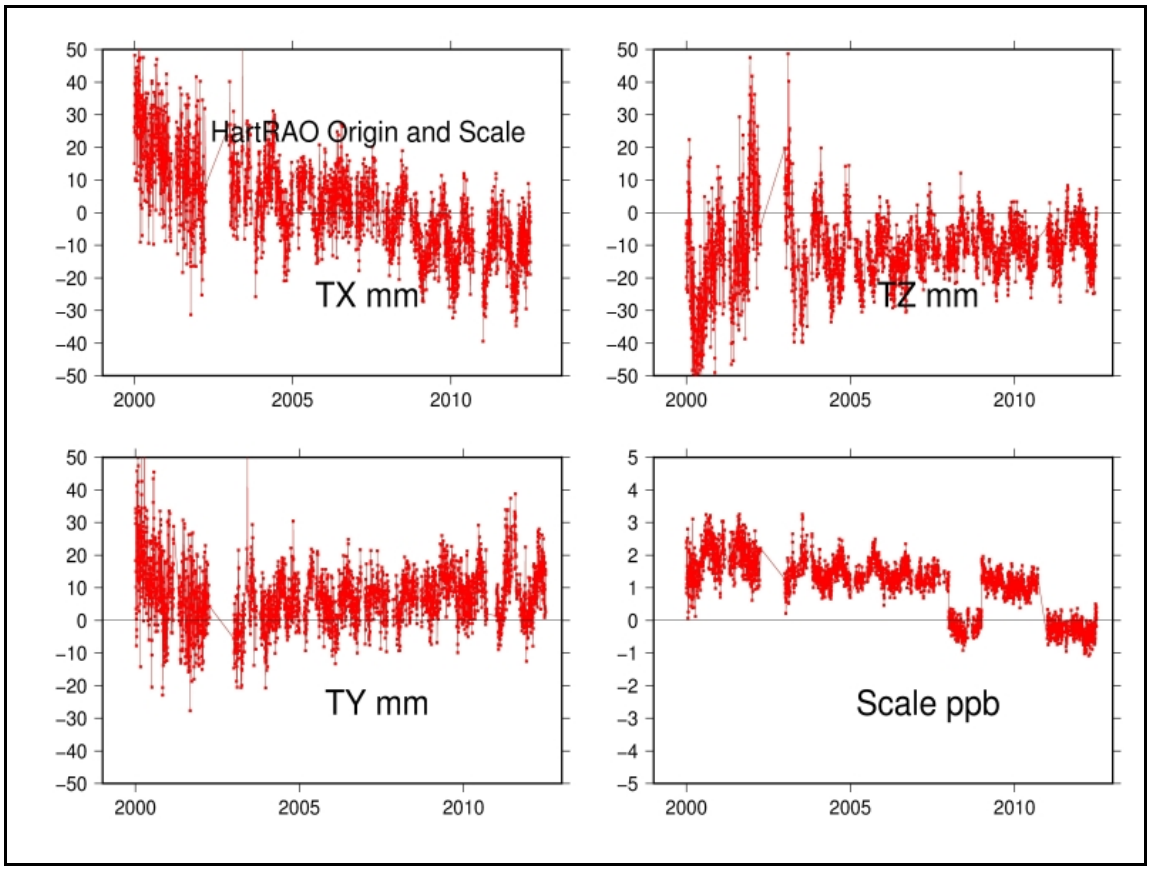


**Figure 50**. The origin and scale-consistency solution derived from the CATREF combination software.

A gradual improvement can be seen in the transformation parameters: TX, TY, TZ and scale from 2000 to 2004, mainly due to the addition of more GNSS stations in the processed network. Results that are more consistent can be noted after 2004 due to an increase in use of available reference stations. The jump in scale during 2011 could be related to inconsistencies during migration of IGS2005 (igs05.atx) to the IGS2008 reference frame (Rebischung *et al.* 2012). The IGS2008 was derived from the ITRF2008. The IGS solution required a slightly different approach, since there was inherent error in station coordinates during migration from the ITRF2005 to ITRF2008. The shift in station coordinates (during ITRF2005 to ITRF2008) was due to antenna calibration updates, which needed to be accounted for. Therefore, the new IGS2008 was also not consistent with the new set of antenna calibrations (igs08.atx). This has resulted in inconsistency between the use of IGS2005 and IGS2008. The reason for the jump during 2008 is not clear at this stage. It is interesting to see the effect of incompatible

antenna calibrations as illustrated from the second scale jump in Figure 50. For more detailed discussions on antenna calibrations, see Rebischung *et al.* (2012).

The estimated horizontal and vertical velocities using CATREF are plotted in Figure 51 and Figure 52, respectively. Generally, the derived velocities are consistent with the NUVEL-1 model (DeMets *et al.* 1990) which is based on geological models or observations. It is also consistent with the ITRF2008 solution from Jet Propulsion Laboratory (JPL, for example see: http://sideshow.jpl.nasa.gov/mbh/series.html) and the GLOBK solution obtained in this study (Figure 39) in terms of direction and magnitude of the velocities. Estimated velocities from CATREF are listed in Table 12 of Appendix A. The magnitude of the horizontal velocities in the network varies up to 3.5 cm/yr. Variable velocity vectors in terms of magnitude and direction can be noted. Stations on the Somalian plate indicate an interesting feature both in magnitude and direction, the vectors clearly indicate that the Somalian plate moves independently from the Nubian plate. The estimated GNSS station rates for Nubian and Somalian plates are 2.5 and 2.8 cm/yr, respectively. The difference supports current understanding of mantle interaction along the East African Rift System resulting in high seismic activity along the plate boundary.

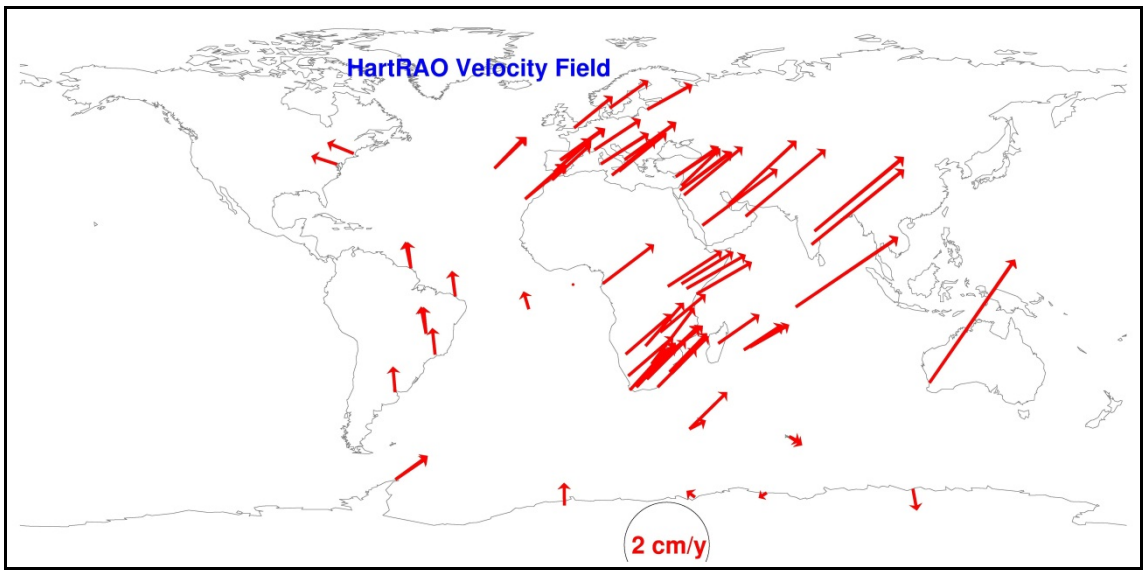


**Figure 51**. Estimated horizontal velocities expressed in ITRF2008. The velocities agree with those derived using the GLOBK software.

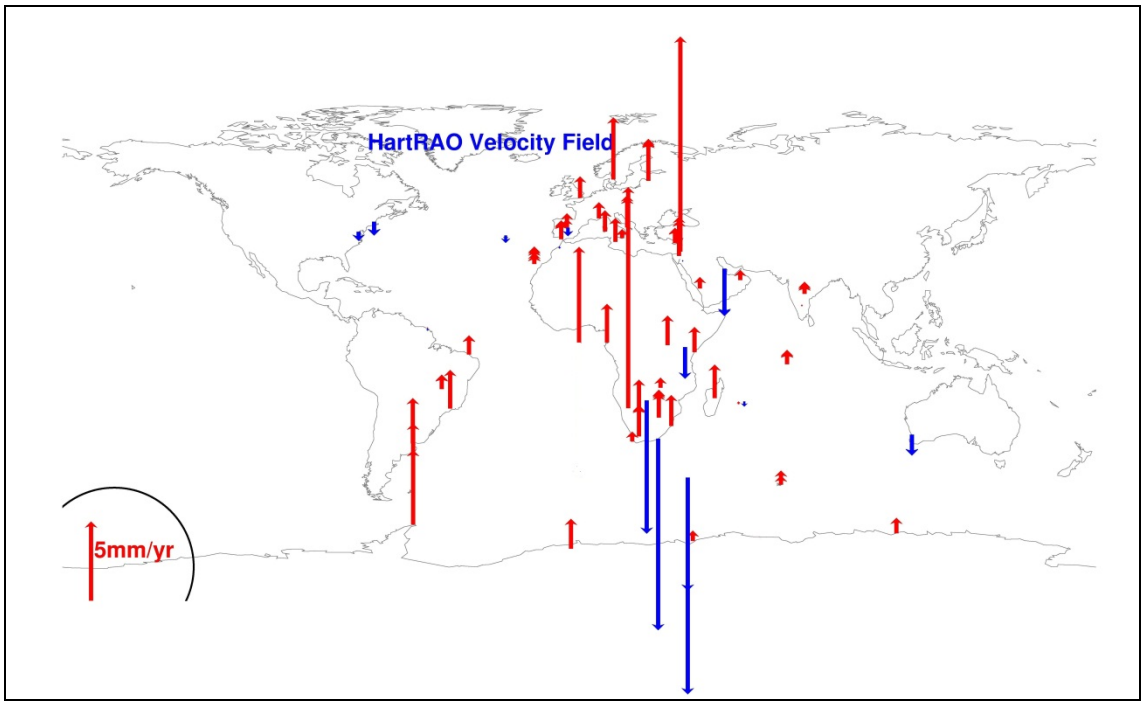


**Figure 52**. Estimated vertical velocity field expressed in ITRF2008. Vertical velocities are associated with high errors. The red arrows indicate upwards movement and blue arrows indicate downwards movement of the GNSS stations.

## 4.5 Concluding remarks

The analyses of GNSS data indicates that most IGS stations are affected by temporal influences, which leads to seasonal, diurnal and sub-diurnal cycles. This results in an increase of daily and longer period RMS values. Statistical evaluation of the combined sub-networks solution indicates an improvement as opposed to an individual solution with short time span network. It was observed that the vertical component contributed higher errors compared with other components. This is due to the fact that the vertical component is highly correlated with atmospheric constituents and is geometrically less constrained.

The GNSS velocities indicate distinctive inter-continental plates or plate boundaries i.e., stations on the Arabian and Somalian plates move independently from stations on the Nubian plate. Even though IGS stations in Africa are too poorly distributed to effectively study neo-tectonic motions, the existing stations provide valuable information about the current local plate motions and no unusual station velocities were observed.

The validity of velocities derived at HartRAO (from this study) was compared against velocities from JPL. A good agreement was obtained with only 1-2 mm/yr deviations in East and North components, while vertical components indicated about 1-3 mm/yr difference between the two solutions.

The results from the VLBI 26 m telescope, MOBLAS-6 and IGS station HRAO using independent techniques indicated good agreement. No significant or obvious vertical motion was found at the HartRAO site. These results confirm that the SDAS software developed at HartRAO produces reliable and high quality results when compared with other independent software packages and techniques. Velocities from GNSS can only be reliable if similar results are obtained from at least two different solutions and in this study, it was illustrated that the HRAO IGS station velocity vectors compare favourably with other techniques. The derived velocity solutions indicated no significant difference between solutions computed from the GLOBK software and CATREF software. Transformation parameters agree well with the ITRF2008.

# CHAPTER 5

## Examples of the application of GNSS velocities to geodynamics

*"It is important to foster individuality for only the individual can produce the new ideas"-Albert Einstein, 1952.*

### 5 Introduction

Plate tectonic processes have played a vital role in shaping our dynamic planet upon which we live. For many years, scientists have been studying the processes underlying the movement of continental plates to enhance their knowledge of plate tectonics (Anderle, 1986). We make use of space geodesy techniques (specifically GNSS stations in this case) to study local neo-tectonics of the African continent and how other plates interact with it, e.g., the Somalian and Arabian plates. We also look at local motion of the proposed Matjiesfontein Observatory site and the Southern Africa plate.

The comprehensive theory of continental drift was first proposed by Alfred Wegener, a German meteorologist, in 1921 (Marshak, 2005). Similarities of the continental shelf margins around the Atlantic Ocean led to the reconstruction of the continental margins (Jacoby, 2001). It was concluded that the continents were once unified landmasses known as supercontinents but over a geological period, they have drifted to their present positions. However, the theory of continental drift remained the subject of controversy and at first few scientists (Holmes, 1928; Du Toit, 1937; Gutenberg, 1930) supported this theory. The controversy was mainly due to insufficient knowledge about the mechanical processes that are responsible for continental drift and very little was known about the mantle at that time (Torge, 1991). Geodetic techniques that could provide near-real time observations of continental plate movement such as GNSS, SLR, DORIS and VLBI were not initially available to be applied to the field of geodynamics. To this end, evidence for continental drifting was firstly derived from studies such as palaeontology, paleoclimatology and paleomagnetism that subsequently led to the development of the global theory of plate tectonics (Jacoby, 2001).

Before the major development of GNSS during 1990's, many researchers in the field of geodynamics used mobile SLR and VLBI instruments to measure crustal

deformation rates precisely (Robaudo, and Harrison., 1993). The mobile systems were mainly used in dedicated campaigns and not in continuous measurements, due to their high operation cost requirements (Torge, 1991). With an increase in GNSS satellite constellation density and GNSS collocation, determination of crustal deformation in 3-D with very high accuracy became feasible for most parts of the Earth (Torge, 2001). Furthermore, Torge (2001) reported that geodynamic modelling requires very high spatial and temporal resolution of the geodetic observations carried out at certain epochs in order to resolve tectonic motions in detail.

## 5.1 Geodynamics of Africa

### 5.2.1 Nubian-Somalian-Arabian Plates

During the late Ordovician (about 445 Ma), the African continent was located at the heart of Gondwanaland, with the South Pole situated off the northern edge of its present location (Bumby and Guiraud, 2005). About 140 Ma ago during the break-up of Gondwana, continental fragments consisting of South America, Africa, Antarctica, India, Madagascar and Australia began to separate. During this process, the African continent nudged northwards away from the South Pole so that it invaded Europe. The African plate remained relatively stable with slow rotation at approximately the same latitude (Burke *et al.* 2003; Bumby and Guiraud, 2005). Other continents such as South America drifted west and Antarctica drifted south (King, 1983) to their present latitudes and longitudes.

Different geological structures formed between the Mesozoic-Cenozoic (250 Ma-0 Ma) periods (Guiraud and Bosworth, 1997; Figure 53). These structures include the East African Rift System (EARS), Central African Rift, and Gulf of Aden, thrust faults along the northern edge of the African continent and other minor structures. These structures are still seismically active (Figure 54; Graham and Brandt, 1999). The seismic data indicate that the eastern part of Africa is highly active compared to the western part.

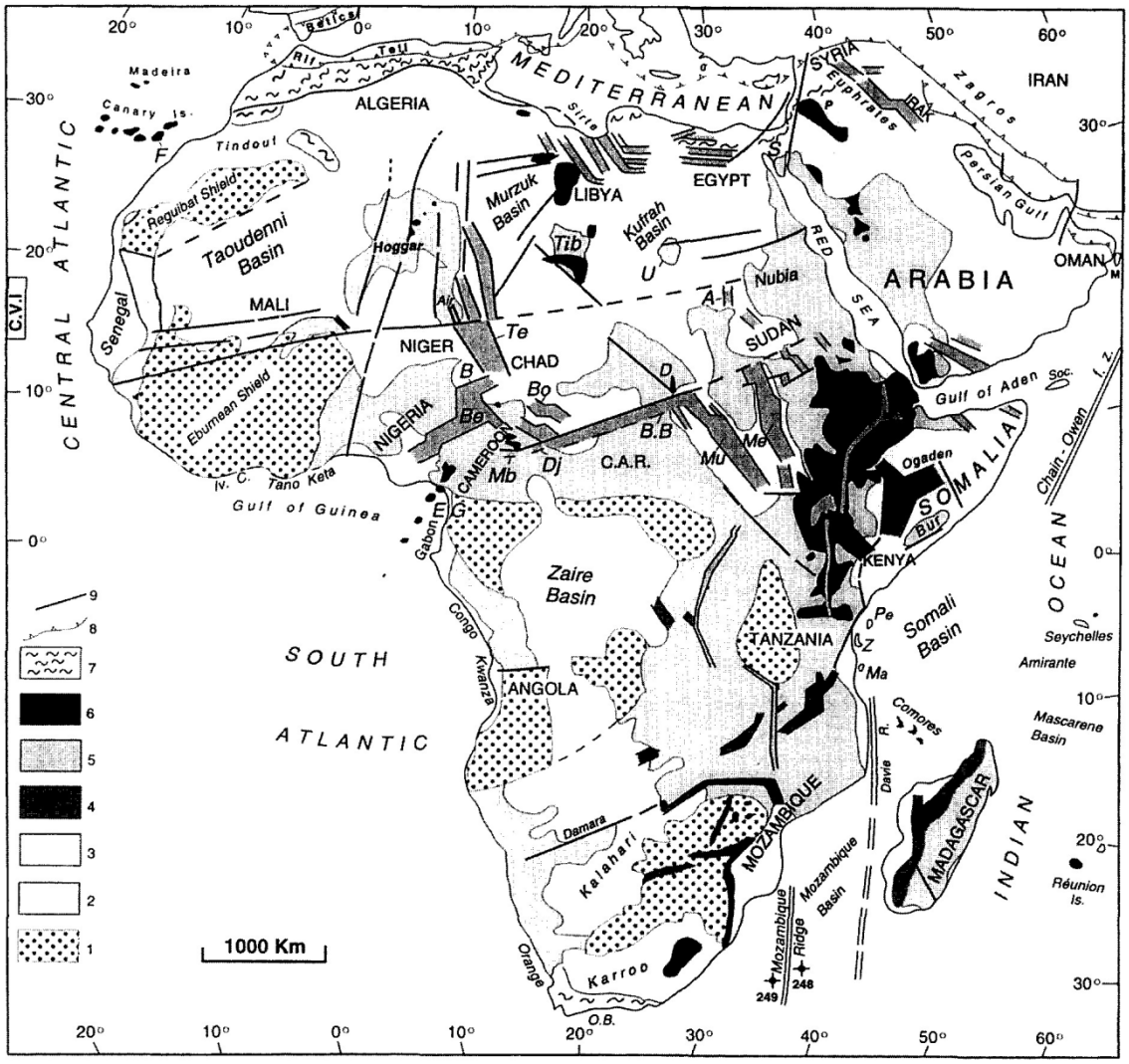


**Figure 53.** Mesozoic-Cenozoic rift-related basins, faulting and magmatism related to the break-up of Gondwana (Guiraud and Bosworth, 1997).

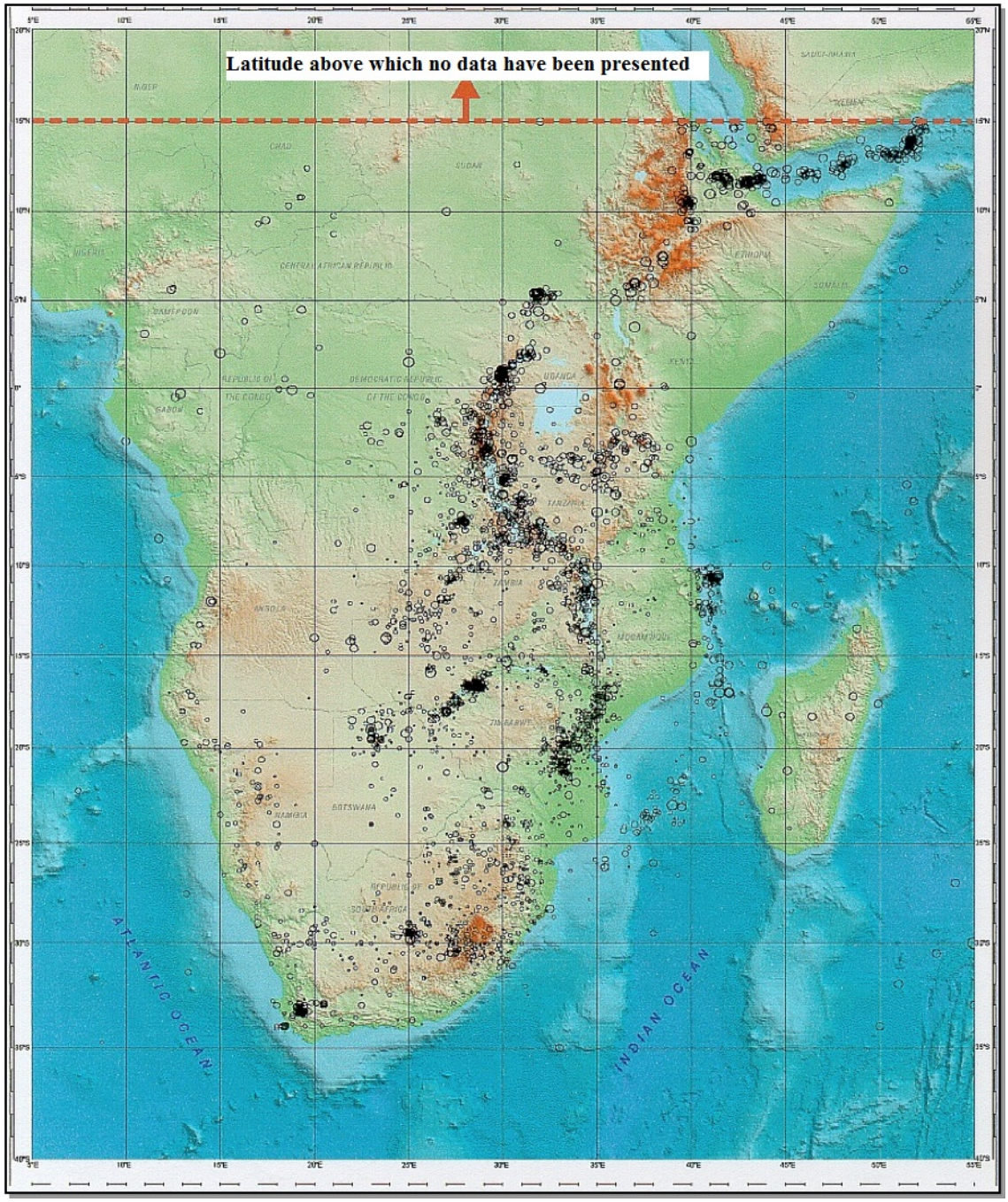


**Figure 54.** Seismicity of sub-Saharan Africa between 1071 and 1996 (Graham and Brandt, 1999).

Using GNSS data from this study, the average calculated rate of station velocities on the Nubian plate is 26.25 ± 0.46 mm/yr and stations on the Somalian plate move at 28.64 ± 0.32 mm/yr. Therefore, stations on the Somalian plate move 2.39 mm/yr faster compared with the Nubian plate. Due to lack of station coverage, the MBAR, RCMN, MAL2 and MOIU stations are used to define the Somalian plate, even though these stations are collocated at different micro-plates such as the Victorian plate for station MBAR. The differential motion between these two plates is indicated by the angular vector of 13.23° between the two groups of stations represented by the Nubian and Somalian plates. The stations on the Arabian plate move at 38.71 ± 0.19 mm/yr i.e., 12.46 mm/yr and 10.07 mm/yr faster compared with the Nubian and Somalian plates, respectively. The angular vectors for Nubian-Arabian plates and Somalian-Arabian plates are 6.92° and 10.07°, respectively (see Table 8 for a summary). Generally, stations on the Nubian-Somalian-Arabian plates indicate interaction which is similar in direction, but independent movement can easily be observed. These results should be considered in terms of the seismic data by Guiraud and Bosworth (1997) presented in Figure 54. The GNSS results clearly indicate differential sub-plate motion delineated by the line of seismic activity.

**Table 8.** Summary of average velocities of Nubian-Somalian-Arabian plates and their associated angular vectors.

| Plates | Average Velocities (mm/yr) | Plate-plate | Angular vectors (deg) |
|---|---|---|---|
| Nubian | 26.25 ± 0.46 | Nubian-Somalian | 13.23 |
| Somalian | 28.64 ± 0.32 | Nubian-Arabian | 6.92 |
| Arabian | 38.71 ± 0.19 | Somalian-Arabian | 10.7 |

This progressive increase of average velocities from the Nubian to Arabian plates indicates mantle interaction along plate boundaries such as the East African Rift System, Red Sea rift and Gulf of Aden rift. Fernandes *et al.* (2004) also illustrated these differences between the Nubian and Arabian plates. This implies that EARS is not an aulacogen i.e., a failed arm of a triple junction of a rift system, it is an independent active rifting system. The DORIS station (DJIB) located at Djibouti area close to the

triple-junction of the Ethiopian Rift, Red Sea and Gulf of Aden measures a local motion of 31.37 mm/yr (see: http://ids-doris.org/network/ids-station-series.html), which is similar to that of the Somalian plate as reported in this dissertation.

### 5.2.2 Southern Africa

South Africa has experienced several earthquakes in the past in different regions, both of natural and anthropogenic origin, e.g., from mining activities. Some of the recorded earthquakes are contained in the South African National Seismological Database (SANSD) and are listed in Table 9 (for the period 1809 to 2005). The SANSD is managed by the Council for Geosciences (CGS). Different programmes have been established to monitor neo-tectonics or seismicity such as the Global Seismic Hazard Assessment Program (GSHAP), which was based on an analysis of the main tectonic features and the correlation with the current seismicity (Singh *et al.* 2009). Nevertheless, because of the large scale of these projects, many structural features on a local scale were not resolved.

The seismotectonic model is currently being developed by Singh *et al.* (2009) and it includes, but is not limited to, fusion of geological mapping, magnetic and gravity surveys, neo-tectonic activity and correlation of seismic data with the above mentioned disciplines. This model will greatly enhance current understanding of neo-tectonics in South Africa.

Space geodesy is slowly growing in South Africa. Currently developing projects include GNSS installations (HartRAO is heavily involved), the SLR and Lunar Laser Ranging (LLR) project destined for installation at Matjiesfontein and the Square Kilometre Array (SKA) project (earmarked for a geophysical observatory at Klerefontein). In order to achieve a high level of understanding of neo-tectonics and to build reliable models to monitor tectonics in South Africa, space geodesy is one of the disciplines that needs to be included in the final integrated model for tectonics.

**Table 9.** A list of earthquakes in the National Database above magnitude 5 for south African regions (Singh *et al.* 2009).

| Year | Month | Day | M | Region |
|---|---|---|---|---|
| 1809 | 12 | 4 | 6.3 | Cape Town Region |
| 1811 | 6 | 2 | 5.7 | Cape Town |
| 1811 | 6 | 19 | 5 | Cape Town |
| 1850 | 5 | 21 | 5 | Grahamstown |
| 1857 | 8 | 14 | 5 | Western Cape |
| 1870 | 8 | 3 | 5 | Harrismith |
| 1899 | 9 | 13 | 5 | Cape Town |
| 1908 | 9 | 26 | 5 | Bloemfontein |
| 1910 | 10 | 21 | 5 | Philipstown |
| 1911 | 11 | 8 | 5 | Windhoek |
| 1912 | 2 | 20 | 6.2 | Koffiefontein |
| 1919 | 10 | 31 | 6.3 | Swaziland |
| 1921 | 10 | 9 | 5 | Tulbagh |
| 1922 | 6 | 23 | 5 | Panbult Siding—Transvaal |
| 1922 | 8 | | 5 | Panbult Siding—Tansvaal |
| 1925 | 10 | 10 | 5 | Leutwein Siding—Nambia |
| 1932 | 8 | 9 | 5 | Grahamstown |
| 1932 | 12 | 31 | 6.3 | Off Cape St. Lucia |
| 1936 | 1 | 12 | 5 | Mooihoek-Swaziland |
| 1936 | 1 | 16 | 5 | Fauresmith (Free State) |
| 1940 | 11 | 10 | 5 | Tzaneen (Transvaal) |
| 1942 | 11 | 1 | 5.5 | Port Shepstone |
| 1950 | 9 | 14 | 6 | Mozambique Channel |
| 1950 | 9 | 30 | 5.5 | Namaqualand |
| 1952 | 1 | 27 | 5 | Sutherland |
| 1952 | 1 | 27 | 5.3 | Sutherland |
| 1952 | 1 | 28 | 5 | Sutherland |
| 1952 | 1 | 28 | 5.4 | Sutherland |
| 1952 | 6 | 9 | 5.5 | Keetmanshoop District (Namibia) |
| 1952 | 9 | 4 | 5 | SWA (Namibia) |
| 1952 | 11 | 8 | 5.2 | SWA (Namibia)—Botswana Border |

| Year | Month | Day | M | Region |
|---|---|---|---|---|
| 1953 | 5 | 1 | 5.8 | Namaqualand |
| 1954 | 2 | 17 | 5.5 | Mozambique |
| 1955 | 1 | 20 | 5.5 | Offshore Mozambique |
| 1955 | 5 | 20 | 5.1 | Fauresmith District (Free State) |
| 1957 | 4 | 13 | 5.5 | Zastron District (Free State) |
| 1963 | 8 | 27 | 5 | Worcester-Ceres |
| 1964 | 6 | 9 | 5 | Luckhoff (Free State) |
| 1966 | 6 | 18 | 5 | Mokhotlong (Lesotho) |
| 1968 | 1 | 12 | 5.5 | Uitenhage |
| 1968 | 1 | 14 | 5 | Sul Do Save Prov (Mozambique) |
| 1969 | 9 | 11 | 5.2 | Heidelberg |
| 1969 | 9 | 29 | 6.3 | Tulbagh |
| 1976 | 12 | 8 | 5.1 | Welkom gold mines |
| 1977 | 3 | 2 | 5.3 | S.W. Cape Province |
| 1977 | 4 | 7 | 5.2 | Klerksdorp gold mines |
| 1979 | 2 | 21 | 5.8 | N. Cape Province SA. |
| 1984 | 1 | 28 | 5.01 | Klerksdorp gold mines |
| 1985 | 5 | 8 | 5.22 | Koffiefontein Region (Free State) |
| 1986 | 10 | 5 | 5.15 | Transkei |
| 1987 | 9 | 30 | 5.04 | Klerksdorp gold mines |
| 1989 | 9 | 29 | 5 | Mandileni Region (Transkei) |
| 1991 | 10 | 31 | 5 | Ceres Area Cape Province |
| 1992 | 12 | 23 | 5.1 | Namibia |
| 1994 | 8 | 20 | 5 | Southern Namibia |
| 1994 | 10 | 30 | 5.1 | Free State gold mines |
| 1994 | 12 | 31 | 5.1 | Brandvlei Region—Northern Cape |
| 1996 | 9 | 15 | 5.1 | Loeriefontein Region |
| 1999 | 4 | 22 | 5.1 | Free State gold mines |
| 2001 | 4 | 6 | 5.2 | Boesmanland Area—N. Cape |
| 2001 | 7 | 31 | 5 | Klerksdorp gold mines |
| 2005 | 3 | 9 | 5.3 | Klerksdorp gold mines |
| 2005 | 10 | 12 | 5.1 | Klerksdorp gold mines |

Seismic data clearly indicate that South Africa is seismically active. The seismological record shows that most parts of South Africa are seismically active (some more than others). Figure 55 depicts earthquakes from magnitude 3 to 6.1 *ML* (Richter scale); different seismic clusters can be seen. Seismic activities around the Wits basin are directly related to blasting in the gold mines. For more information on each cluster refer to (Singh *et al.* 2009).

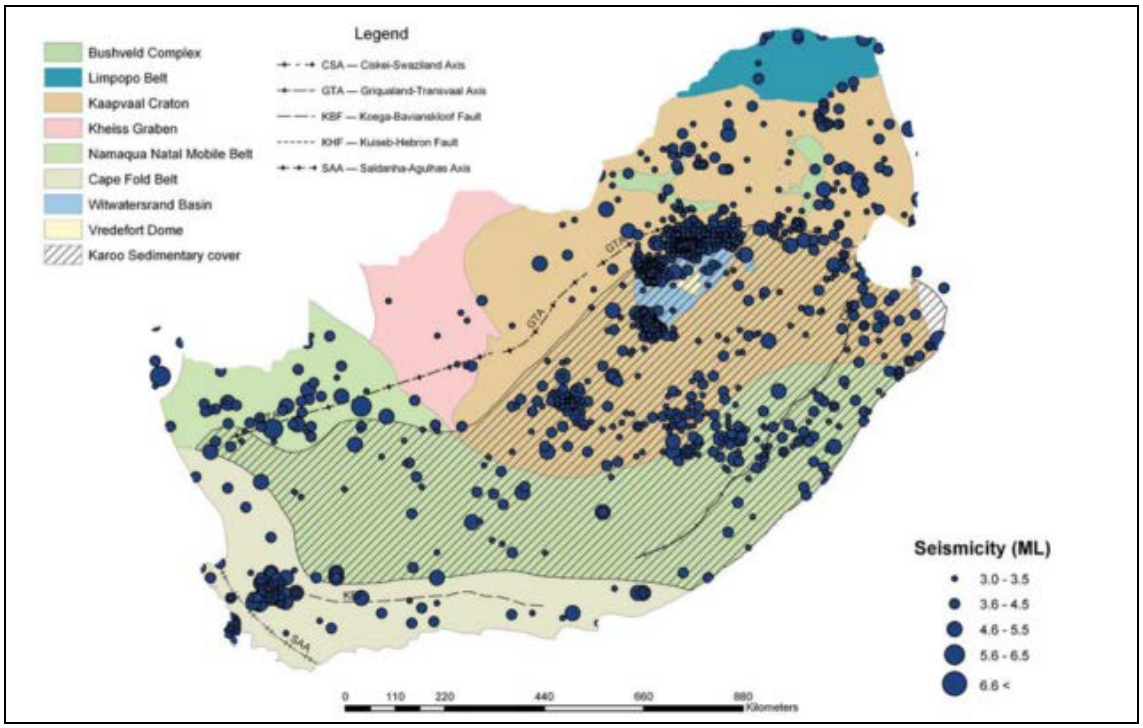


**Figure 55.** Distribution of earthquakes, major structures and geological provinces in South Africa (Source: Nguuri *et al.* 2001 In: Singh *et al.* 2009).

Different studies have been carried out to explore the lithospheric/crustal structure of Southern Africa using different techniques such as geophysics and seismology. Much potential exists to measure local tectonic motion of the crust using space geodesy techniques. Presented in Figure 56 are GNSS velocities for Southern Africa, illustrating the horizontal component, which indicates systematic movement of the crust towards the northeast at a rate of 26.25 ± 0.46 mm/yr. The vertical components of most stations are within error margins and the results are inconclusive.

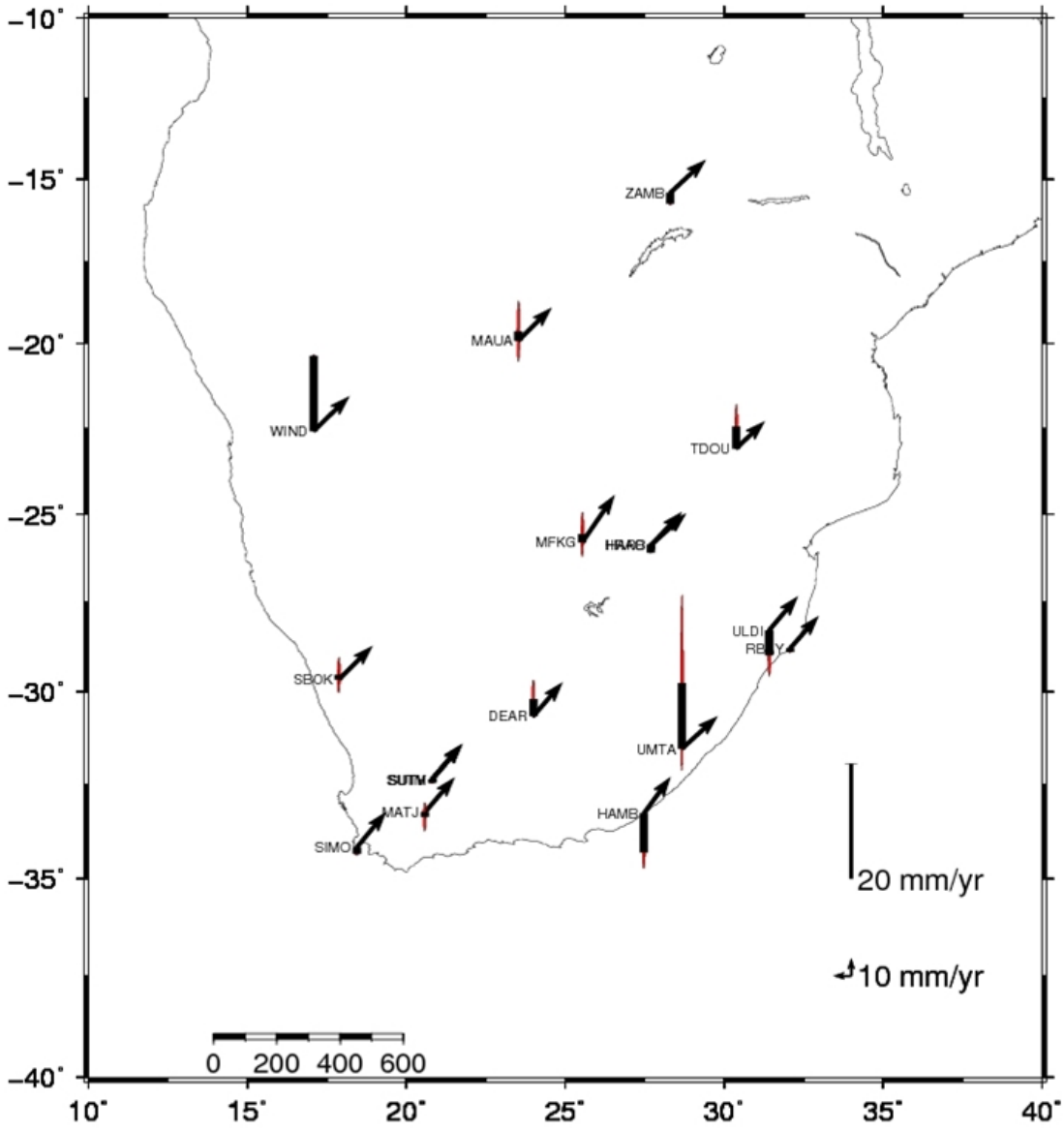


**Figure 56.** Vertical and horizontal velocities plotted at 95% confidence interval for the South African region.

### 5.2.3 Proposed Matjiesfontien observatory site

Matjiesfontein is set to host the SLR/LLR system. The proposed site is located 5 km south of Matjiesfontein in the Great Karoo. This state of the art technology is led by HartRAO of the National Research Foundation (NRF), South Africa. The proposed site resides in the small depression to protect geodetic instruments from radio interference (see Figure 57 and Figure 58). The site underwent extensive investigations, which

include geophysical surveys by utilizing magnetic, electromagnetic and seismic refraction surveys. The site was declared suitable and stable to host geodetic instruments (Combrinck *et al.* 2007).

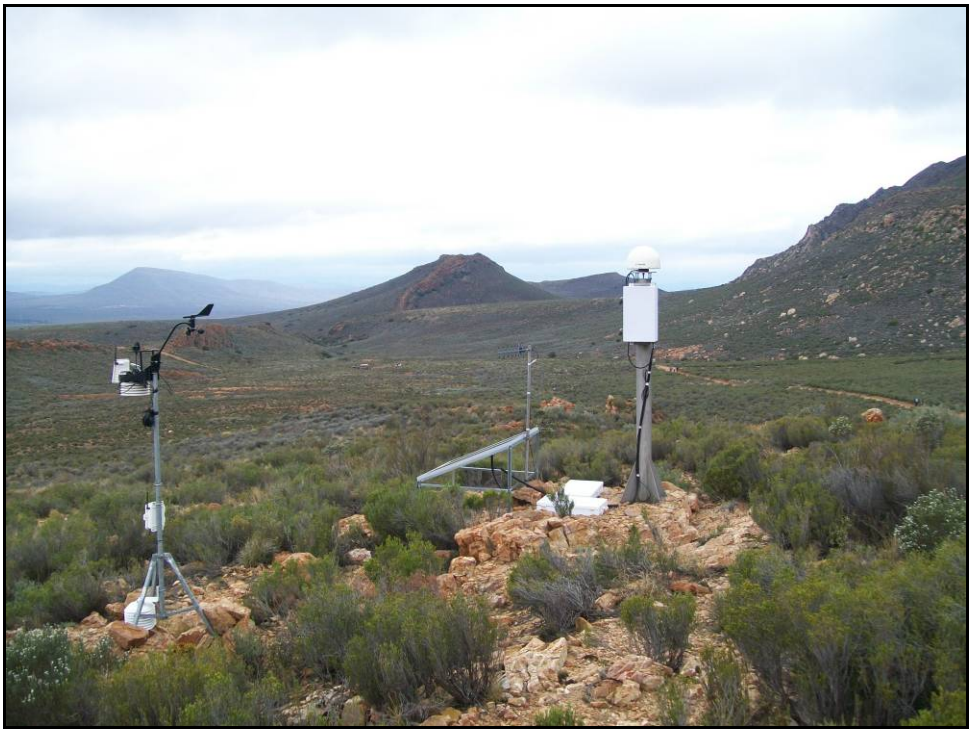

**Figure 57.** Matjiesfontein (MATJ) GNSS station located at the proposed site to host the S/LLR system, on the left is the meteorological instrument; this will be replaced by a MET4 unit in December 2013.


**Figure 58.** Left: Google map of the proposed site. Right: an insert map depicting the location of Matjiesfontein in the Western Cape of South Africa.

The proposed observatory is already equipped with a GNSS station and meteorological station as pictured in Figure 57. A seismic vault was constructed during the first quarter of 2013. The site data were processed together with other stations to investigate any significant tectonic motions on the proposed site. A time-series plot of the station is depicted in Figure 59.

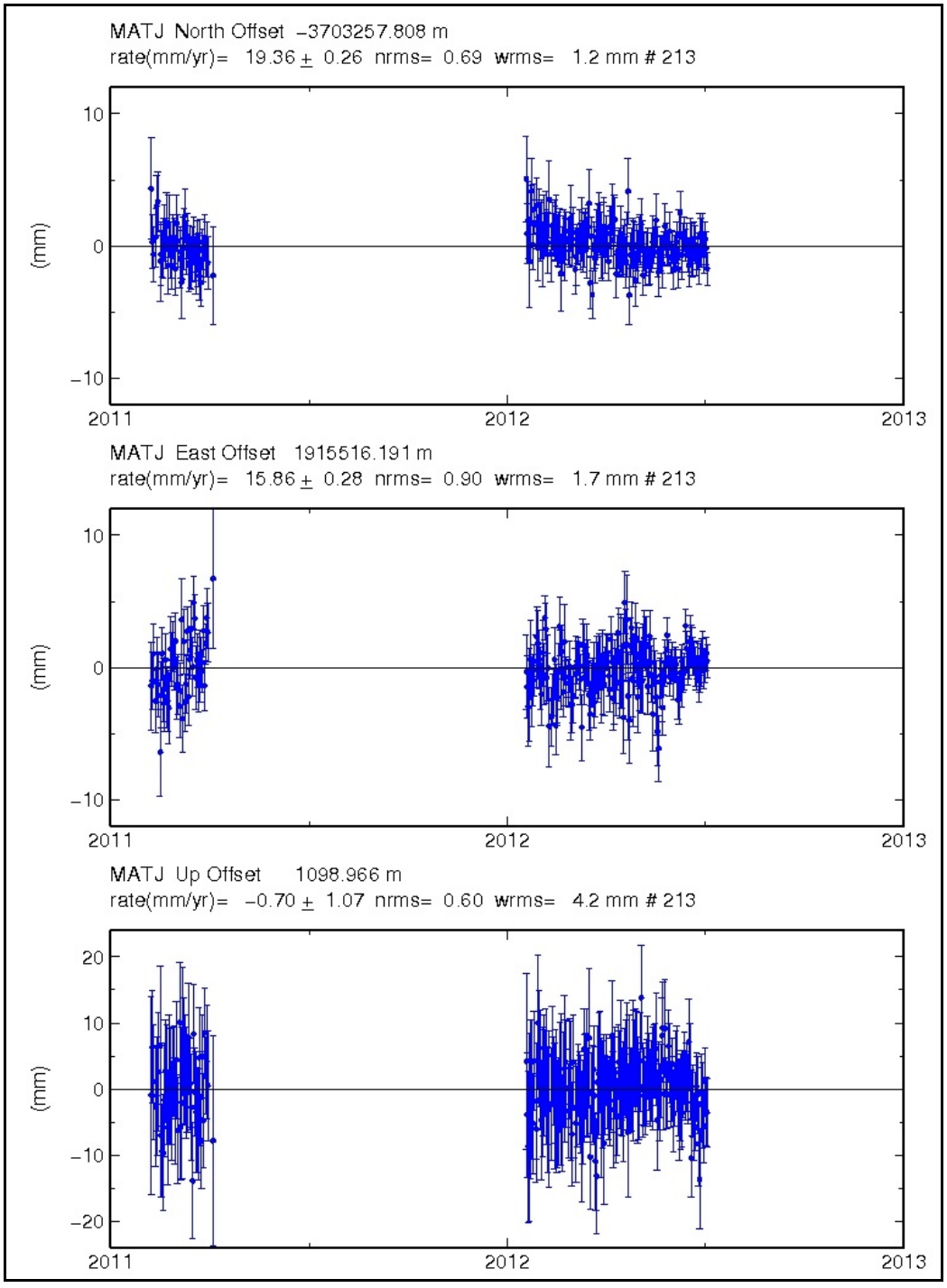


**Figure 59.** Time-series plot for MATJ GNSS station, Great Karoo, South Africa.

Velocities of 19.36 ± 0.26 mm/yr, 15.86 ± 0.28 mm/yr and -0.7 ± 1.07 mm/yr in North, East and Up components, respectively, were obtained. The geodetic site should be stable as bedrock is very shallow and all instruments can be located on bedrock. There is no significant vertical motion that is measured by the MATJ station and the vertical vector is within the error bar. As more data becomes available, conclusive results will be achieved. Monitoring of the vertical component will be required during the process of foundation installation for the S/LLR system as geodetic instruments require a stable foundation. This monitoring will reveal any local motion due to foundation settlement. None is expected; however, as there are no deep soils or soil below bedrock.

The preliminary results obtained to investigate atmospheric and astronomical seeing conditions by Combrinck *et al.* (2007) using a small astronomical refractor (10.8 cm aperture) indicated good seeing conditions ranging between 1-2 arc seconds. These values represent the stability of the atmosphere for carrying out astronomical measurements, the lower the value, the better the seeing conditions for geodetic instruments. Extinction is usually increased by the presence of dust, cloud coverage or smoke particles in the atmosphere. These particles interfere with the light source from a star or reflectors on the Moon or with SLR calibration reflectors on the ground. A series of polar sky plots (Figure 60; Figure 65 of Appendix B) from the MATJ station were utilized to also investigate the atmospheric conditions of the proposed observatory site.

The results indicate that the site is partly affected by water vapour content in the atmosphere that seems to last for not more than four hours of the day. This could be due to partial cloud coverage that occurred around the site on this particular day. This is illustrated by the computed series of polar sky plots from day 90 to 95 of year 2012, where the associated RMS values range from 5.5 mm to 9.4 mm. The results from the investigation by Combrinck *et al.* (2007) are supported by the results obtained from this study in that the sky is mostly clear (rainfall is only about 200 mm per year). The site is stable and shows no significant vertical motion. It is envisaged that as more data become available for this station, a longer time-series and results that are more conclusive will be achieved. A local survey, using purpose-built calibration piers will be done in the future to monitor site stability. This will improve

monitoring of local motion to confirm the local crustal stability of the Matjiesfontein observatory site over time.

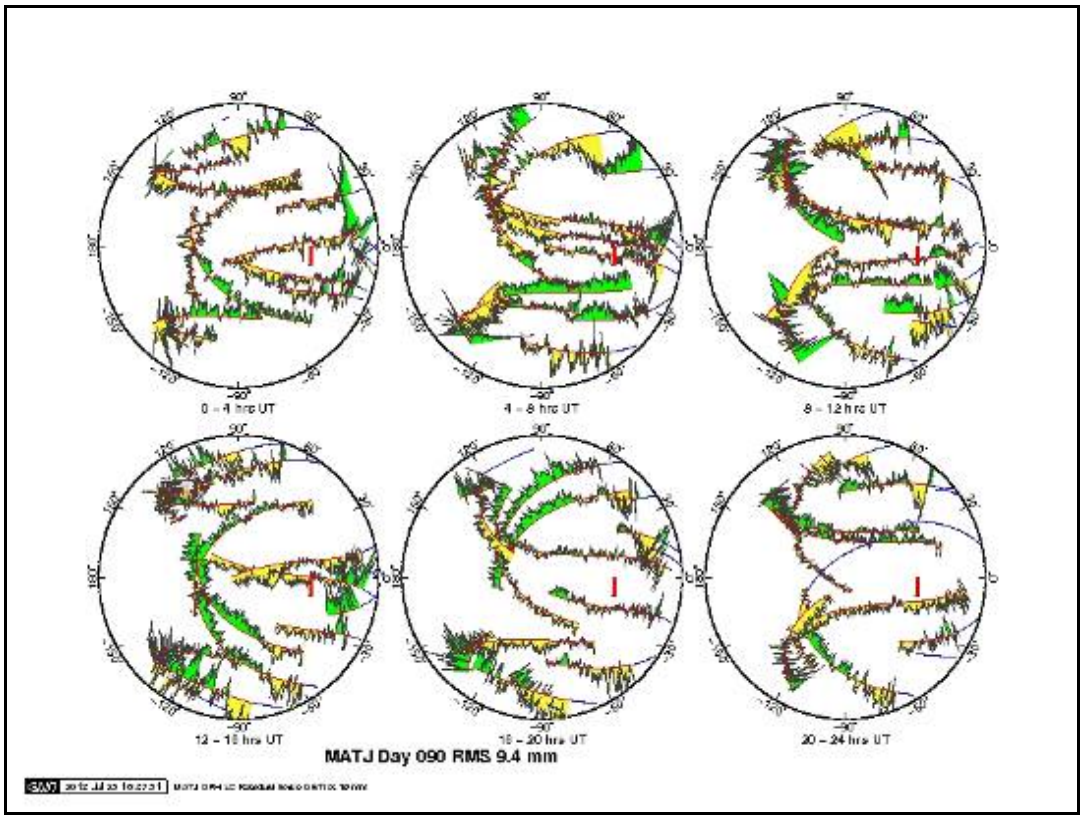


**Figure 60.** Polar sky plots for station MATJ, South Africa, for day 90 of 2012.

## 5.2 Concluding remarks

This study has presented examples of application of the derived GNSS velocities in the framework of geodynamics. The current plate motion interactions of Nubian-Somalian-Arabian plates have been presented. Differential motions of the Nubian and Somalian plate were observed. The results indicate that the Nubian plate is moving at 26.25 ± 0.46 mm/yr, the Somalian plate moves at 28.64 ± 0.32 mm/yr and the Arabian plate moves at 38.71 ± 0.19 mm/yr. The angular velocity vector between the Nubian-Arabian plates and Somalian-Arabian plates are $6.92^{\circ}$ and $10.07^{\circ}$, respectively. The GNSS station (MATJ) located at the proposed Matjiesfontein Observatory site outside Matjiesfontein village indicates that the geodetic site is relatively stable and there is no significant vertical motion measured by MATJ station.

# CHAPTER 6

## Conclusion and recommendations

*"I have not eaten enough of the tree of knowledge, though in my profession I am obligated to feed on it regularly"- Albert Einstein, 1919.*

### 6.1 Summary

Space geodesy is one of the disciplines that contributes uniquely to global society; its applications have grown to such an extent that system Earth is better understood today. The accuracy that space geodesy has reached allows determination of geophysical parameters such as velocities, Earth tides, polar motion and implementation and maintenance of geodetic reference frames. This study has presented a velocity field solution for Africa derived using GNSS stations in ITRF2008 in support of the establishment of AFREF.

The velocities of selected IGS stations processed in this study were compared with their solutions from JPL. Good agreement was achieved with correlation coefficient ($R^2$) values of 0.991, 0.993 and 0.578 in the North, East and Up components, respectively. The obtained differences are thought to be due to a network effect as described by Bruyninx *et al.* (2010) and due to the different processing strategies employed in this study and used by JPL.

Furthermore, the results from the VLBI 26 m telescope, MOBLAS-6 and IGS station HRAO using independent techniques indicated good agreement. No significant or obvious vertical motion was found at the HartRAO site. These results confirm that the SDAS software developed at HartRAO (used to process SLR data by L Combrinck) produces reliable and high quality results when compared with other independent software packages and techniques. The results presented in this thesis compared favourably with current published ITRF2008 velocities.

One of the most important outcomes of the study is the static coordinate solution for AFREF, which was submitted to IGN for combination analysis by Zuheir Altamimi (IGN) as a contribution towards AFREF.

The SINEX file computed from GAMIT as loosely constrained solutions where combined and analysed using the CATREF software. The derived velocity

solution indicated no significant difference between the solution computed from GLOBK. Transformation parameters indicated a good agreement with ITRF2008.

The proposed Matjiesfontein observatory site was found to be relatively stable and no significant vertical motion was observed. This information could be utilized during the process of designing a foundation for the telescope. Figure 61 illustrates the current development of the Lunar Laser Ranger (LLR) at HartRAO; the station will be moved to Matjiesfontein once it is completed.

**Figure 61.** The Lunar Laser Ranger (LLR) is currently being developed at HartRAO (left) and MOBLAS-6 SLR station (right). Once the development is completed, the LLR station will be moved to Matjiesfontein.

Furthermore, this study used GNSS technology to create a colour-enhanced image of velocities of the African plate. It is envisaged that as more stations are added to the sparsely distributed current network, more accurate results and better tectonic models can be derived.

## 6.2 Future work and recommendations

Currently the author is developing a web page that will publish velocity maps and time-series plots similar to those from JPL (see: http://sideshow.jpl.nasa.gov/mbh/series.html) with more focus on the African continent. This will allow easy transfer of information to science communities and to the general public (see Figure 62 and Figure 63). It is recommended that more GNSS stations be installed; especially in the areas above the equator, to increase the density of the current GNSS network. This will ensure that the estimation of geophysical parameters determined from GNSS stations are of good quality. A dedicated analysis centre needs to be established and maintained for continuous processing of GNSS data to monitor inter-continental plate motion in Africa needs. This will ensure that the new reference frame for Africa (AFREF) will be maintained and updated as tectonic plates exhibit differential motions at a particular epoch.

Since HartRAO also focus on training students, the following projects can be used to train students on GNSS. The study area of space geodesy in South Africa has limited number of expertise. Hence, these projects could attract young scientists to specialize also in space geodesy.

- Velocity field for South African sub-continental plates.
- Integrated water vapour for the Southern Hemisphere.
- Noise analysis from GPS data time-series.
- Using GNSS to model strain-stress for the South African sub-continental plates.
- Develop and integrated system (GNSS + Geophysical instruments) to monitor seismic activities in South Africa.
- Install more GNSS stations to increase the current network and upgrade some of the receivers.

# References

1. AFREF: Windhoek Declaration on an African Geodetic Reference Frame, (2002). Viewed 30 January 2011. Available from: http://geoinfo.uneca.org/afref/Reports.htm
2. Agnew, D.C. (1992). The time-domain behaviour of power-law noises. *Geophys. Ress. Lett*, 19, 333-336 pp.
3. Altamimi, Z., Sillard, P and Boucher, C. (2012). CATREF Software: *Combination and Analysis of Terrestrial Reference Frames*. Technical Manual, IGN, France.
4. Altamimi, Z., Collilieux, X. and Metivier, L. (2011). ITRF2008: an improved solution of the international terrestrial reference frame. *J Geod*, DOI 10.1007/s00190-011-0444-4.
5. Altamimi, Z and Collilieux, X. (2009). IGS contribution to ITRF. *J Geod*, 83, 375-383 pp.
6. Altamimi, Z., Sillard, P and Boucher, C. (2007). CATREF software: Combination and analysis of terrestrial references. LAREG, Technical, Institut Géographique National, Paris, France.
7. Altamimi, Z and Boucher, C. (2003). Multi-technique Combination of Time Series of Station Positions and Earth Orientation Parameters. IERS Technical Note, No.30. IGN/ENSG/LAREG/Marne-La-Vallee, France, 102-106 pp.
8. Altamimi, Z. (2002). Discussion on How to Express a Regional GPS Solution in the ITRF, Report on the Symposium of the IAG Sub-commission for Europe (EUREF), Dubrovnik.
9. Anderle, R.J. (1986). Doppler Satellite Measurements and their Interpretation, In: Anderson, A.J and Cazenave, A. Space Geodesy and Geodynamics. *Academic Press*, Landon, 114-165 pp.
10. Andrzej, A., Mariusz, F and Krzysztof, F. (2010). Combining of GNSS solutions from BERNESE and GAMIT Software. EGU General Assembly 2010 held 2-7 May, 2010 in Vienna, Austria, p.4588. Viewed 29 March 2012. Available from: http://adsabs.harvard.edu/abs/2010EGUGA.12.4588A.
11. Bartone, C.P.E. (2006). GNSS Solutions: *will I need a new antenna for the new GPS and Galileo signals? Will one antenna work for both systems?* Inside GNSS (21). Viewed 08 March 2013. Available from: www.insidegnss.com.
12. Bastos, L., Bos, M and Fernandes, R.M. (2010). Deformation and Tectonics: Contribution of GPS Measurements to Plate Tectonics - Overview and Recent Developments. In: Xu, G.

(Ed), Sciences of Geodesy-1: Advances and Future Directions. *Springer-Verlag, Berlin*. 155-180 pp.

13. Bock, Y., Prawirodirdjo, L., Genrich, J.F., Stevens, C.W., McCaffrey, R., Subarya, C., Puntodewo, S.S.O and Calais, E. (2003). Crustal motion in Indonesia from Global Positioning System measurements. Journal of Geophysical Research, 108 (B8).

14. Botai, O.J., Combrinck, L and Rautenbach, C.J.H. (2013). On the global geodetic observing system: Africa's preparedness and challenges. *Acta Astronautica*, 83, 119-124 pp.

15. Bruyninx, C., Altamimi, Z., Becker, M., Craymer, M., Combrinck, L., Combrink, A., Dawson, J., Dietrich, R., Fernandes, R., Govind, R., Herring, T., Kenyeres, A., King, R., Kreemer, C., Lavallée, D., Legrand, J., Sánchez, L., Shen, Z., Sella, G and Woppelmann, G. (2009). Progress of IAG SC1.3 Working Group in Providing a Dense Global Velocity Field Based on GNSS Observations. Poster presented in May 27-30, Florence, Italy. Viewed 14 March 2011. Available from: http://www.epncb.oma.be/IAG/documents/WG_presentations/EUREF200905.pdf

16. Bruyninx, C., Legrand, J., Altamimi, Z., Becker, M., Craymer, M., Combrinck, L., Combrink, A., Dawson, J., Dietrich, R., Fernandes, R., Govind, R., Griffiths, J., Herring, T., Kenyeres, A., King, R., Kreemer, C., Lavallée, D., Sánchez, L., Sella, G., Shen, Z., Santamaría-Gómez, A and Wöppelmann G. (2010).IAG WG SC1.3 on Regional Dense Velocity Fields: First Results and Steps Ahead. "Reference Frames for Applications in Geosciences 2010", IAG Symposia *Series, accepted.* Viewed 20 May 2012. Available from: http://epncb.oma.be/IAG

17. Bruyninx, C., Altamimi, Z., Becker, M., Craymer, M., Combrinck, L., Combrink, A., Dawson, J., Dietrich, R., Fernandes, R., Govind, R., Herring, T., Kenyeres, A., King, R., Kreemer, C., Lavallée, D., Legrand, J., Sánchez, L., Sella, G., Shen, Z., Santamaría-Gómez, A and Wöppelmann, G. (2012). A Dense Global Velocity Field based on GNSS Observations: Preliminary Results, IAG Symposia Series due “Geodesy for Planet Earth”, Springer. International Association of Geodesy Symposia, 136, Part 1, 19-26 pp.

18. Bumby, A.J and Guiraud, R. (2005). The geodynamics settings of the Phanerozoic basins of Africa. *Journal of African Earth Sciences*, 43, 1-12 pp.

19. Burke, K., MacGregor, D.S and Cameron, N.R. (2003). Africa petroleum systems: four tectonic Aces in the past 600 million years. In: Arthur, T.J., MacGregor, D.S., Cameron, N.R. (Eds.), Petroleum Geology of Africa: New Themes and Developing Technologies. *The Geological Society*, London. Special Publication, 207, 21–60 pp.

20. Combrinck, L. (2011). Testing the General Relativity Theory through the estimation of PPN parameters $\gamma$ and $\beta$ using Satellite Laser Ranging data, *South African Journal of Geology*, December 2011, v. 114, p. 549-560, doi:10.2113/gssajg.114.3-4.549.

21. Combrinck, L. (2011). Proposal for the establishment of a Space Geodesy Centre at the University of Pretoria. Presented at the Department of Geography, Geoinformatics and Meteorology, *Version 2*, February 2011, not published.

22. Combrinck, L. (2010). Satellite Laser Ranging. In: Xu, G. (Ed), Sciences of Geodesy-1: Advances and Future Directions. Spriger-Verlag, Berlin. 302-336 pp.

23. Combrinck, W.L and Chin, M. (2001). IGS Stations: Stations and Regional Issues. *Phys. Chem. Earth (A)*, 26, (6-8), 539-544 pp.

24. Combrinck, L. (2009). MOBLAS6 Satellite Laser Ranger: Technology and Applications of Data, Proceedings of the IEEE International Geoscience & Remote Sensing Symposium: Earth observation, origins to applications, July 12-17, 2009, Cape Town, South Africa. IEEE, 2009. 4 p. IEEE Catalog No.: CFP09IGA-CDR ISBN: 978-1-4244-3395-7 Library of Congress: 2008910215.

25. Combrinck, L. (2000). Hartebeesthoek Radio Astronomy Observatory (HartRAO), In: IGS Data Center Reports, IGS 2000 Technical Report. Viewed 01 February 2011, Available from: igscb.jpl.nasa.gov/igscb/resource/pubs/00_tec/2000_techreports.pdf

26. Combrinck, W.L. (1993). Space Geodesy at HartRAO. Viewed 24 May 2012. Available from: www.hartrao.ac.za/geodesy/figtalk.ps.gz.

27. Combrinck, L., Fourie, C.J.S., Croukamp, L and Saunders, I. (2007). Report on preliminary geotechnical and tropospheric site investigation for a proposed space geodetic observatory near Matjiesfontein in the Great Karoo, South Africa. *Journal of Geology*, 110, 225-234 pp., doi:10.2113/gssajg.110.2/3.225.

28. Combrinck, L and Suberlak, V. (2007). Earth-tide as parameter of crustal motion to correction for SLR station displacement. *South African Journal of Geodesy*. 110. p 203-210.

29. Combrink, A.Z.A., Combrinck, W.L. and Moraal, H. (2004). Near real-time detection of atmospheric water vapour using the SADC GPS network. *SA. J. Science*. 100, pp.436-442.

30. DeMets, C., Gordon, R.G and Argus, D.F. (2010). Geologically current plate motions. *Geophys. J. Int.*181, 1-80 pp.

31. Degnan, J.J. (1985). Satellite Laser Ranging: Current status and further prospects. IEEE Trans. Geosci. Remote Sens., GE-23, 389-413 pp.

32. DeMets, C., Gordon, R.G., Argus, D.F and Stein, S. (1990). Current plate motions. *Geophys. J. Int*.101, 425-478 pp.

33. DMA (Defense Mapping Agency). (1983). Geodesy for the Layman, DMA Technical Report 80-003, pp. 29-39.

34. Dodo, J.D and Idowu, T.O. (2010). Regional Assessment of the GPS Tropospheric Delay Model on the African GNSS Network. *Journal of Emerging Trends in Engineering and Applied Science*, 1 (1), 113-121 pp.

35. Dong, D., Herring, T.A. and King, R.W. (1998): Estimating regional deformation from a combination of space and terrestrial geodetic data, *J. Geod.*, 72, 200-214 pp.

36. Drewes, H., Hornik, H., Ádám, J and Rózsa S. Eds. (2008). The geodesist handbook. (2008). *Journal of Geodesy, Springer*, 82 (11), 661 – 846 pp.

37. Drewes, H and Hornik, H. Eds. (2005). International Association of Geodesy (IAG): IAG-Commission 1 – Reference Frames. Bulletin No. 19, Mid-Term Report 2005. Viewed 17 May 2012. Available from: http://www.iag aig.org/attach/9316bd52b9894897de444a340660ae5f/commission1.pdf

38. Du Toit, A.L. (1937). Our Wandering Continents. Oliver & Boyd, London.

39. Erdogan, S., Sahin, M., Tiryakioglu, I., Gulal, E and Telli, A.K. (2009). GPS velocity and strain rate fields in Southwest Anatolia from Repeated GPS Measurements. Sensor, 9, 2017-2034 pp.

40. Estey, L. (2011). TEQC. Accessed: 20 September 2011, last update: 13 September 2001. Available from: http://facility.unavco.org/software/teqc/teqc.html#executables

41. Feigl, K.L., Agnew, D.C., Bock, Y., Dong, D., Donnellan, A., Hager, B.H., Herring, T.A., Jackson, D.D., Jordan, T.H., King, R.W., Larsen, S., Larson, K.M., Murry, M.H., Shen, Z and Wedd, F. (1993). Space geodetic measurement of crustal deformation in Central and Southern California, 1984-1992. *Journal of Geophys res*, 98(21), 677-21,712 pp.

42. Fernandes, R.M.S., Ambrosius, B.A.C., Noomen, R., Bastos, L., Combrinck, L., Miranda, J.M and Spakman, W. (2004). Angular velocities of Nubia and Somalia from continuous GPS data: implications on present-day relative kinematics. *Earth and planetary Science, Letters*, 222, 197-208 pp.

43. Graham, G and Brandt, M.B.C. (1999). Seismicity of sub-Saharan Africa (1071-1996) (1:10 000 000 seismic map). Council for Geoscience, Pretoria, South Africa.

44. Grejner-Brezezinska, D.A. (1995). Analysis of GPS Data Processing Techniques: In Search of Optimized Strategy of Orbit and Earth Rotation Parameters Recovery. Report No.432,

Department of Geodetic Science and Surveying, the Ohio State University, Columbus, Ohio 1247-4321- pp.

45. Gutenberg, B. (1930). Hypotheses on the development of the E. J. Wash. Acad. Sci. 20, 17–25 pp.

46. Gurtner, W and Neil, R.E. (1994).IGS: Densification of the IERS Terrestrial Reference Frame through Regional GPS Network: Position Paper 3, Network Operations, Standards and Data Flow Issues. Workshop Proceeding, Novermber 30 - December 02, viewed: 2011 October 04. Available from: ftp.igs.org/igs/resources/pubs/zumberge_94.pdf

47. Guiraud, R and Bosworth, W. (1997). Senonian basin inversion and rejuvenation of rifting in Africa and Arabia: synthesis and implications to plate-scale tectonics. *Tectonophysics*, 282, 39–82 pp.

48. Herring, T. A., (1997). GLOBK: Global Kalman Filter VLBI and GPS analysis program, v. 4.1 Mass. Inst. of Technol., Cambridge.

49. Herring, T.A., King, R.W and Mc Clusky, S.C. (2010). Introduction to GAMIT/GLOBK. Release 10.4, viewed 25 March 2011. Available from: http://www-gpsg.mit.edu/~simon/gtgk/

50. Herring, T.A., Altamimi, Z., Plag, H.P and Poli, P. (2009). The future Geodetic Reference Frame. Plag, H.P and Pearlman, M. (Eds). Global Geodetic Observing System: Meeting the Requirements of a Global Society on a Changing Planet in 2020. *Springer*, London, New York. 225-232 pp.

51. Hofmann-Wellenhof, B., Lichtenegger, H and Collins, J. (1992). GPS: Theory and Practice. *Springer-Verlag Wien*, New York, -261 pp.

52. Holmes, A. (1928). Radioactivity and Earth movements. *Trans. Geol. Soc*. Glasgow 18, 559–606 pp.

53. Hopfield, H.S. (1969). "Two-quartic tropospheric refractivity profile for correcting satellite data."*Journal of Geophysical Research*, Vol. 74, No. 18, 4487-4499 pp.

54. Iliffe, J.C. (2000). Datums and map projections for remote sensing, GIS and Surveying. *Whittle Publishing*, Boca Raton.

55. Jacoby, W.R. (2001). Successes and failures of Geodynamics: from past to future. *Journal of Geodynamics*, 32, 3-27 pp.

56. Jin, S.G. (2003). Global plate tectonic motions from GPS measurements. Ph.D. dissertation, Shanghai Observatory, Chinese Academy of Sciences.

57. Kahmen, H and Faig, W. (1988). Surveying. *Walter de Gruyter*. Berlin, 477- 492 pp.

58. Kaiser, A., Reicherter, K., Hubsher, C and Gajewski, D. (2005). Variation of the present-day stress field within the North German Basin-insights from thin FE modelling based on residual GPS velocities. *Tectonophysics*, 397, 55-72 pp.

59. Kamamia, M. (2004). AFREF establishment of a common and modern African reference frame. Presented during the 5th AARSE International Conference held at UNON HQs, Nairobi, Kenya 18-2nd October 2004. Viewed 20 June 2011. Available from: http://geoinfo.uneca.org/afref

60. Kendrick, E., Bevis, M.G., Smalley, R and Brooks, B.A. (2001). An integrated crustal velocity field for the central Andes. *Geochem. Geophys, Geosyst*, 2, 10.1029/2001GC000191.

61. King, L.C. (1983). Wandering Continents and Spreading Sea Floor on an Expanding Earth, *Wiley-Interscience*, New York, -14 pp.

62. King, R. W. and Bock, Y. (1995): Documentation of the GAMIT GPS analysis software v. 9.4, Mass. Inst. of Technology and Scripps Inst. of Oceanography.

63. Komjathy, A. (1997). Global Ionospheric Total Electron Content Mapping Using the Global Positioning System. Ph.D. dissertation, Department of Geodesy and Geomatics Engineering Technical Report No. 188, University of New Brunswick, Fredericton, New Brunswick, Canada, 136 pp.

64. Kouba, J. (2009). A guide to using international GNSS service (IGS) products. Viewed 31 October 2011. Available from: http://igscb.jpl.nasa.gov/components/usage.html

65. Kovalevsky, J., Mueller, I.I and Kolaczek, B. (Eds). (1989). Reference Frames in Astronomy and Geophysics. *Kluwer Academic Publishers*, Dordrecht. Vol: 154, -241 pp.

66. Lambeck, K. (1988). Geological Geodesy. *Oxford, Clarendon press*, 102-234 pp.

67. Ma, C., Jee, G.I., MacGougan, G., Lachapelle, G., Bloebaum, S., Cox, G., Garin, L and Shewfelt, J. (2001). GPS Signal Degradation Modeling. GPS01, Session C2, Salt Lake City, September 11-14. Viewed 17 May 2011. Available from:

http://0-plan.geomatics.ucalgary.ca.innopac.up.ac.za/papers/01gpscma.pdf

68. Marshak, S. (2005). Earth: Portrait of a planet. 2nd edition, *W.W. Norton & Company*, New York, -25 pp.

69. McClusky, S., Reilinger, R., Mahmoud, S., Sari, B.D and Tealeb. (2003). GPS constraints on Africa (Nubia) and Arabia plate motions. *Geophys. J. Int*. 155, 126-138 pp.

70. Moeketsi, D.M., McKinell, L.A and Combrinck, W.L. (2009). Validation of University of New Brunswick Ionospheric Modeling Technique with ionosonde TEC estimation over South Africa. *J. Adv. Space Res*. 44, 725-735, doi:10.1016/j.asr.2008.07.

71. Nguuri, T., Gore, J., James, D.E., Webb, S.J., Wright, C.T., Zengeni, G., Gwavava, O., Snoke, J.A and Kaapvaal Seismic Group (2001). Crustal structure beneath Southern Afr*ica and its impli*cations for the formation and evolution of the Kaapvaal and Zimbabwe cratons. Geophysical Research Letters 28 (13), 2,501–2,504 pp.

72. Nilforoushan, F., Masson, F., Vernant, P., Vigny, C., Martinod, J., Abbassi, M., Nankali, H., Hatzfeld, D., Bayer, R., Tavakoli, F., Ashtiani, A., Doerflinger, M., Deagnieres, M., Collard, P and Chery, J. (2003). GPS network monitors the Arabi a-Eurasia collision deformation in Iran. *Journal of Geodesy*, 77, 411-422 pp.

73. Pavlis, E.C. (2010). Satellite Laser Ranging (SLR) and Applications. Last modified date, Thursday, August 12, 2010. Available at: http://ilrs.gsfc.nasa.gov/.

74. Perez, J.A.S., Monica, J.F.G and Chaves, J.C. (2003). Velocity field estimation using GPS precise point positioning: The South America Case. *Journal of Global Positioning System*, 2 (2), 90-99 pp.

75. Plag, H.P., Beutler. G., Gross. R., Herring. T.A., Rizos. C., Rummel. R., Sahagian. D and Zumberge, J. (2009a). Introduction. Plag, H,-P and Pearlman, M. (Eds). Global Geodetic Observing System: Meeting the Requirements of a Global Society on a Changing Planet in 2020. *Springer*, London, New York. 1-13 pp.

76. Plag, H.P., Altamimi. Z., Bettadpur. S., Beutler. G., Beyerle. G., Cazenave. D., Crossley. D., Donnellan. A., Forsberg. R., Gross. R., Hinderer. J., Komjathy. A., Ma. C., Mannucci. J., Noll. C., Nothnagel. A., Pavlis. E., Pearlman. M., Poli. P., Schrieber. U., Senior. K., Woodworth. P., Zerbini. S and Zuffada. C. (2009b). The goals, achievements, and tools of modern geodesy. Plag, H,-P and Pearlman, M. (Eds). Global Geodetic Observing System: Meeting the Requirements of a Global Society on a Changing Planet in 2020. *Springer*, London, New York. 15-88 pp.

77. Rebischung, P., Griffiths, J., Ray, J., Schmid, R., Collilieux, X and Garayt, B. (2012). IGS08: the IGS realization of ITRF2008. *GPS Solut*, 16, 483-494 pp, DOI 10.1007/s10291-011-0248-2.

78. Robaudo, S and Harrison. C.G.A. (1993). Plate Tectonics from SLR and VLBI Global Data. Smith, D, E and Turcotte, D.L (Eds): Contributions of Space Geodesy to Geodynamics: Crustal Dynamics, *Geodynamics*, (23), 51-71 pp.

79. Rodrigues, E.P. (2007). Estimation of Crustal Vertical Movements Due To Atmospheric Loading Effects By GPS Observation. Revista Brasileira de Geofísica, 25(1), 45-50 pp.

80. Rothacher, M., Beutler, D., Behrend, D., Donnellan, A and Hinderer, J. (2009). The future Global Geodetic Observing System. Plag, H.P and Pearlman, M. (Eds). Global Geodetic

Observing System: Meeting the Requirements of a Global Society on a Changing Planet in 2020. *Springer*, London, New York. 237-270 pp.

81. Seeber, G. (1993). Satellite Geodesy. *Walter de Gruyter*, Berlin, -305 pp.
82. Singh, M., Kijko, A and Durrheim, R. (2009). Seismotectonic Models for South Africa: Synthesis of Geoscientific Information, Problems, and the Way Forward. *Seismological Research Letter*, 80 (1), doi: 10.1785/gssrl.80.1.71.
83. Smith, M.A. (1964). Laser Tracking Success. Published in Flight International, Chief editor M.A. Smith, Number 2908, Vol. 86.
84. Sovers, O.J., Thomas, J.B., Fanselow, J.L., Cohen, E.J., Purcel, Jr. G.J., Rogstad, D.H., Skjerve. L.J and Spitzmesser. D.J. (1984). Radio interferometric determination of intercontinental baselines and Earth orientation utilizing deep space network antennas: 1971-1980. *J. Geophys. Res*, 89 (7), 597-7,607 pp.
85. Stebler, Y. (2008). GPS/INS Integrity in Airborne Mapping. Published master's thesis, Swiss Federal institute of Technology, Lausanne, Geodetic Engineering Laboratory. Viewed 06 May 2011. Available from http://infoscience.epfl.ch/record/128436/files/20080711_GPSINSIntegrityALS.pdf
86. Stein, S. (1993). Space Geodesy and Plate Motions. Smith, D, E and Turcotte, D.L (Eds): Contributions of Space Geodesy to Geodynamics: Crustal Dynamics, *Geodynamics*, (23), 5-20 pp.
87. Thomas, J.B., Fanselow, J.L, MacDoran, P.F., Skjerve. L.J., Spitzmesser. D.J and Fliegel. H.F. (1976). A demonstration of an independent-station radio interferometry system with 4-cm precision on a 16-km baseline. *J. Geophys. Res.*81, 995-1005 pp.
88. Torge, W. (1991). Geodesy. 2nd edition. *Walter de Gruyter*, Berlin *GmbH & Co. KG*, -127 pp.
89. Torge, W. (2001). Geodesy. 3nd edition. *Walter de Gruyter GmbH & Co. KG*, Berlin, -120 pp.
90. Tranquill, J.M. (1988). The experimental study of global positioning satellite antenna/backplane configurations. Contract Rep. NASA/Jet Propulsion Lab, Contract 957959, Radiating Syst. Res. Lab, Univ. New Brunswick, Fredericton, Canada.
91. Wells, D. (1986).Guide to GPS Positioning. Canadian GPS Association, *New Brunswick Graphics Services*, Canada,-11.12 pp.
92. Weston, N.D and Schwieger, V. (2010). Cost Effective GNSS Positioning Techniques. FIG Commission 5 publications. Viewed 29 September 2011. Available at www.fig.net/pub/figpub/pub49/figpub49.pdf

93. Wonnacott, R., Fernandes, R.M.S., Combrinck, L., Farah, H and Nonguierma, A. (2010). The African Reference Frame (AFREF), Presented at IAG Reference Frames for Applications in Geosciences REFAG2010, Paris, 5 October 2010.

94. Wonnacott, R. (2005). The African Geodetic Reference Frame (AFREF) project. Viewed 04 October 2011. Available from http://geoinfo.uneca.org/afref/

95. Yang, M. (1995). New GPS Measurement Modelling Techniques of Orbit Determination and precise Kinematic Positioning. Report No. 431, Department of geodetic Science and Surveying, The Ohi State University, Columbus, 4321-1247 pp.

96. Yu, S.B., Chen, H.Y and Kuo, L.C. (1997). Velocity field of GPS stations in the Taiwan area. Tectonophysics, 274, 41-59 pp.

# **Appendix A:** Tables

**Table 10.** Comparison of GNSS velocities derived at HartRAO and from the Jet Propulsion Laboratory (JPL; http://sideshow.jpl.nasa.gov/mbh/series.html).

| | ***JPL (mm/yr)*** | | | | | | ***HARTRAO (mm/yr)*** | | | | | |
|---|---|---|---|---|---|---|---|---|---|---|---|---|
| **Site** | **North** | **±** | **East** | **±** | **Up** | **±** | **North** | **±** | **East** | **±** | **Up** | **±** |
| **ASC1** | 11 | 0.005 | -5.213 | 0.005 | -0.557 | 0.021 | 8.89 | 0.27 | -5.52 | 0.36 | -0.98 | 1.15 |
| **BAHR** | 30.255 | 0.004 | 31.464 | 0.004 | 0.033 | 0.015 | 31.01 | 0.1 | 29.36 | 0.12 | 0.05 | 0.4 |
| **BRFT** | 13.11 | 0.011 | -4.537 | 0.012 | -0.669 | 0.049 | 11.33 | 0.03 | -4.41 | 0.03 | -1.26 | 0.11 |
| **CAS1** | -9.9 | 0.004 | 1.828 | 0.003 | 1.648 | 0.012 | -10.38 | 0.01 | 1.34 | 0.01 | -0.7 | 0.03 |
| **CHPI** | 12.36 | 0.005 | -3.904 | 0.005 | -0.052 | 0.019 | 12.54 | 0.02 | -3.44 | 0.02 | 1.38 | 0.07 |
| **GRAS** | 16.07 | 0.004 | 20.407 | 0.003 | 0.196 | 0.013 | 15.65 | 0.01 | 20.79 | 0.01 | -0.38 | 0.03 |
| **HALY** | 22.88 | 0.03 | 26.825 | 0.027 | 0.213 | 0.118 | 23.37 | 0.03 | 26.57 | 0.03 | -1.96 | 0.11 |
| **HARB** | 18.5 | 0.003 | 17.727 | 0.003 | -0.045 | 0.013 | 18.38 | 0.01 | 16.9 | 0.01 | -0.65 | 0.04 |
| **HERS** | 16.56 | 0.004 | 16.764 | 0.003 | -0.05 | 0.013 | 15.86 | 0.02 | 14.76 | 0.02 | -0.81 | 0.05 |
| **HRAO** | 18.05 | 0.01 | 17.889 | 0.01 | -0.618 | 0.041 | 17.62 | 0.01 | 19.59 | 0.01 | -1.29 | 0.03 |
| **KERG** | -2.3 | 0.008 | 4.826 | 0 | 1.243 | 0.024 | -2.37 | 0.01 | 5.95 | 0.01 | -2.11 | 0.04 |
| **KOUR** | 13.33 | 0.003 | -4.272 | 0.003 | 0.249 | 0.011 | 12.59 | 0.02 | -4.11 | 0.02 | -0.25 | 0.06 |
| **LAMP** | 18.54 | 0.004 | 19.722 | 0.004 | 0.444 | 0.015 | 17.47 | 0.13 | 18.88 | 0.13 | 2.09 | 0.48 |
| **LPGS** | 11.76 | 0.004 | -1.104 | 0.003 | 2.42 | 0.016 | 11.63 | 0.02 | -2.82 | 0.02 | 1.89 | 0.07 |
| **MAL2** | 16.02 | 0.016 | 26.189 | 0.019 | 0.775 | 0.068 | 15.16 | 0.1 | 24.14 | 0.11 | 3.67 | 0.41 |
| **NKLG** | 18.92 | 0.005 | 22.258 | 0.006 | 0.563 | 0.023 | 18.9 | 0.02 | 22.13 | 0.02 | 0.06 | 0.07 |
| **NOT1** | 19.72 | 0.003 | 21.238 | 0.003 | -0.703 | 0.012 | 18.99 | 0.01 | 20.92 | 0.01 | -1.2 | 0.04 |

| | | | | | | | | | | | | |
|---|---|---|---|---|---|---|---|---|---|---|---|---|
| **OHI2** | 10.63 | 0.004 | 14.581 | 0.003 | 4.385 | 0.013 | 11 | 0.02 | 14.2 | 0.02 | 4.97 | 0.04 |
| **OHI3** | 9.79 | 0.005 | 14.256 | 0.004 | 3.827 | 0.016 | 11 | 0.02 | 14.2 | 0.02 | 4.97 | 0.04 |
| **ONSA** | 14.69 | 0.003 | 17.057 | 0.002 | 2.893 | 0.008 | 13.9 | 0.02 | 16.93 | 0.02 | 2.65 | 0.04 |
| **PDEL** | 16.08 | 0.007 | 12.452 | 0.005 | -1.681 | 0.021 | 16.23 | 0.01 | 12.61 | 0.02 | -1.92 | 0.04 |
| **RABT** | 17.77 | 0.007 | 16.073 | 0.006 | -0.47 | 0.0024 | 17.22 | 0.01 | 16.06 | 0.01 | -2.25 | 0.04 |
| **RAMO** | 19.39 | 0.005 | 23.224 | 0.005 | 1.273 | 0.018 | 19.19 | 0.01 | 23.82 | 0.01 | 0.39 | 0.04 |
| **RBAY** | 17.6 | 0.006 | 16.473 | 0.006 | 0.117 | 0.025 | 17.77 | 0.02 | 15.62 | 0.02 | -0.58 | 0.07 |
| **REUN** | 11.49 | 0.007 | 18.546 | 0.007 | -0.765 | 0.029 | 12.44 | 0.02 | 16.23 | 0.02 | -5.13 | 0.08 |
| **SIMO** | 19.41 | 0.008 | 16.607 | 0.008 | 0.003 | 0.033 | 19.58 | 0.03 | 16.08 | 0.03 | -1.1 | 0.1 |
| **SUTH** | 18.79 | 0.005 | 16.991 | 0.005 | -0.128 | 0.018 | 19.36 | 0.01 | 16.46 | 0.01 | -0.51 | 0.03 |
| **SUTM** | 19.26 | 0.004 | 17.215 | 0.004 | 0.503 | 0.014 | 19.36 | 0.01 | 16.46 | 0.01 | -0.51 | 0.03 |
| **SYOG** | 2.93 | 0.005 | -4.031 | 0.003 | 0.115 | 0.017 | 2.83 | 0.01 | -4.74 | 0.01 | -1.19 | 0.05 |
| **VASC** | 11.34 | 0.0017 | 17.722 | 0.017 | 0.33 | 0.072 | 10.94 | 0.04 | 16.74 | 0.05 | -2.05 | 0.2 |
| **VILL** | 16.57 | 0.005 | 19.365 | 0.004 | -2.588 | 0.018 | 16.09 | 0.02 | 18.8 | 0.02 | -2.22 | 0.05 |
| **YIBL** | 31.45 | 0.012 | 35.752 | 0.012 | 2.045 | 0.049 | 32.81 | 0.17 | 34.83 | 0.2 | 3.83 | 0.69 |
| **ZAMB** | 18.14 | 0.009 | 20.332 | 0.01 | 0.758 | 0.004 | 18.26 | 0.02 | 19.55 | 0.02 | -1.9 | 0.07 |

**Table 11.**Estimated station velocities from GLOBK software.

| Long. | Lat. | E & N Rate | | E & N | ± | H Rate | ± | SITE |
|---|---|---|---|---|---|---|---|---|
| (deg) | (deg) | (mm/yr) | | (mm/yr) | | (mm/yr) | | |
| 357.158 | -71.674 | -0.95 | 10.70 | 0.01 | 0.01 | 0.47 | 0.04 | VESL* |
| 356.048 | 40.4436 | 18.80 | 16.09 | 0.02 | 0.02 | -2.22 | 0.05 | VILL |
| 355.75 | 40.4292 | 18.57 | 15.46 | 0.02 | 0.02 | -0.72 | 0.04 | MADR |
| 353.794 | 36.4644 | 14.46 | 16.10 | 0.01 | 0.01 | 0.06 | 0.03 | SFER |
| 353.146 | 33.9981 | 16.06 | 17.22 | 0.01 | 0.01 | -2.25 | 0.04 | RABT |
| 345.588 | -7.9512 | -5.52 | 8.89 | 0.36 | 0.27 | -0.98 | 1.15 | ASC1 |
| 344.367 | 27.7637 | 16.82 | 17.15 | 0.01 | 0.01 | -1.78 | 0.03 | MAS1 |
| 344.366 | 27.7648 | 16.82 | 17.15 | 0.01 | 0.01 | -1.78 | 0.03 | GMAS |
| 337.017 | 16.7548 | 16.11 | -0.88 | 11.14 | 8.76 | 62.64 | 39.52 | TGCV |
| 334.337 | 37.7478 | 12.61 | 16.23 | 0.02 | 0.01 | -1.92 | 0.04 | PDEL |
| 321.574 | -3.8775 | -4.41 | 11.33 | 0.03 | 0.03 | -1.26 | 0.11 | BRFT |
| 315.015 | -22.687 | -3.44 | 12.54 | 0.02 | 0.02 | 1.38 | 0.07 | CHPI |
| 312.122 | -15.947 | -4.42 | 12.35 | 0.01 | 0.01 | -0.87 | 0.05 | BRAZ* |
| 307.194 | 5.25218 | -4.11 | 12.59 | 0.02 | 0.02 | -0.25 | 0.06 | KOUR |
| 302.099 | -63.321 | 14.20 | 11.00 | 0.02 | 0.02 | 4.97 | 0.04 | OHI2 |
| 302.099 | -63.321 | 14.20 | 11.00 | 0.02 | 0.02 | 4.97 | 0.04 | OHI3 |
| 302.068 | -34.907 | -2.82 | 11.63 | 0.02 | 0.02 | 1.89 | 0.07 | LPGS |
| 288.507 | 42.6133 | -15.12 | 4.73 | 0.02 | 0.02 | -3.02 | 0.06 | WES2 |
| 283.173 | 39.0217 | -14.44 | 3.44 | 0.03 | 0.02 | -2.19 | 0.08 | GODE |
| 115.885 | -31.802 | 39.07 | 57.55 | 0.02 | 0.02 | -4.59 | 0.05 | PERT |
| 110.52 | -66.283 | 1.34 | -10.38 | 0.01 | 0.01 | -0.7 | 0.03 | CAS1 |
| 78.5509 | 17.4173 | 41.23 | 33.57 | 0.03 | 0.02 | -0.72 | 0.07 | HYDE |
| 77.5116 | 13.0343 | 44.21 | 35.19 | 0.03 | 0.02 | -0.71 | 0.1 | BAN2 |
| 72.3702 | -7.2697 | 47.28 | 33.36 | 0.02 | 0.01 | -1.1 | 0.05 | DGAR |
| 70.2555 | -49.351 | 5.95 | -2.37 | 0.01 | 0.01 | -2.11 | 0.04 | KERG |
| 62.8707 | -67.605 | -4.38 | -2.5 | 0.01 | 0.01 | -1.9 | 0.03 | MAW1 |
| 57.497 | -20.297 | 16.74 | 10.94 | 0.05 | 0.04 | -2.05 | 0.2 | VACS |
| 56.1123 | 22.1865 | 34.83 | 32.81 | 0.2 | 0.17 | 3.83 | 0.69 | YIBL |

**Table 11.** (continued).

| Long. | Lat. | E & N Rate | | E & N | ± | H Rate | ± | SITE |
|---|---|---|---|---|---|---|---|---|
| (deg) | (deg) | (mm/yr) | | (mm/yr) | | (mm/yr) | | |
| 55.5717 | -21.208 | 16.23 | 12.44 | 0.02 | 0.02 | -5.13 | 0.08 | REUN |
| 50.6082 | 26.2091 | 29.36 | 31.01 | 0.12 | 0.1 | 0.05 | 0.4 | BAHR |
| 50.6082 | 26.2091 | 29.36 | 31.01 | 0.12 | 0.1 | 0.05 | 0.4 | BHR1 |
| 47.2292 | -19.018 | 17.39 | 13.81 | 0.04 | 0.03 | 0.96 | 0.15 | ABPO |
| 46.4006 | 24.9107 | 27.20 | 28.87 | 1.38 | 1.2 | -20.5 | 5.25 | SOLA |
| 42.0447 | 19.2114 | 34.17 | 26.93 | 0.03 | 0.03 | -0.2 | 0.11 | NAMA |
| 40.1941 | -2.9961 | 24.14 | 15.16 | 0.11 | 0.1 | 3.67 | 0.41 | MAL2 |
| 39.5837 | -69.007 | -4.74 | 2.83 | 0.01 | 0.01 | -1.19 | 0.05 | SYOG |
| 37.861 | -46.876 | 6.26 | 3.88 | 0.1 | 0.11 | -10.2 | 0.35 | MARI |
| 37.861 | -46.876 | 6.26 | 3.88 | 0.1 | 0.11 | -10.2 | 0.35 | MARN |
| 36.8935 | -1.2208 | 26.06 | 16.15 | 0.05 | 0.04 | -2.95 | 0.17 | RCMN |
| 36.0999 | 29.1389 | 26.57 | 23.37 | 0.03 | 0.03 | -1.96 | 0.11 | HALY |
| 35.29 | 0.28832 | 22.87 | 16.21 | 0.54 | 0.43 | -1.55 | 1.79 | MOIU |
| 35.2093 | 32.1024 | 20.32 | 20.76 | 0.39 | 0.39 | 4.83 | 1.58 | AREL |
| 34.7631 | 30.5976 | 23.82 | 19.19 | 0.01 | 0.01 | 0.39 | 0.04 | RAMO |
| 33.3965 | 35.141 | 18.98 | 15.17 | 0.01 | 0.01 | 0.18 | 0.04 | NICO |
| 32.0784 | -28.796 | 15.62 | 17.77 | 0.02 | 0.02 | -0.58 | 0.07 | RBAY |
| 31.4209 | -28.293 | 15.81 | 18.74 | 0.47 | 0.37 | -4.32 | 1.49 | ULDI |
| 30.7379 | -0.6015 | 23.81 | 17.14 | 0.02 | 0.02 | -0.25 | 0.07 | MBAR |
| 30.384 | -23.08 | 15.50 | 14.75 | 0.49 | 0.37 | 3.71 | 1.58 | TDOU |
| 28.6725 | -31.549 | 19.59 | 17.86 | 1.95 | 1.58 | 11.45 | 6.23 | UMTA |
| 28.311 | -15.426 | 19.55 | 18.26 | 0.02 | 0.02 | -1.9 | 0.07 | ZAMB |
| 27.7073 | -25.887 | 16.90 | 18.38 | 0.01 | 0.01 | -0.65 | 0.04 | HARB* |
| 27.687 | -25.89 | 19.59 | 17.62 | 0.01 | 0.01 | -1.29 | 0.03 | HRAO* |
| 27.4734 | -33.291 | 14.61 | 19.99 | 0.33 | 0.3 | -6.81 | 1.13 | HAMB |
| 25.54 | -25.805 | 17.96 | 26.29 | 0.49 | 0.37 | 1.4 | 1.59 | MFKG |
| 24.0588 | 56.9486 | 20.05 | 12.86 | 0.02 | 0.02 | 0.81 | 0.05 | RIGA |
| 23.9926 | -30.665 | 16.03 | 18.55 | 0.4 | 0.34 | 2.99 | 1.35 | DEAR |

**Table 11.** (continued).

| Long. | Lat. | E & N Rate | | E & N | ± | H Rate | ± | SITE |
|---|---|---|---|---|---|---|---|---|
| (deg) | (deg) | (mm/yr) | | (mm/yr) | | (mm/yr) | | |
| 23.5284 | -19.90224 | 18.37 | 18.23 | 0.6 | 0.49 | 1.57 | 2.14 | MAUA |
| 20.8109 | -32.38143 | 16.46 | 19.36 | 0.01 | 0.01 | -0.51 | 0.03 | SUTM* |
| 20.8105 | -32.38021 | 16.46 | 19.36 | 0.01 | 0.01 | -0.51 | 0.03 | SUTH* |
| 20.8105 | -32.38021 | 16.46 | 19.36 | 0.01 | 0.01 | -0.51 | 0.03 | SUTV |
| 20.5797 | -33.26693 | 16.41 | 19.26 | 0.26 | 0.24 | -0.73 | 1 | MATJ |
| 18.4396 | -34.18794 | 16.08 | 19.58 | 0.03 | 0.03 | -1.1 | 0.1 | SIMO |
| 17.8792 | -29.66932 | 18.57 | 18.52 | 0.39 | 0.31 | 0.77 | 1.25 | SBOK |
| 17.0894 | -22.57492 | 19.69 | 19.14 | 0.03 | 0.02 | 13.01 | 0.1 | WIND |
| 16.7045 | 40.64913 | 22.48 | 18.52 | 0.01 | 0.01 | 0.12 | 0.04 | MATE |
| 14.9898 | 36.87585 | 20.92 | 18.99 | 0.01 | 0.01 | -1.2 | 0.04 | NOT1 |
| 12.6057 | 35.49978 | 18.88 | 17.47 | 0.13 | 0.13 | 2.09 | 0.48 | LAMP |
| 11.9255 | 57.3953 | 16.93 | 13.90 | 0.02 | 0.02 | 2.65 | 0.04 | ONSA |
| 9.67213 | 0.35391 | 22.13 | 18.90 | 0.02 | 0.02 | 0.06 | 0.07 | NKLG |
| 8.97275 | 39.13591 | 21.60 | 15.22 | 0.01 | 0.01 | -0.63 | 0.04 | CAGL |
| 6.92058 | 43.75474 | 20.79 | 15.65 | 0.01 | 0.01 | -0.38 | 0.03 | GRAS* |
| 0.33627 | 50.86731 | 14.76 | 15.86 | 0.02 | 0.02 | -0.81 | 0.05 | HERS |

* Represents stations used to stabilize the network.

**Table 12.** Estimated velocities utilising the CATREF software.

| *Name* | *Long* | *Lat* | *E(mm/yr)* | *N(mm/yr)* | *Up(mm/yr)* |
|---|---|---|---|---|---|
| **BRAZ** | 312.1221 | -15.9475 | -2.3985 | 12.6303 | 0.9076 |
| **CAGL** | 8.9728 | 39.1359 | 22.3885 | 14.3097 | 1.3366 |
| **CAS1** | 110.5197 | -66.2834 | 1.8442 | -10.117 | 0.9771 |
| **DGAR** | 72.3702 | -7.2697 | 48.0408 | 32.4299 | 0.9047 |
| **GRAS** | 6.9206 | 43.7547 | 21.514 | 14.1961 | 0.9909 |
| **HERS** | 0.3363 | 50.8673 | 17.9573 | 14.5745 | 1.3533 |
| **HRAO** | 27.687 | -25.8901 | 19.2028 | 17.3253 | 1.508 |
| **KERG** | 70.2555 | -49.3515 | 4.9265 | -2.5546 | 0.8812 |
| **KOUR** | 307.194 | 5.2522 | -2.61 | 12.4198 | -0.1583 |
| **LPGS** | 302.0677 | -34.9067 | -1.0175 | 11.9421 | 2.8608 |
| **MAS1** | 344.3667 | 27.7637 | 18.2095 | 15.7255 | 0.5796 |
| **MAW1** | 62.8707 | -67.6048 | -3.6882 | -2.2958 | 0.0267 |
| **NICO** | 33.3964 | 35.141 | 20.2859 | 13.3205 | 0.9837 |
| **ONSA** | 11.9255 | 57.3953 | 18.0451 | 12.8334 | 3.9059 |
| **PERT** | 115.8853 | -31.802 | 39.8997 | 57.6906 | -1.3191 |
| **RIGA** | 24.0588 | 56.9486 | 21.2018 | 11.6489 | 2.4603 |
| **SFER** | 353.7944 | 36.4643 | 17.5598 | 15.6843 | 1.0787 |
| **SUTH** | 20.8105 | -32.3802 | 17.8929 | 18.821 | 1.9562 |
| **SYOG** | 39.5837 | -69.007 | -3.9283 | 2.9347 | 0.6571 |
| **VESL** | 357.1582 | -71.6738 | -0.1605 | 10.6429 | 1.8892 |
| **WES2** | 288.5067 | 42.6133 | -12.4219 | 5.0592 | -0.8704 |
| **RAMO** | 34.7631 | 30.5976 | 23.7705 | 18.0118 | 2.2601 |
| **MATE** | 16.7045 | 40.6491 | 24.1792 | 17.1448 | 1.8756 |
| **GODE** | 283.1732 | 39.0217 | -12.1033 | 3.8986 | -0.5806 |
| **PDEL** | 334.3372 | 37.7477 | 14.0829 | 14.691 | -0.4656 |
| **RABT** | 353.1457 | 33.9981 | 17.8569 | 16.4081 | -0.1416 |
| **MADR** | 355.7503 | 40.4292 | 20.3839 | 14.7412 | 0.9049 |
| **ZAMB** | 28.311 | -15.4255 | 21.3476 | 17.7706 | 0.626 |
| **HYDE** | 78.5509 | 17.4173 | 42.0636 | 34.7792 | 0.7685 |
| **REUN** | 55.5717 | -21.2082 | 18.6525 | 11.426 | 0.119 |
| **CHPI** | 315.0148 | -22.6871 | -1.2969 | 12.4907 | 2.4361 |
| **WIND** | 17.0894 | -22.5749 | 21.6257 | 18.7453 | 13.949 |
| **MAL2** | 40.1941 | -2.9961 | 26.026 | 14.9773 | 1.5808 |
| **LAMP** | 12.6057 | 35.4998 | 20.4443 | 16.5574 | 1.5043 |
| **YIBL** | 56.1123 | 22.1865 | 37.5936 | 31.3619 | 0.6259 |
| **HALY** | 36.0999 | 29.1389 | 27.5011 | 22.5054 | -0.0821 |
| **BRFT** | 35.2093 | 32.1024 | 18.1787 | 17.4165 | 13.568 |
| **BAN2** | 77.5116 | 13.0343 | 43.5372 | 35.1563 | 0.0745 |
| **MARN** | 37.861 | -46.8765 | 17.6829 | 17.3221 | -7.1368 |
| **BRFT** | 321.5745 | -3.8774 | -1.5873 | 11.9777 | 1.2127 |
| **RCMN** | 36.8935 | -1.2208 | 27.7889 | 15.7803 | -1.9894 |
| **VACS** | 57.497 | -20.2971 | 18.4462 | 10.4548 | -0.3155 |
| **ABPO** | 47.2292 | -19.0183 | 19.3592 | 13.4852 | 2.1152 |

| | | | | | |
|---|---|---|---|---|---|
| **SIMO** | 18.4396 | -34.1879 | 17.6364 | 19.4132 | 0.6167 |
| **OHI2** | 302.0987 | -63.3211 | 15.2283 | 11.1063 | 4.6964 |
| **RBAY** | 32.0784 | -28.7955 | 17.2335 | 17.4643 | 1.9491 |
| **NKLG** | 9.6721 | 0.3539 | 23.9987 | 18.2395 | 2.4369 |
| **VILL** | 356.048 | 40.4436 | 20.659 | 14.7193 | -0.5328 |
| **NOT1** | 14.9898 | 36.8758 | 22.3285 | 18.0232 | 0.5706 |

**Table 13**. List of GNSS station positions computed using GLOBK.

| *SITE* | *Long.* | *Lat.* | *dE adj.* | *dN adj.* | *dE +* | *dN +* | *RHO* | *dH adj.* | *dH +* |
|---|---|---|---|---|---|---|---|---|---|
| | (deg) | (deg) | (mm) | (mm) | (mm) | (mm) | | (mm) | (mm) |
| **VESL** | 357.158 | -71.674 | -1.32 | 3.94 | 0.09 | 0.08 | -0.024 | -16.57 | 0.33 |
| **VILL** | 356.048 | 40.4436 | -13.6 | -4.94 | 0.1 | 0.1 | 0.074 | 8.07 | 0.31 |
| **MADR** | 355.75 | 40.4292 | 1.63 | -4.57 | 0.1 | 0.1 | 0.046 | -65.31 | 0.31 |
| **SFER** | 353.794 | 36.4644 | 32.15 | -4.85 | 0.08 | 0.07 | 0.076 | 22.45 | 0.22 |
| **RABT** | 353.146 | 33.9981 | -6.8 | -6.75 | 0.09 | 0.08 | 0.079 | -2.1 | 0.26 |
| **ASC1** | 345.588 | -7.9512 | -5.97 | -16.36 | 3.06 | 2.37 | 0.019 | -2.01 | 9.98 |
| **MAS1** | 344.367 | 27.7637 | -2.73 | 0.42 | 0.08 | 0.07 | 0.083 | 1.98 | 0.23 |
| **GMAS** | 344.366 | 27.7648 | 0.29 | -2.17 | 0.08 | 0.07 | 0.087 | -43.92 | 0.21 |
| **PDEL** | 334.337 | 37.7478 | 2.33 | 1.11 | 0.07 | 0.07 | 0.1 | 10.79 | 0.26 |
| **BRFT** | 321.574 | -3.8775 | -0.94 | -8.07 | 0.14 | 0.12 | 0.029 | 3.68 | 0.48 |
| **CHPI** | 315.015 | -22.687 | -6.1 | 6.32 | 0.11 | 0.1 | -0.007 | -14.67 | 0.36 |
| **BRAZ** | 312.122 | -15.947 | -6.56 | -3.91 | 0.08 | 0.07 | -0.026 | 5.75 | 0.34 |
| **KOUR** | 307.194 | 5.25218 | 0.14 | -2.46 | 0.13 | 0.11 | 0.01 | -16.3 | 0.41 |
| **OHI2** | 302.099 | -63.321 | -4.3 | 6.87 | 0.09 | 0.11 | 0.038 | 12.78 | 0.26 |
| **OHI3** | 302.099 | -63.321 | -4.13 | 4.4 | 0.09 | 0.11 | 0.038 | 15.71 | 0.26 |
| **LPGS** | 302.068 | -34.907 | -15.86 | -4.87 | 0.11 | 0.12 | 0.073 | 7.94 | 0.44 |
| **WES2** | 288.507 | 42.6133 | -8.07 | -5.86 | 0.15 | 0.12 | -0.25 | -21.49 | 0.45 |
| **GODE** | 283.173 | 39.0217 | 6.5 | -1.81 | 0.21 | 0.18 | -0.144 | 8.44 | 0.65 |
| **PERT** | 115.885 | -31.802 | -5.46 | -14.05 | 0.12 | 0.11 | 0.149 | 12.09 | 0.35 |
| **CAS1** | 110.52 | -66.283 | -9.62 | -8.34 | 0.1 | 0.1 | 0.073 | -5.31 | 0.25 |
| **HYDE** | 78.5509 | 17.4173 | 1.62 | -13.35 | 0.15 | 0.11 | 0.096 | 18.01 | 0.44 |
| **BAN2** | 77.5116 | 13.0343 | 23.3 | -0.95 | 0.19 | 0.14 | 0.041 | -20.59 | 0.56 |
| **DGAR** | 72.3702 | -7.2697 | 9.84 | 5.23 | 0.12 | 0.1 | 0.004 | -17.53 | 0.34 |
| **KERG** | 70.2555 | -49.351 | 10.26 | 0.17 | 0.1 | 0.11 | -0.011 | 1.25 | 0.31 |
| **MAW1** | 62.8707 | -67.605 | -8.44 | -3.72 | 0.09 | 0.1 | -0.032 | 1.36 | 0.24 |
| **VACS** | 57.497 | -20.297 | -22.39 | -3.48 | 0.16 | 0.14 | 0.007 | -70.32 | 0.6 |
| **YIBL** | 56.1123 | 22.1865 | -8.42 | 4.71 | 1.57 | 1.32 | -0.019 | 15.68 | 5.49 |
| **REUN** | 55.5717 | -21.208 | -18.73 | 2.61 | 0.12 | 0.11 | 0.001 | -21.24 | 0.42 |
| **BAHR** | 50.6082 | 26.2091 | 241.32 | 258.95 | 0.95 | 0.82 | -0.055 | 9.87 | 3.29 |
| **BHR1** | 50.6082 | 26.2091 | 246.25 | 256.23 | 0.99 | 0.86 | -0.052 | 15.1 | 3.46 |
| **ABPO** | 47.2292 | -19.018 | 67.53 | 61.75 | 0.14 | 0.13 | 0.035 | -26.46 | 0.5 |
| **NAMA** | 42.0447 | 19.2114 | 271.95 | 232.86 | 0.12 | 0.1 | -0.069 | -108.1 | 0.39 |
| **MAL2** | 40.1941 | -2.9961 | 184.52 | 124.59 | 0.4 | 0.35 | 0.029 | 10.45 | 1.49 |
| **SYOG** | 39.5837 | -69.007 | -8.08 | -1.16 | 0.09 | 0.1 | -0.016 | -8.32 | 0.26 |

**Table 13.** (Continued).

| *SITE* | *Long.* | *Lat.* | *dE adj.* | *dN adj.* | *dE +* | *dN +* | *RHO* | *dH adj.* | *dH +* |
|---|---|---|---|---|---|---|---|---|---|
| | (deg) | (deg) | (mm) | (mm) | (mm) | (mm) | | (mm) | (mm) |
| **MOIU** | 35.29 | 0.28832 | 75.4 | 58.12 | 0.3 | 0.24 | 0.009 | -6.4 | 1 |
| **AREL** | 35.2093 | 32.1024 | 144.19 | 184.28 | 2.97 | 2.99 | -0.06 | 25.89 | 12.11 |
| **RAMO** | 34.7631 | 30.5976 | 16.23 | -14.65 | 0.1 | 0.08 | -0.083 | -16.91 | 0.28 |
| **NICO** | 33.3965 | 35.141 | -13.43 | 2.54 | 0.09 | 0.09 | -0.068 | 4.04 | 0.28 |
| **RBAY** | 32.0784 | -28.796 | -7.33 | 2.84 | 0.12 | 0.11 | 0.022 | 0.6 | 0.4 |
| **ULDI** | 31.4209 | -28.293 | 31.46 | 44.1 | 0.29 | 0.24 | 0.128 | -28.6 | 0.95 |
| **MBAR** | 30.7379 | -0.6015 | -8.57 | -0.88 | 0.14 | 0.12 | -0.011 | -23.74 | 0.43 |
| **TDOU** | 30.384 | -23.08 | 40.04 | 46.9 | 0.32 | 0.25 | 0.142 | -12.91 | 1.03 |
| **UMTA** | 28.6725 | -31.549 | 32.37 | 48.72 | 1.15 | 0.97 | 0.137 | -8.11 | 3.86 |
| **ZAMB** | 28.311 | -15.426 | 0.29 | -0.4 | 0.15 | 0.11 | 0.099 | -22.99 | 0.55 |
| **HARB** | 27.7073 | -25.887 | -11.66 | 0.57 | 0.09 | 0.08 | -0.007 | 4.08 | 0.25 |
| **HRAO** | 27.687 | -25.89 | 12.29 | -3.78 | 0.09 | 0.08 | -0.001 | -2.5 | 0.25 |
| **HAMB** | 27.4734 | -33.291 | -87.29 | 60.17 | 0.57 | 0.51 | 0.141 | 73.52 | 1.89 |
| **MFKG** | 25.54 | -25.805 | 37.42 | 47.81 | 0.27 | 0.22 | 0.112 | -17.62 | 0.89 |
| **RIGA** | 24.0588 | 56.9486 | -5.16 | -3.53 | 0.15 | 0.17 | 0.063 | -5.8 | 0.47 |
| **DEAR** | 23.9926 | -30.665 | 33.83 | 44.53 | 0.25 | 0.21 | 0.109 | -9.2 | 0.82 |
| **MAUA** | 23.5284 | -19.902 | 16.97 | 23.98 | 0.39 | 0.32 | 0.098 | 11.07 | 1.38 |
| **SUTM** | 20.8109 | -32.381 | -7.95 | 1.32 | 0.08 | 0.07 | -0.031 | 7.9 | 0.18 |
| **SUTH** | 20.8105 | -32.38 | -10.13 | 2.22 | 0.08 | 0.08 | -0.022 | 3.09 | 0.2 |
| **SUTV** | 20.8105 | -32.38 | 142.87 | 172.99 | 0.08 | 0.08 | -0.005 | -5.86 | 0.22 |
| **MATJ** | 20.5797 | -33.267 | 67.61 | 12.42 | 7.84 | 7.34 | 0.087 | -83.6 | 30.85 |
| **SIMO** | 18.4396 | -34.188 | -7.2 | -2.53 | 0.24 | 0.23 | -0.083 | 1.42 | 0.88 |
| **SBOK** | 17.8792 | -29.669 | 38.84 | 46.53 | 0.24 | 0.2 | 0.094 | -8.6 | 0.76 |
| **WIND** | 17.0894 | -22.575 | -1.89 | -6.36 | 0.13 | 0.1 | 0.005 | 56.56 | 0.36 |
| **MATE** | 16.7045 | 40.6491 | -4.01 | -5.53 | 0.09 | 0.08 | -0.035 | -5.73 | 0.25 |
| **NOT1** | 14.9898 | 36.8759 | -4.66 | -6.71 | 0.1 | 0.08 | -0.026 | -3.23 | 0.27 |
| **LAMP** | 12.6057 | 35.4998 | -6.47 | -5.58 | 1.02 | 1.01 | -0.017 | 19.7 | 3.77 |
| **ONSA** | 11.9255 | 57.3953 | -6.4 | -6.05 | 0.13 | 0.14 | 0.058 | -8.88 | 0.38 |
| **NKLG** | 9.67213 | 0.35391 | -1.87 | -2.61 | 0.14 | 0.11 | -0.001 | -1.7 | 0.43 |
| **CAGL** | 8.97275 | 39.1359 | -3.12 | -6.51 | 0.09 | 0.08 | 0.017 | -7.66 | 0.25 |
| **GRAS** | 6.92058 | 43.7547 | 4.06 | -3.39 | 0.07 | 0.07 | 0.021 | 8.15 | 0.23 |
| **HERS** | 0.33627 | 50.8673 | -20.02 | 2.51 | 0.13 | 0.14 | 0.052 | -20.79 | 0.39 |
| **MARI** | 37.861 | -46.876 | -95.24 | -34.8 | 0.48 | 0.53 | 0.119 | -104 | 1.66 |
| **MARN** | 37.861 | -46.876 | -73.02 | -25.07 | 0.18 | 0.2 | 0.165 | -54.67 | 0.65 |
| **RCMN** | 36.8935 | -1.2208 | 20.22 | 58.42 | 0.17 | 0.14 | 0.02 | -46.85 | 0.54 |
| **HALY** | 36.0999 | 29.1389 | 203.83 | 198.23 | 0.13 | 0.12 | -0.057 | -84.16 | 0.45 |

**Table 14.** List of IGS stations used in this study with their receiver and antenna types.

| *Station* | *Receiver* | *Antenna* |
|---|---|---|
| **ABPO** | ashtech uz-12 | ash701945g_m |
| **ADIS** | jps legacy | trm29659.00 |
| **BRAZ** | trimble netrs | trm41249.00 |
| **BRFT** | leica grx1200pro | leiat504 |
| **CAGL** | trimble 4700 | trm29659.00 |
| **CAS1** | leica grx1200ggpro | aoad/m_t |
| **CHPI** | ashtech uz-12 | ash701945c_m |
| **DGAR** | ashtech uz-12 | ash701945e_m |
| **GMAS** | trimble netrs | trm29659.00 |
| **GODE** | ashtech uz-12 | aoad/m_t |
| **GRAS** | trimble netr5 | ash701945e_m |
| **HALY** | ashtech z-xii3 | ash701945c_m |
| **HAMB** | tps gb-1000 | tpscr.g3 |
| **HARB** | ashtech uz-12 | trm29659.00 |
| **HERS** | sept polarx3etr | leiar25.r3 |
| **HRAO** | ashtech uz-12 | ash701945e_m |
| **HYDE** | leica grx1200ggpro | leiat504gg |
| **KERG** | ashtech uz-12 | ash701945e_m |
| **KOUR** | jps legacy | ash701946.3 |
| **LPGS** | aoa benchmark act | aoad/m_t |
| **MADR** | ashtech z-xii3 | aoad/m_t |
| **MAL2** | jps legacy | ash701945c_m |
| **MAS1** | jps legacy | ash701945e_m |
| **MATE** | leica grx1200ggpro | leiat504gg |
| **MAW1** | leica grx1200ggpro | aoad/m_t |
| **NAMA** | ashtech z-xii3 | ash701945c_m |
| **NICO** | leica grx1200ggpro | leiat504gg |
| **NKLG** | trimble netr5 | trm59800.00 |
| **NOT1** | trimble 4000ssi | trm29659.00 |
| **OHI2** | jps e_ggd | tpscr.g3 |
| **OHI3** | leica grx1200ggpro | leiar25.r3 |
| **ONSA** | jps e_ggd | aoad/m_b |
| **PDEL** | leica grx1200ggpro | leiat504gg |
| **PERT** | ashtech uz-12 | ash701945c_m |

**Table 14**. (Continued).

| *Station* | *Receiver* | *Antenna* |
|---|---|---|
| **RABT** | ashtech uz-12 | trm29659.00 |
| **RBAY** | rogue snr-8000 | aoad/m_t |
| **RCMN** | leica grx1200ggpro | leiat504gg |
| **REUN** | trimble netr5 | trm55971.00 |
| **RIGA** | leica grx1200pro | leiat504 |
| **SFER** | trimble netrs | trm29659.00 |
| **SUTH** | ashtech uz-12 | ash701945g_m |
| **SUTM** | aoa benchmark act | aoad/m_t |
| **SUTV** | jps eggdt | ash701945g_m |
| **SYOG** | trimble netrs | aoad/m_t |
| **VACS** | trimble netrs | trm41249.00 |
| **VILL** | ashtech uz-12 | aoad/m_t |
| **WES2** | leica grx1200ggpro | aoad/m_ta_ngs |
| **WIND** | ashtech z-xii3 | ash700936c_m |

# **Appendix B:** Sky plots

**A series of sky plots for IGS station HRAO.**

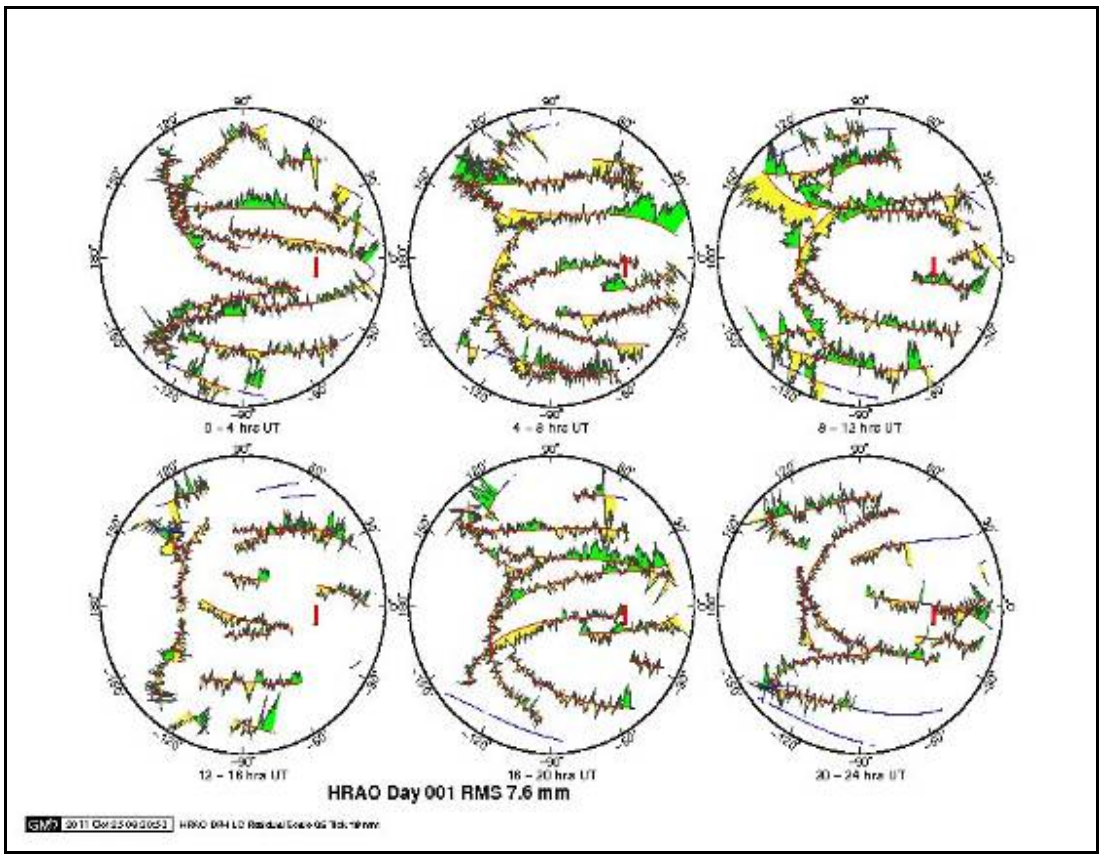

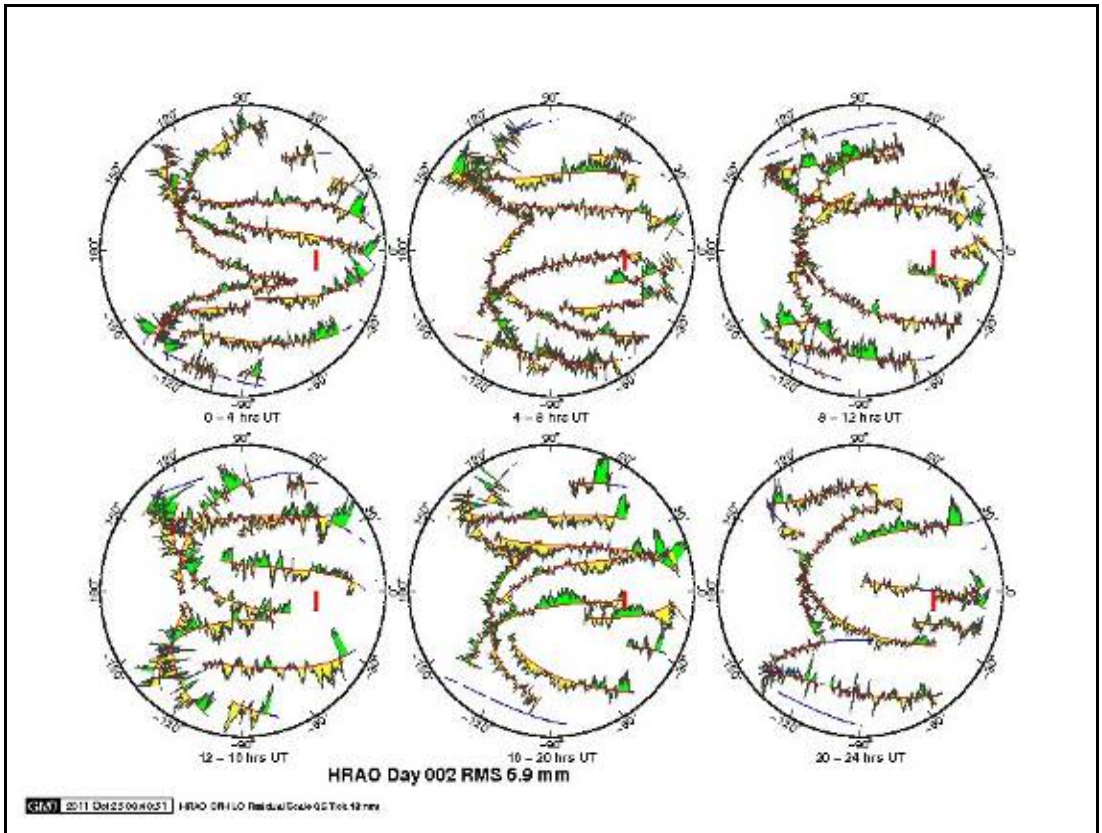


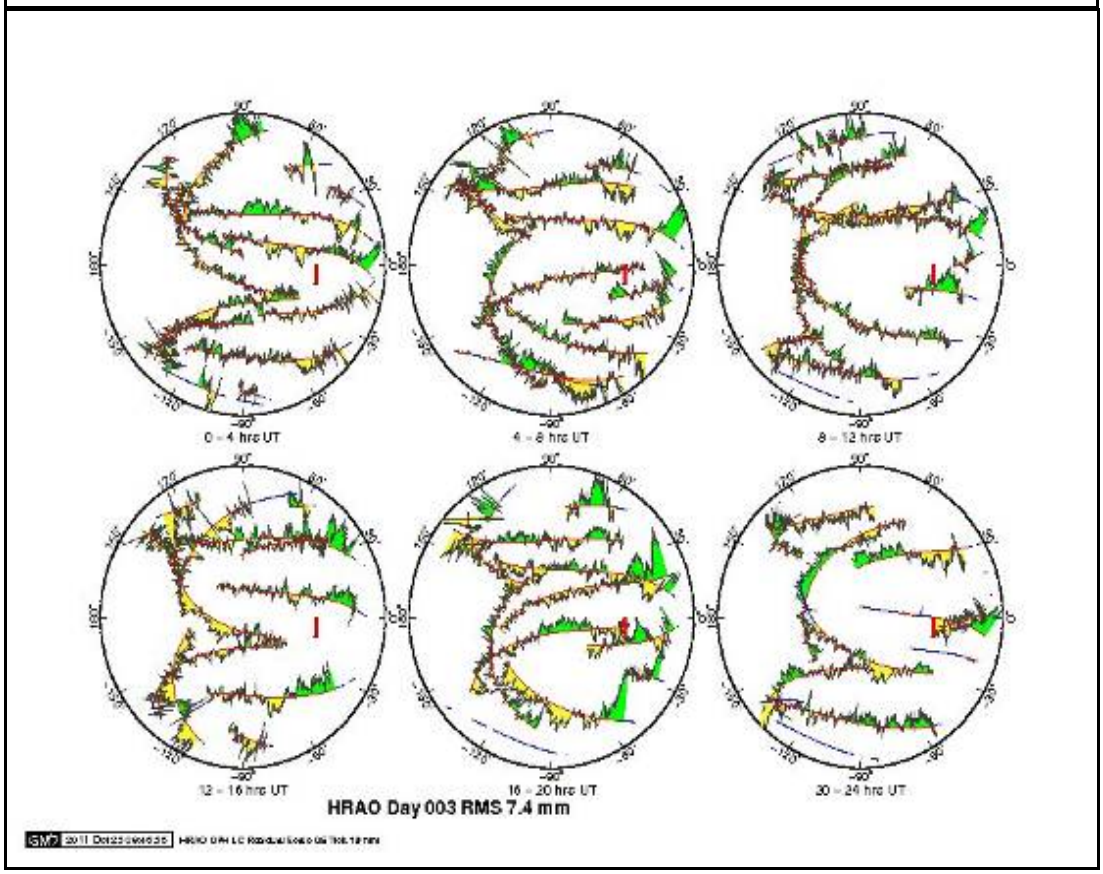

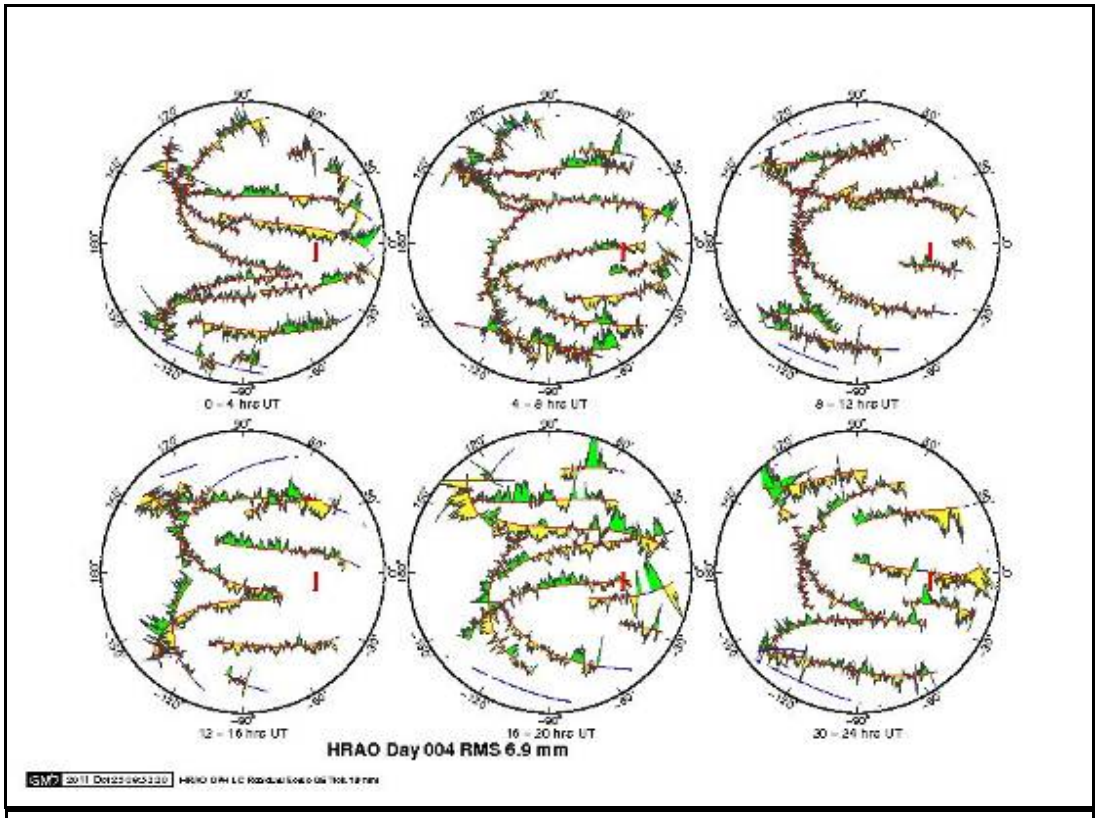


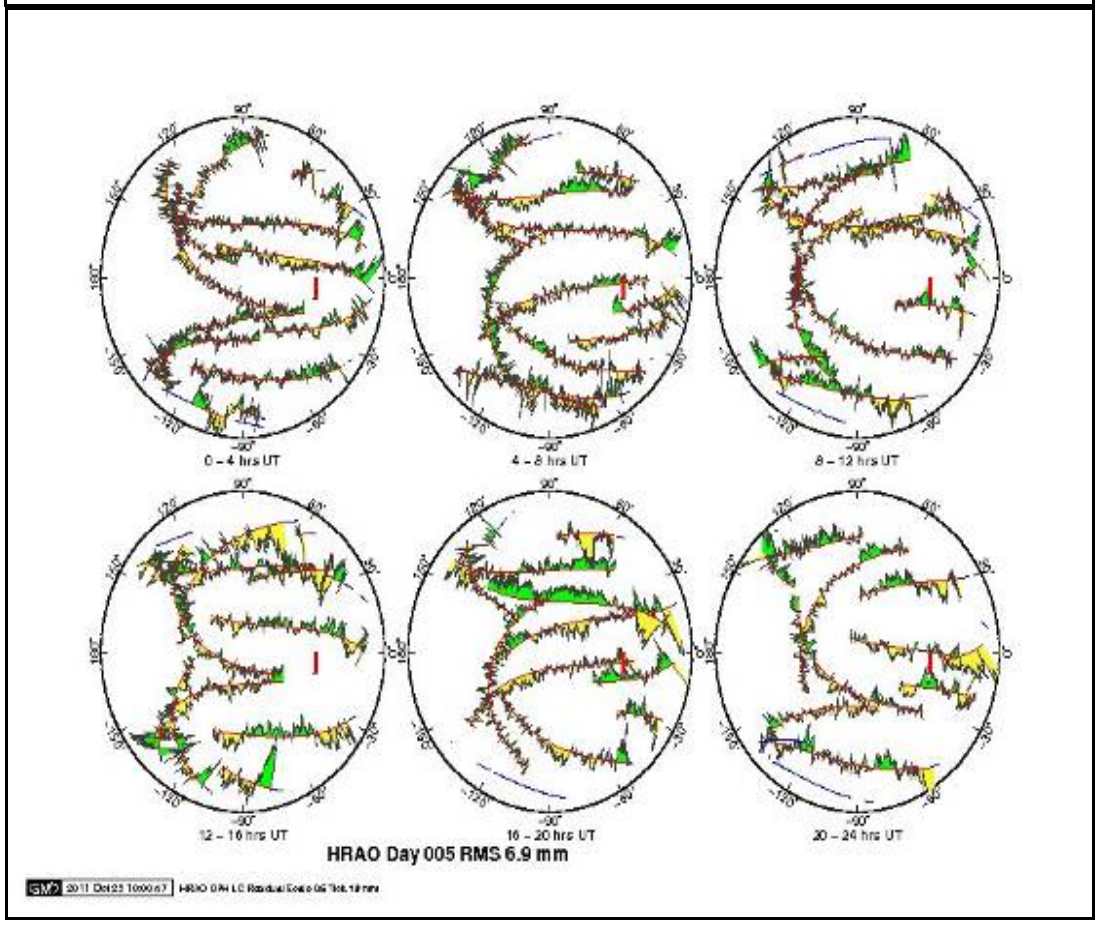

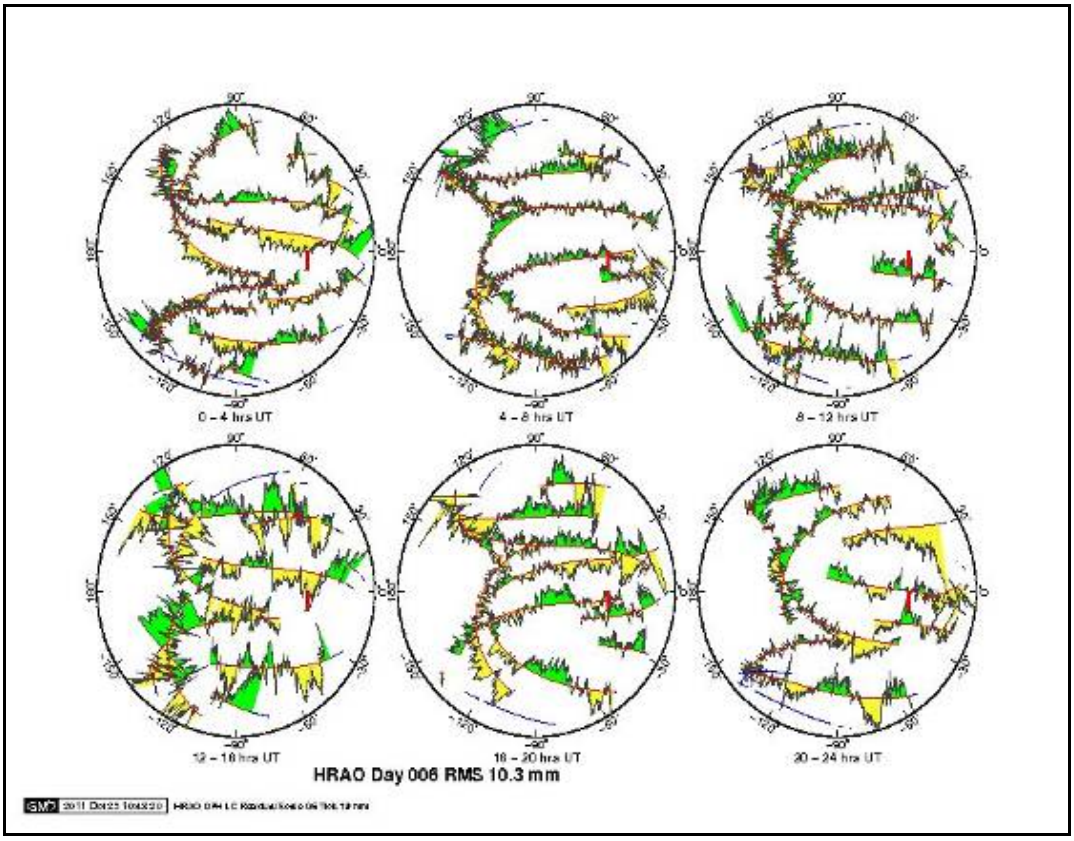


**Figure 64.** Polar sky plots for IGS station HRAO, Hartebeesthoek, South Africa, from 1 to 6 January 2000. Note the effects of cloud on the sky plots on different days and the associated RMS. The red bar on the sky plot represents a scale which is equivalent to 10 mm.

**A series of sky plots for station MATJ (2012).**

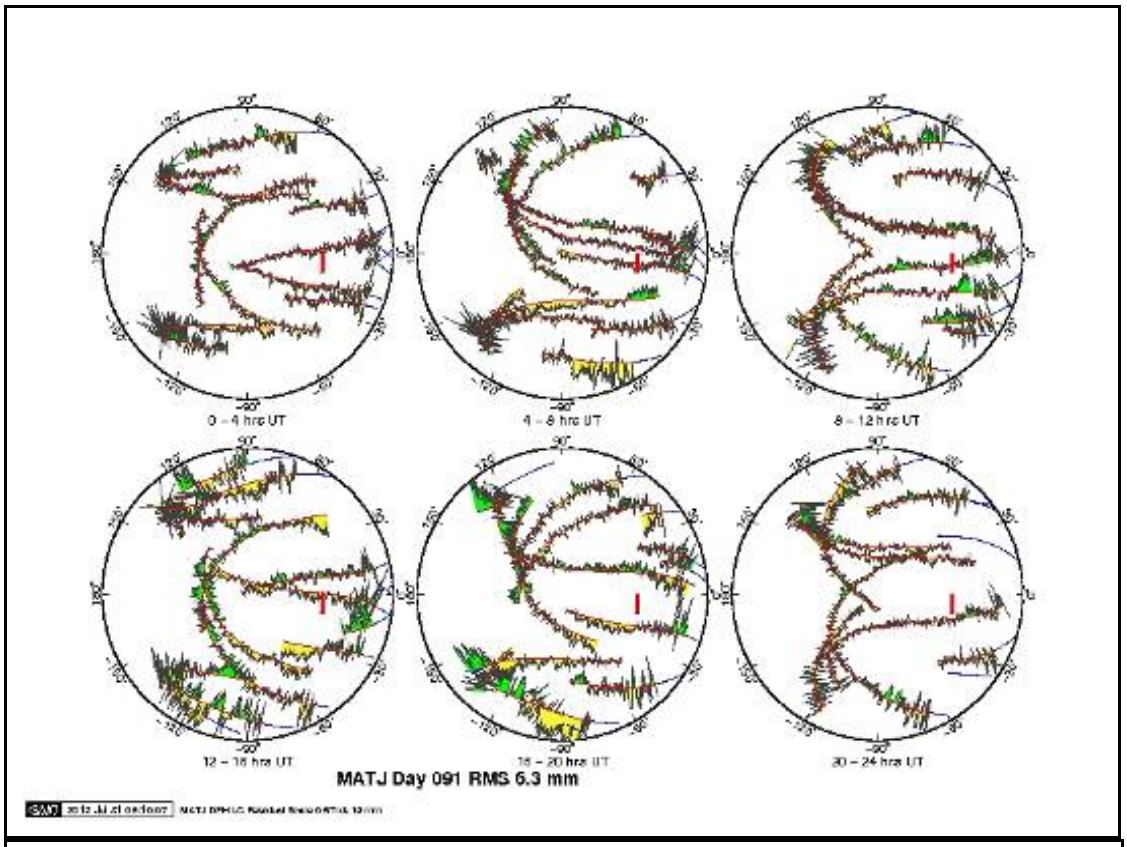


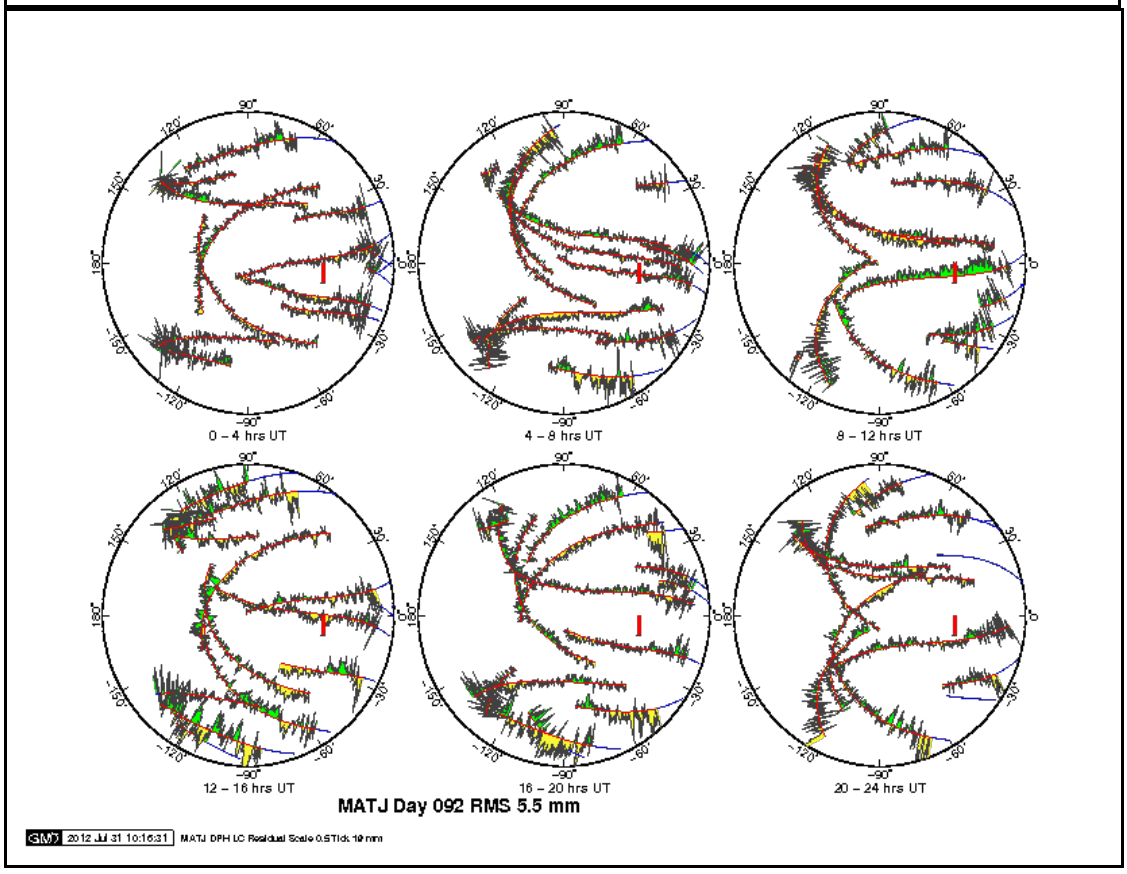

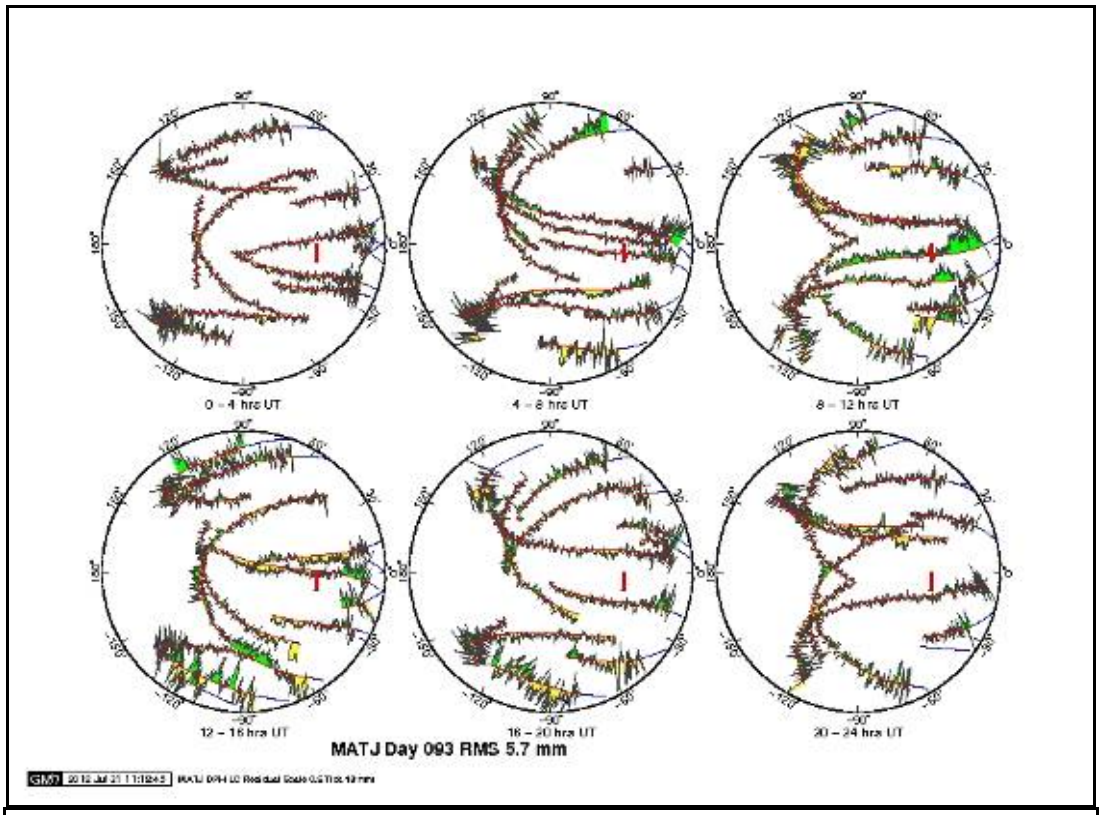


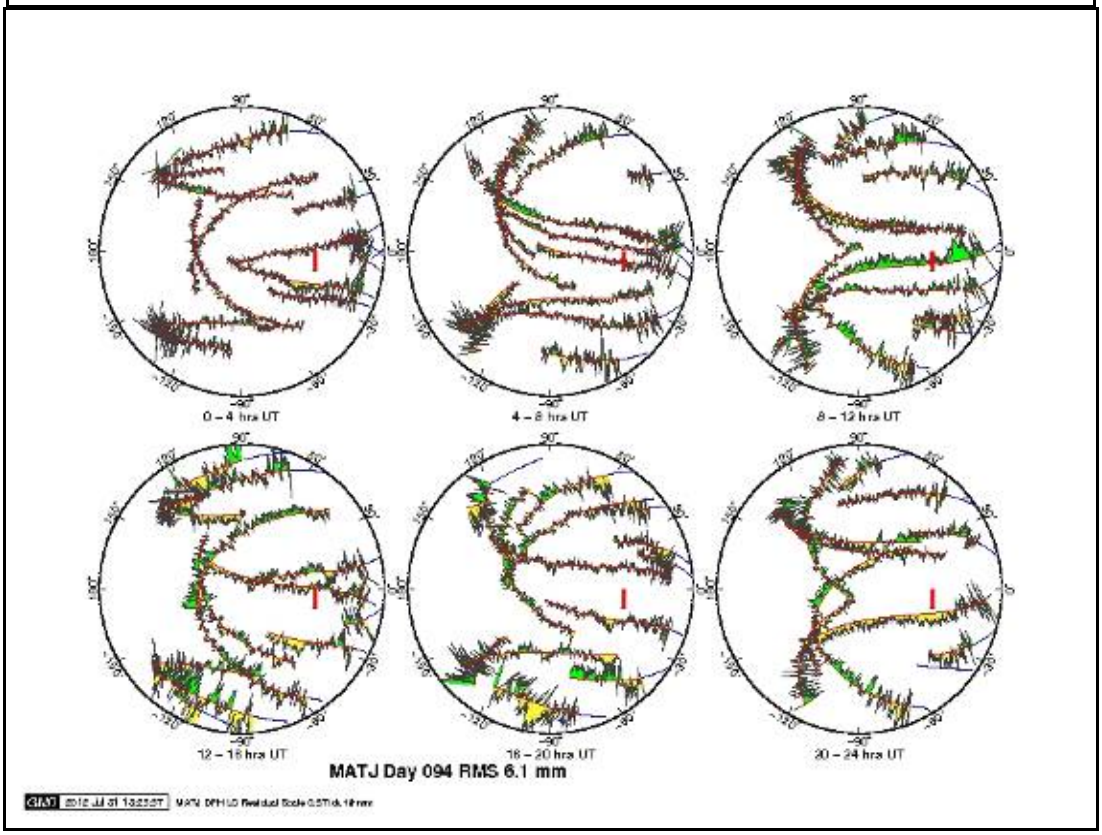

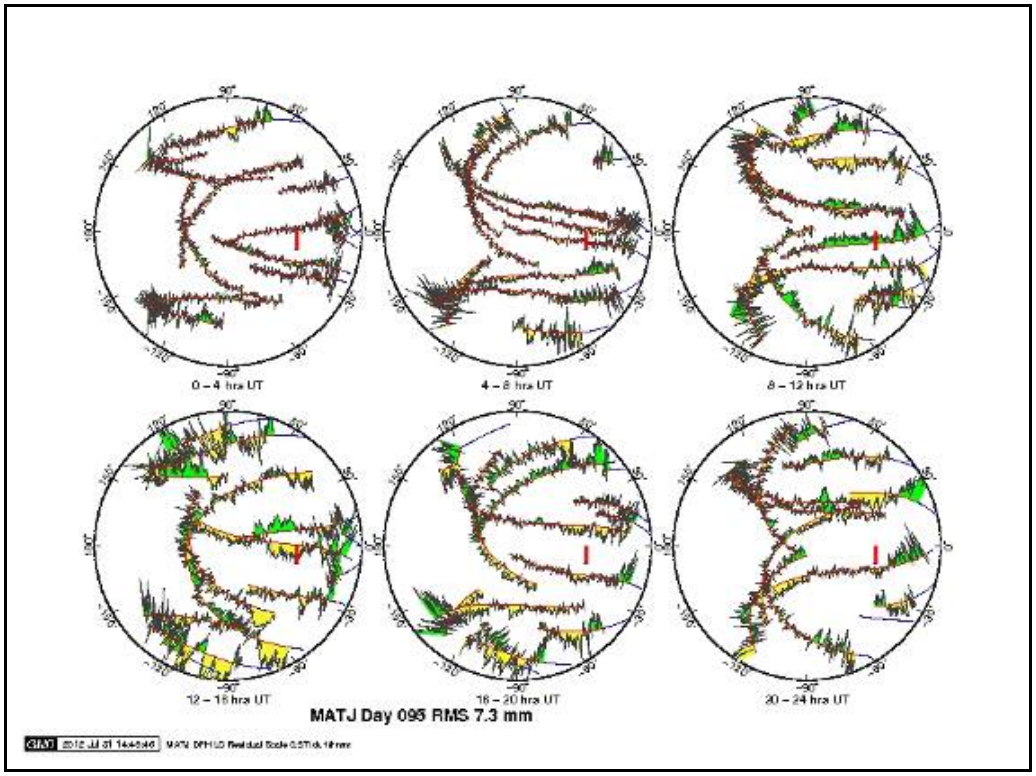


**Figure 65**. Polar sky plots for the MATJ station, South Africa, from days 90-95, 2012, cut off elevation: $10^{o}$. Note the effects of cloud on the sky plots on different days and the associated RMS. The red bars on the sky plot represent a scale which is equivalent to 10 mm. The sky above the proposed site remains relatively clear which is the most important criteria for observations made by geodetic instruments.

**Appendix C:** Network statistics from 2000 to 2012.4.

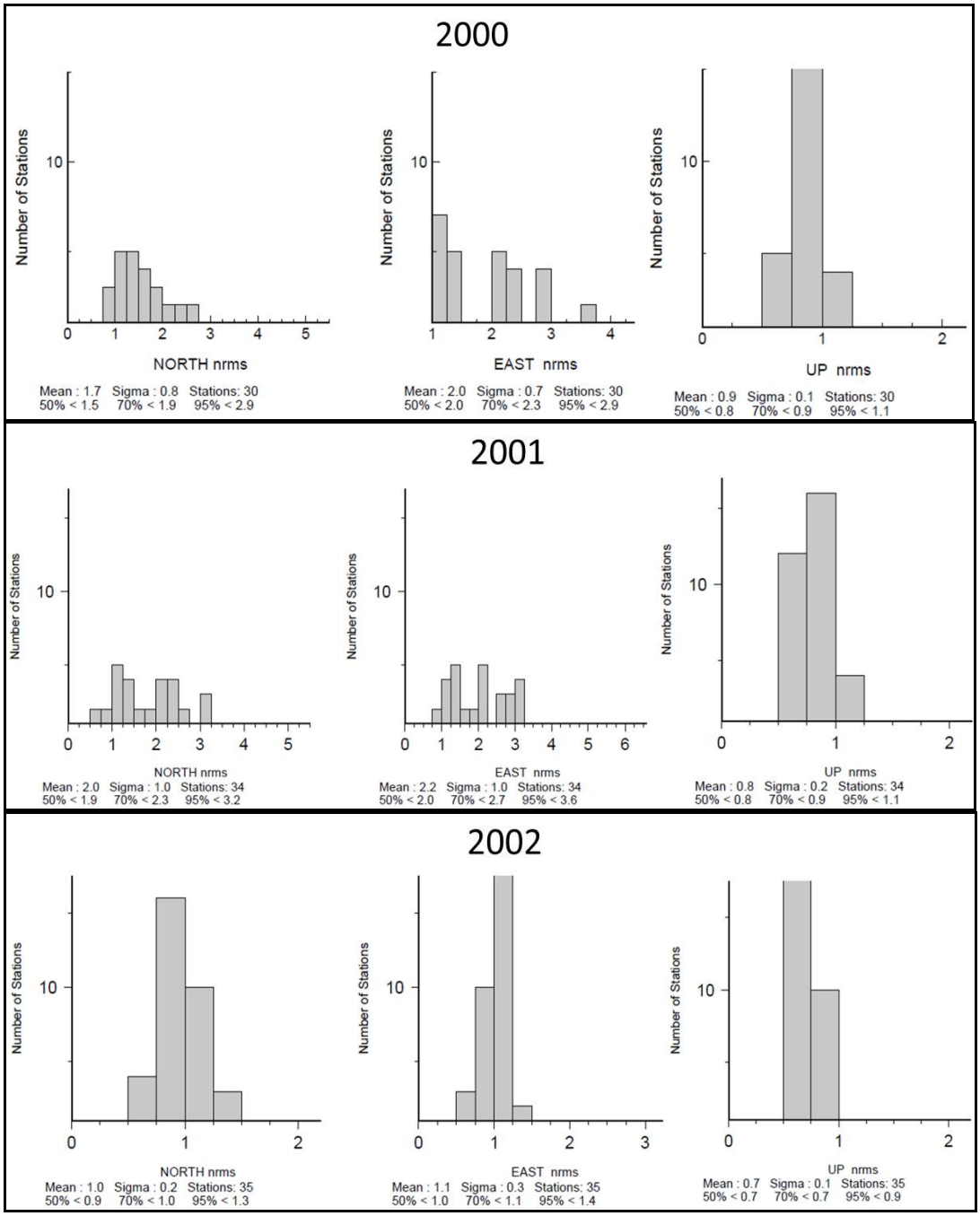

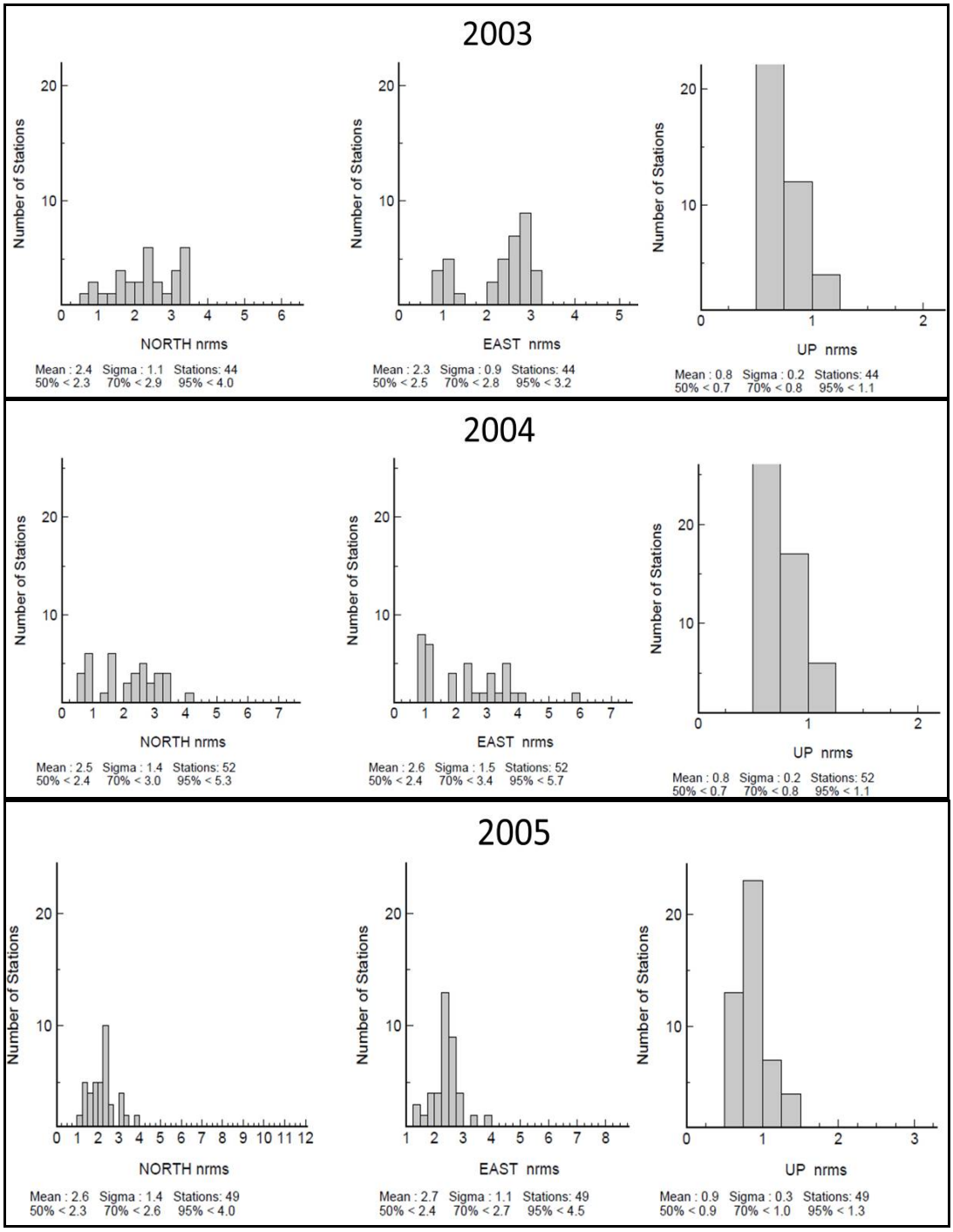

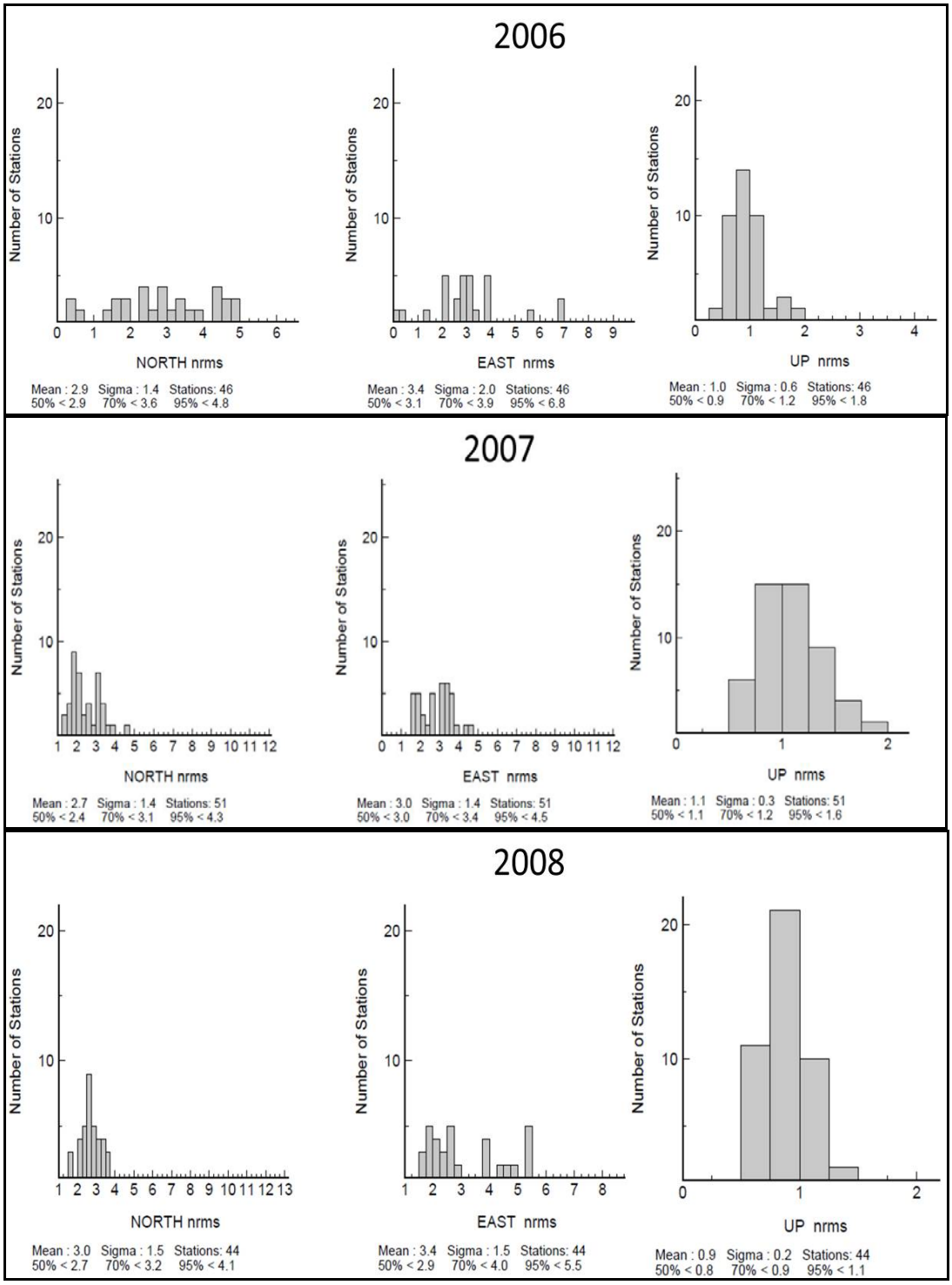

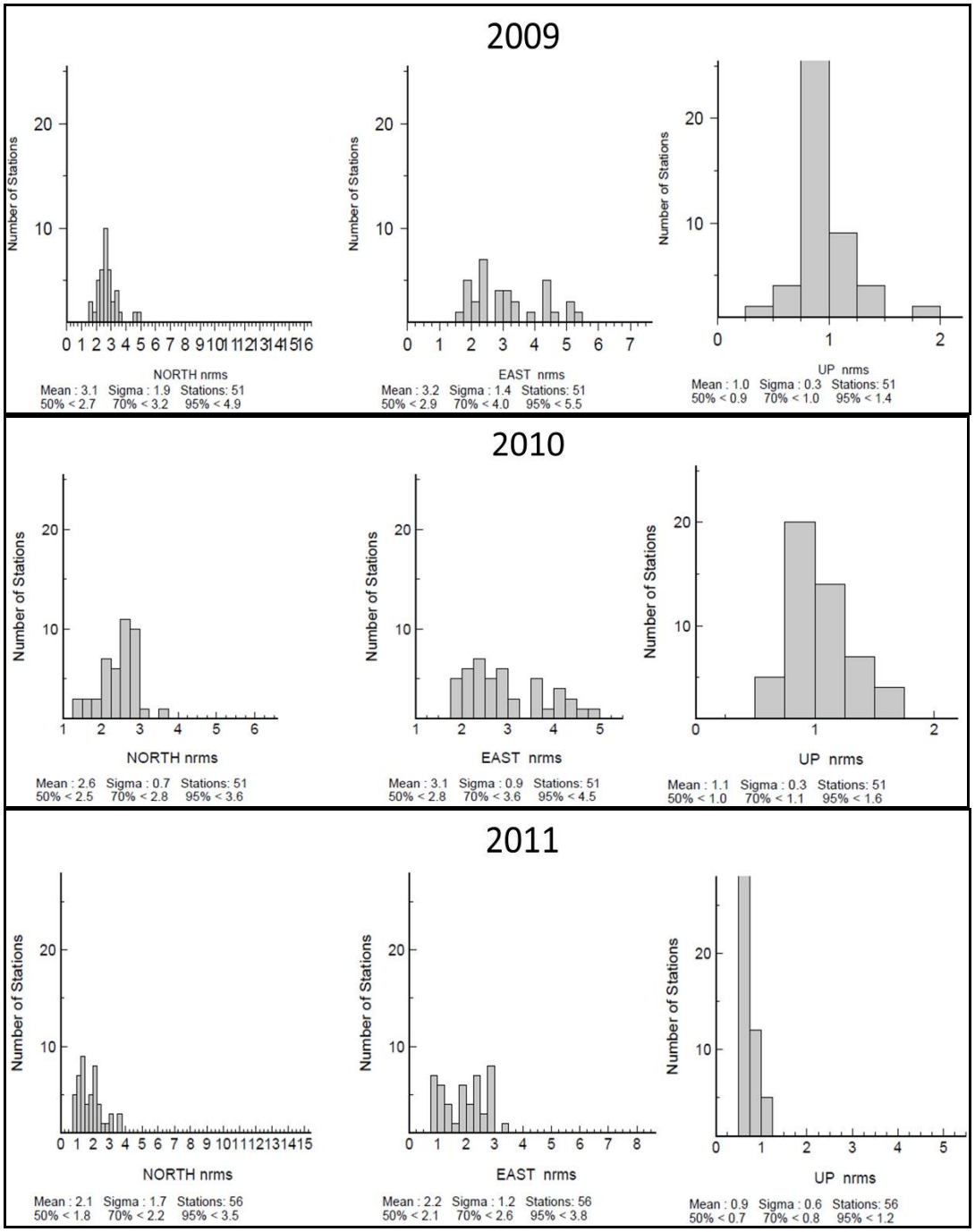

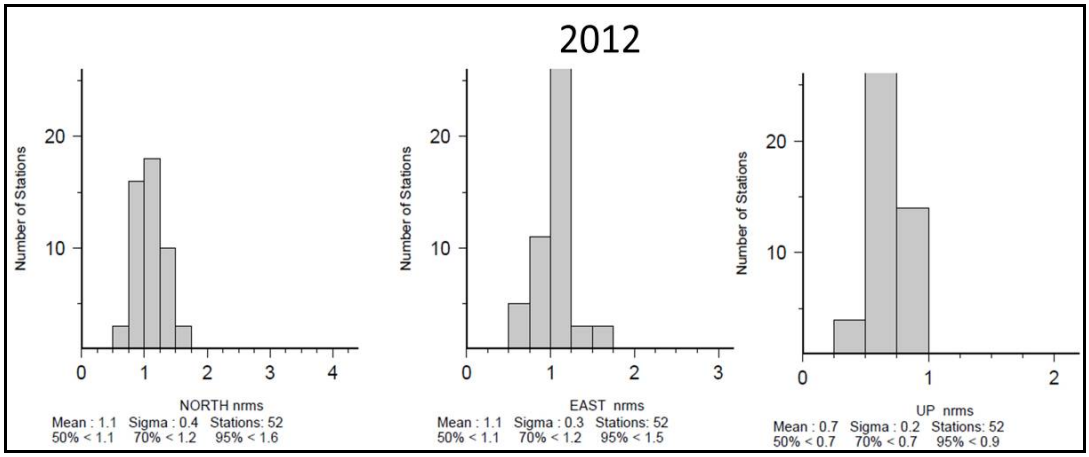


**Figure 66.** Series of NRMS histograms from 2000 to 2012.4 for all GNSS stations processed. The NRMS values are calculated for East, North and Up components.

**Appendix D:** List of GNSS station time-series plots.

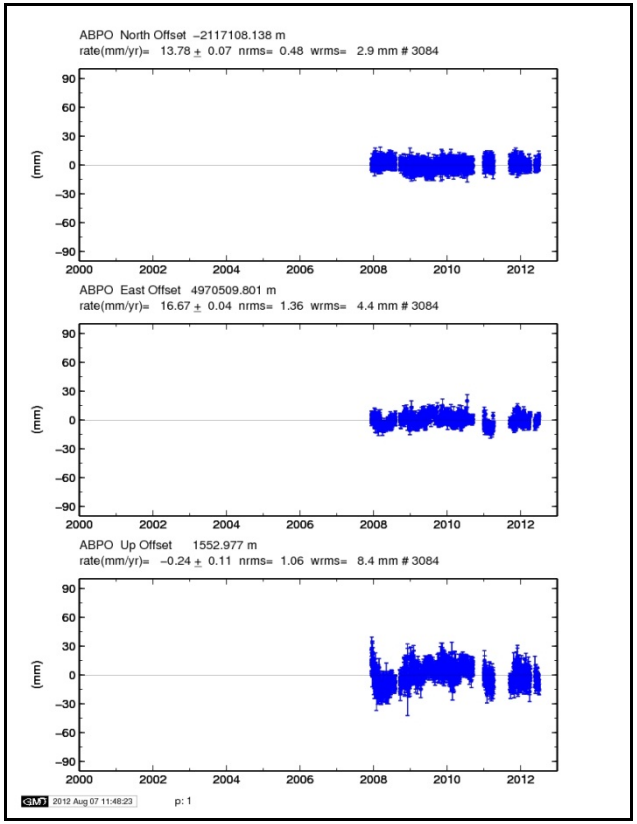


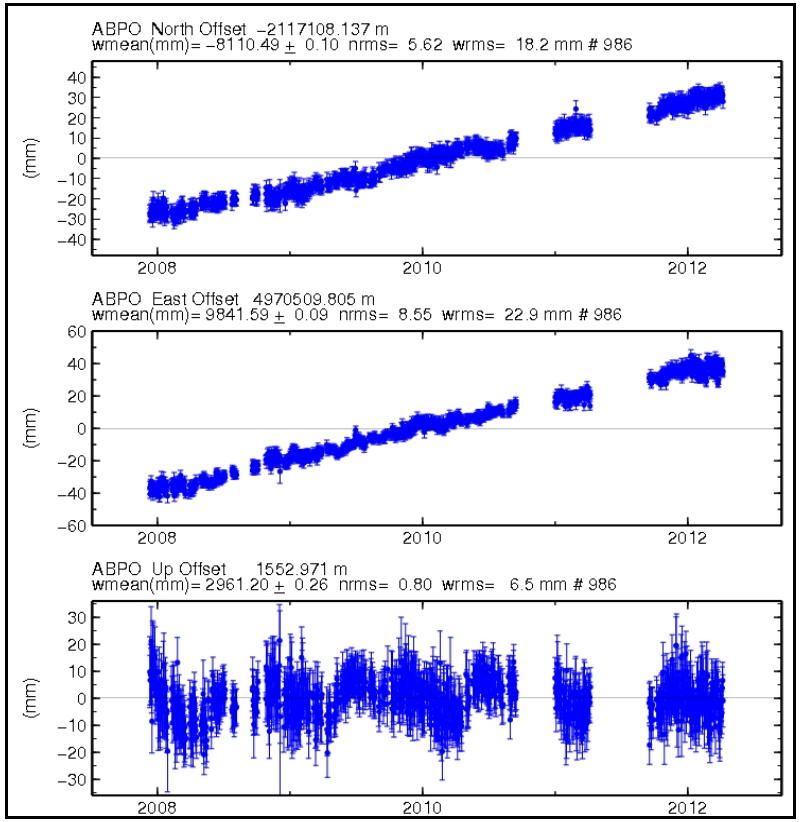


**GPS station (ABOP), Madagascar**

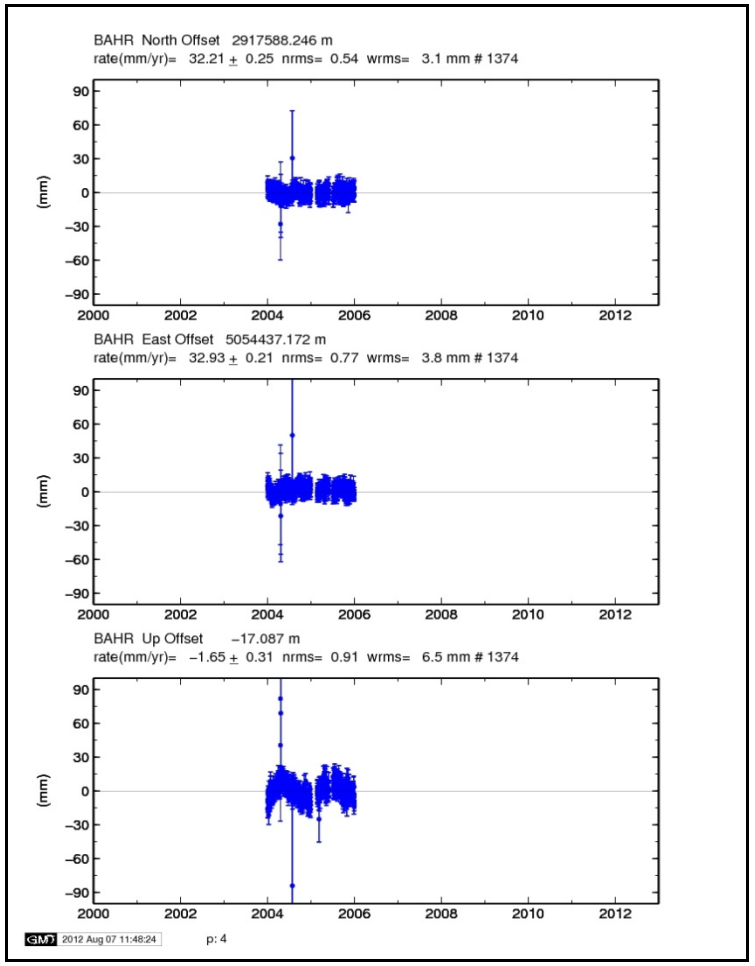


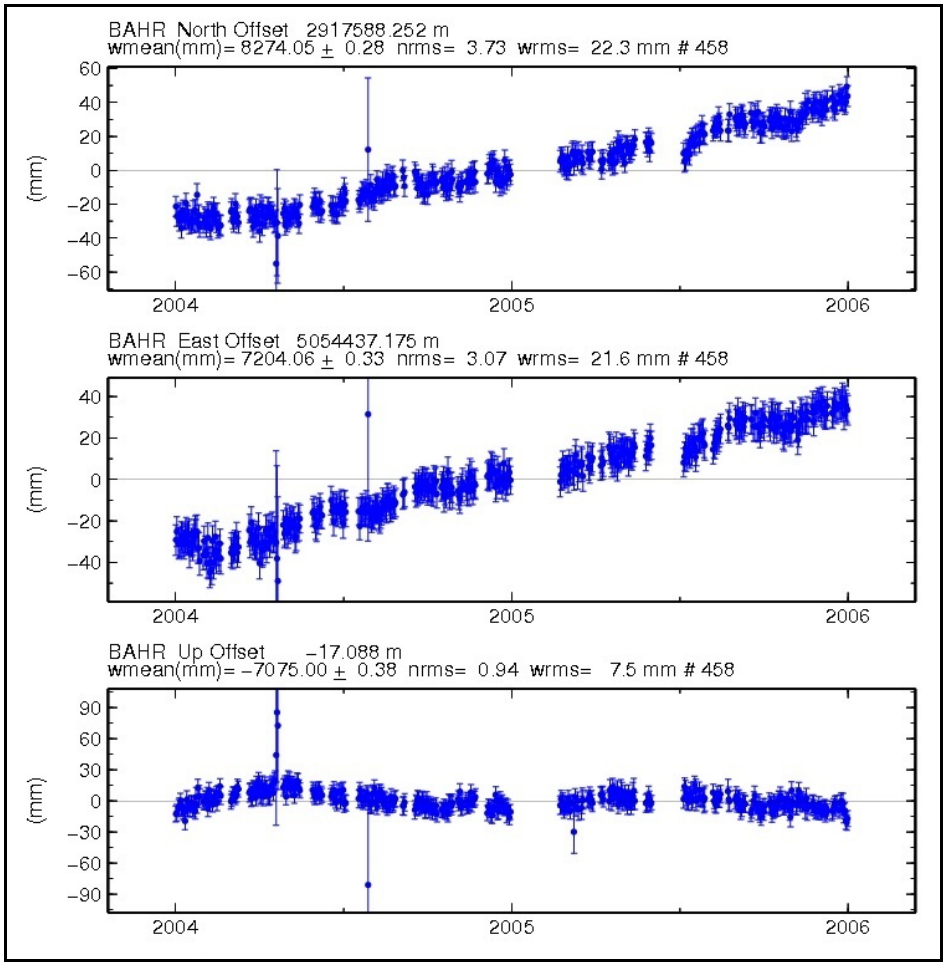


# Bahrain GPS station (BAHR), Bahrain

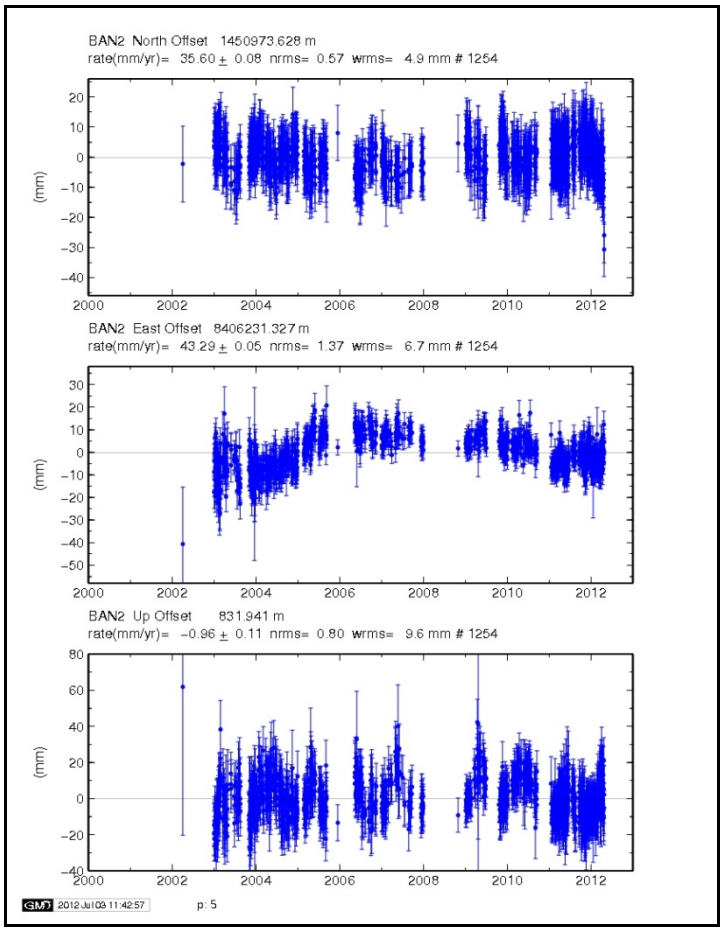


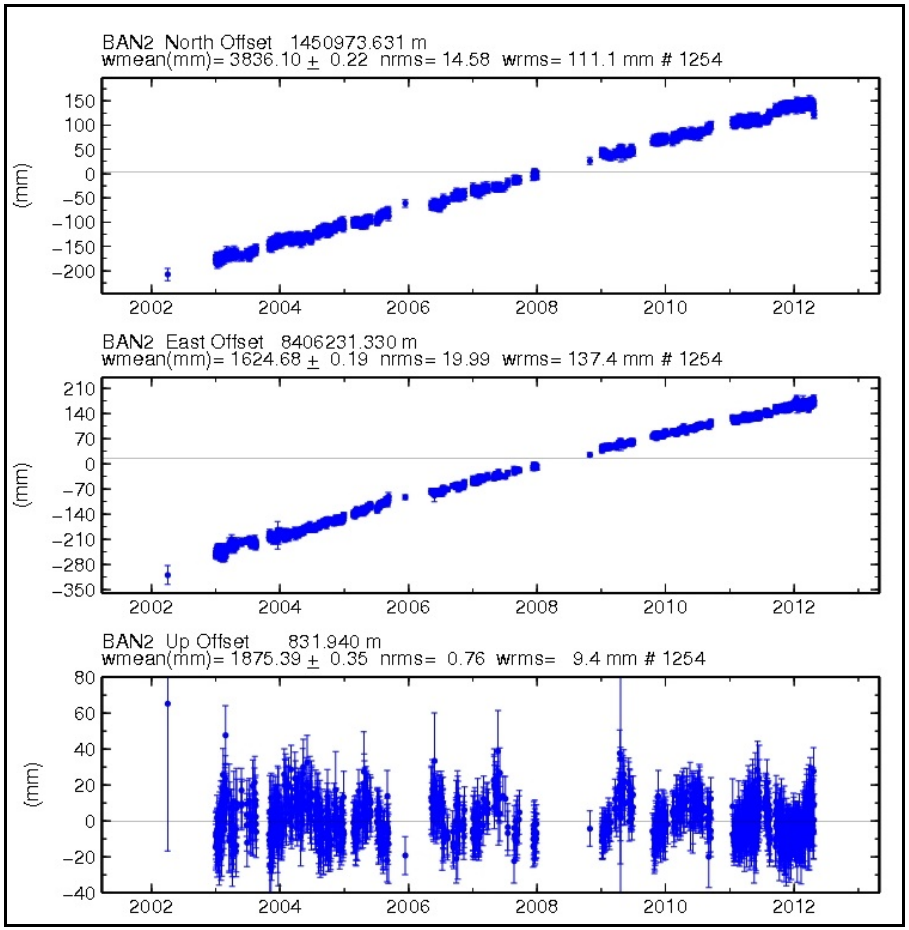


# Bangalore GPS station (BAN2), India

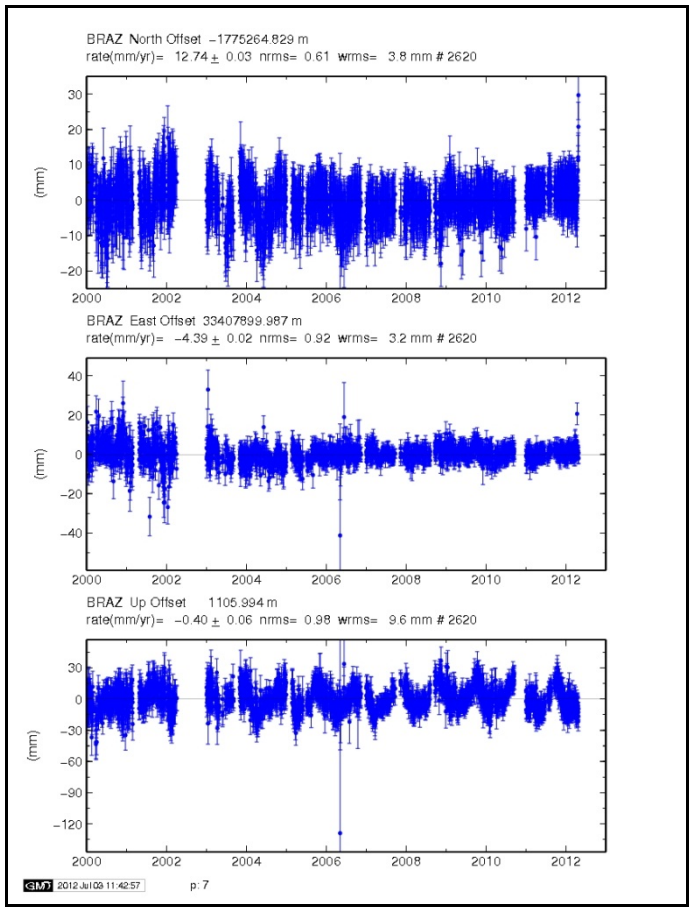


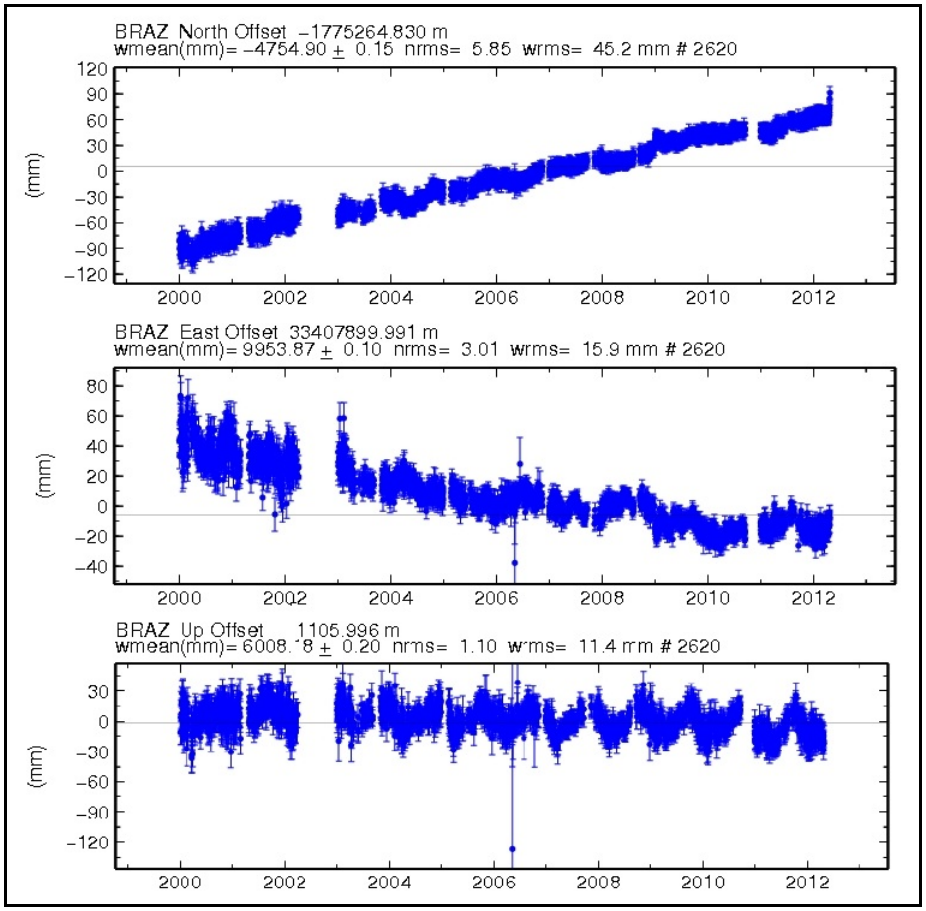


# Brasilia GPS station (BRAZ), Brazil

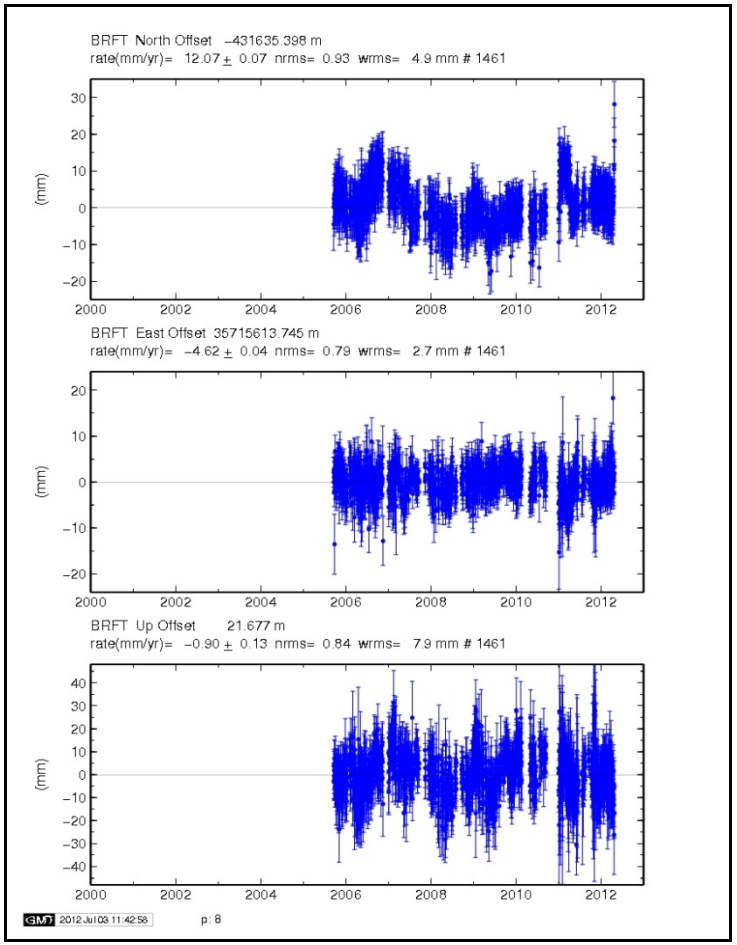


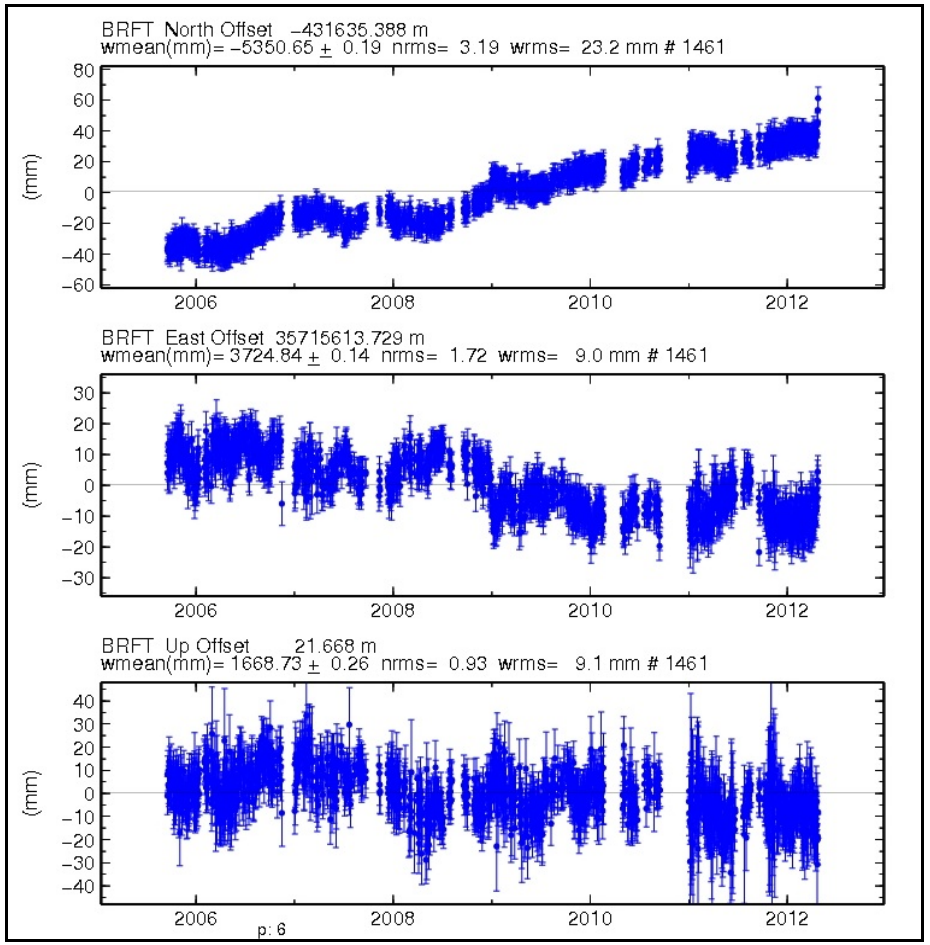


# Fortaleza GPS station (BFRT), Brazil

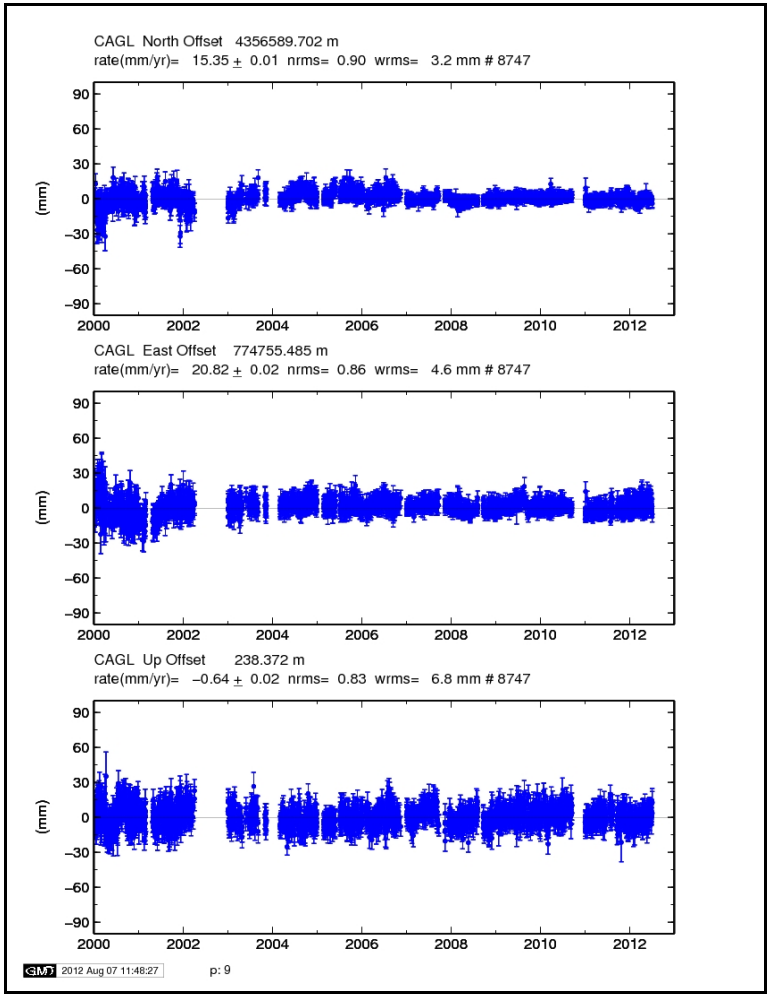


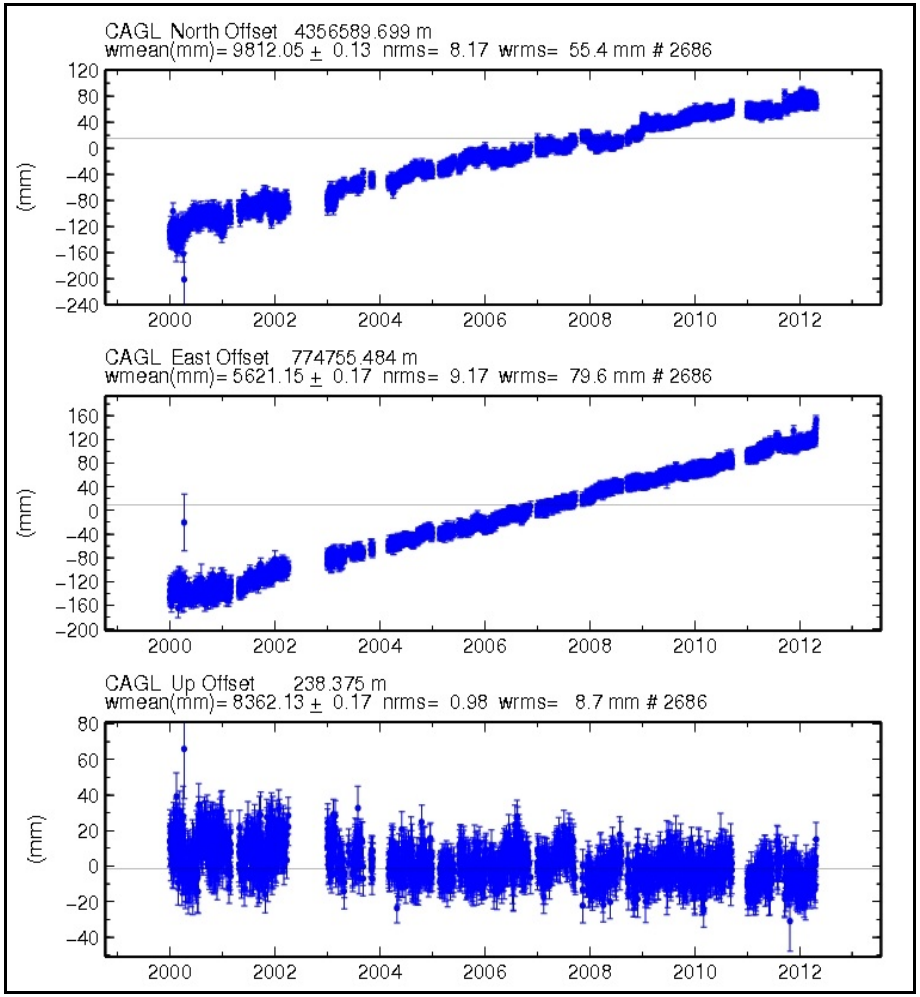


# Cagliari GPS station (CAGL), Sardinia

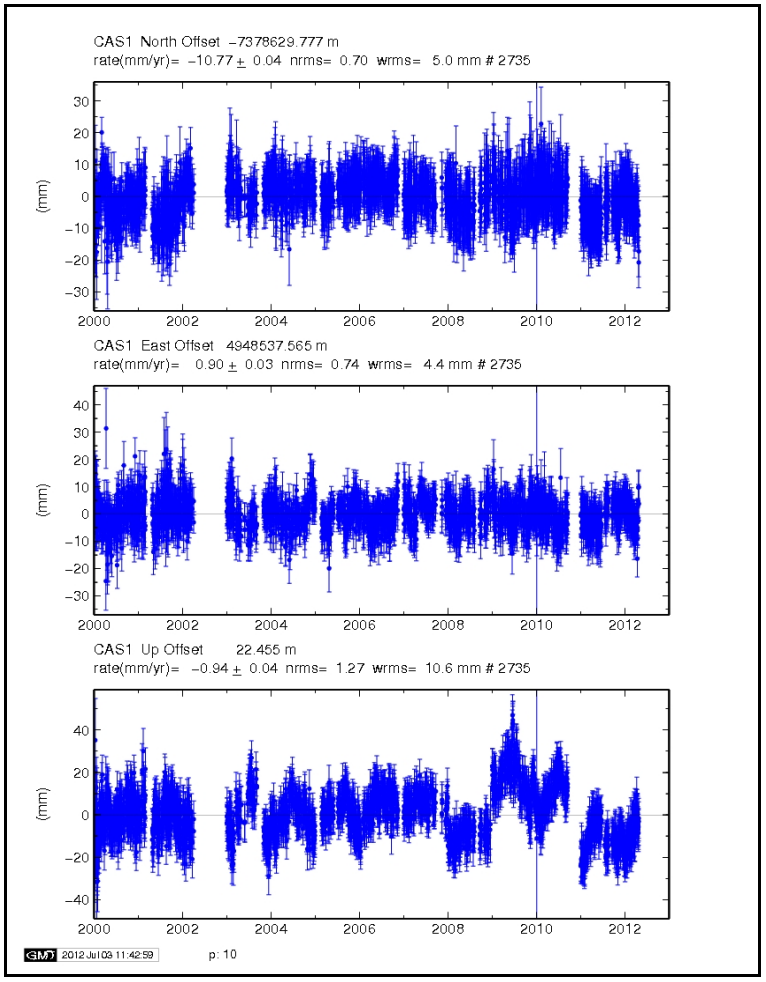


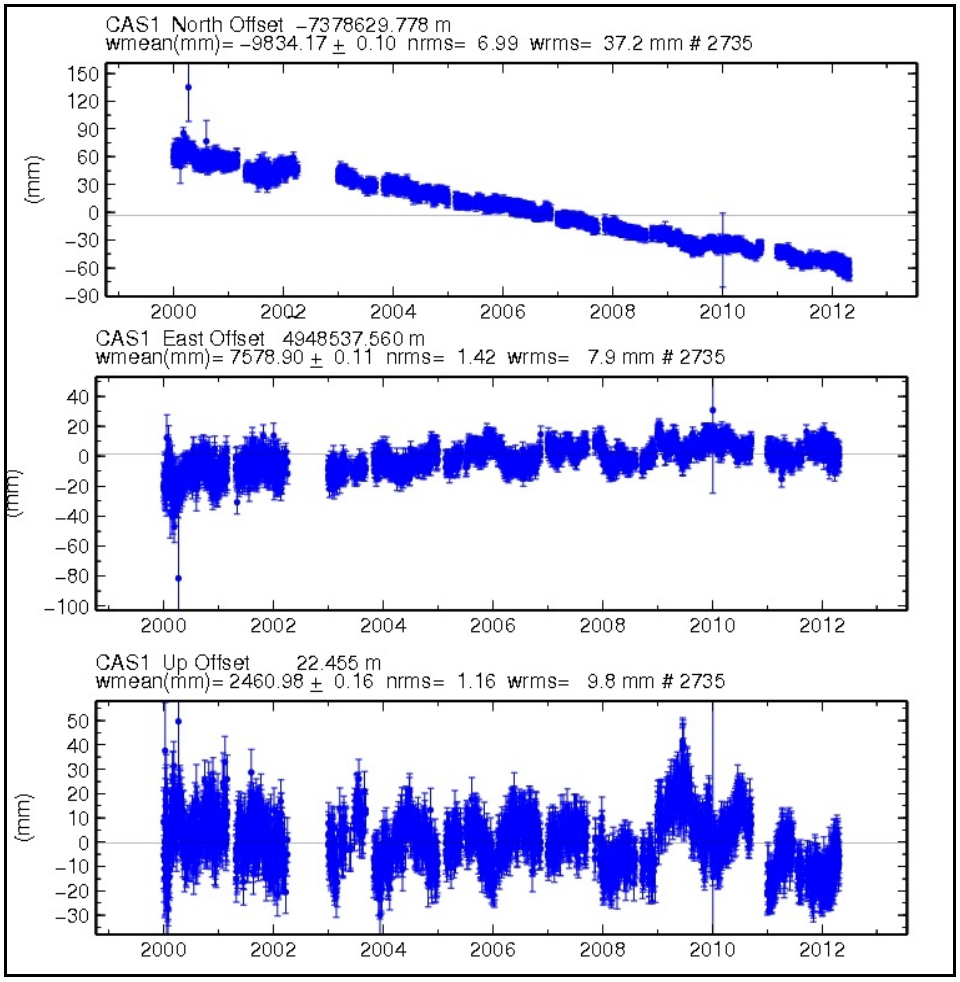


# Casey GPS station (CAS1), Antarctica

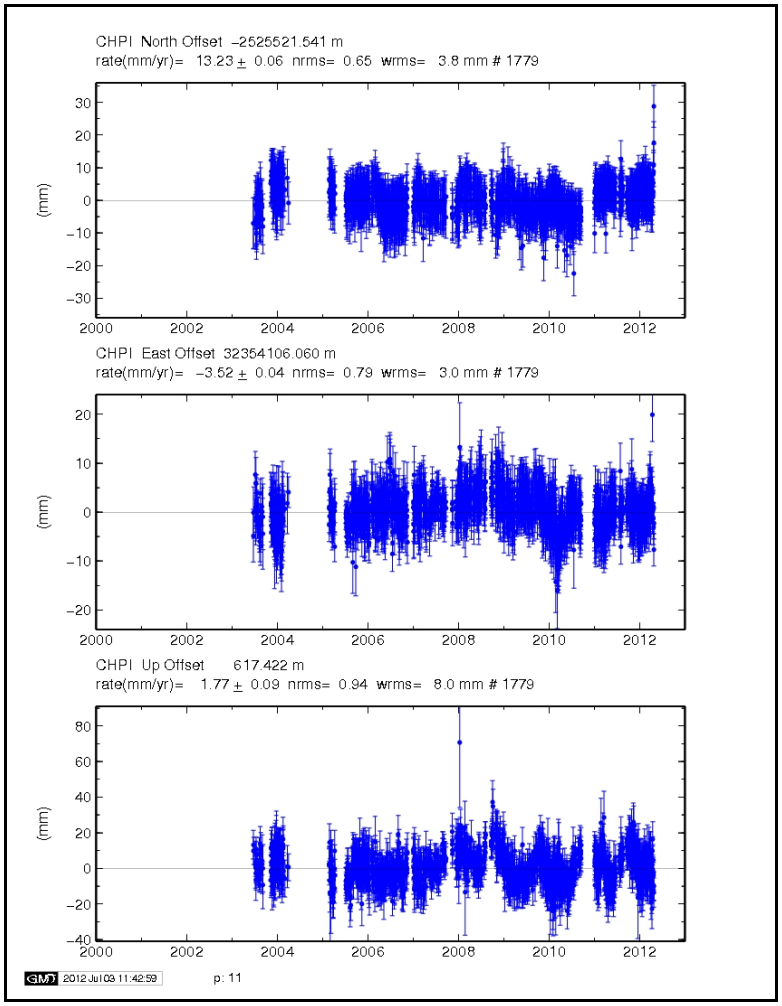


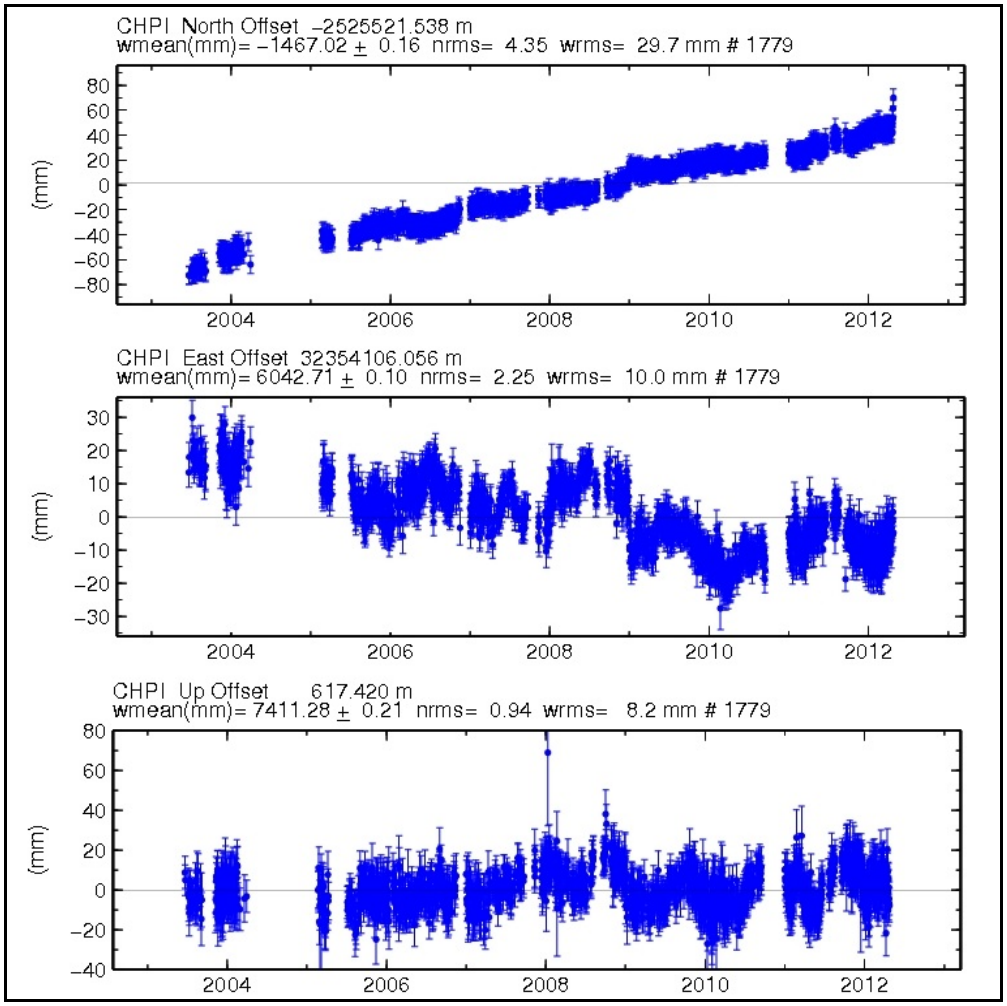


# Cachoeira Pa GPS station (CHIP), Brazil

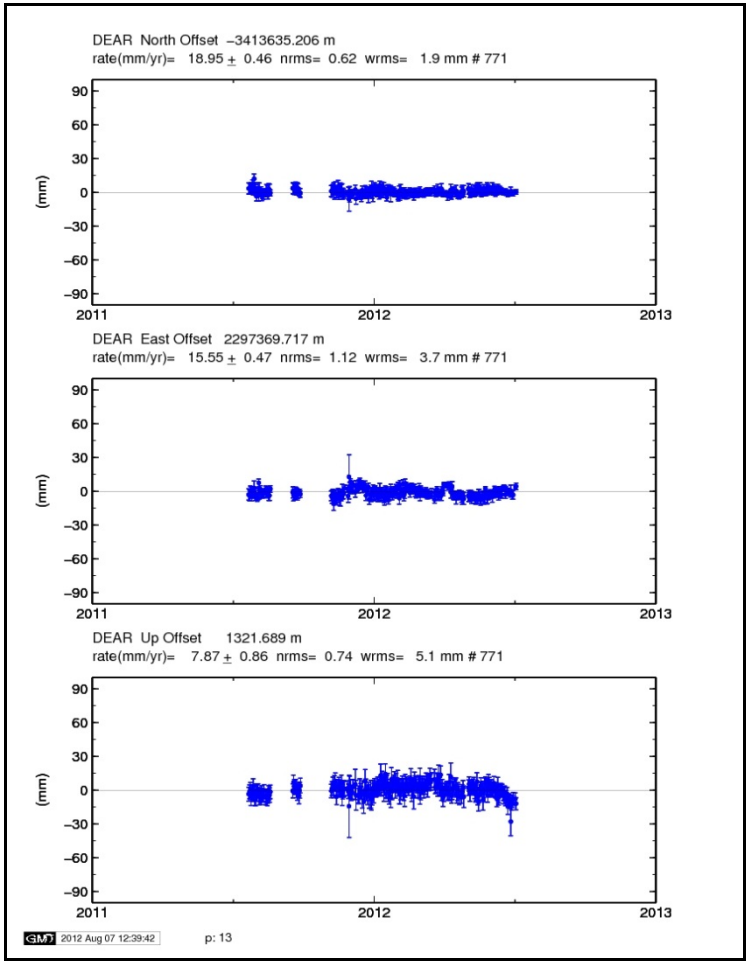


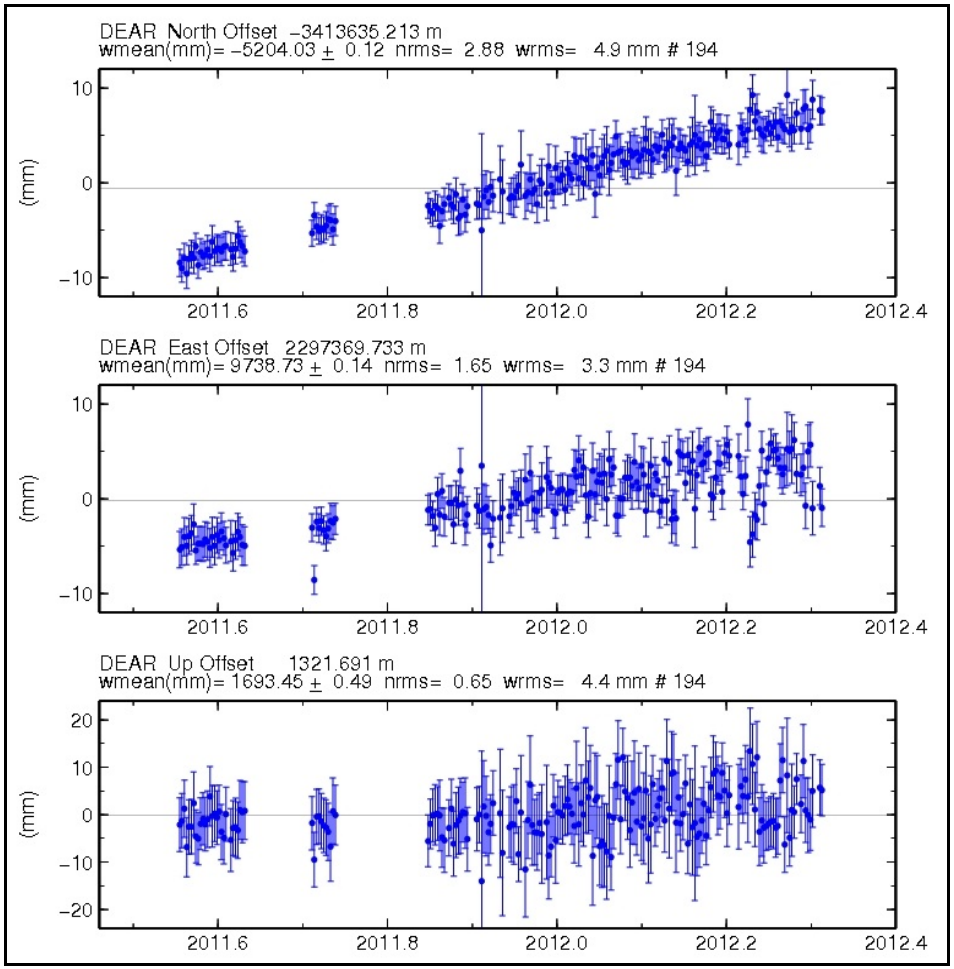


# De AAR GPS station (DEAR), South Africa

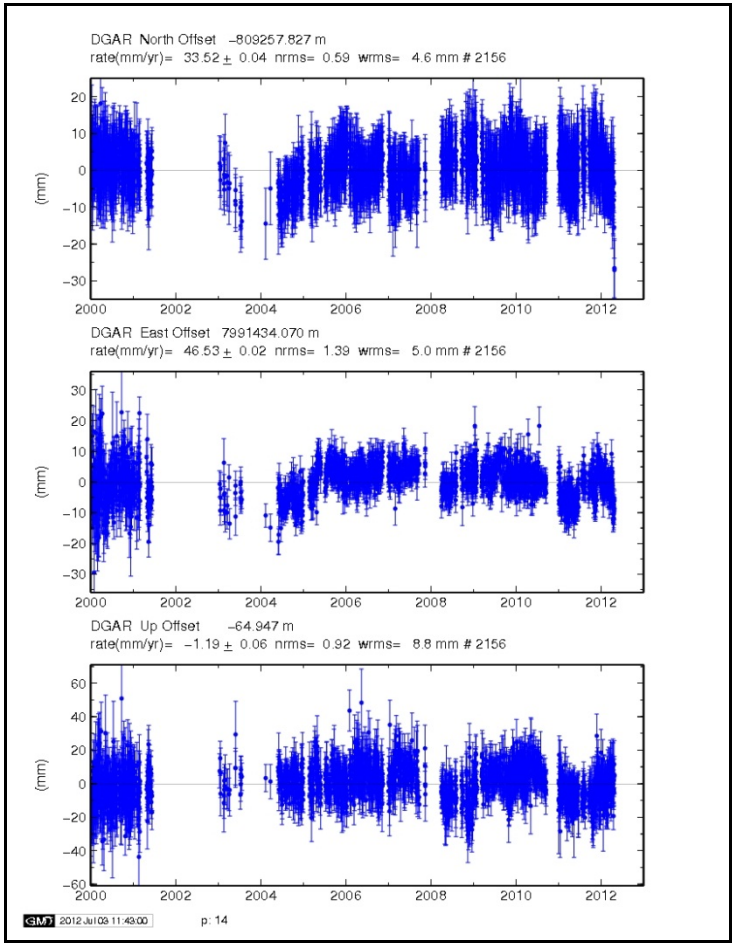


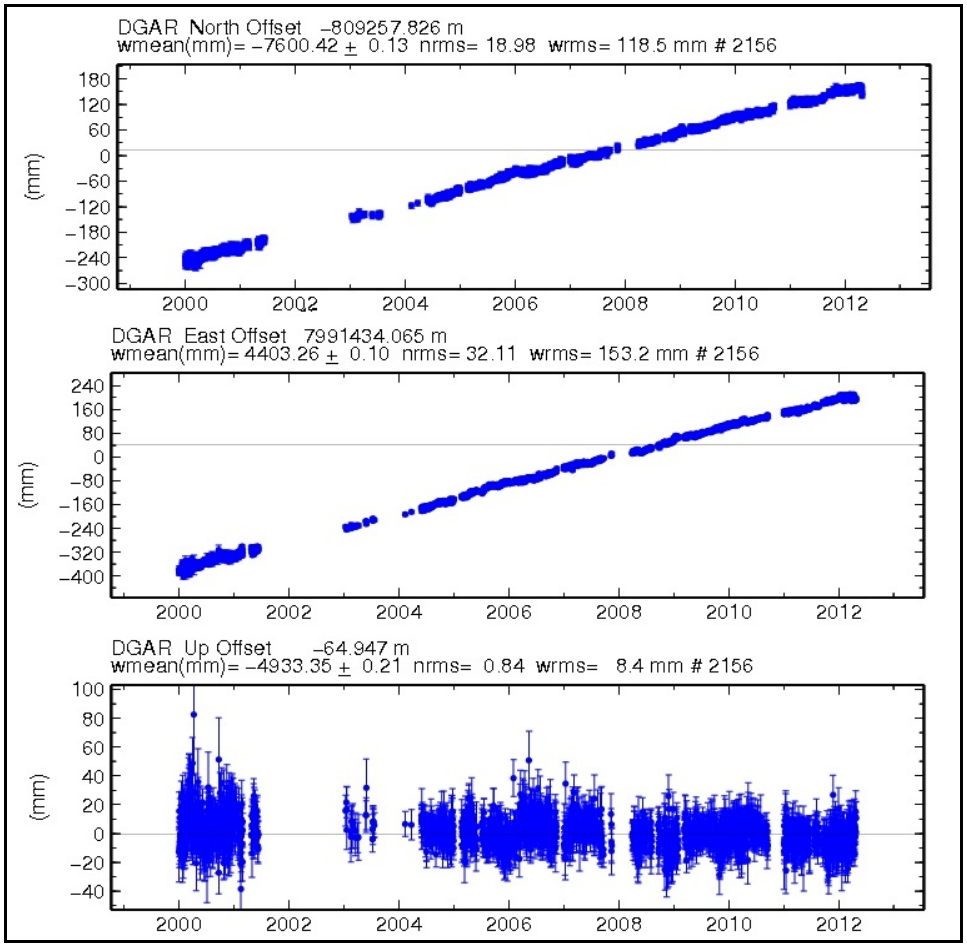


# Diego Garcia GPS station (DGAR), U.K.

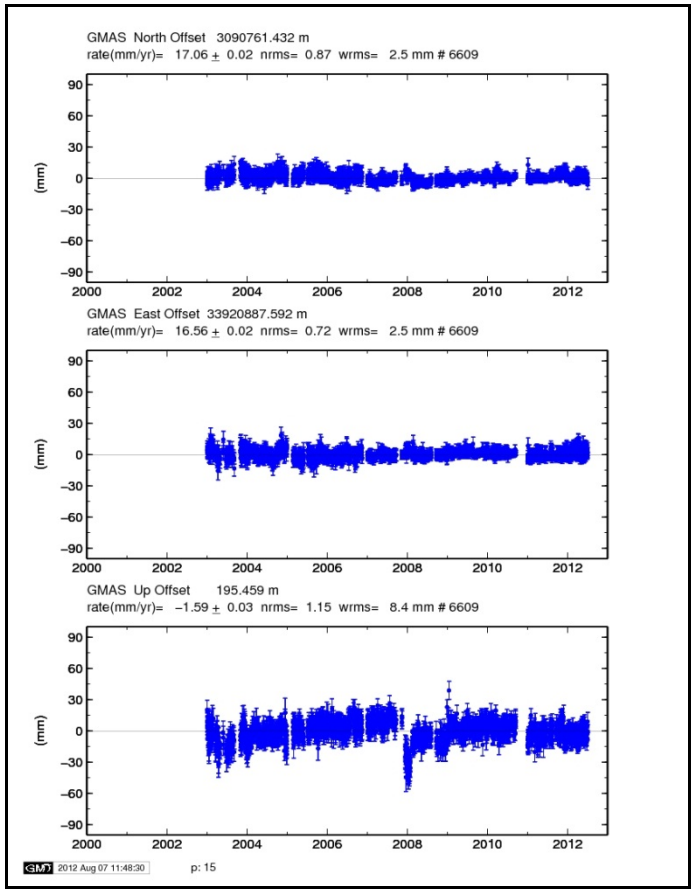


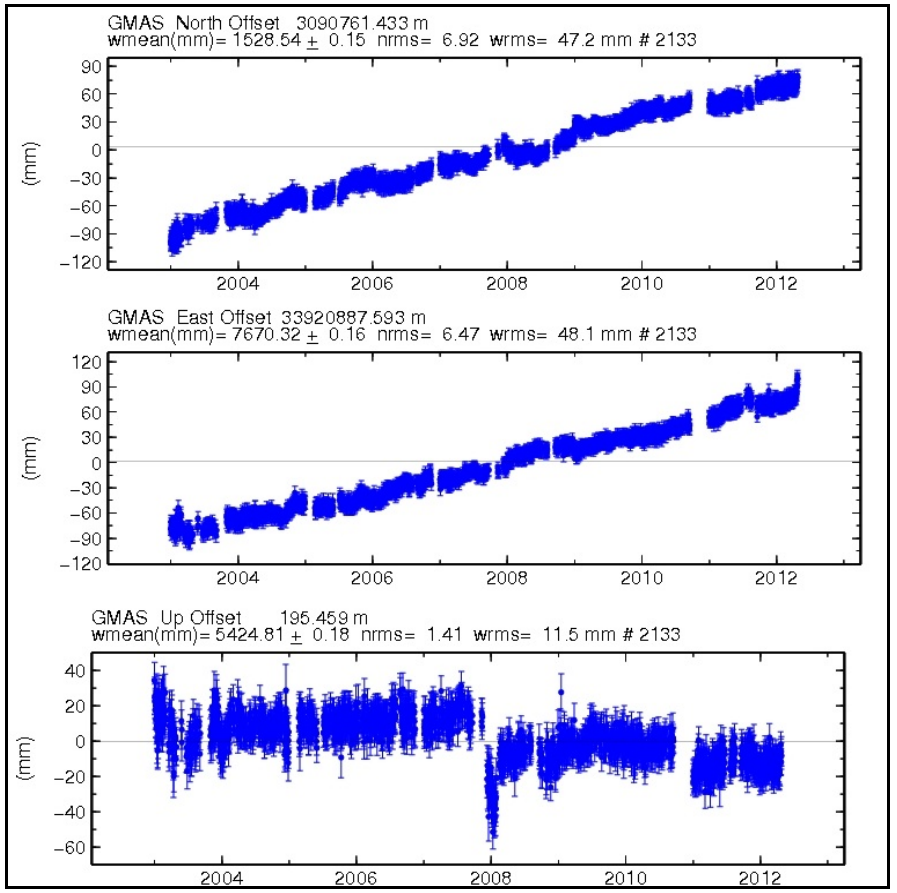


# GUTS Maspalomas GPS station (GMAS), Spain

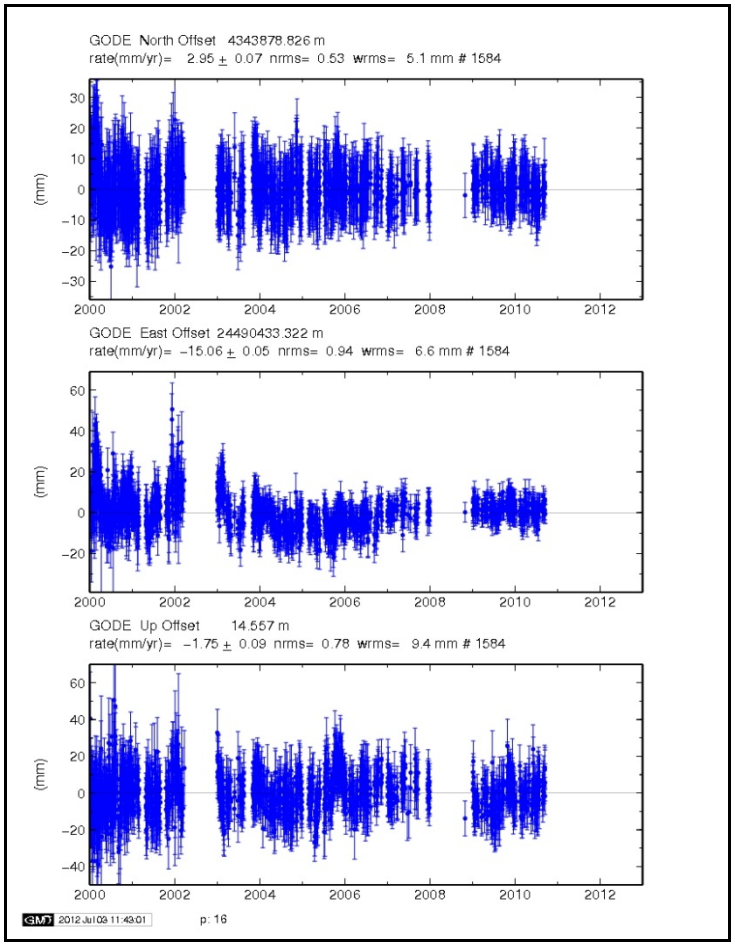


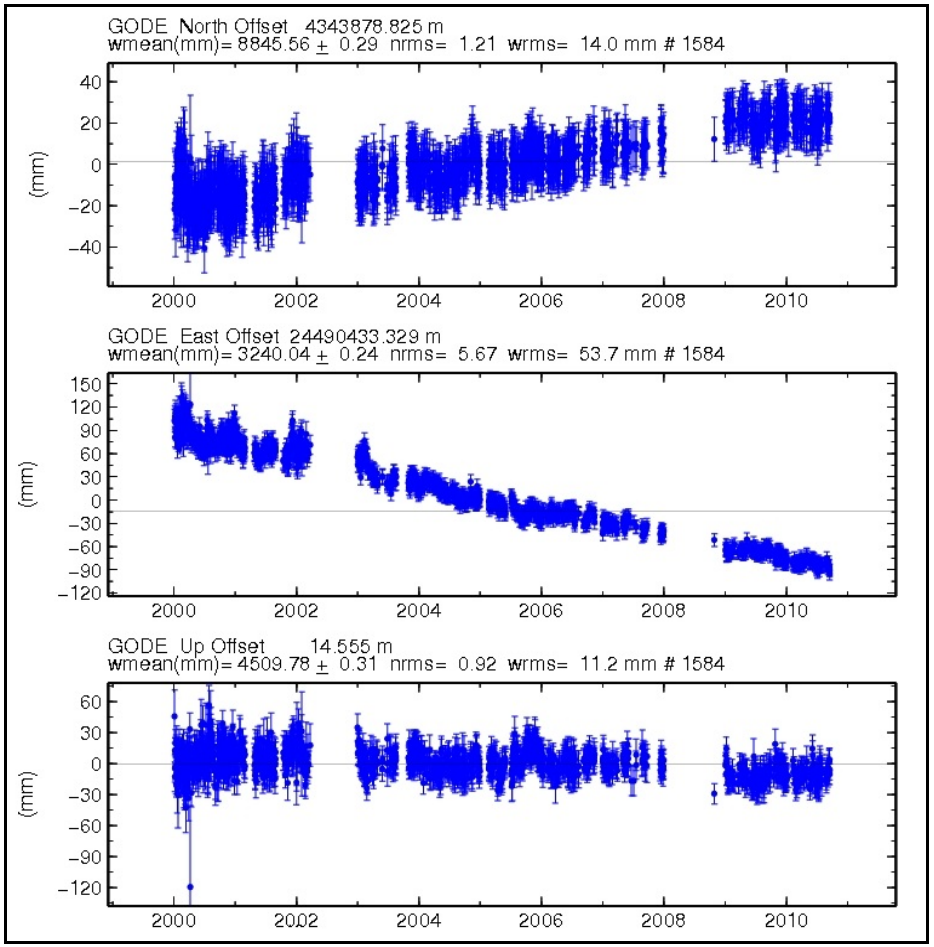


# GGAO (Greenbelt) GPS station (GOGE), USA

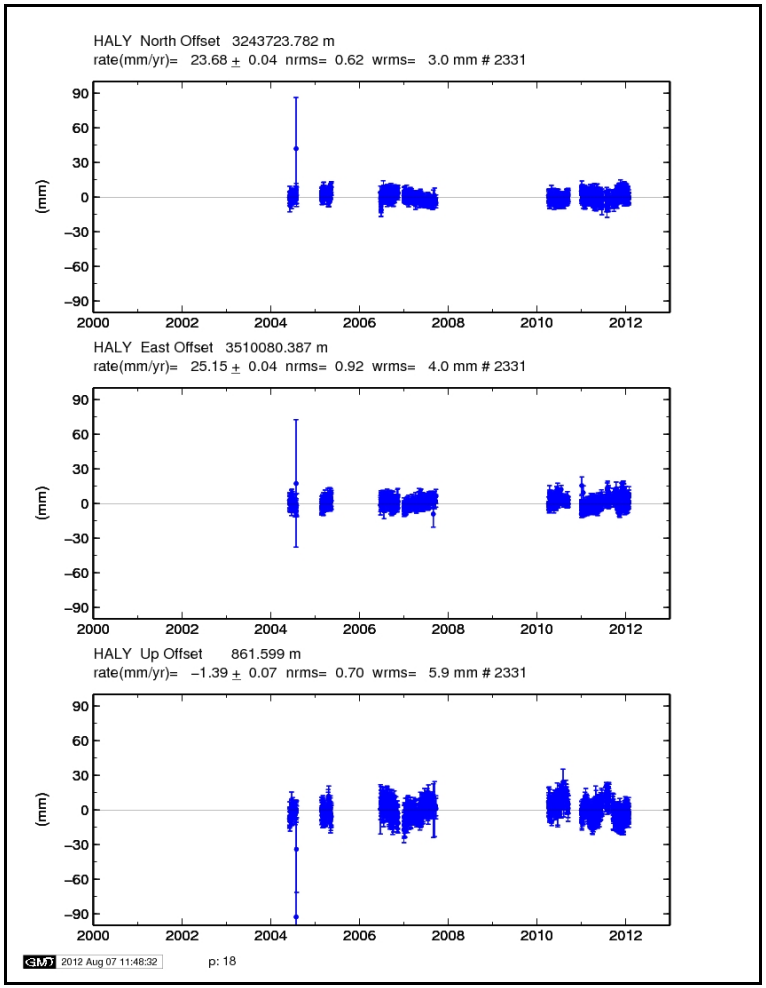


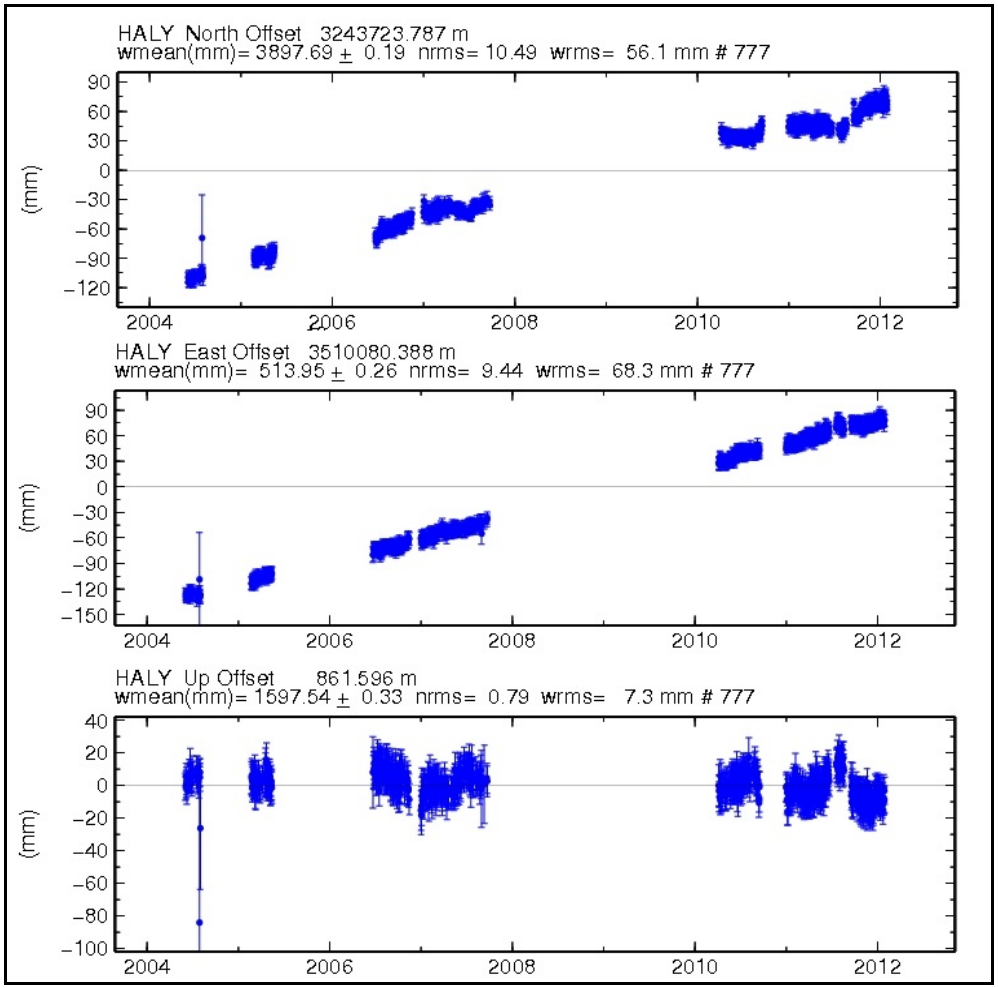


# Halat Ammar GPS station (HALY), Saudi Arabia

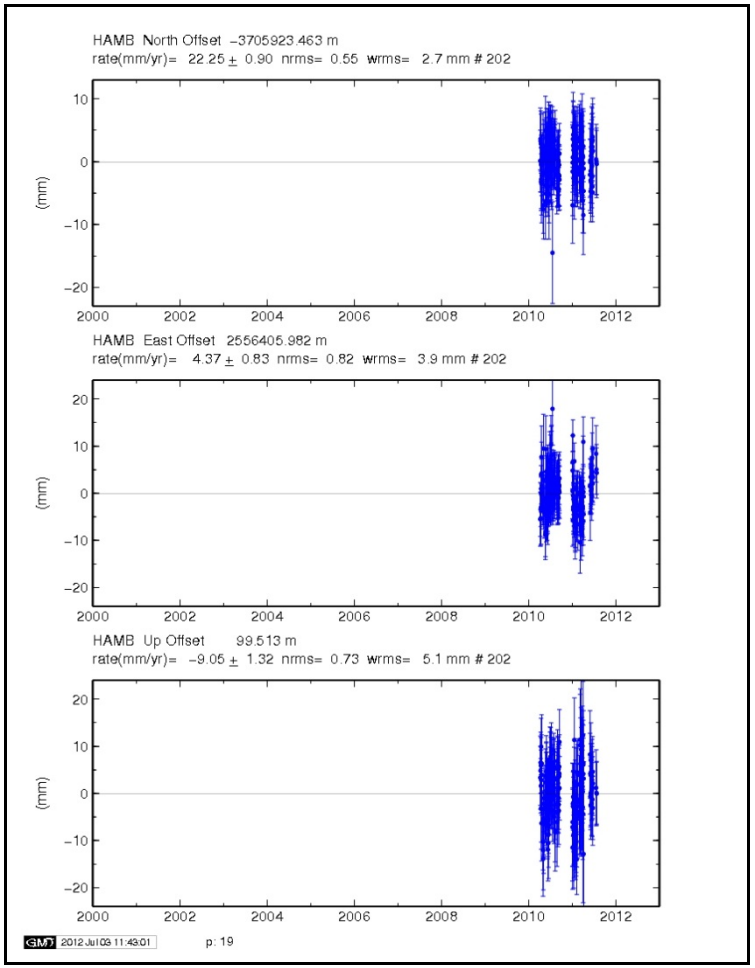


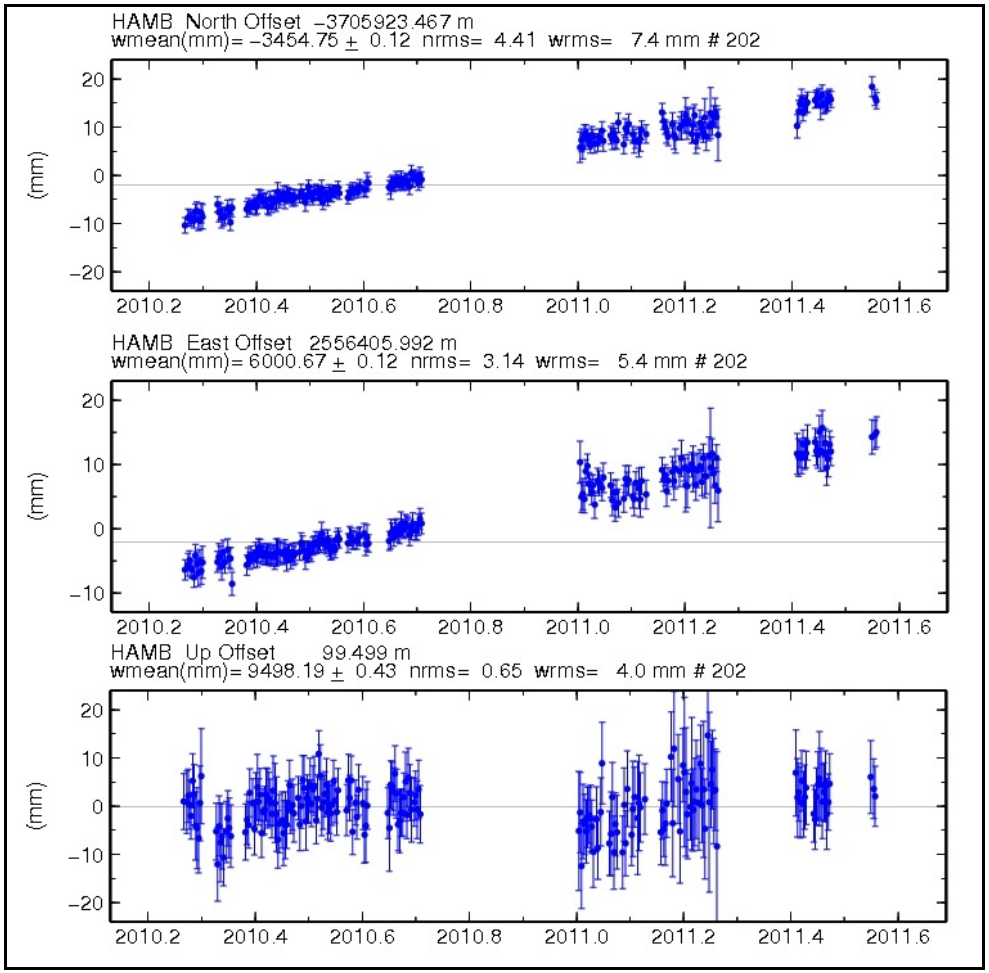


# Hamburg GPS station (HAMB), South Africa

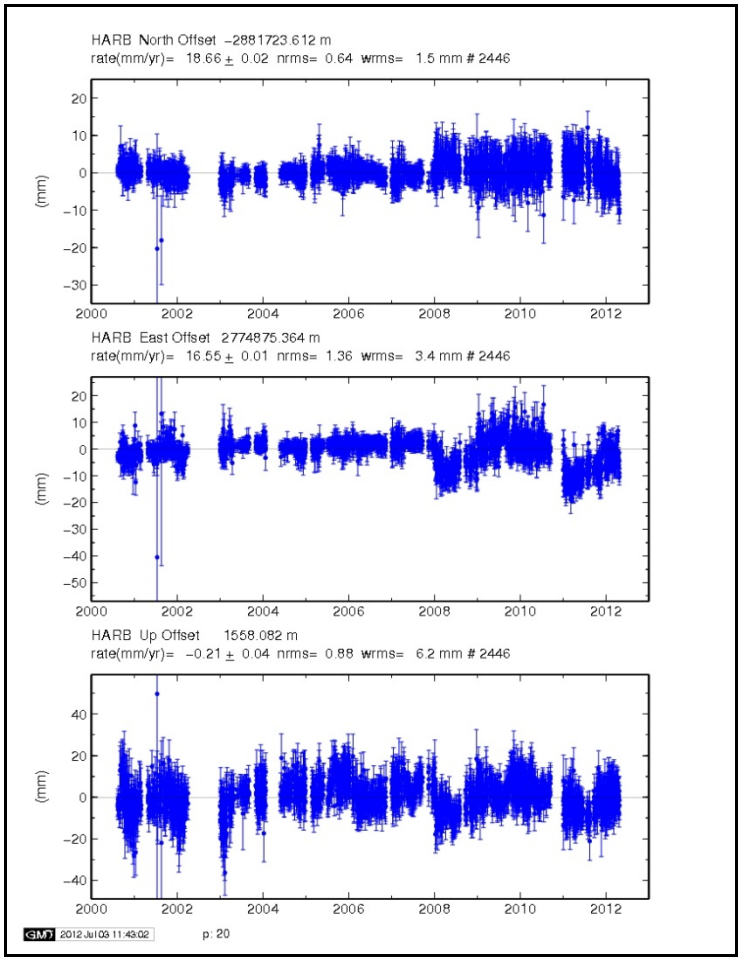


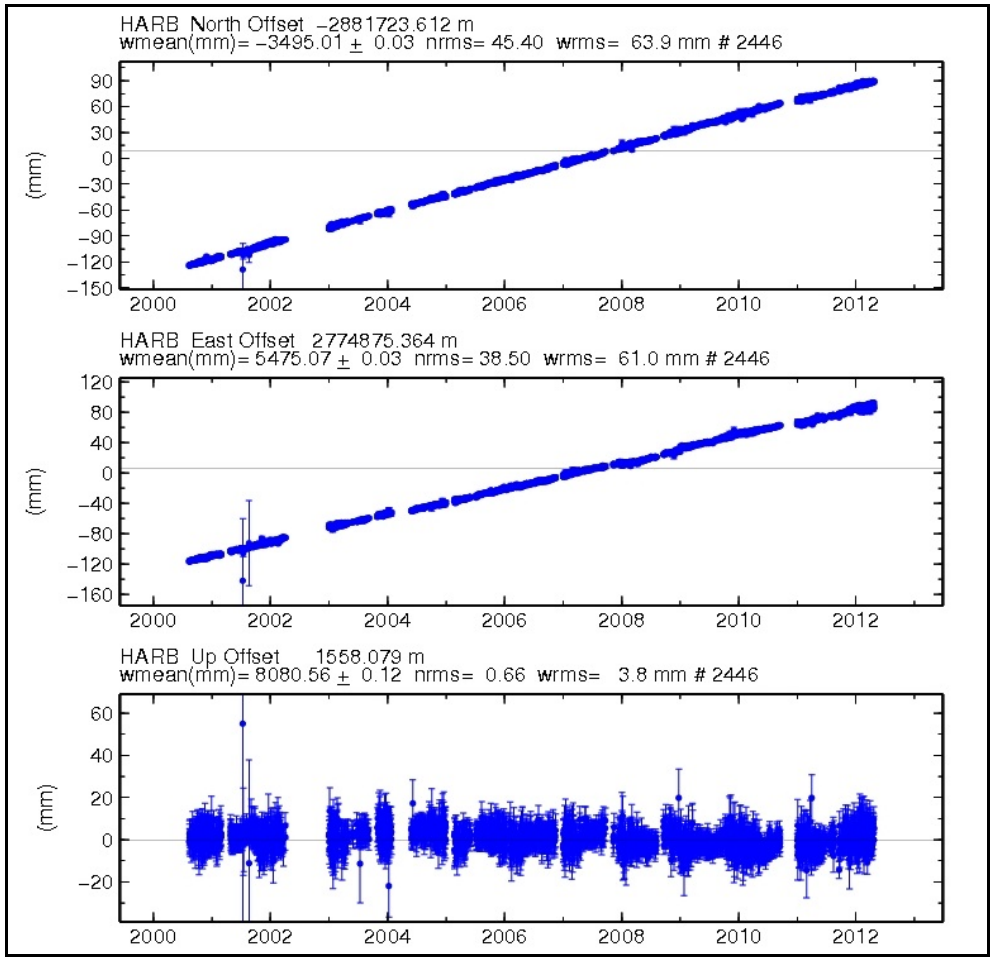


# Hartebeesthoek GPS station (HARB), South Africa

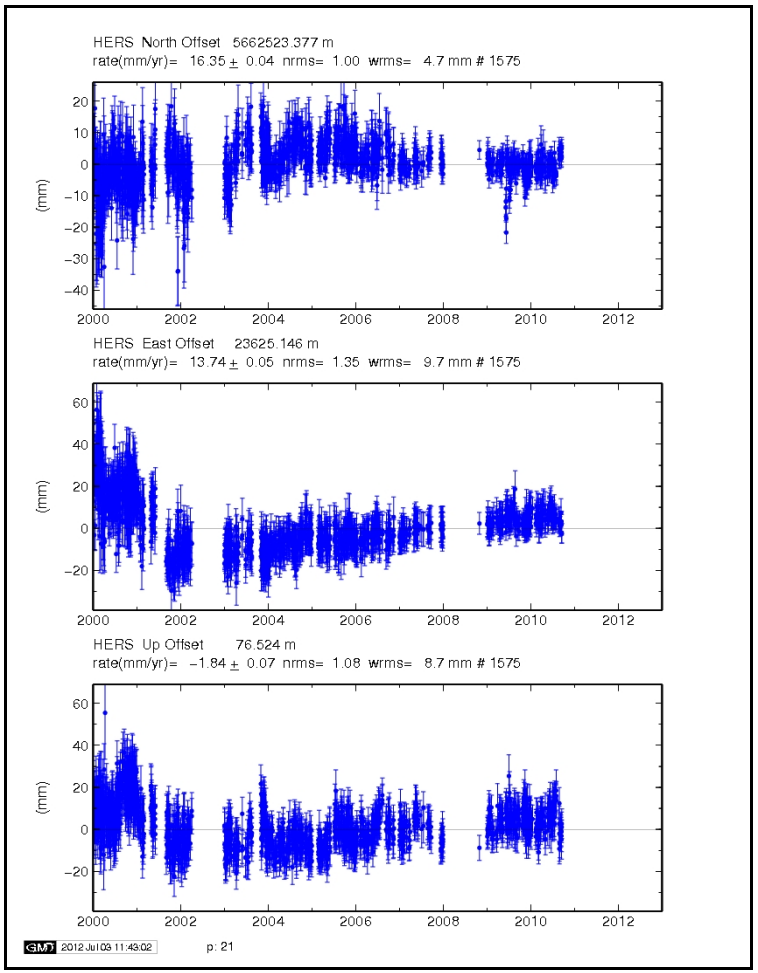


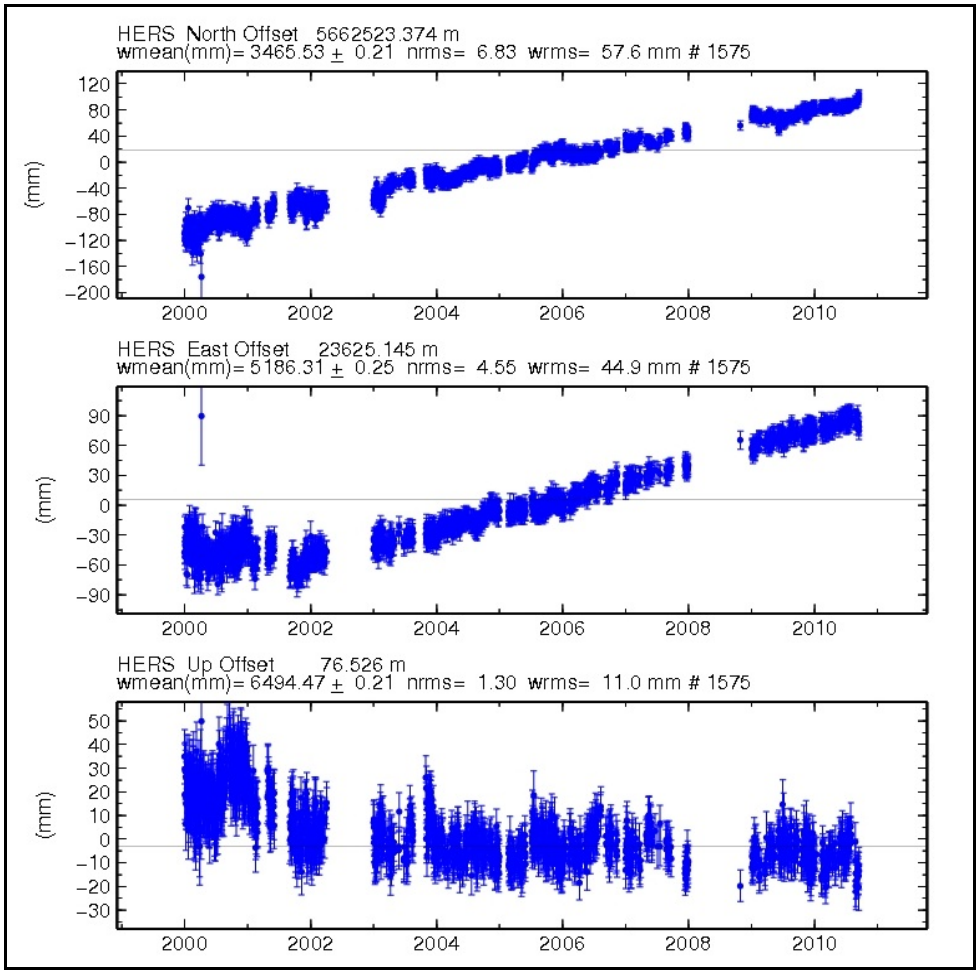


# Herstmonceux GPS station (HERS), United Kingdom

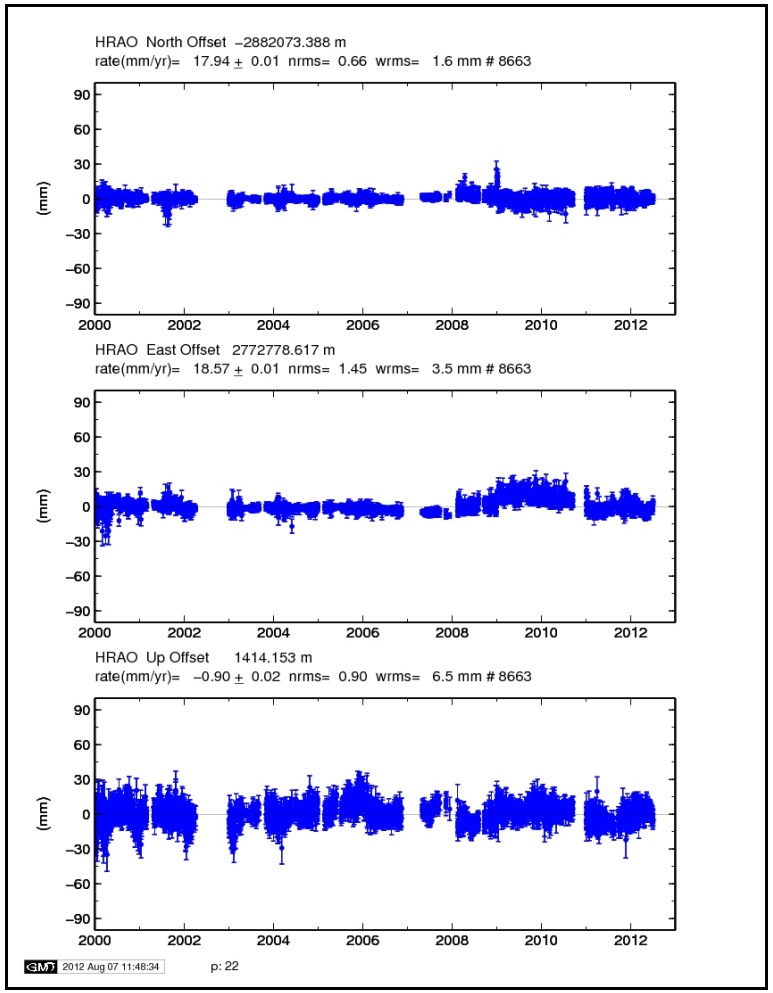


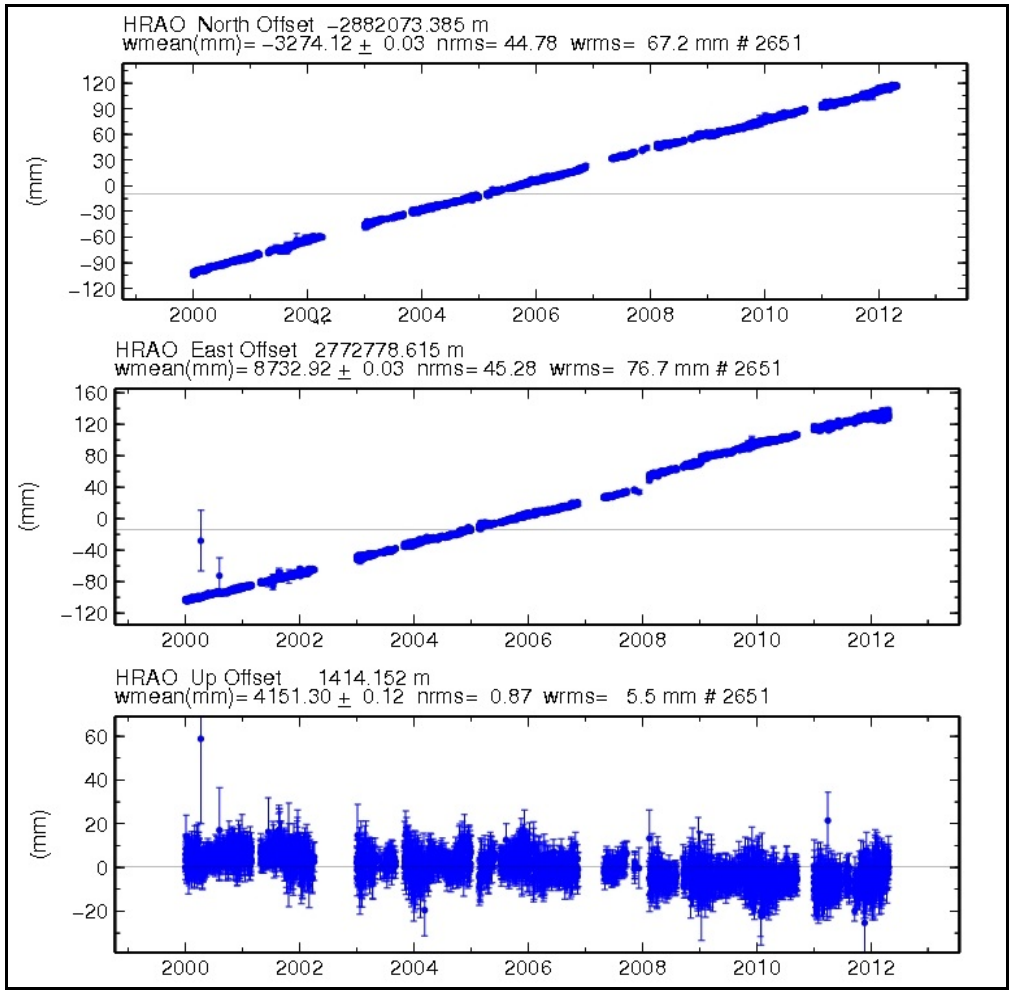


# Hartebeesthoek GPS station (HRAO), South Africa

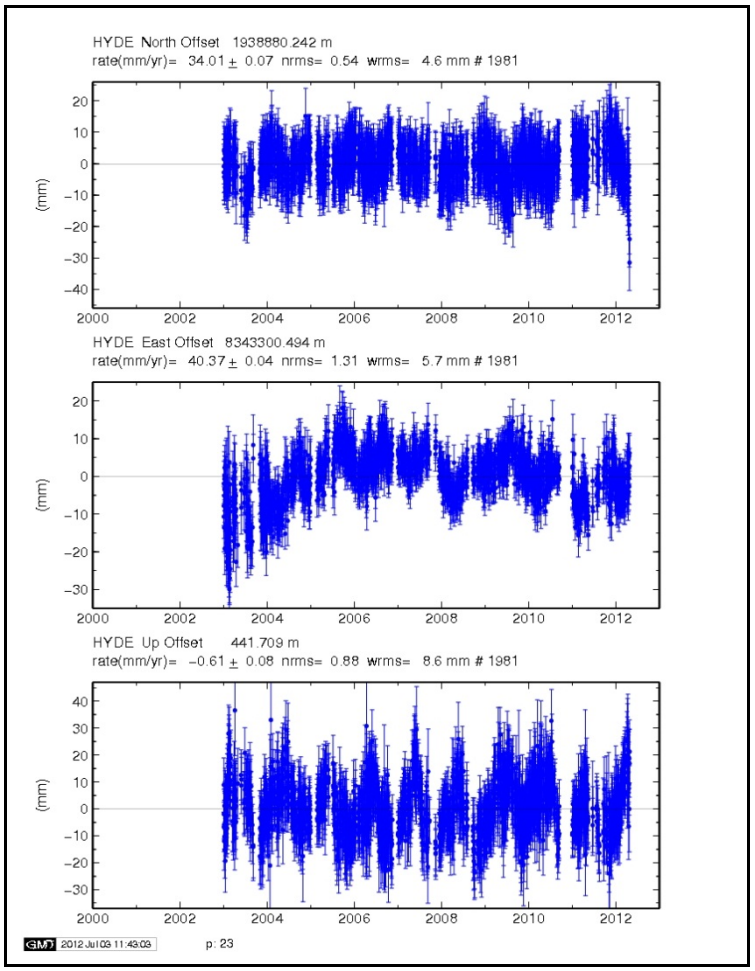


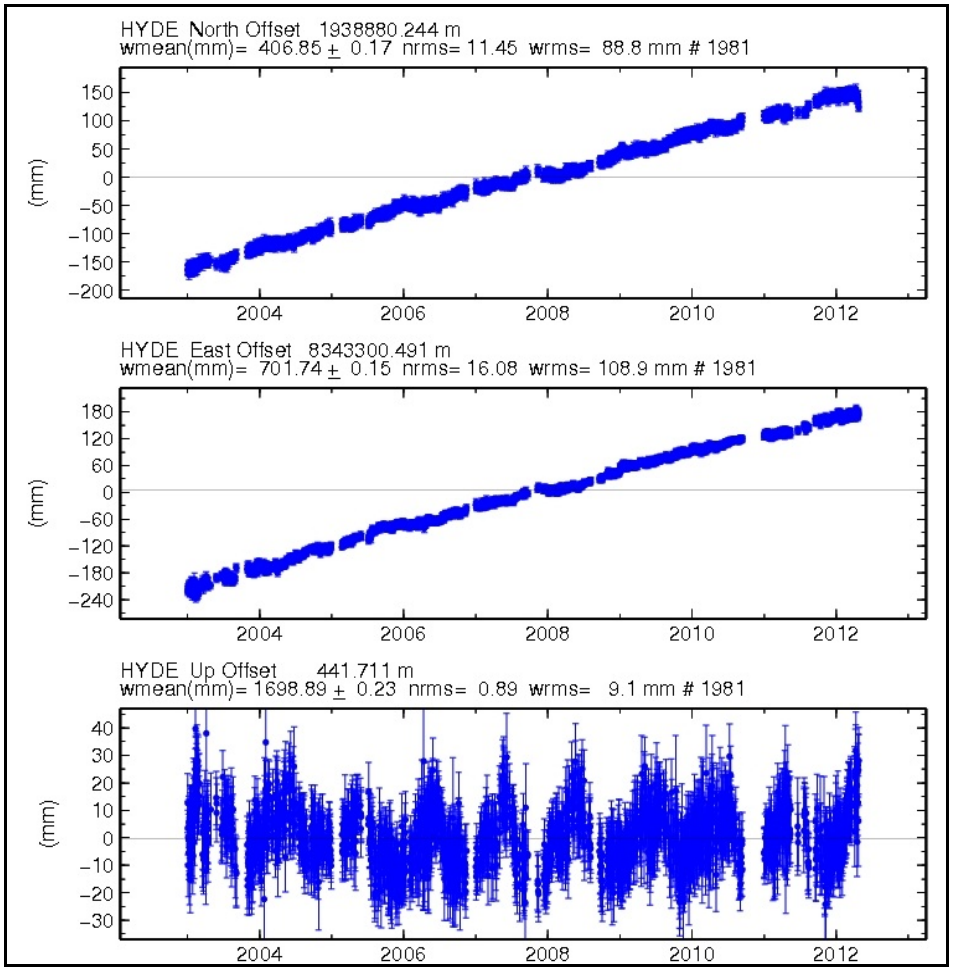


**National Geophysical Research Institute GPS station (HYDE), India**

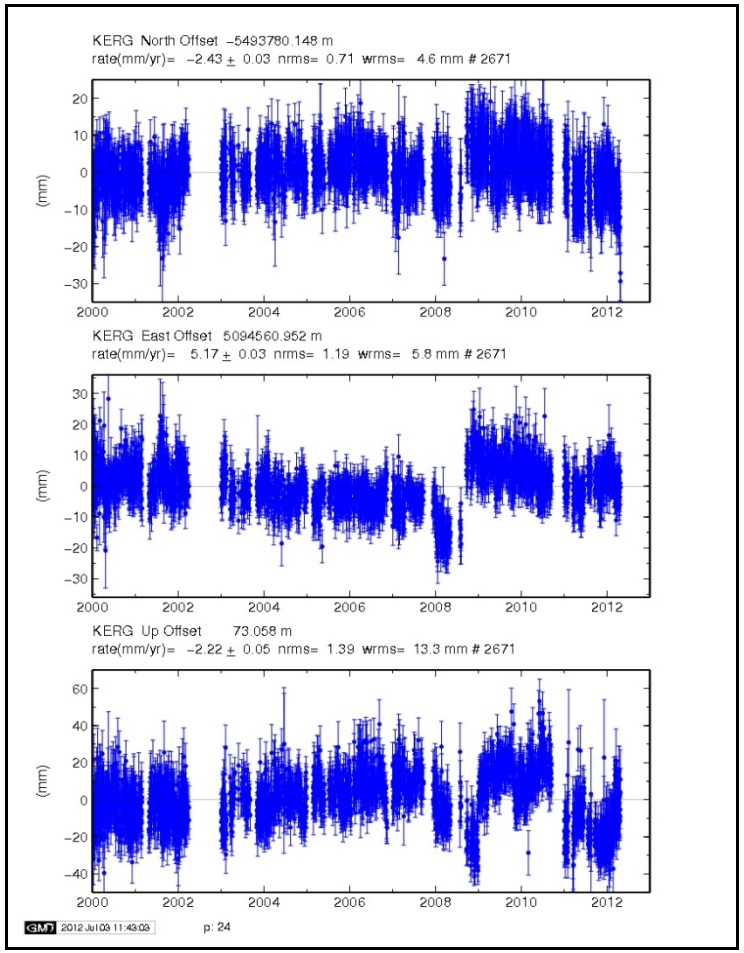


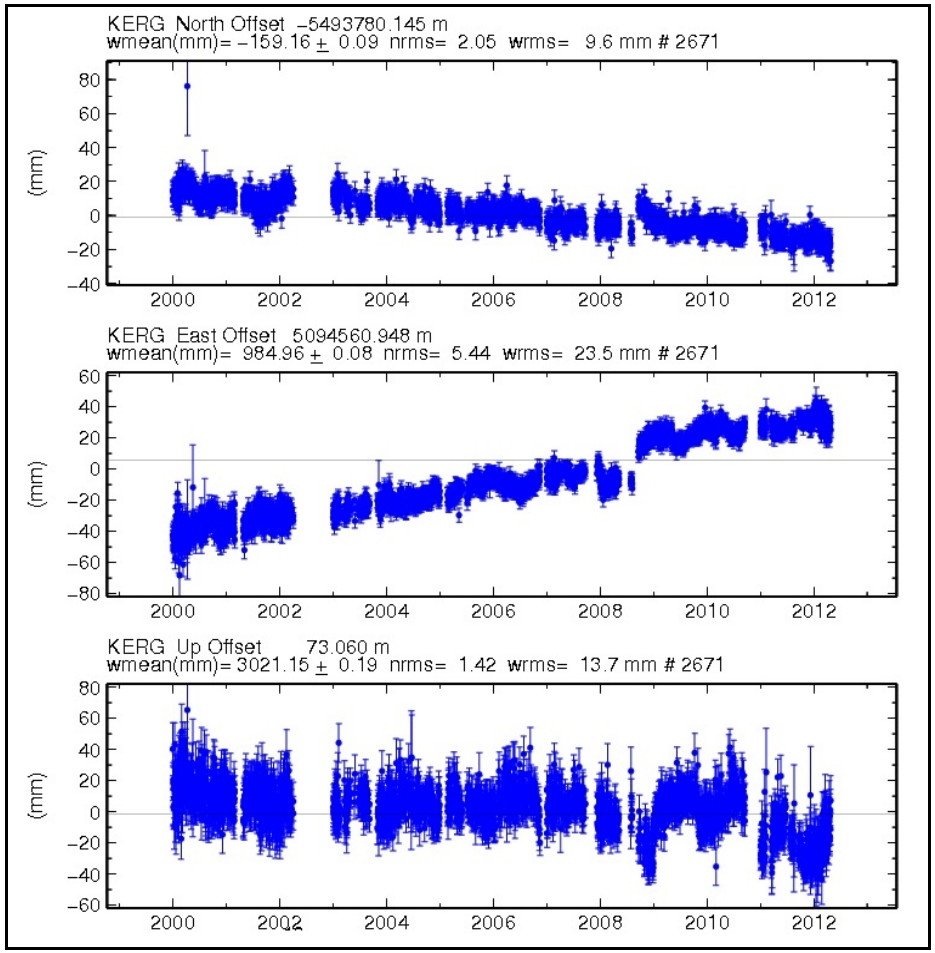


# Kerguelen Islands GPS station (KERG), Antarctica

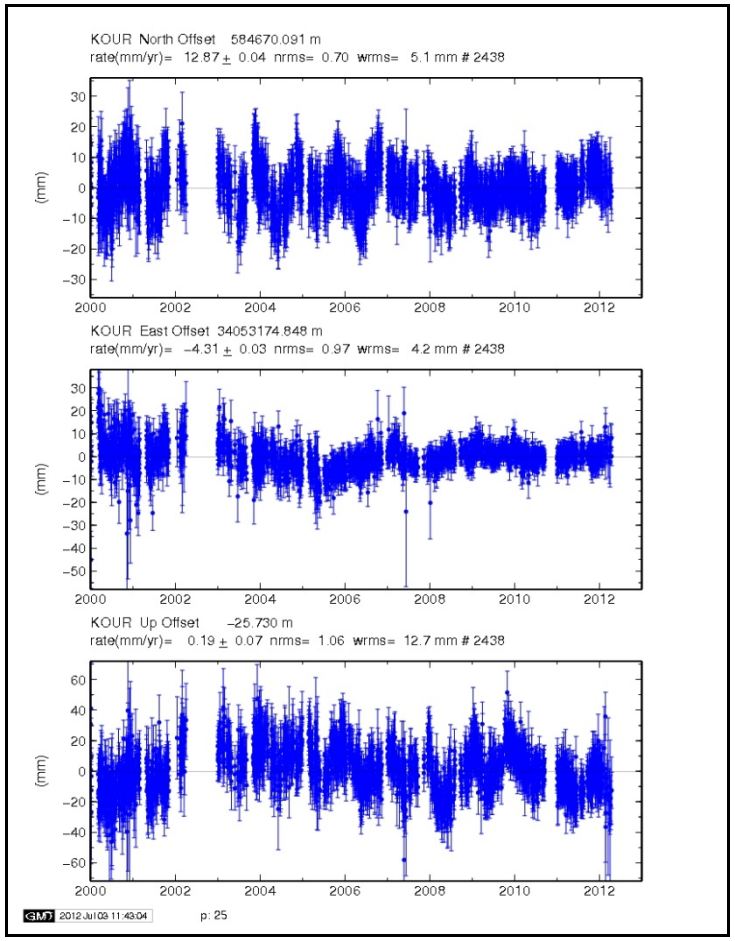


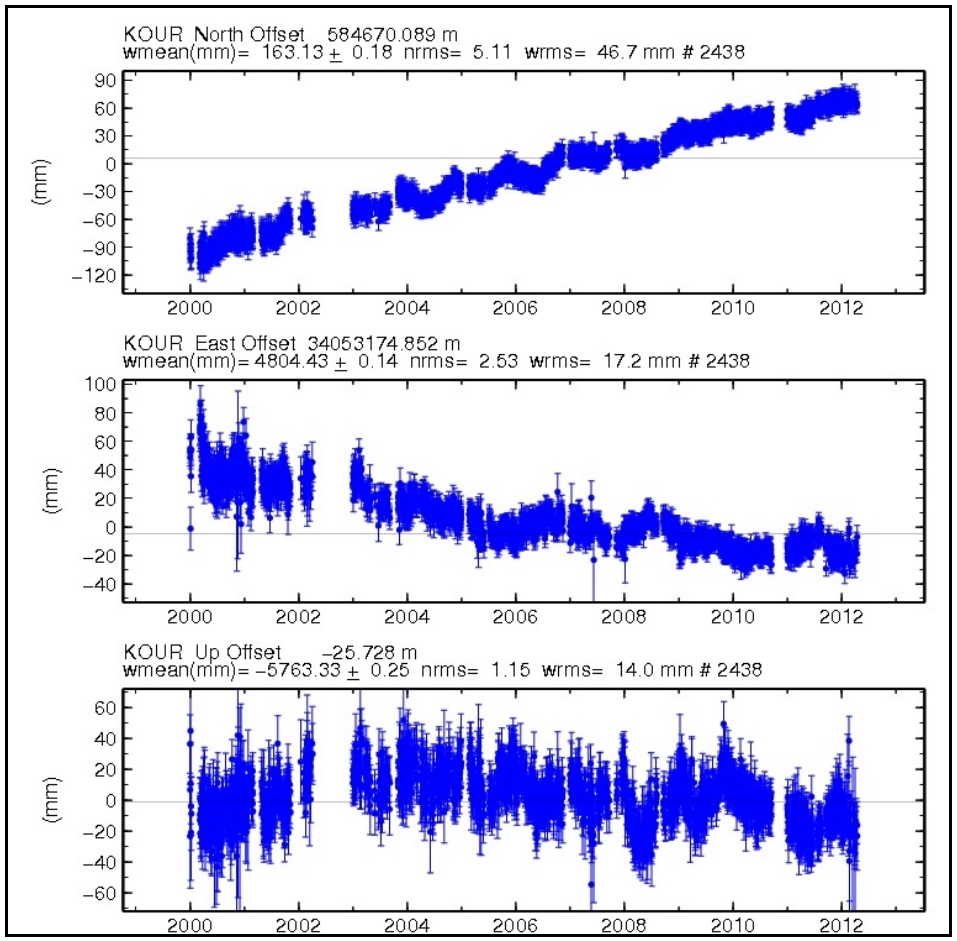


# Kourou GPS station (KOUR), French Guyana

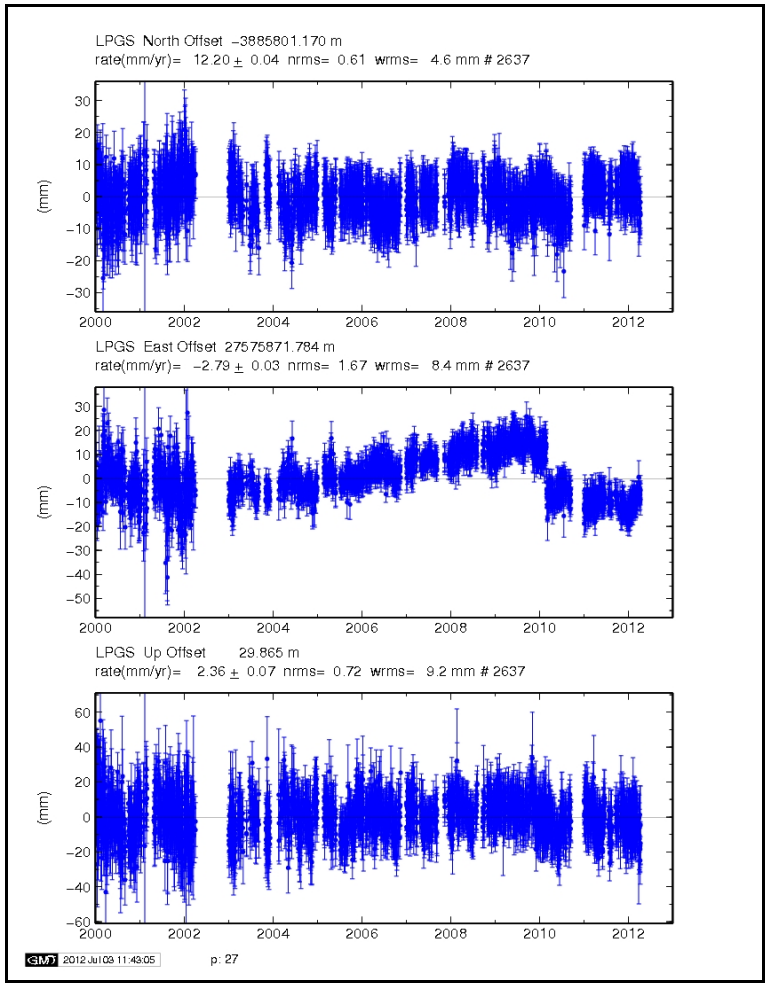


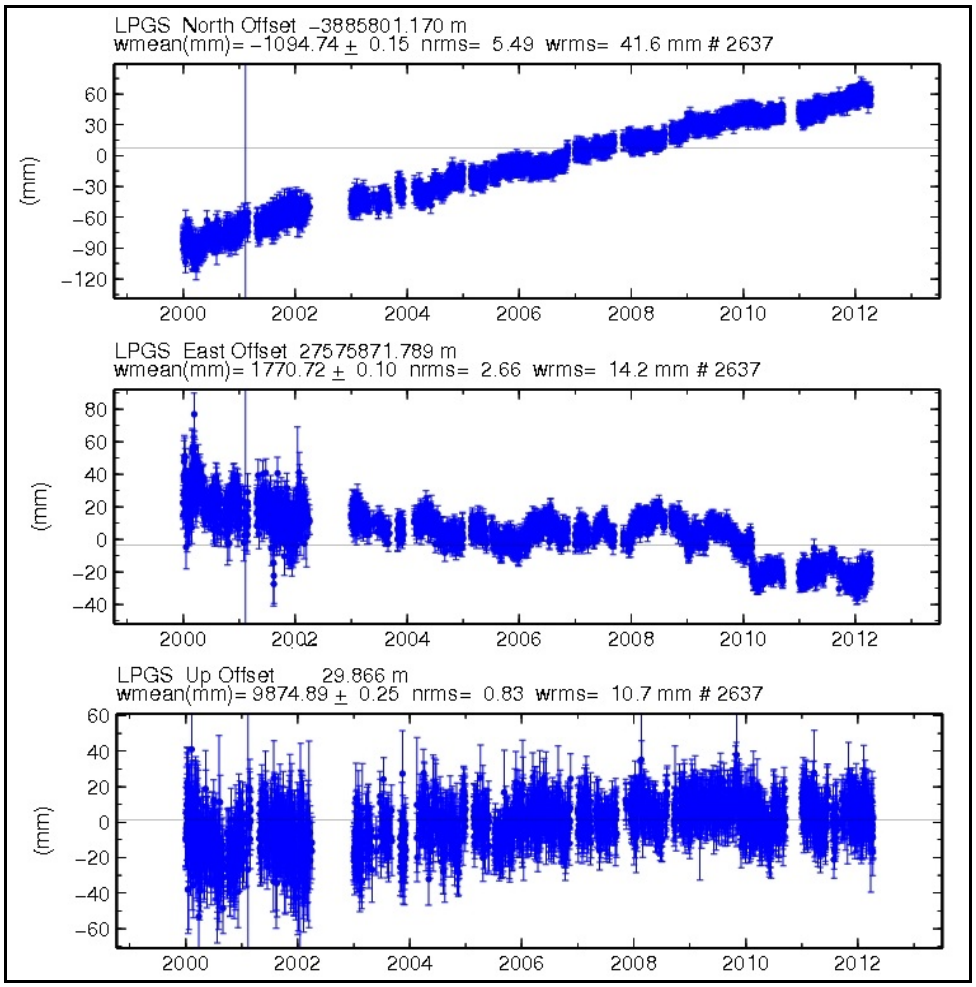


# La Plata GPS station (LPGS), Argentina

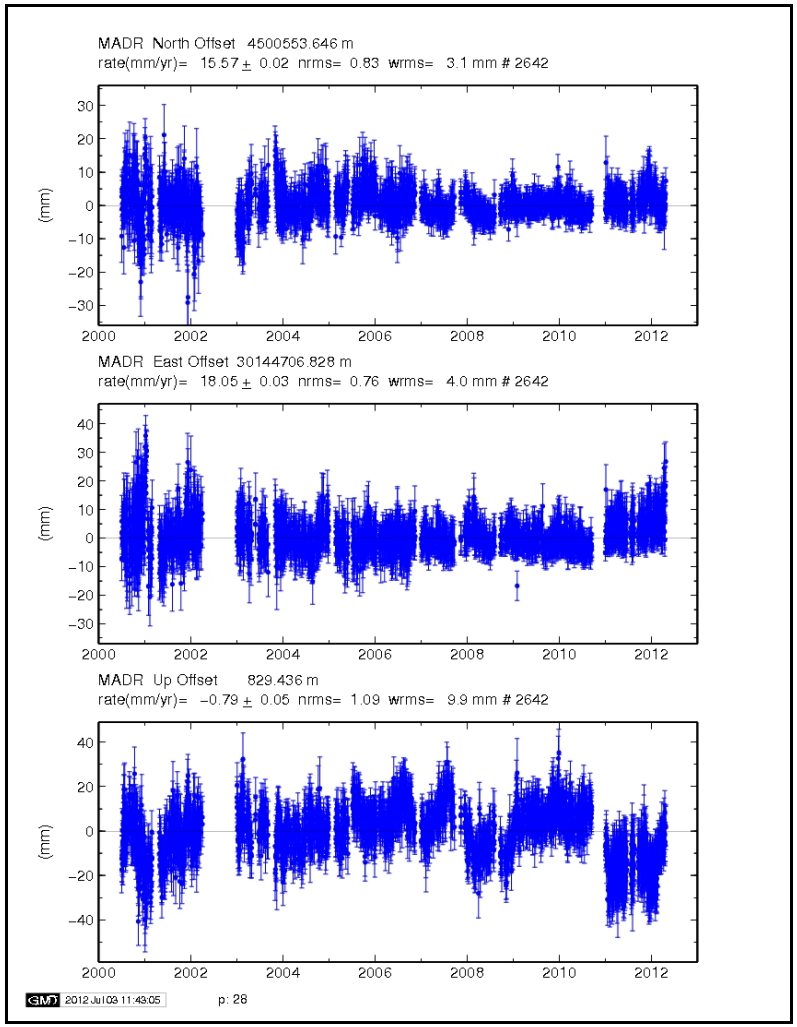


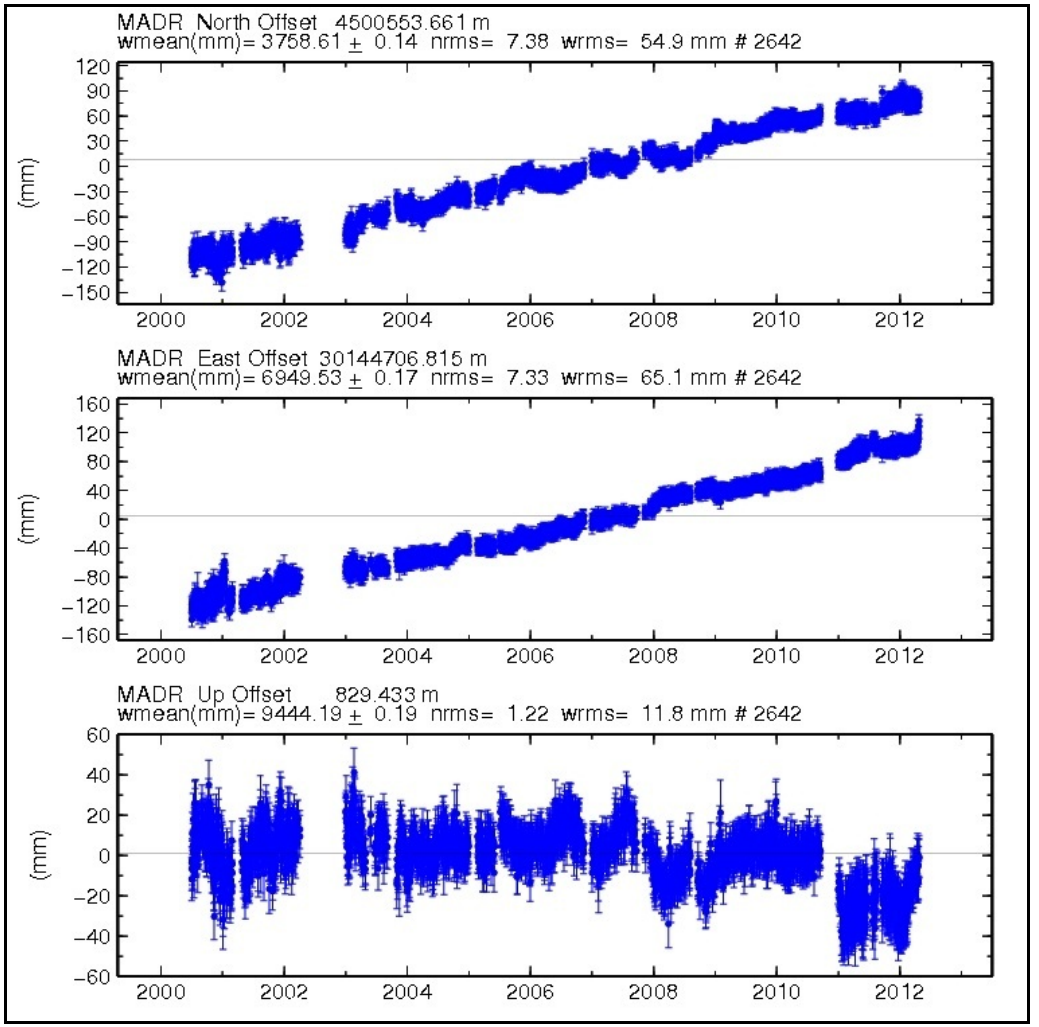


# Madrid Deep Space Tracking GPS station (MADR), Spain

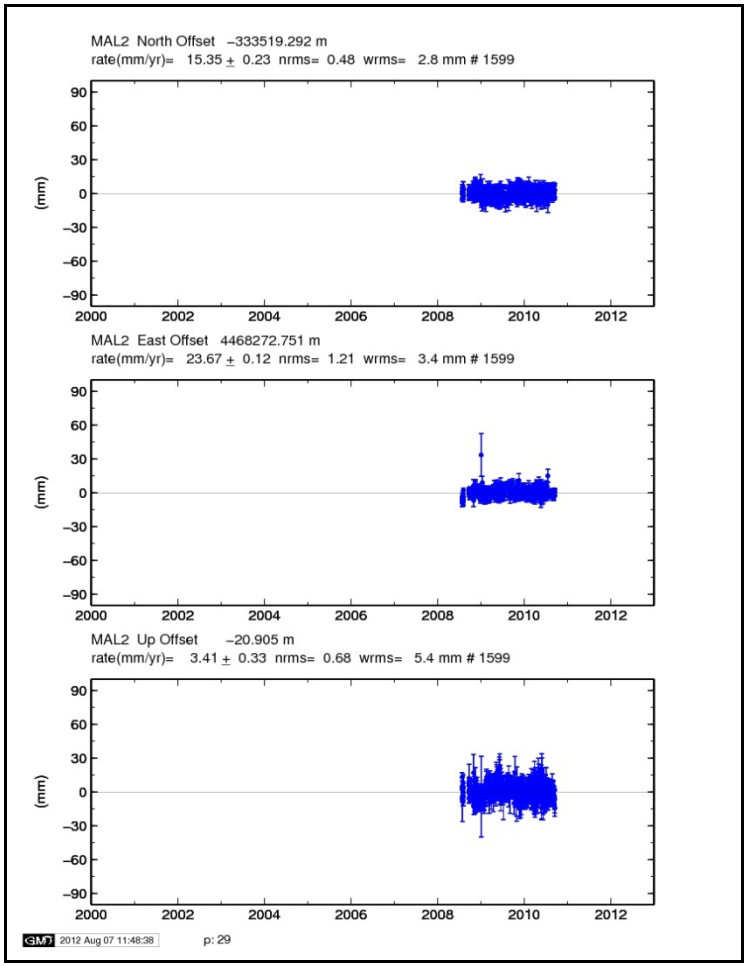


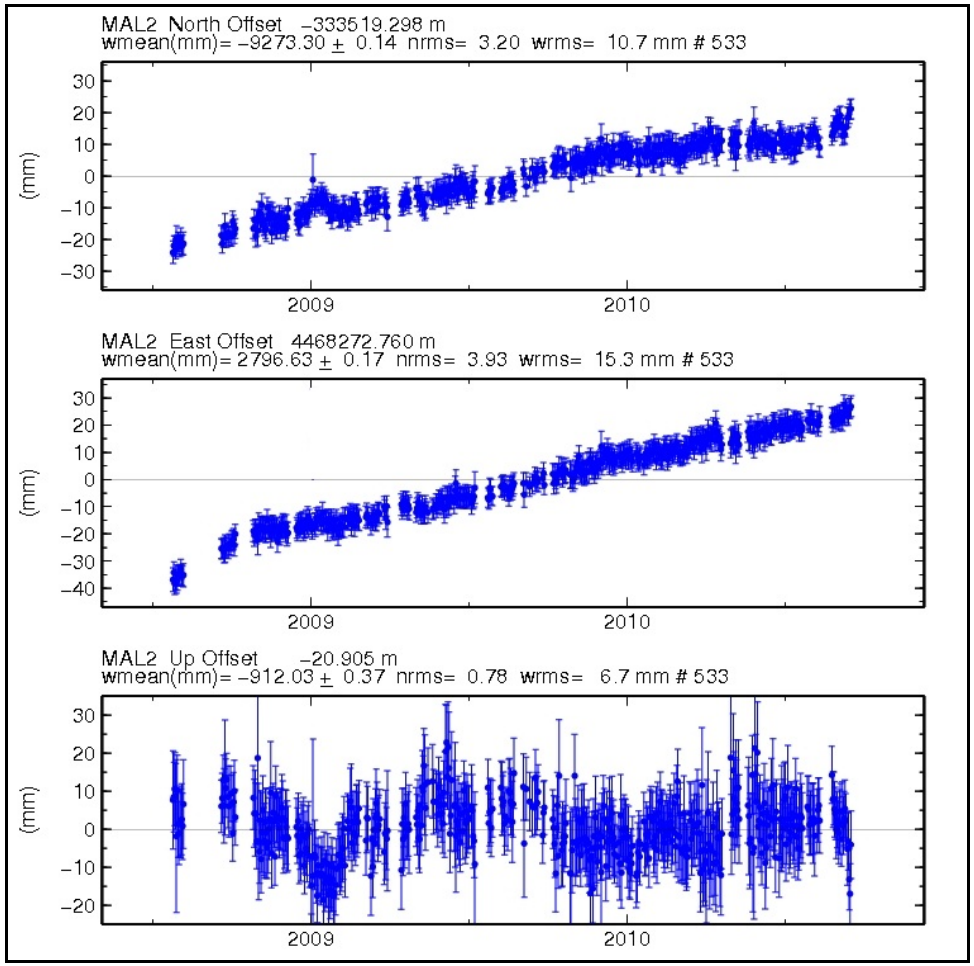


**Malindi GPS station (MAL2), Kenya**

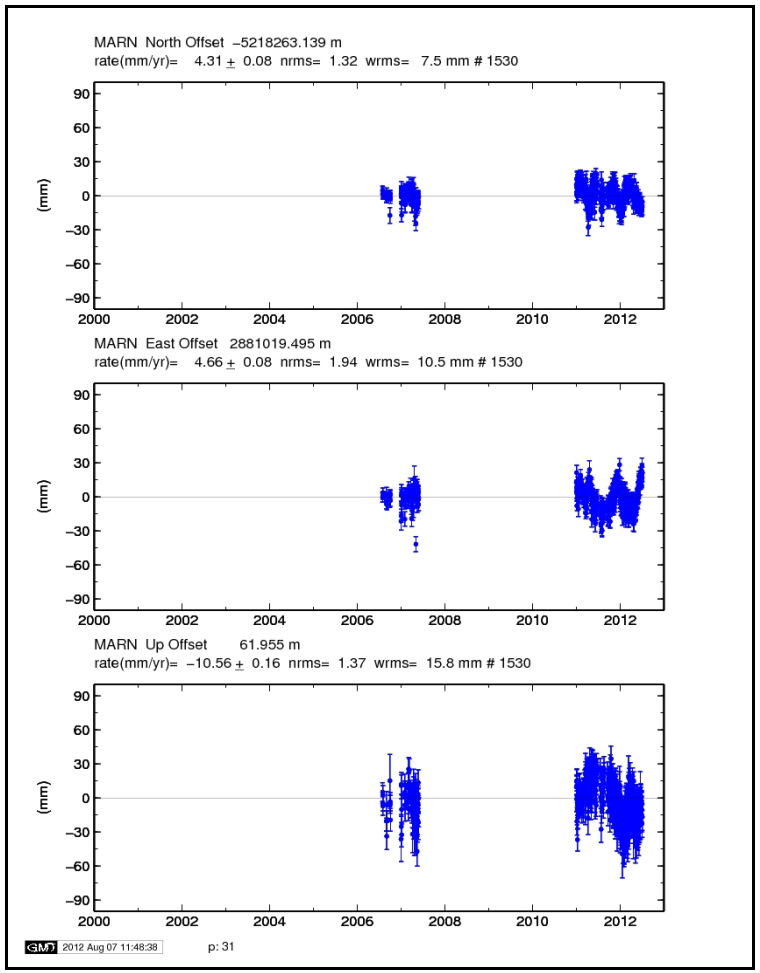


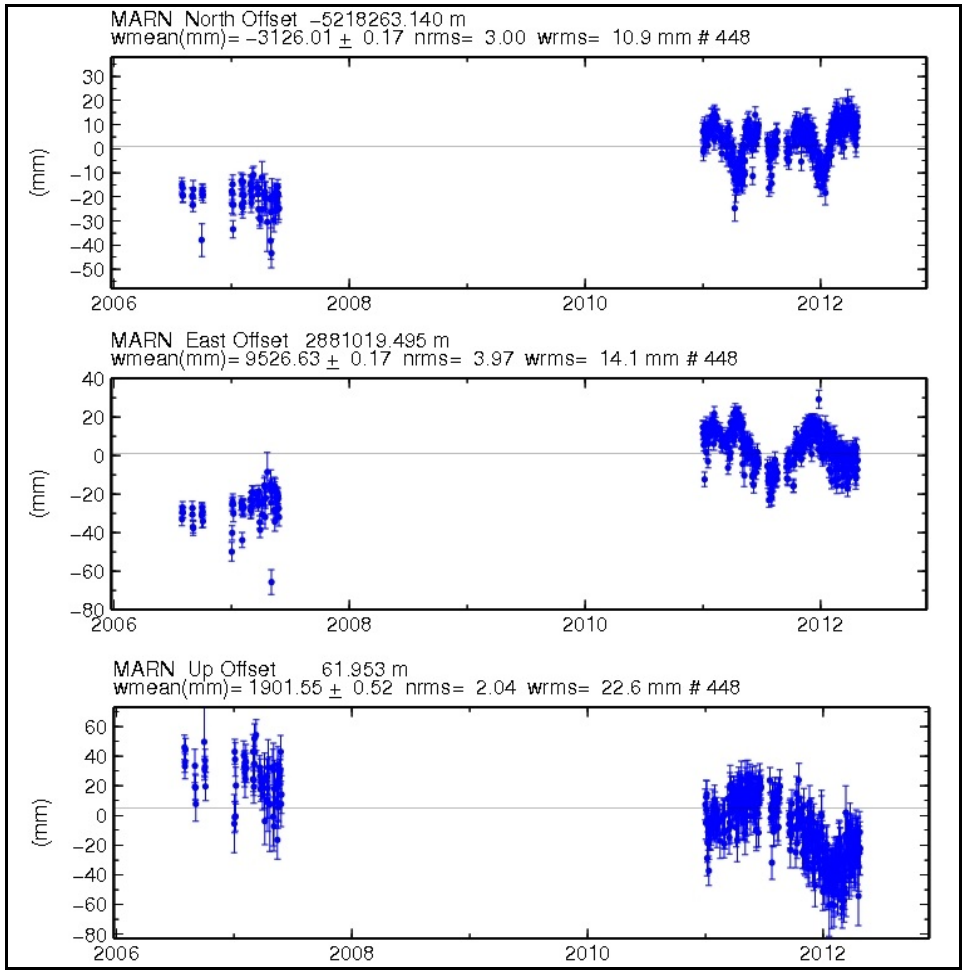


**Marion Island GPS station (MARN),**
**Prince Edward Islands**

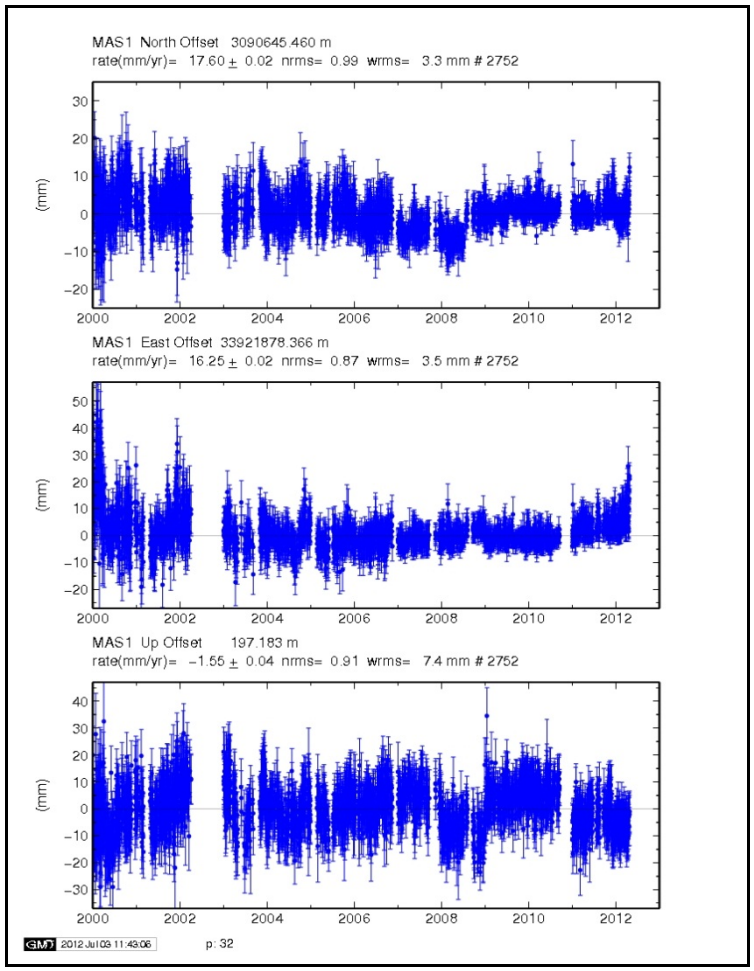


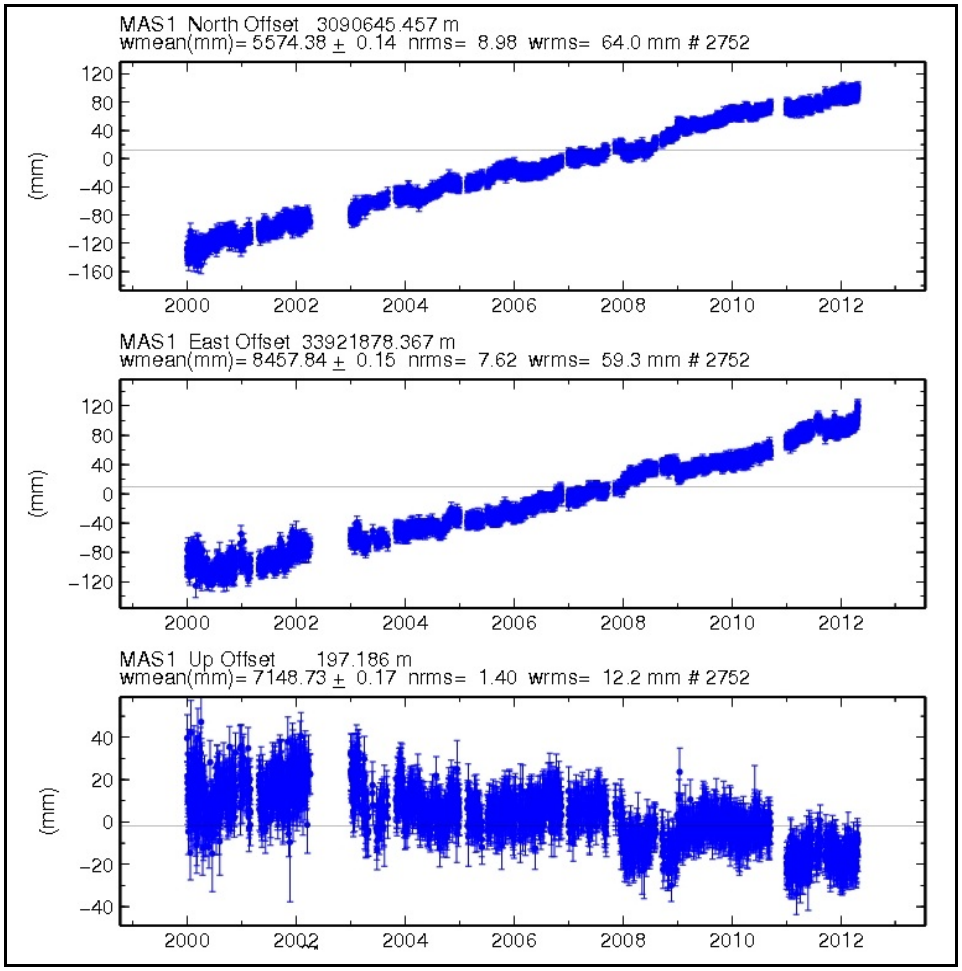


# Maspalomas GPS station (MAS1), Spain

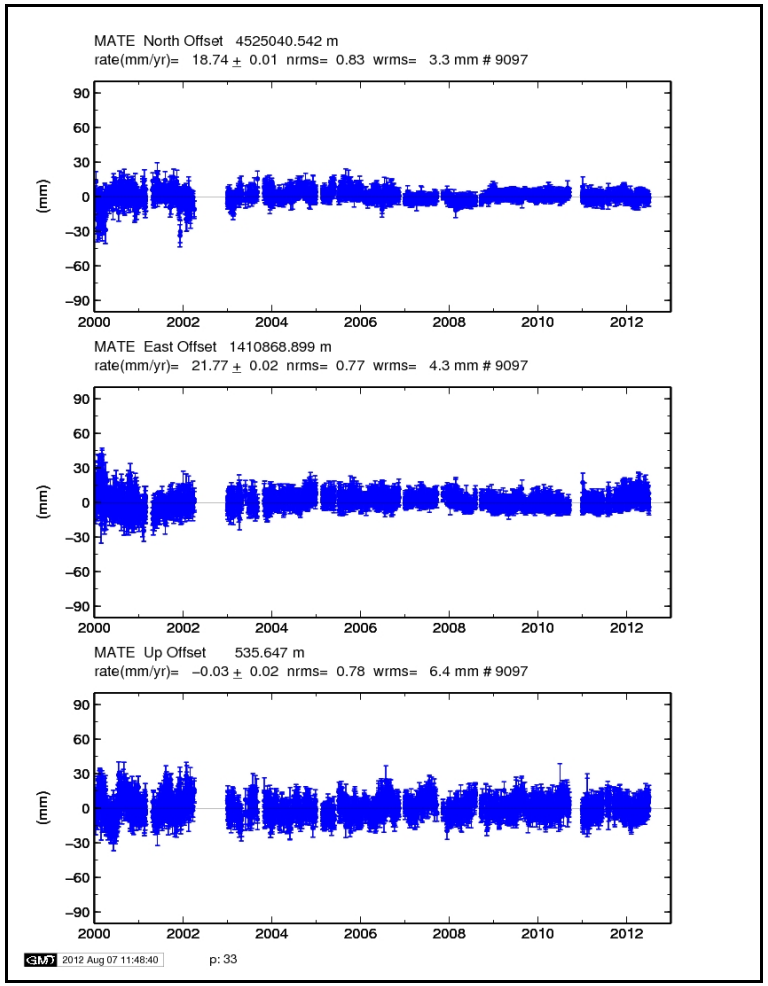


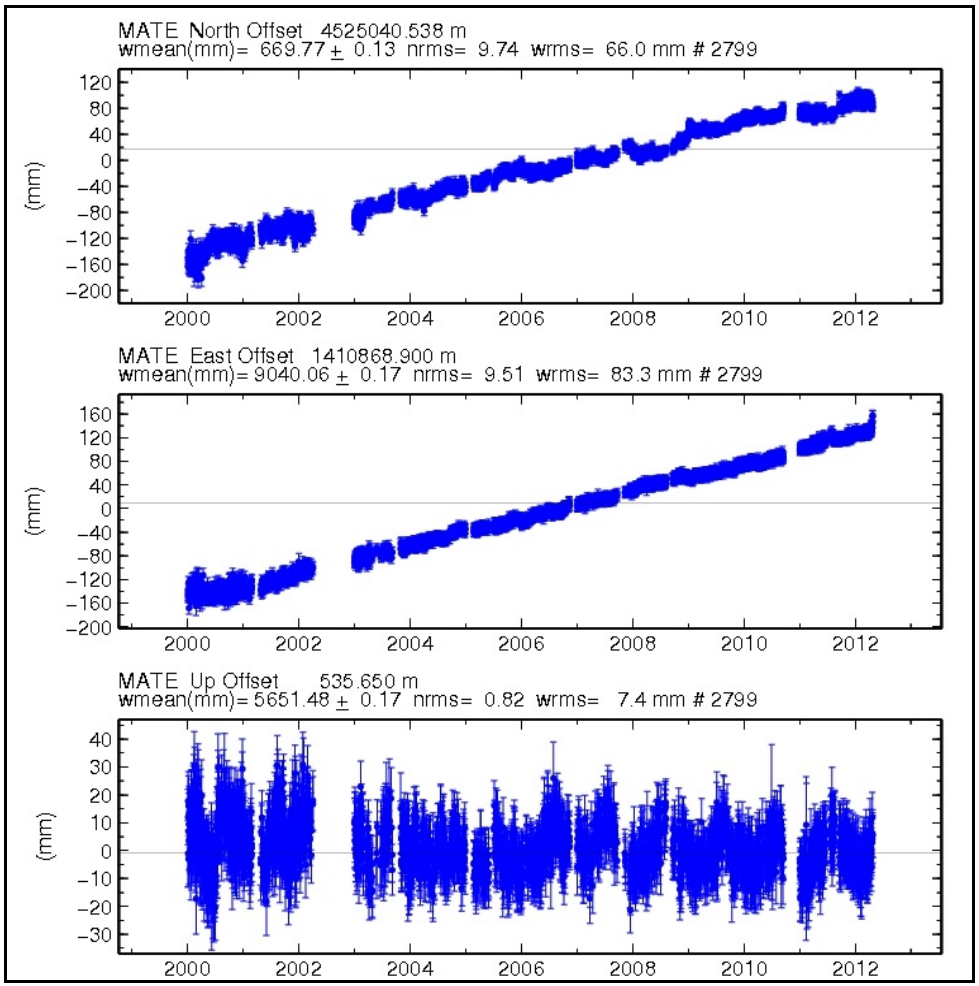


# Matera GPS station (MATE), Italy

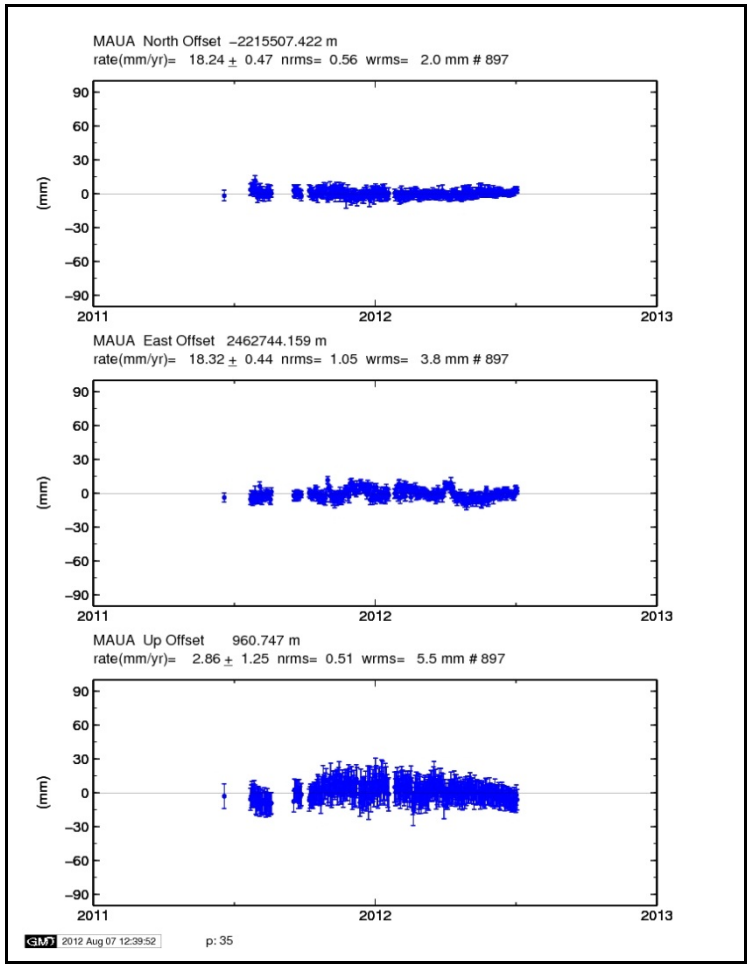


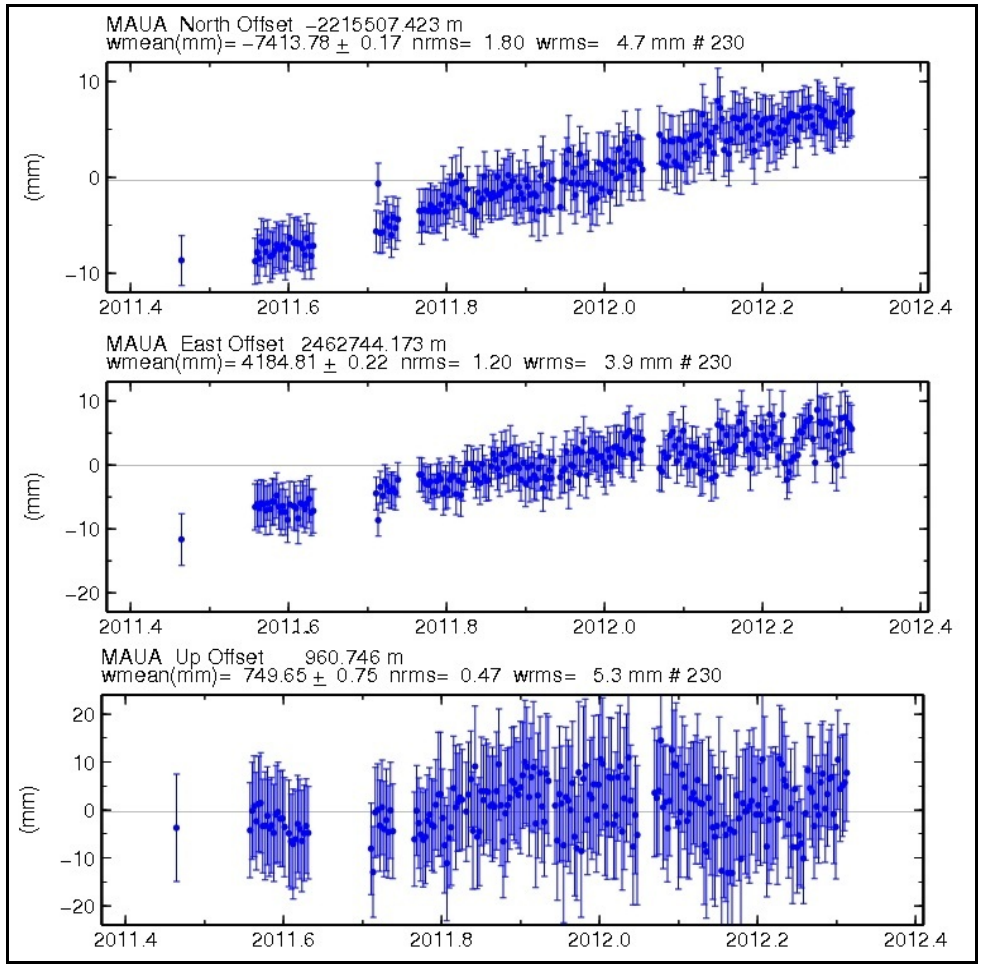


# Maun GPS station (MAUA), Botswana

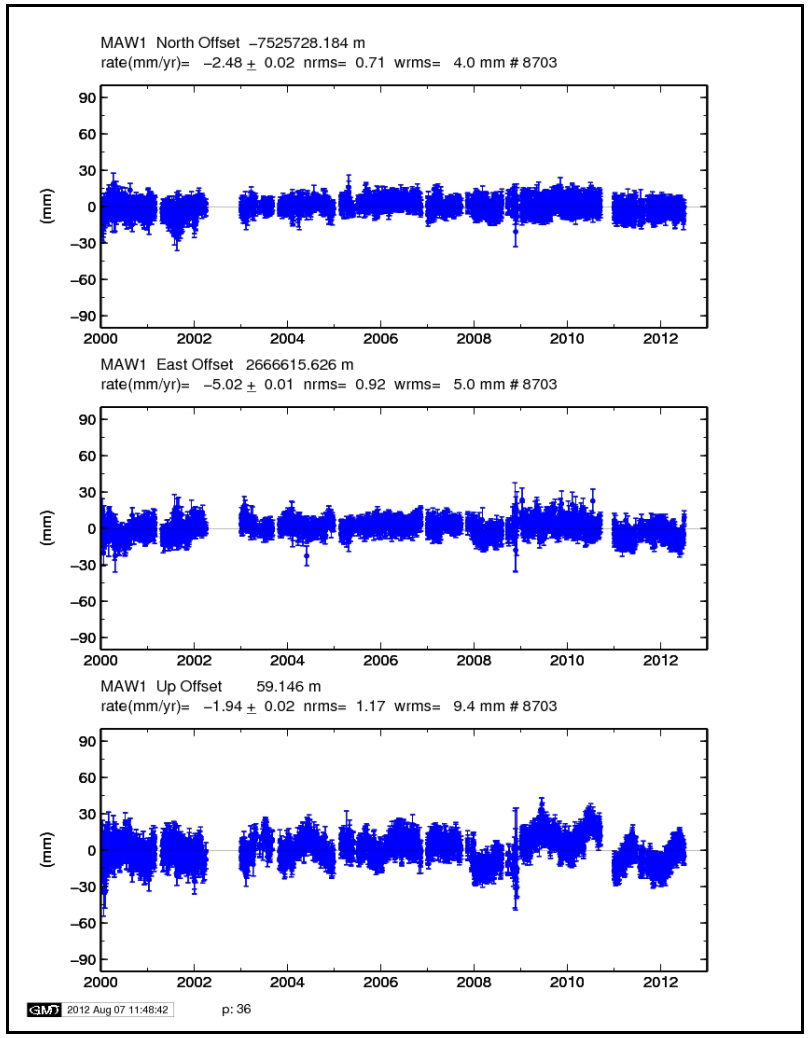


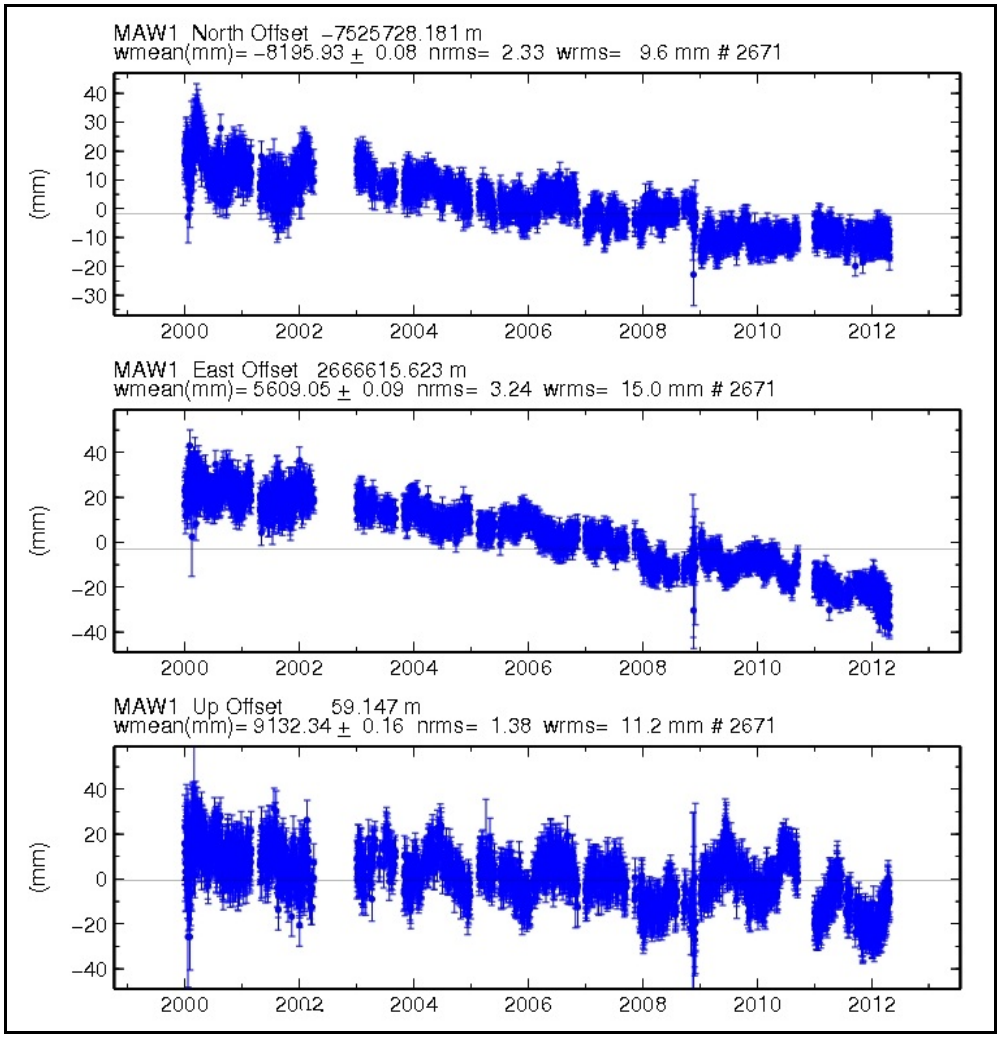


# Mawson GPS station (MAW1), Antarctica

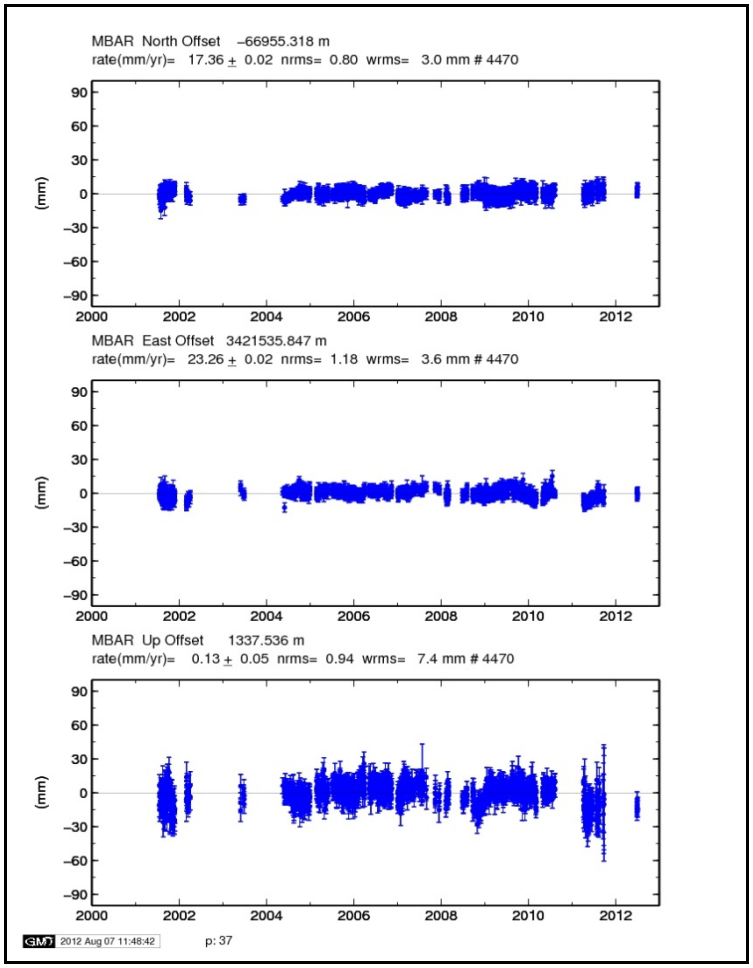


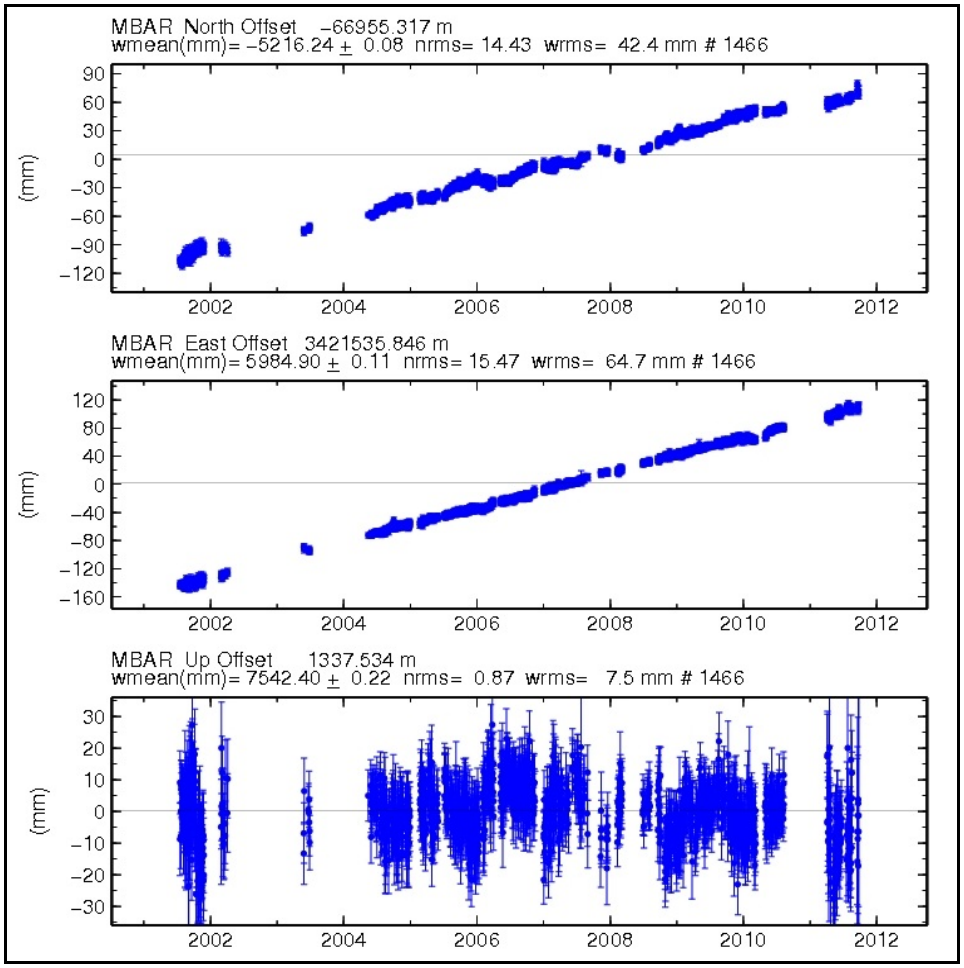


# Mbarara GPS station (MBAR), Uganda

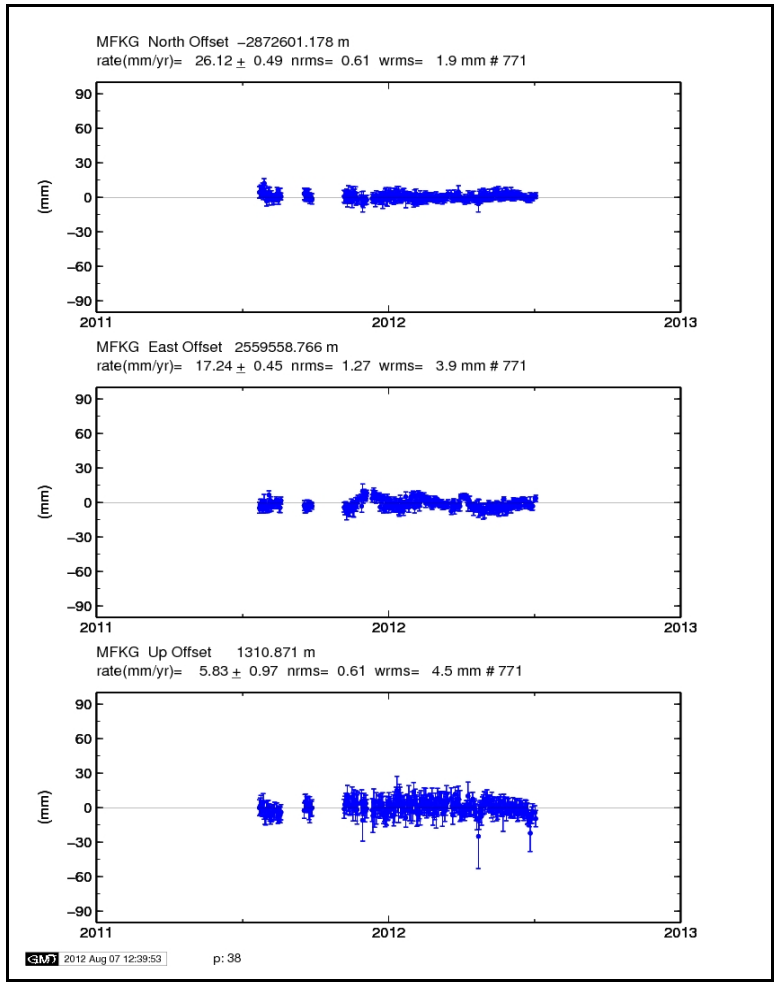


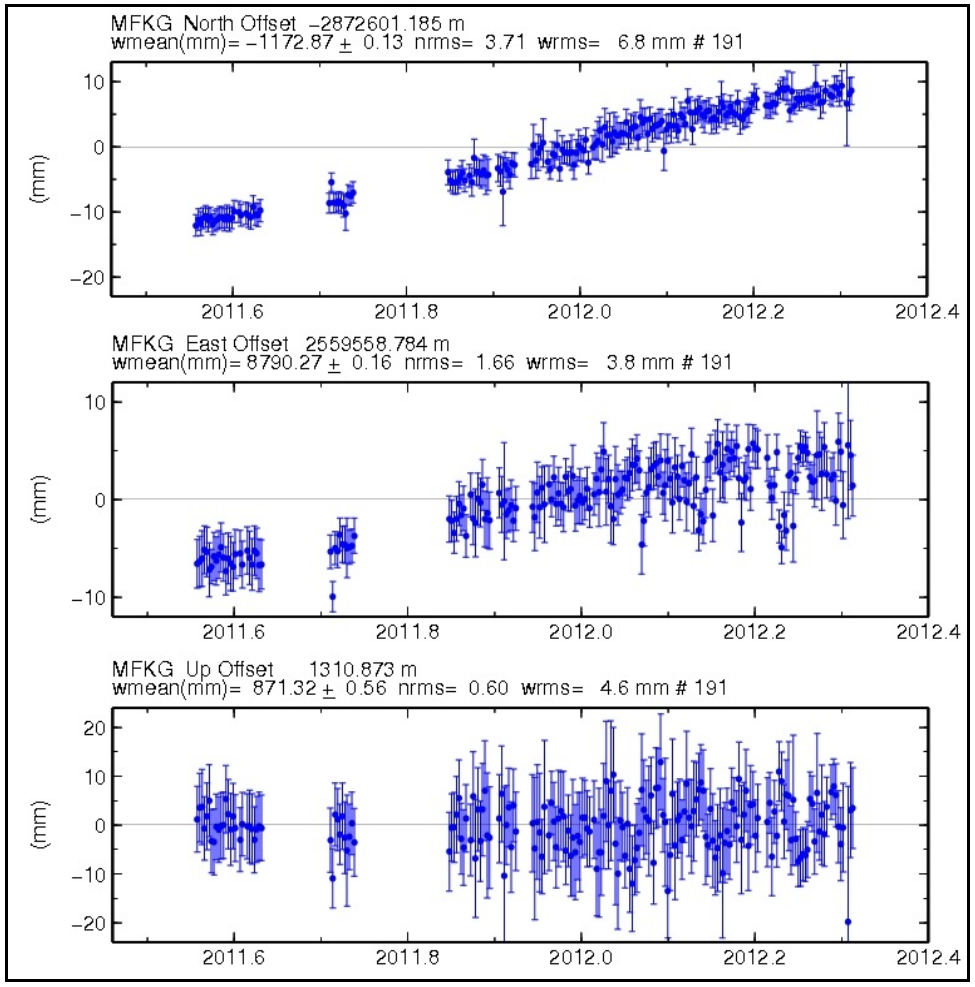


# Mafikeng GPS station (MFKG), South Africa

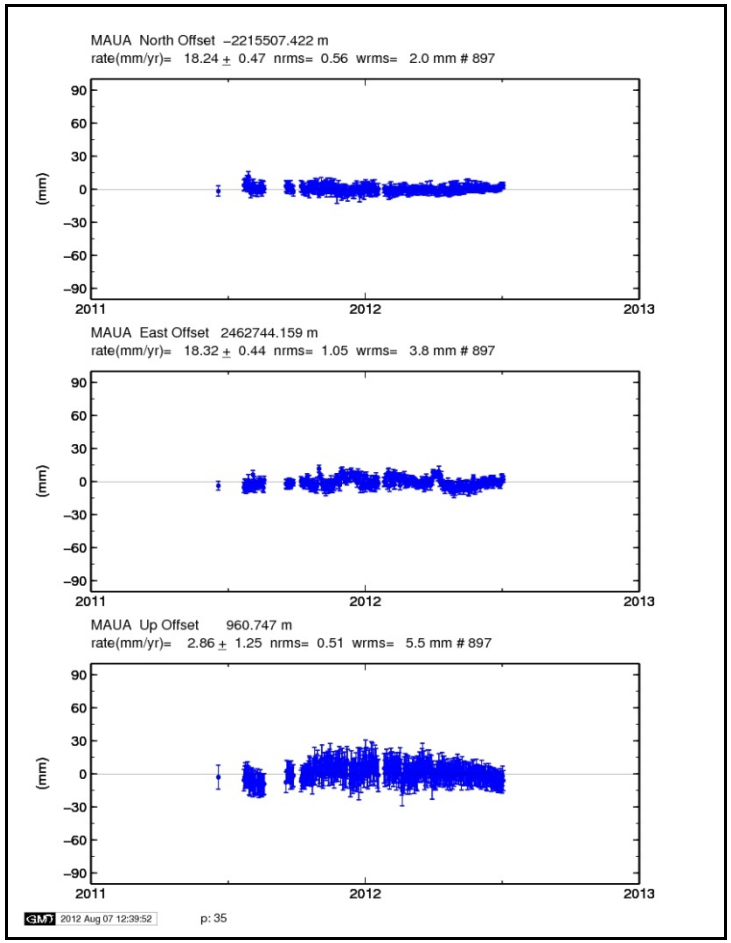


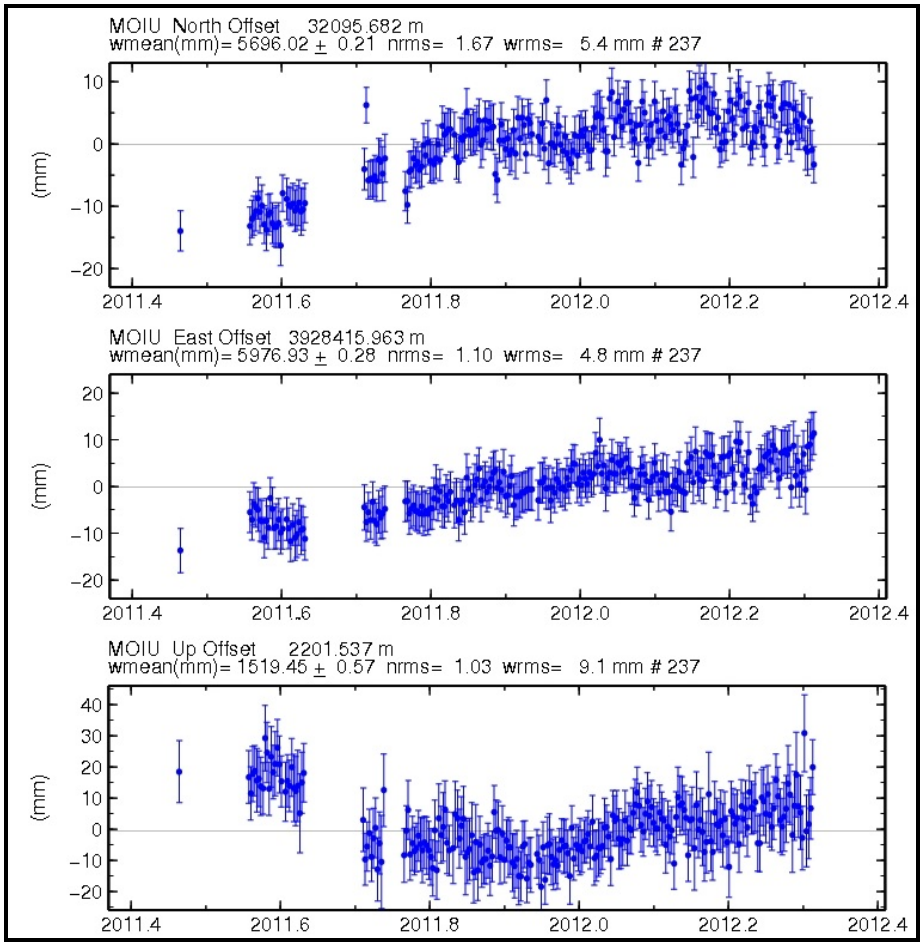


# Eldoret GPS station (MOIU), Kenya

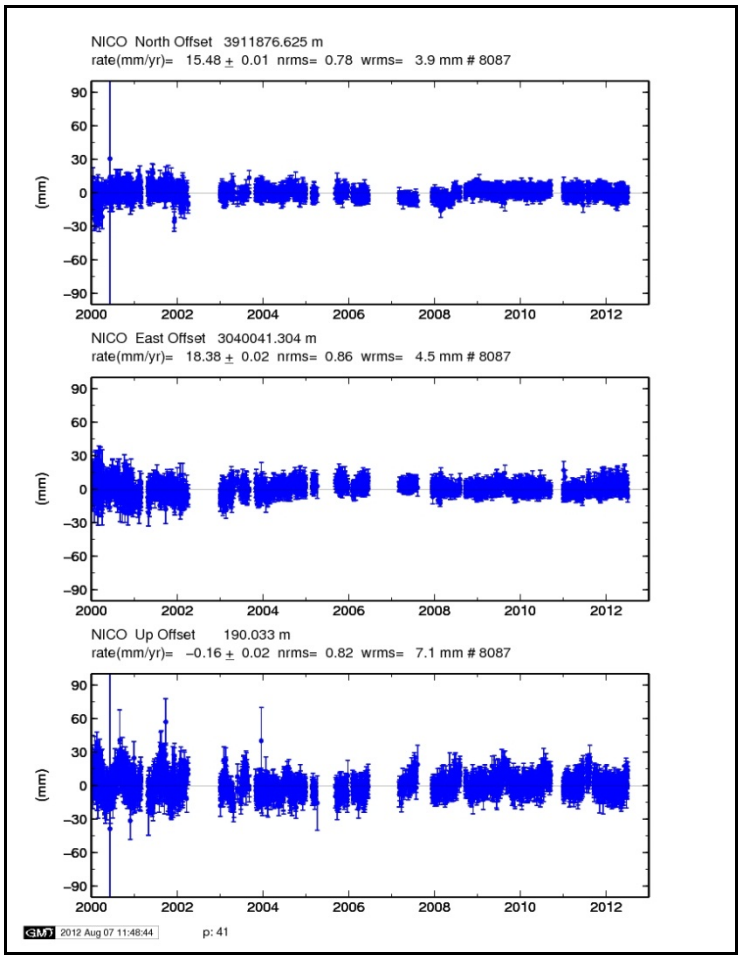


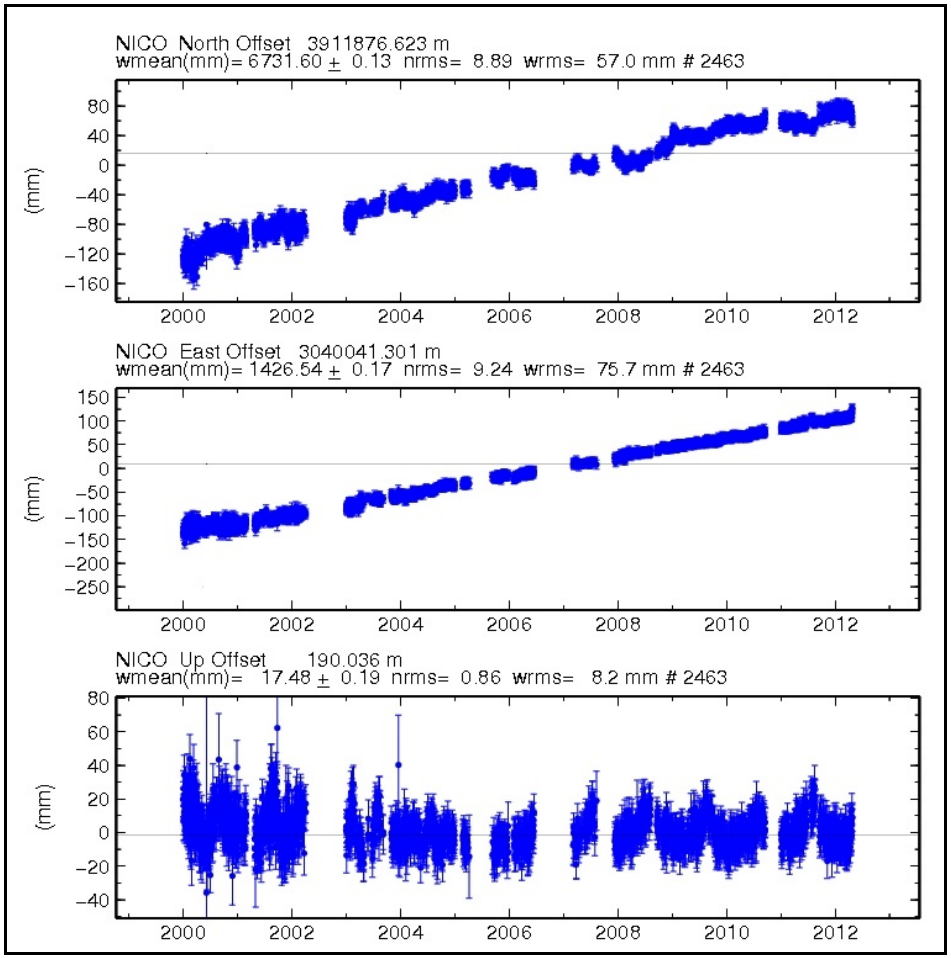


# Nicosia-athalassa GPS station (NICO), Cyprus

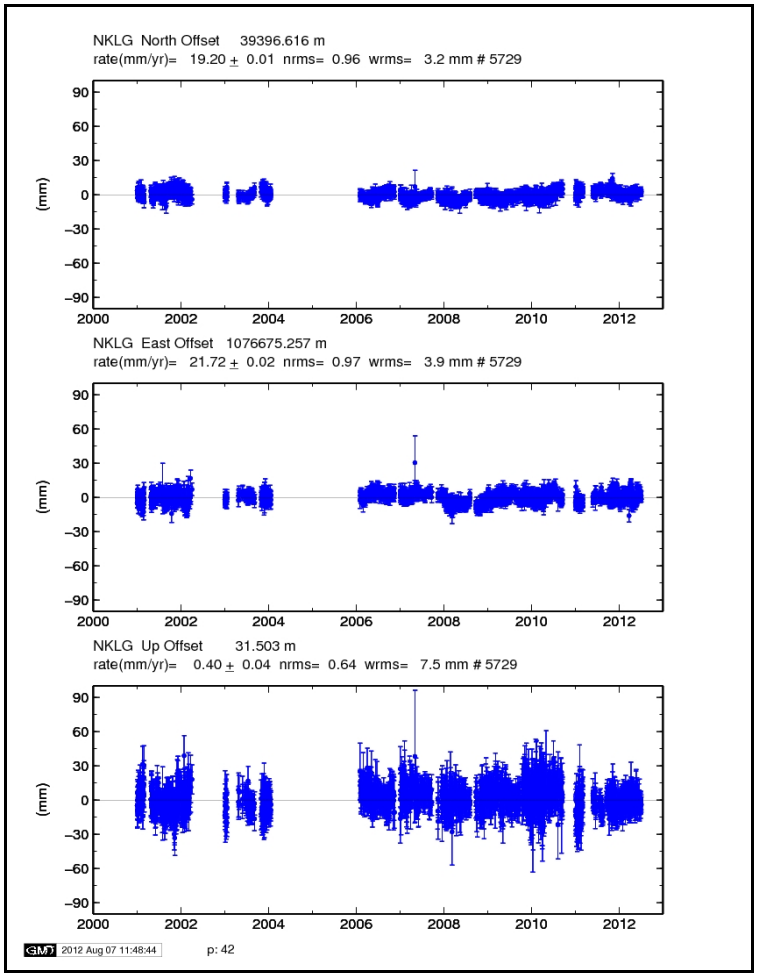


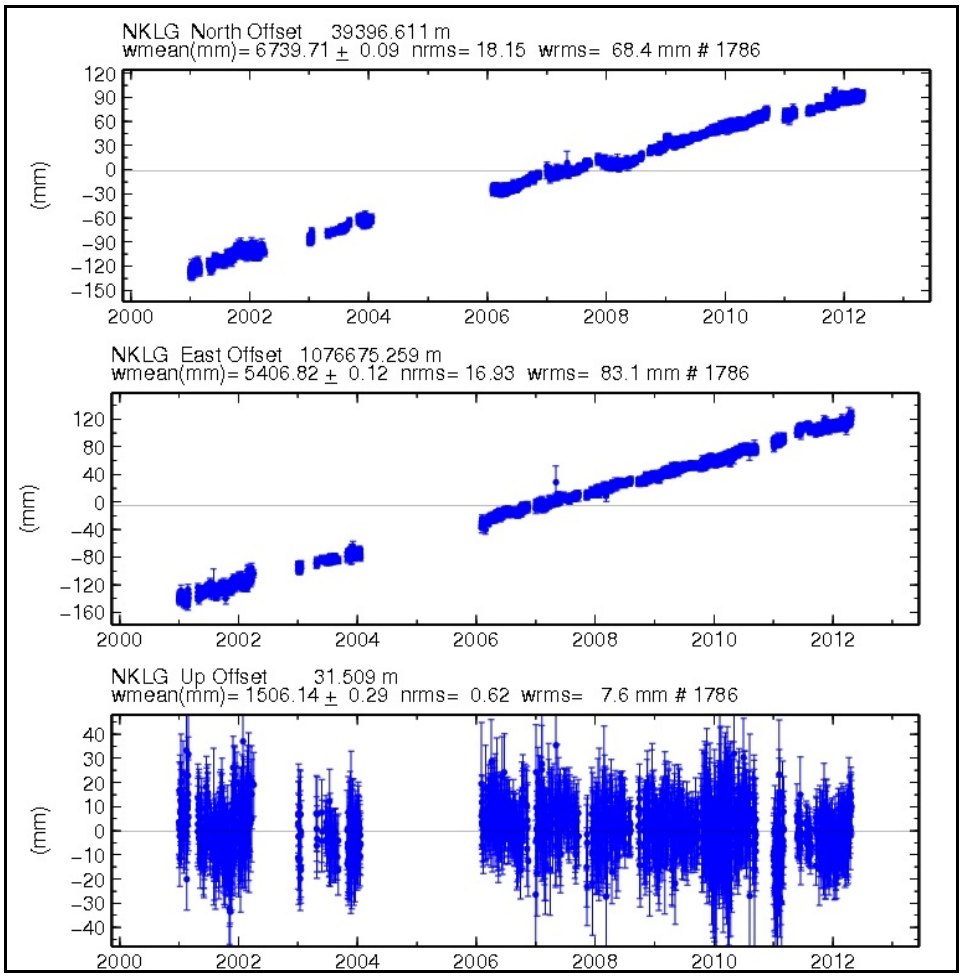


**N’koltang GPS station (NKLG), Gabon**

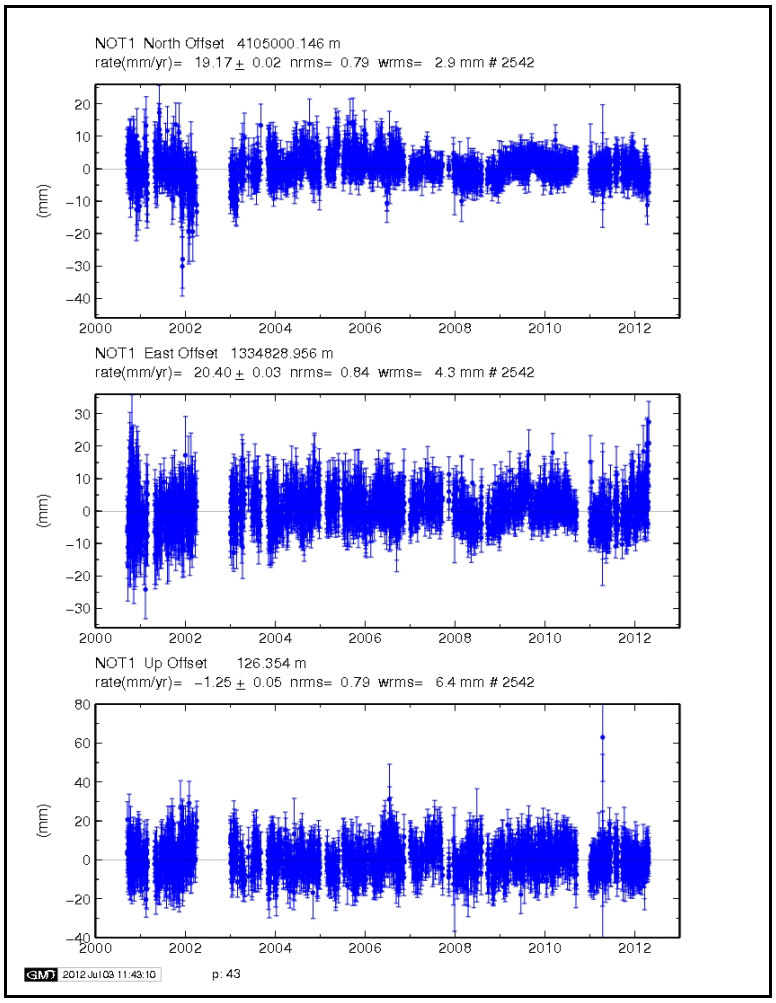


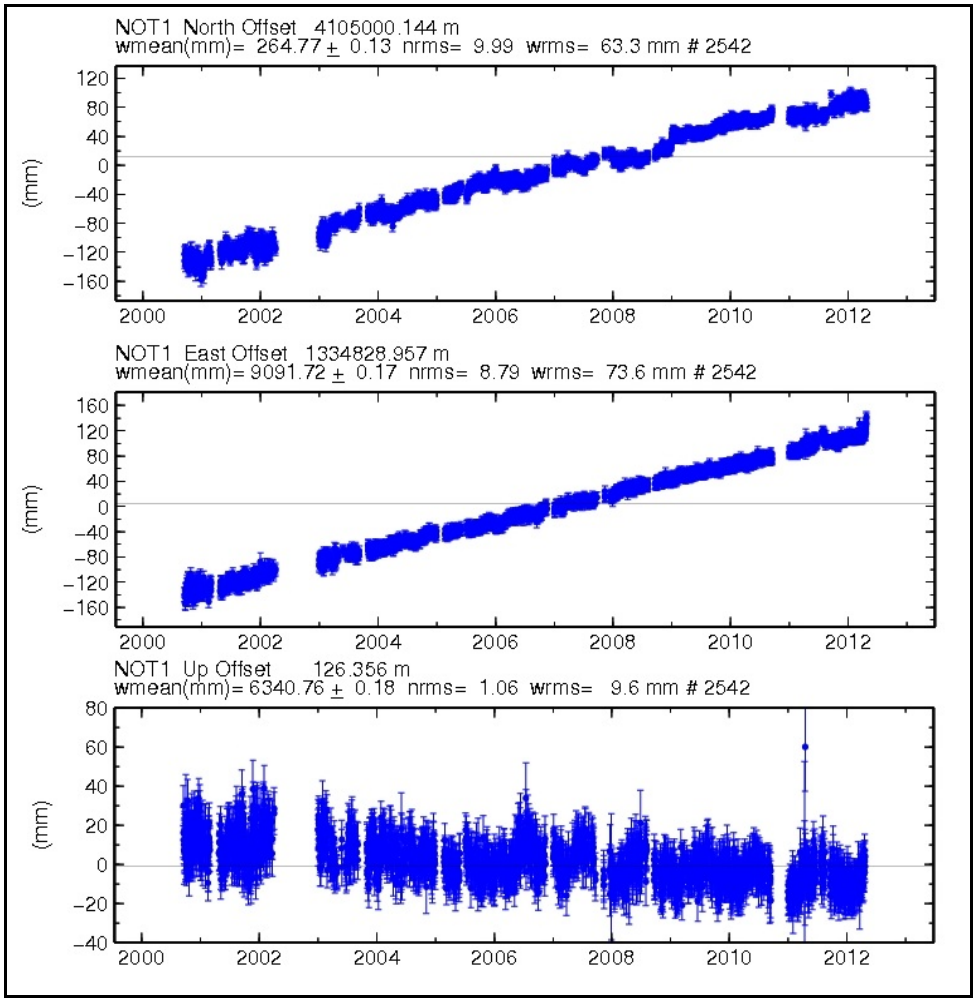


# Noto-Radioastronomy GPS station of C.N.R. (NOT1), Italy

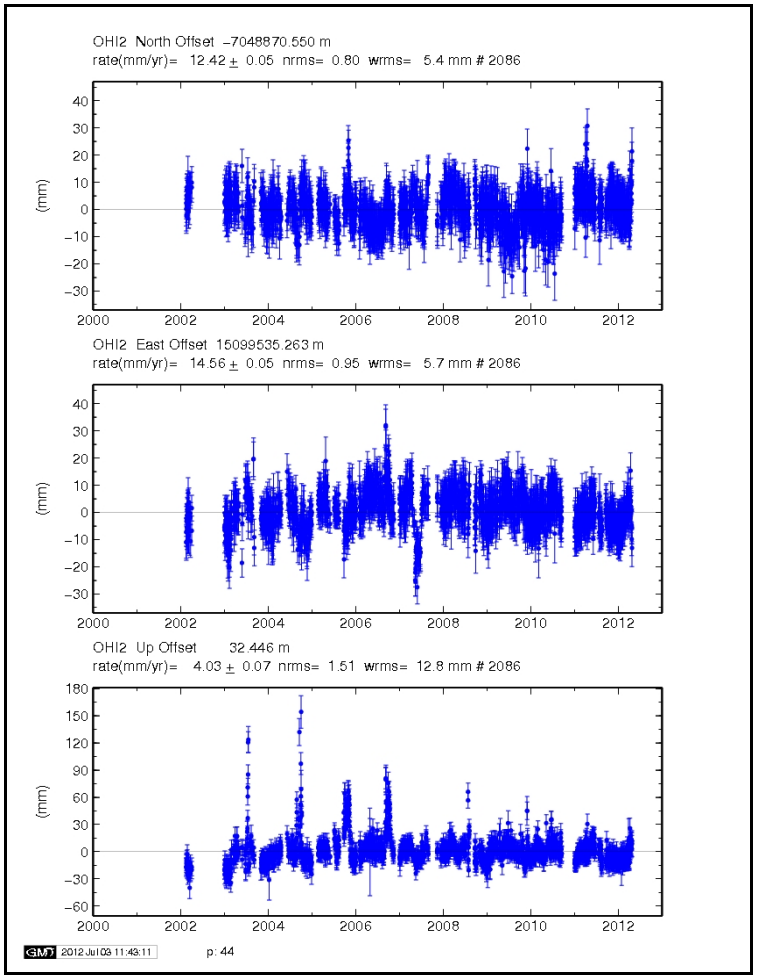


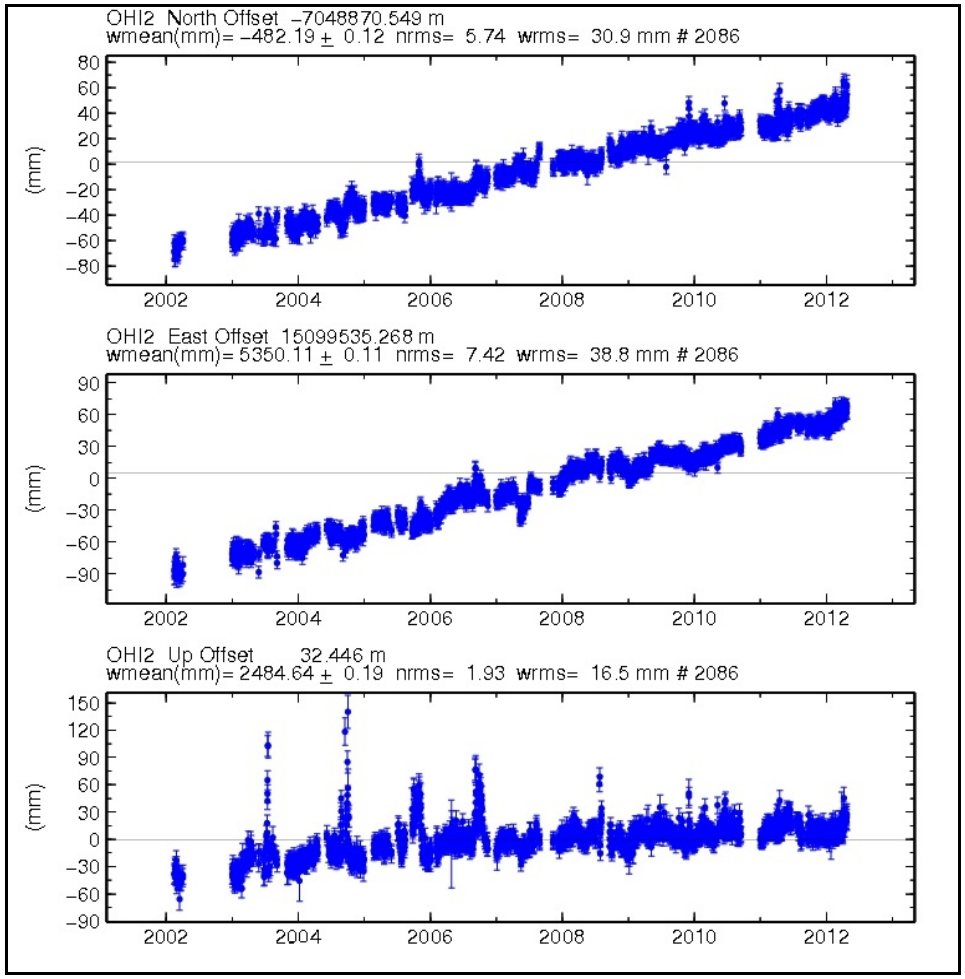


# O'Higgins 2 GPS station (OHI2), Antarctica Peninsula

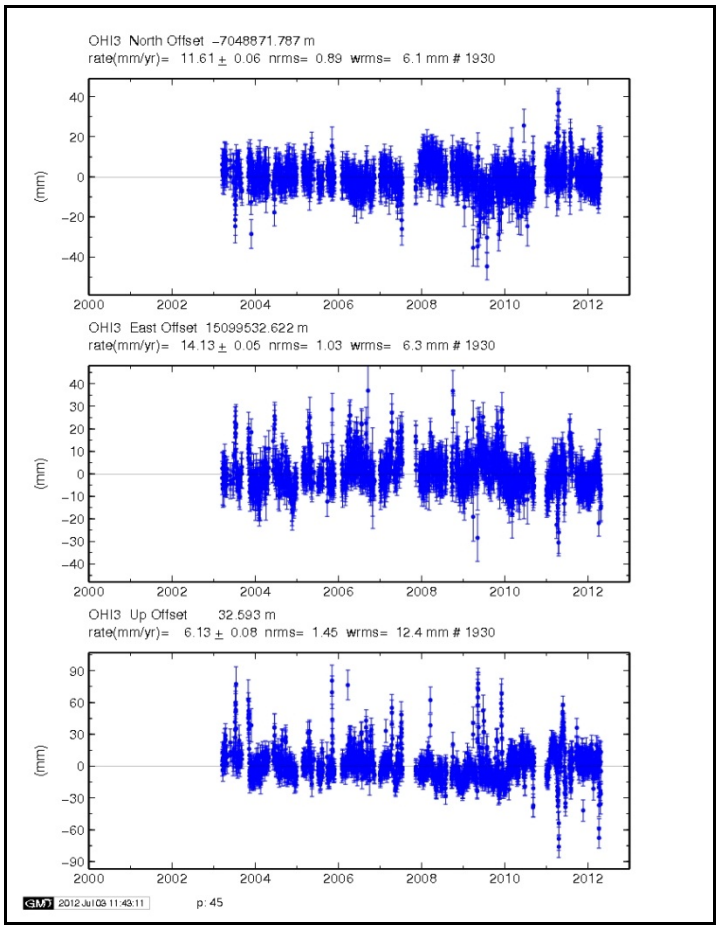


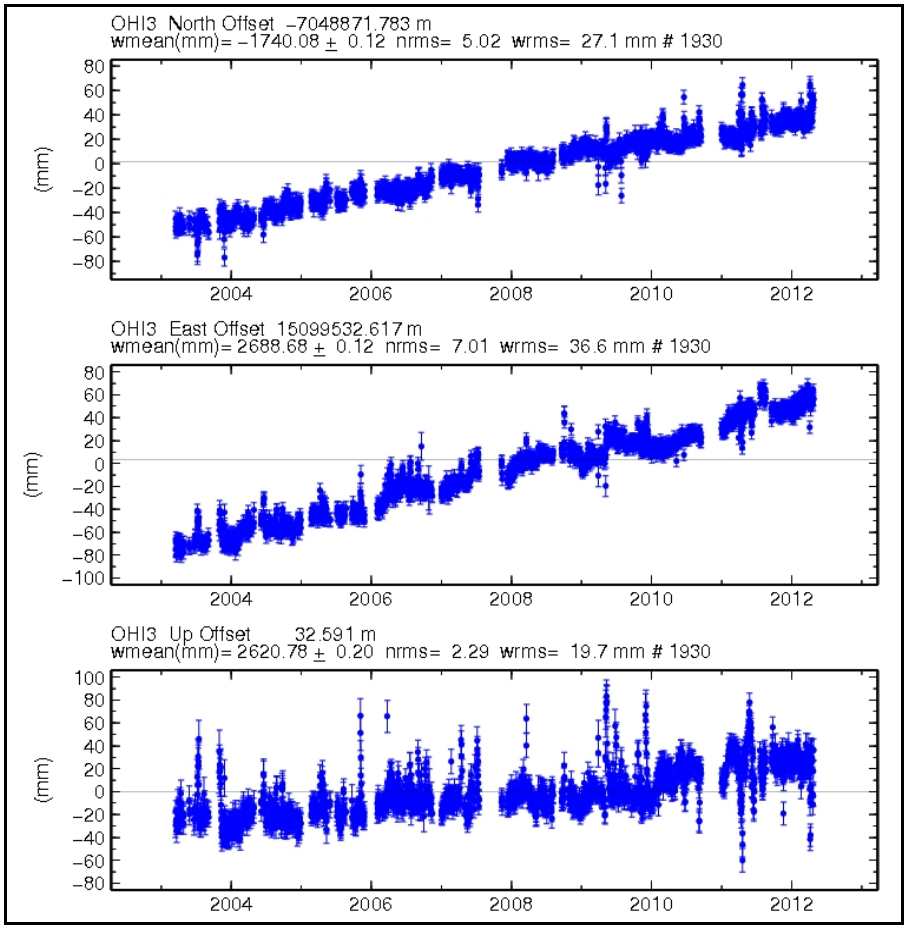


# O'Higgins 3 GPS station (OHI3), Antarctica Peninsula

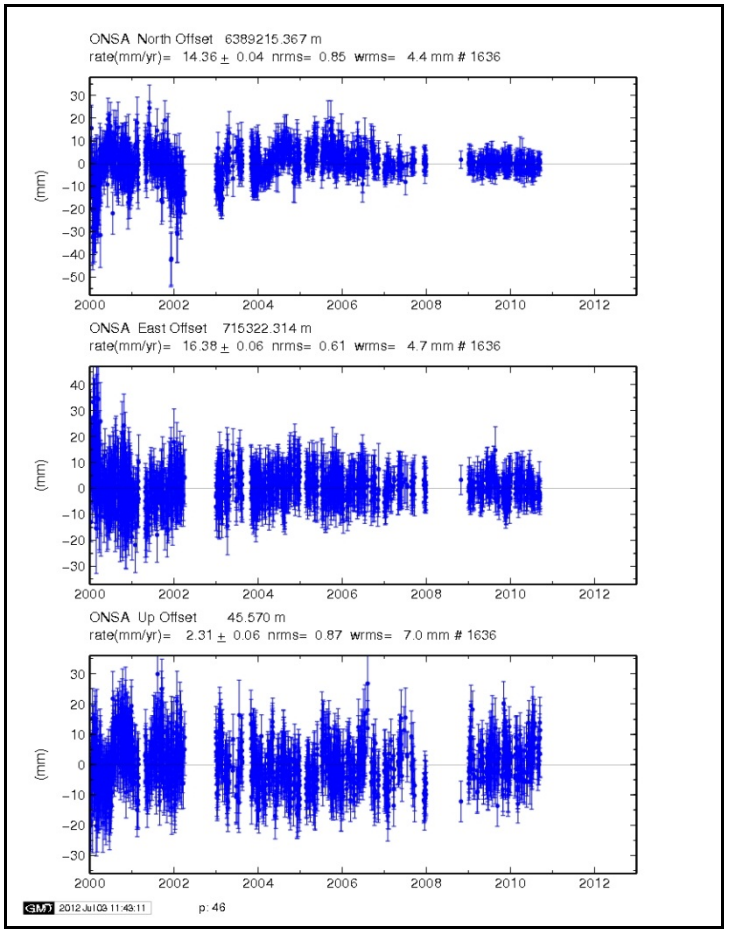


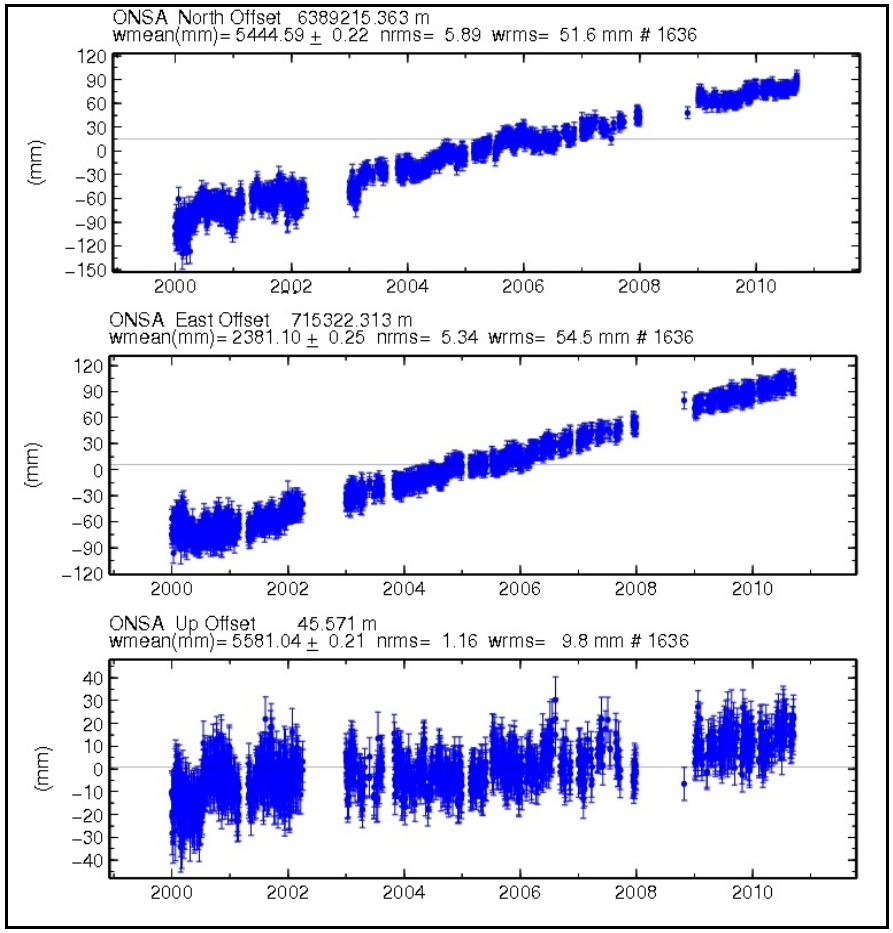


# Onsala GPS station (ONSA), Sweden

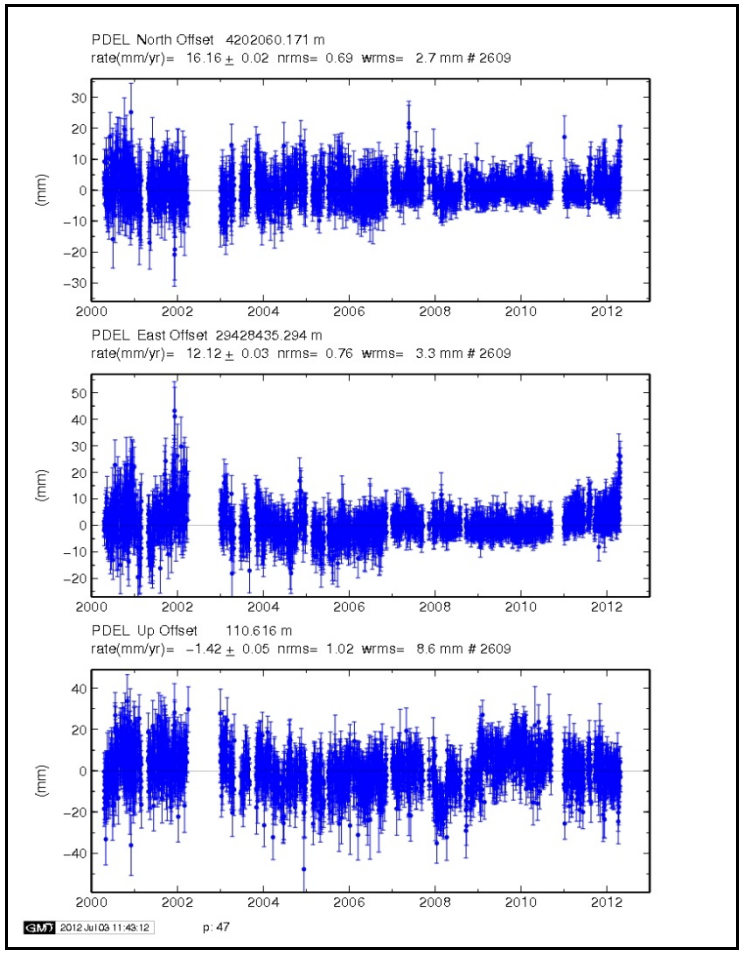


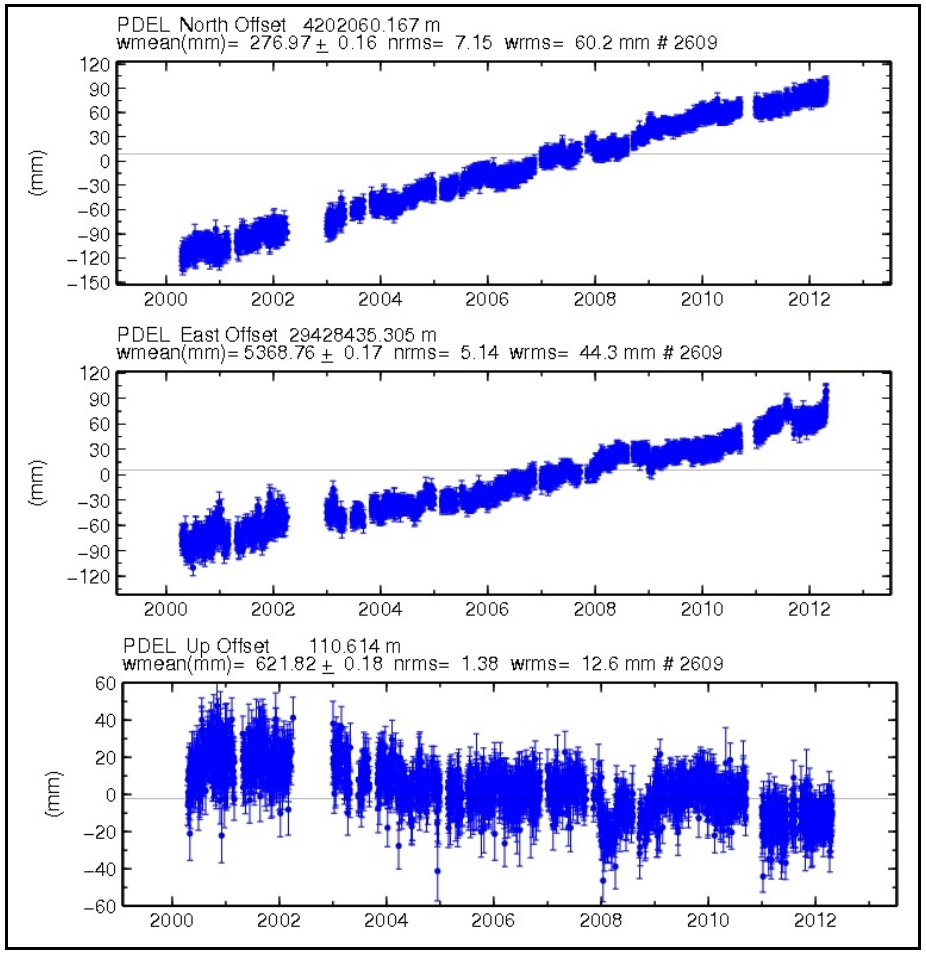


# Ponta Delgada GPS station (PDEL), Portugal

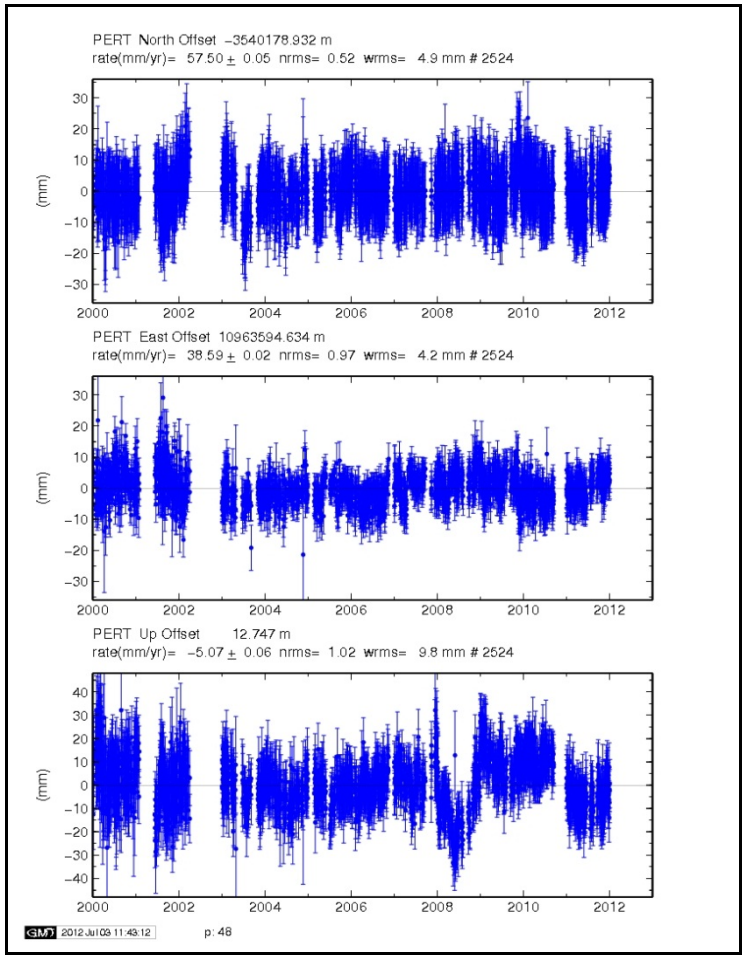


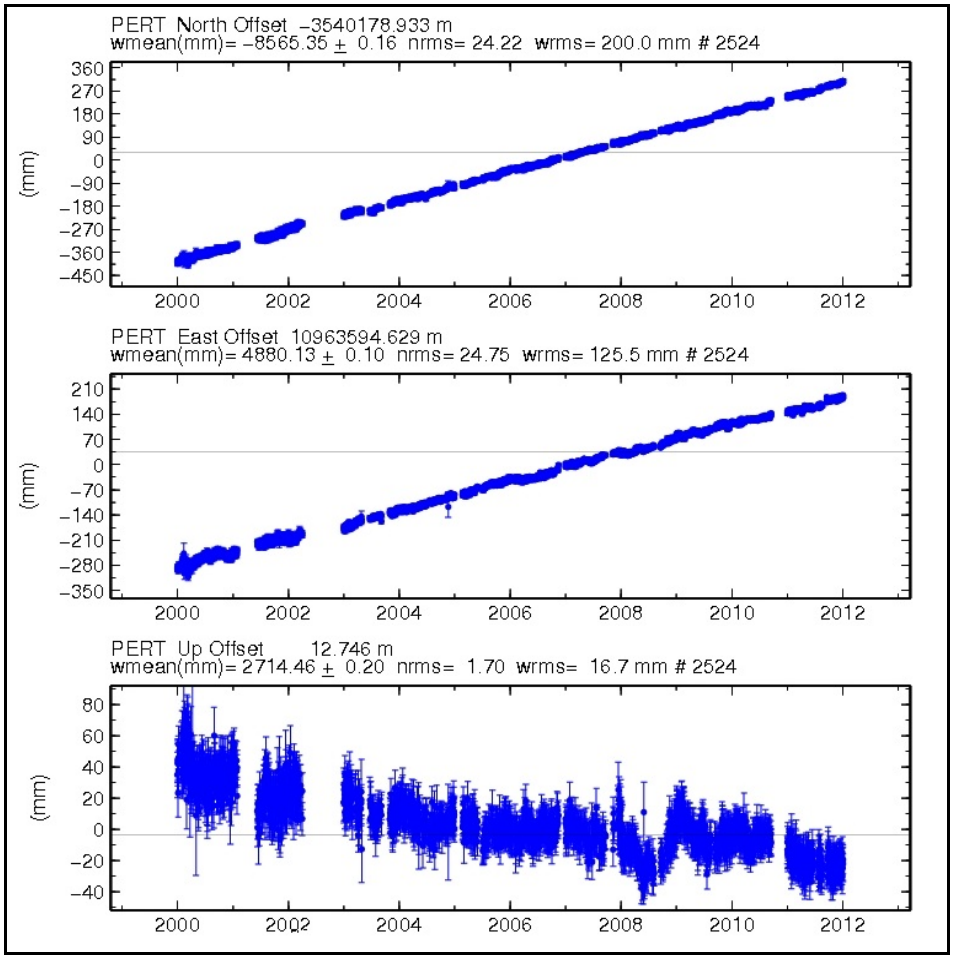


# Perth GPS station (PERT), Australia

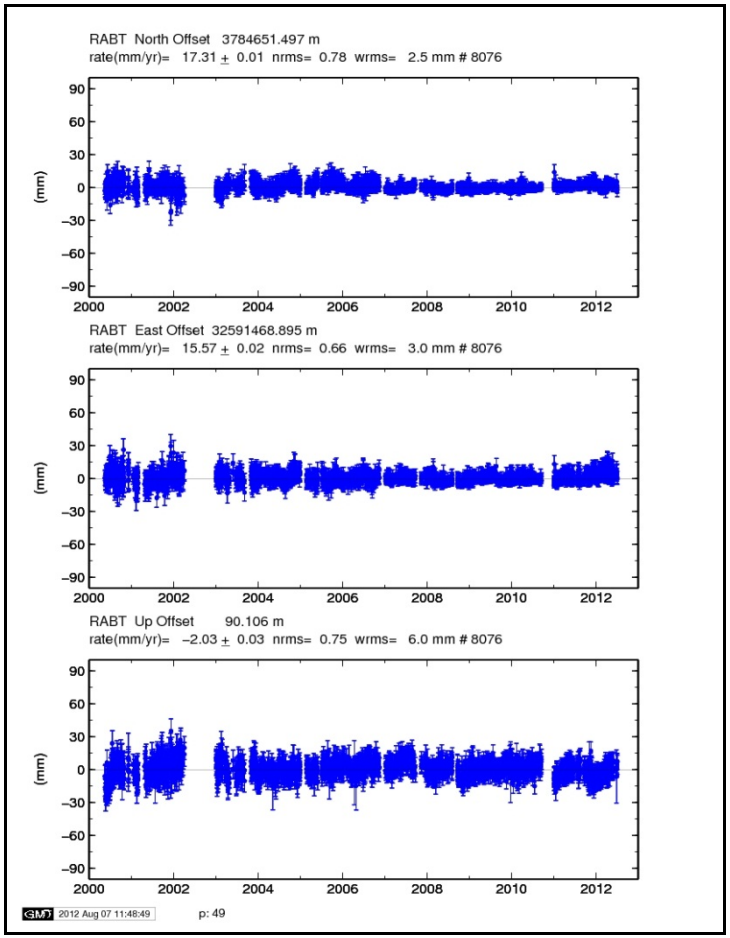


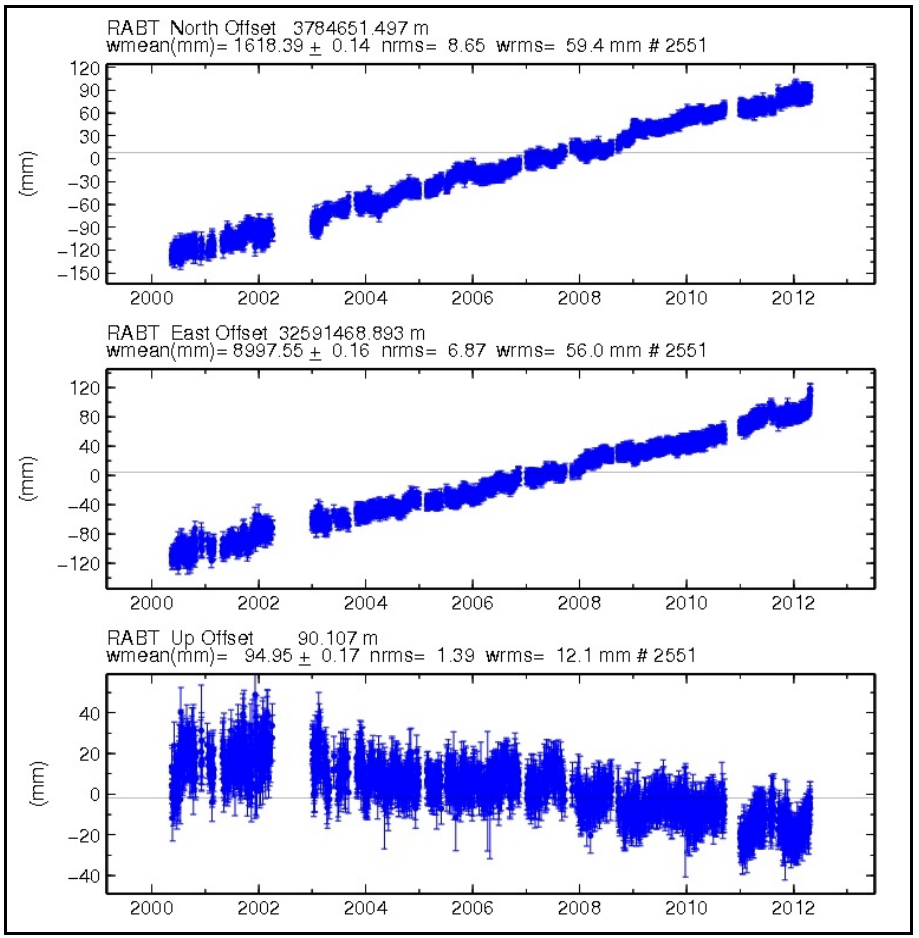


# Rabat, EMI GPS station (RABT), Morocco

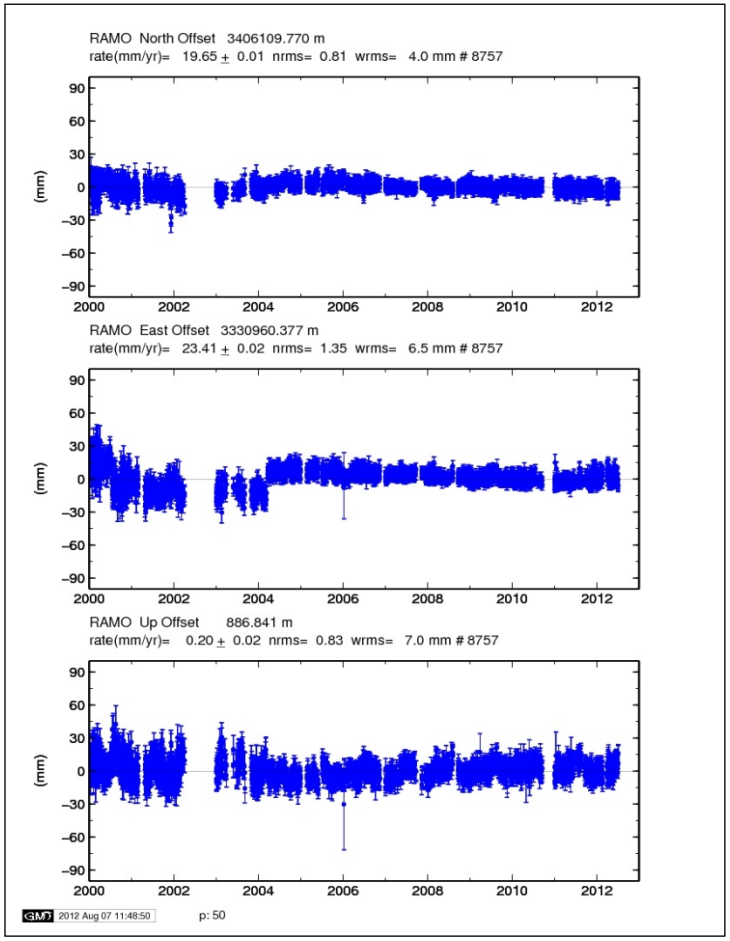


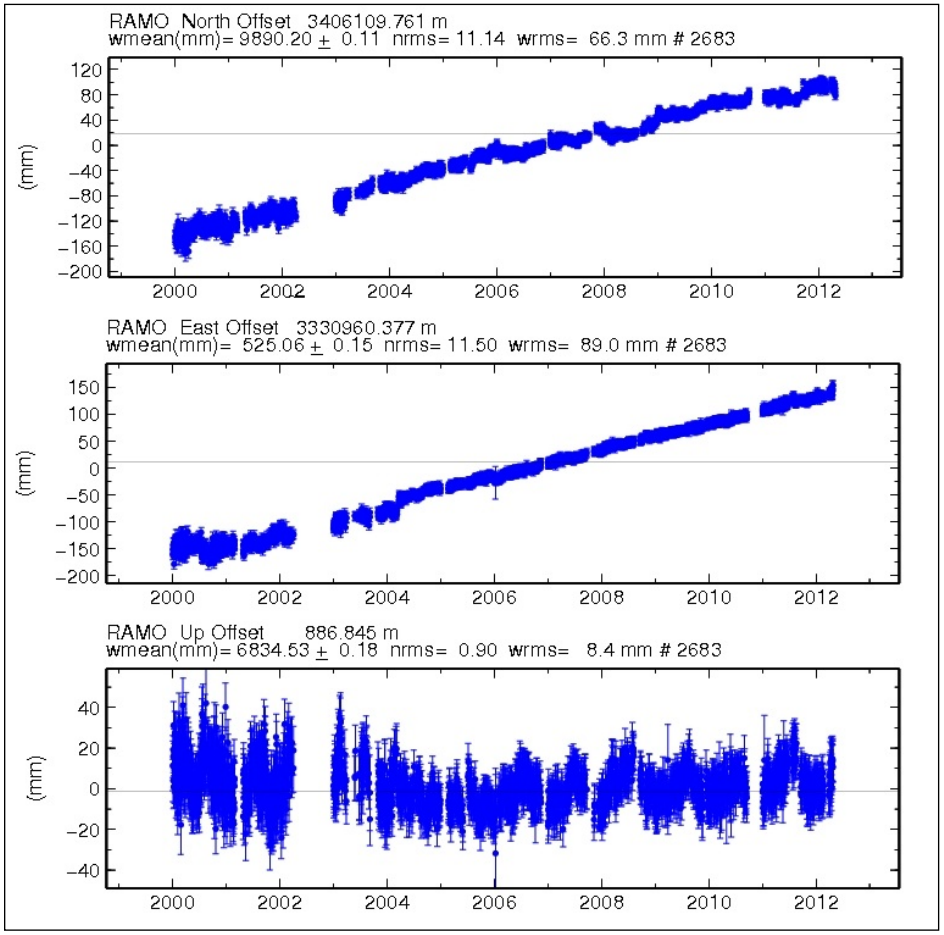


# Mitzpe Ramo GPS station (RAMO), Israel

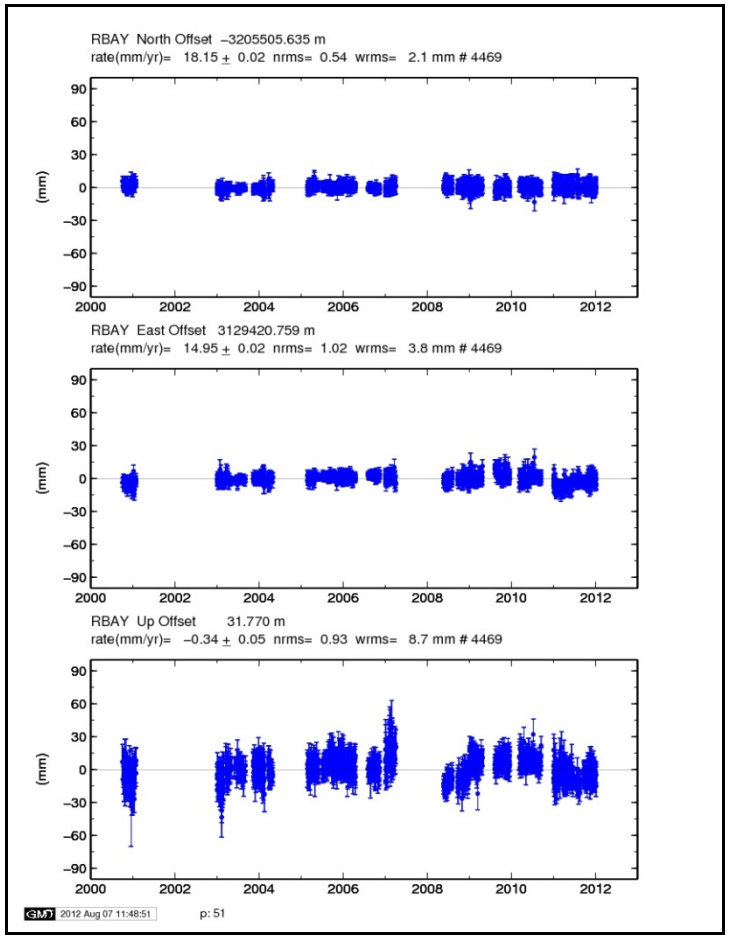


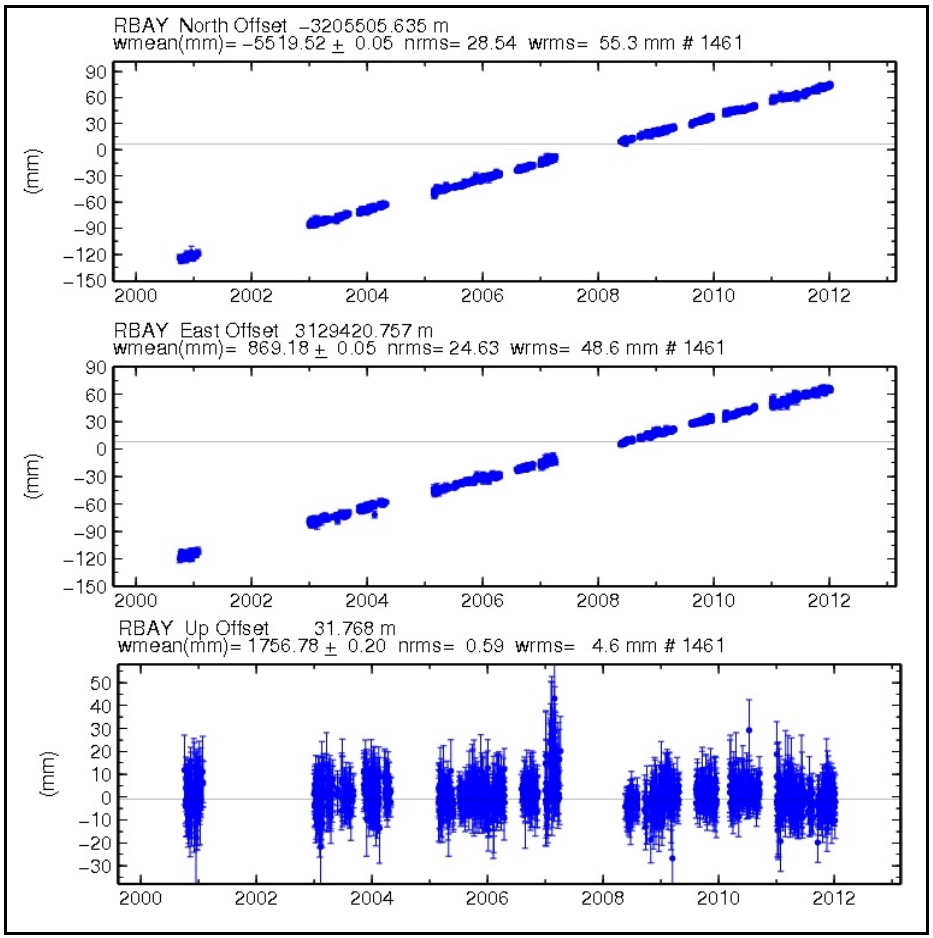


# Richardsbay GPS station (RBAY), South Africa

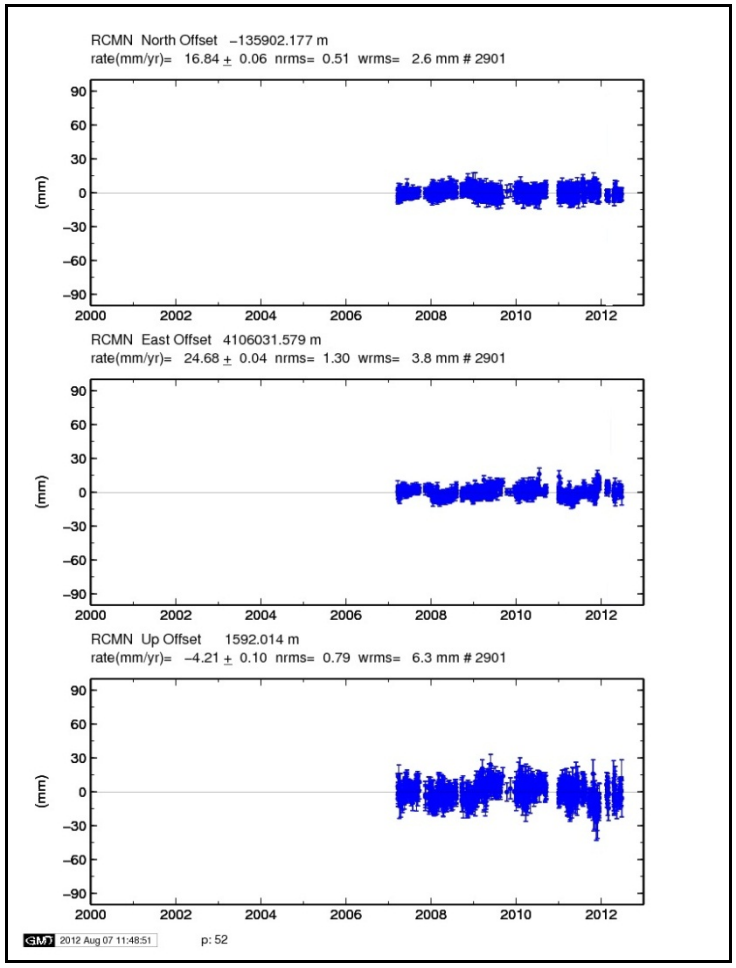


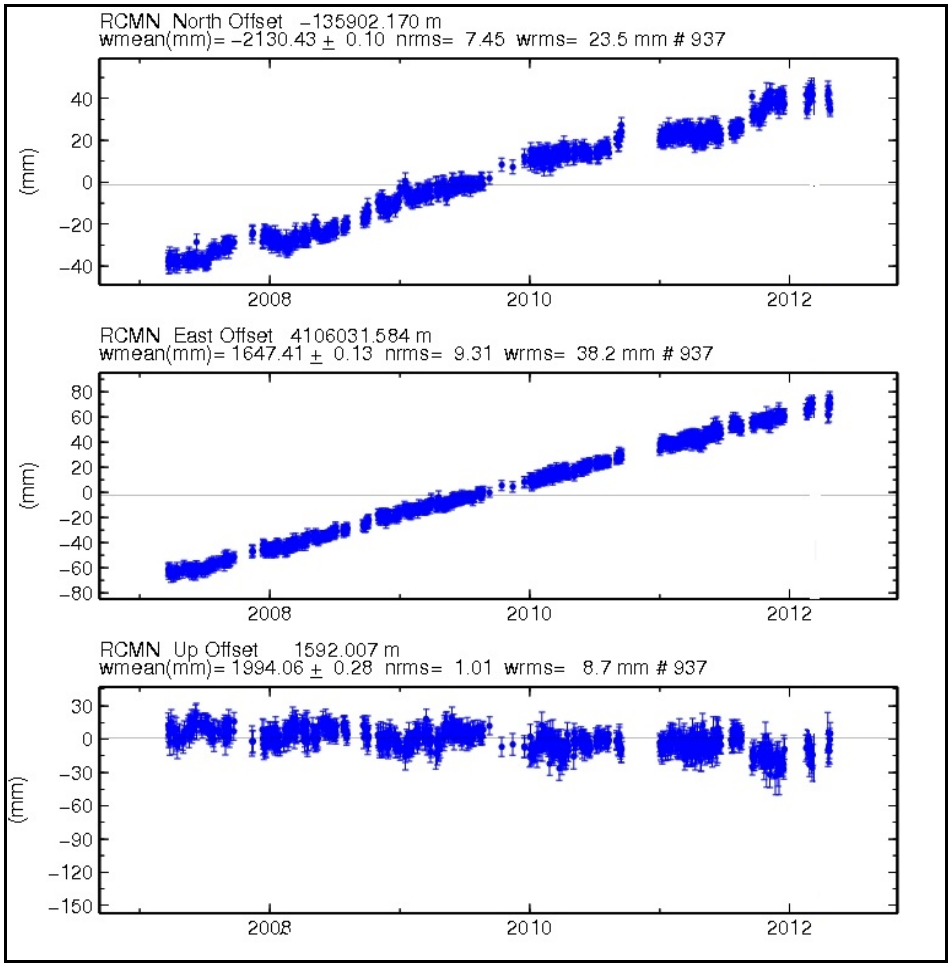


# RCMRD Nairobi GPS station (RCMN), Kenya

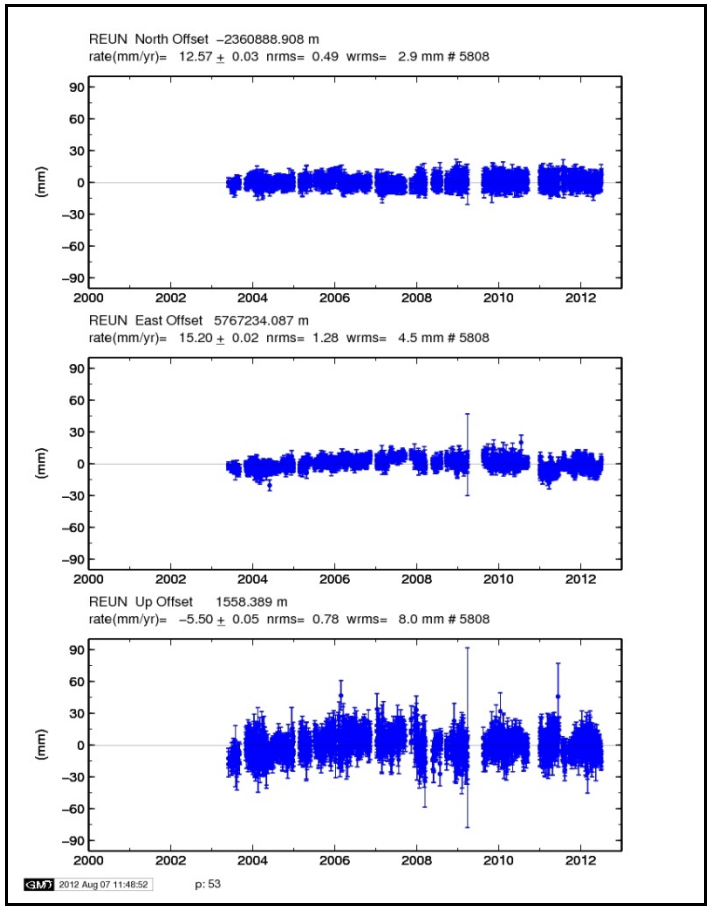


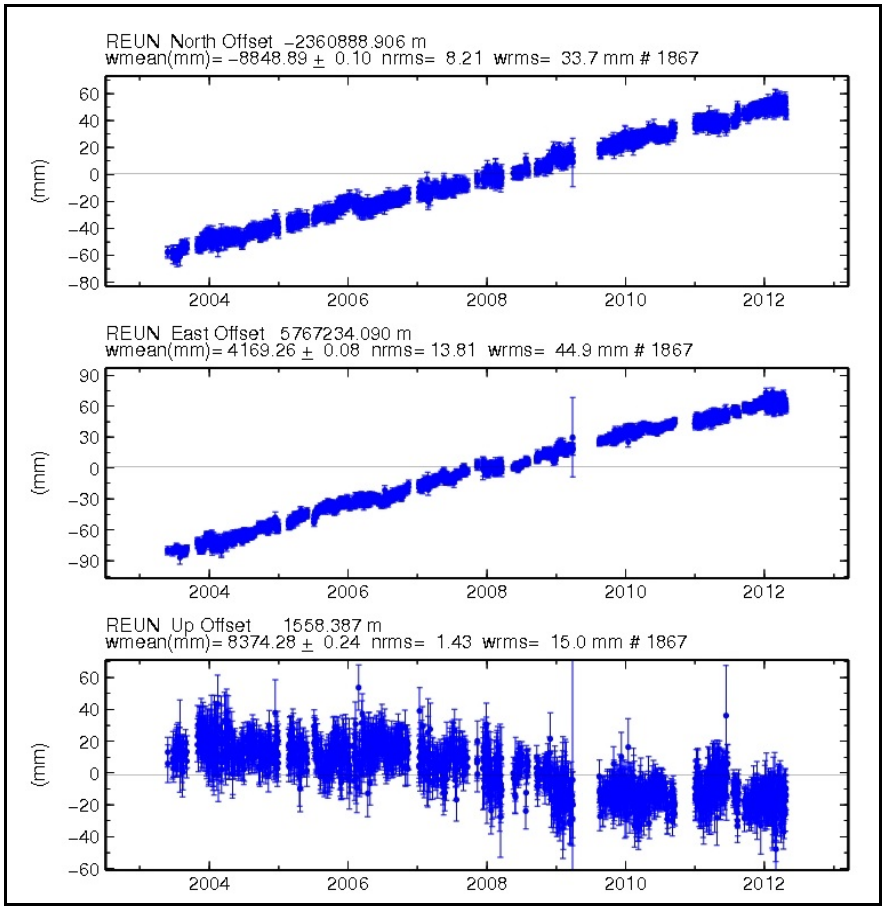


# La Reunion GPS station (REUN), South Africa

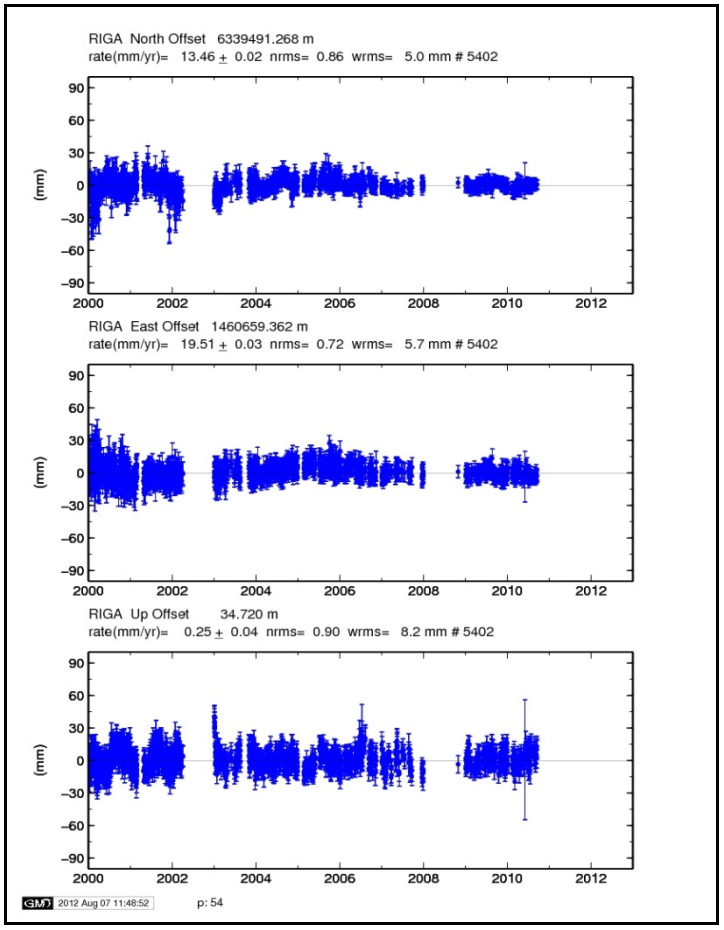


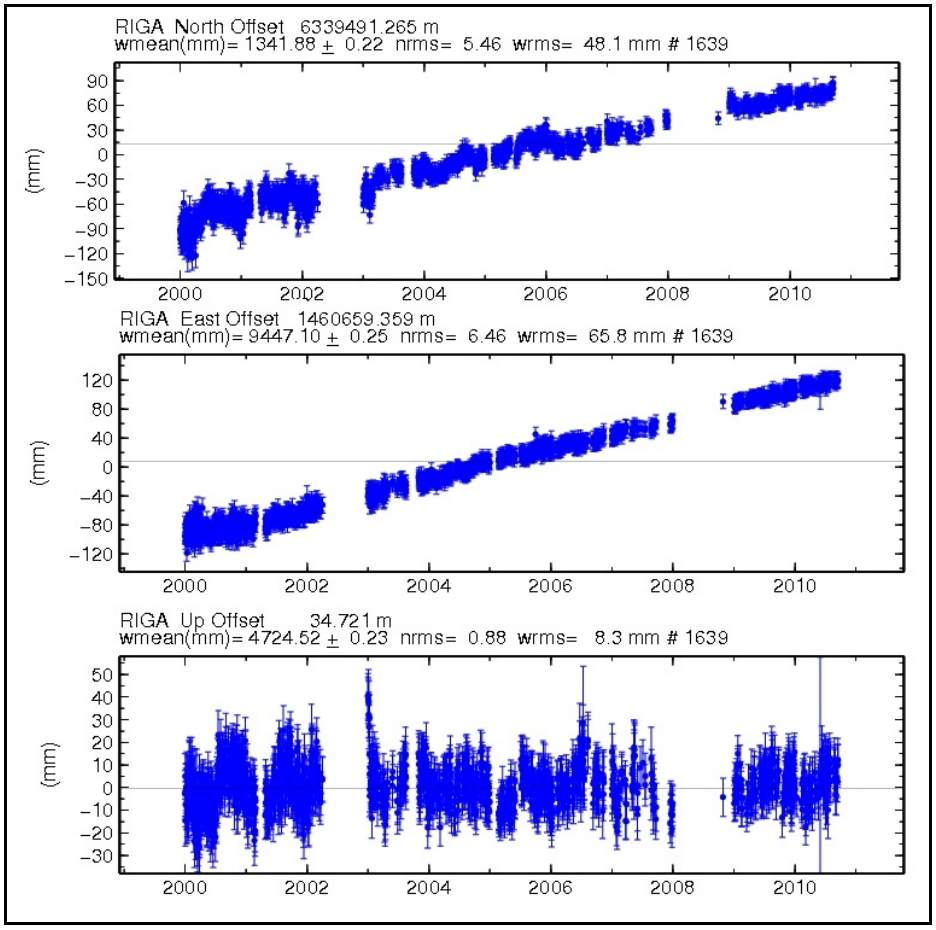


# Riga GPS station (RIGA), Latvia

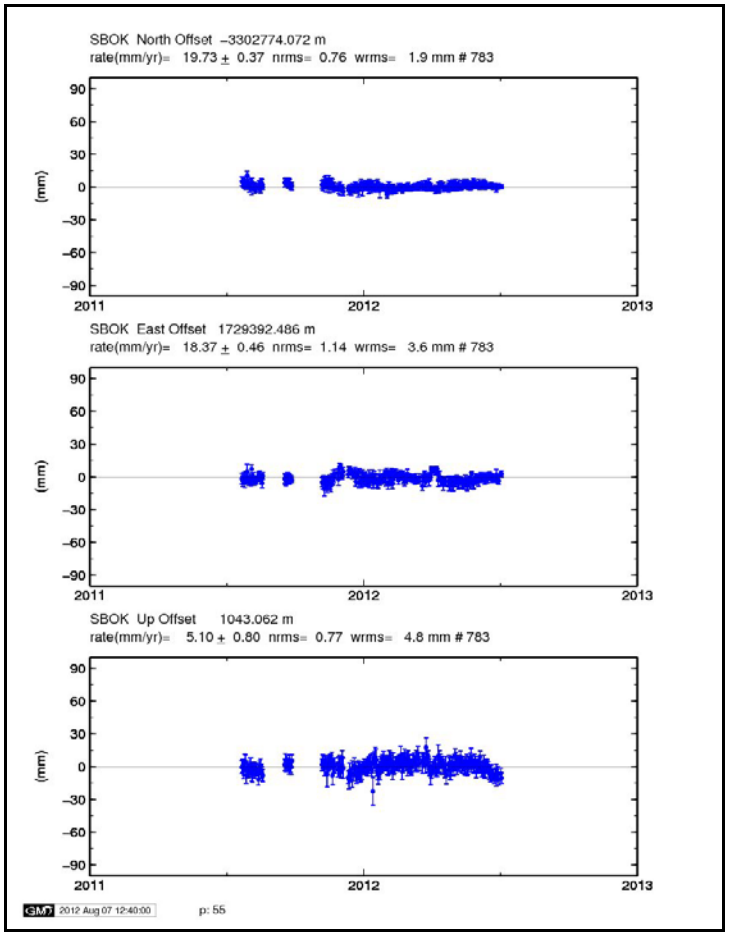


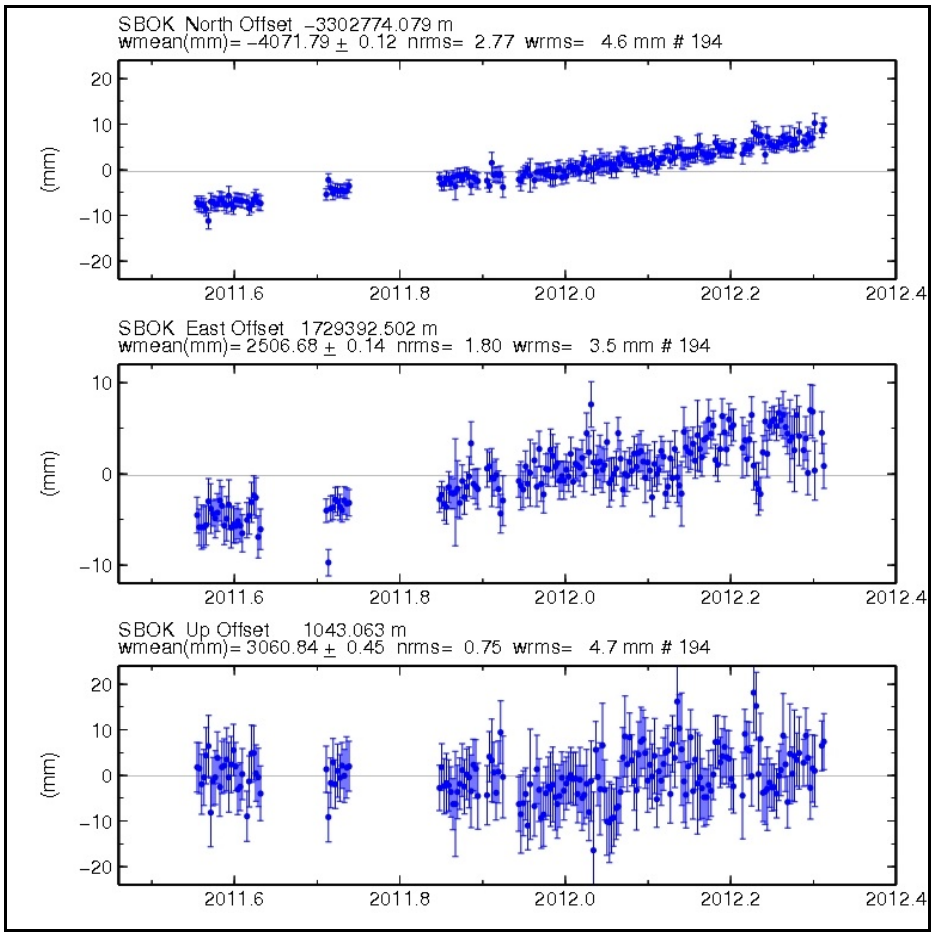


**Springbok GPS station (SBOK), South Africa**

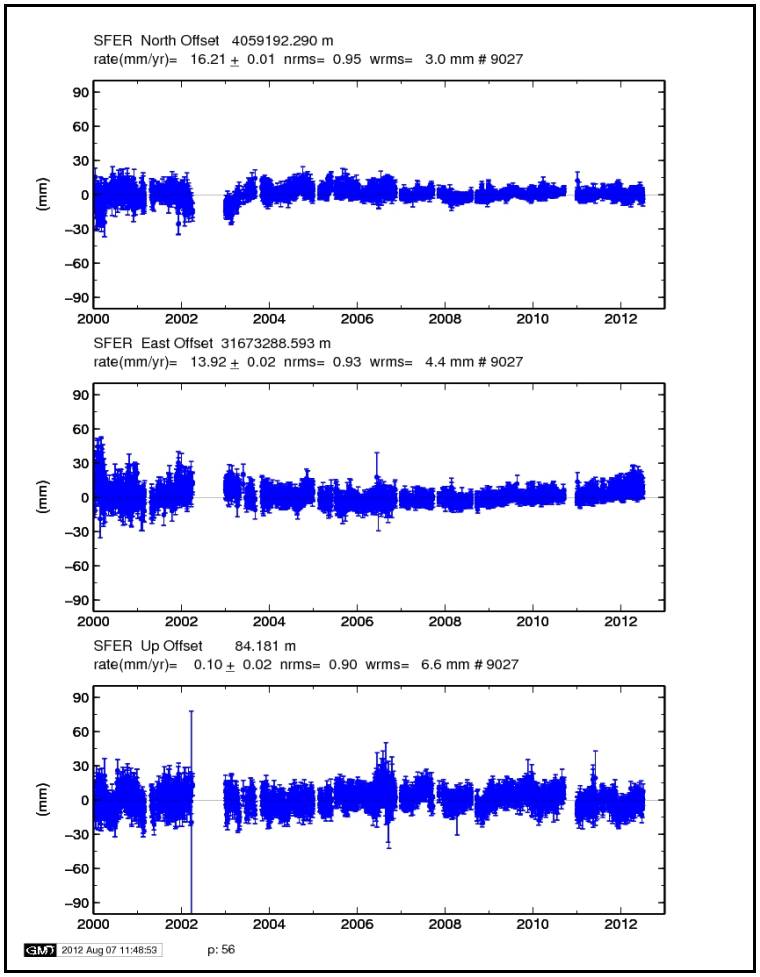


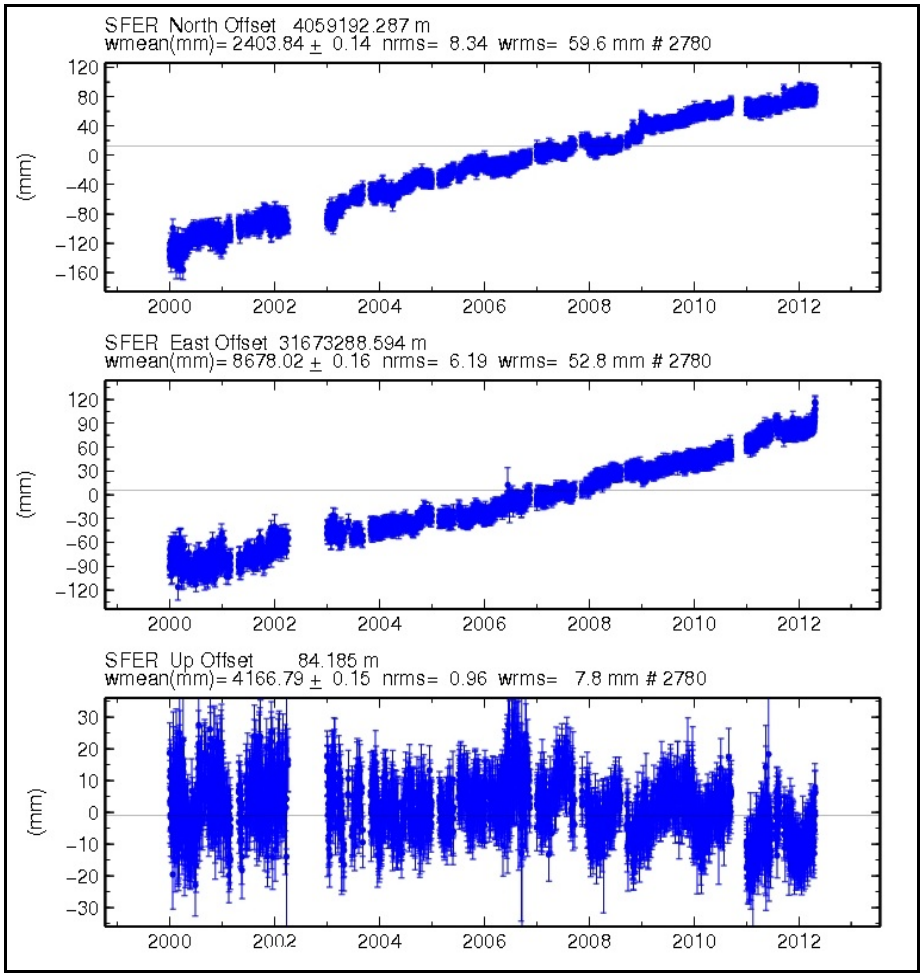


# San Fernando GPS station (SFER), Spain

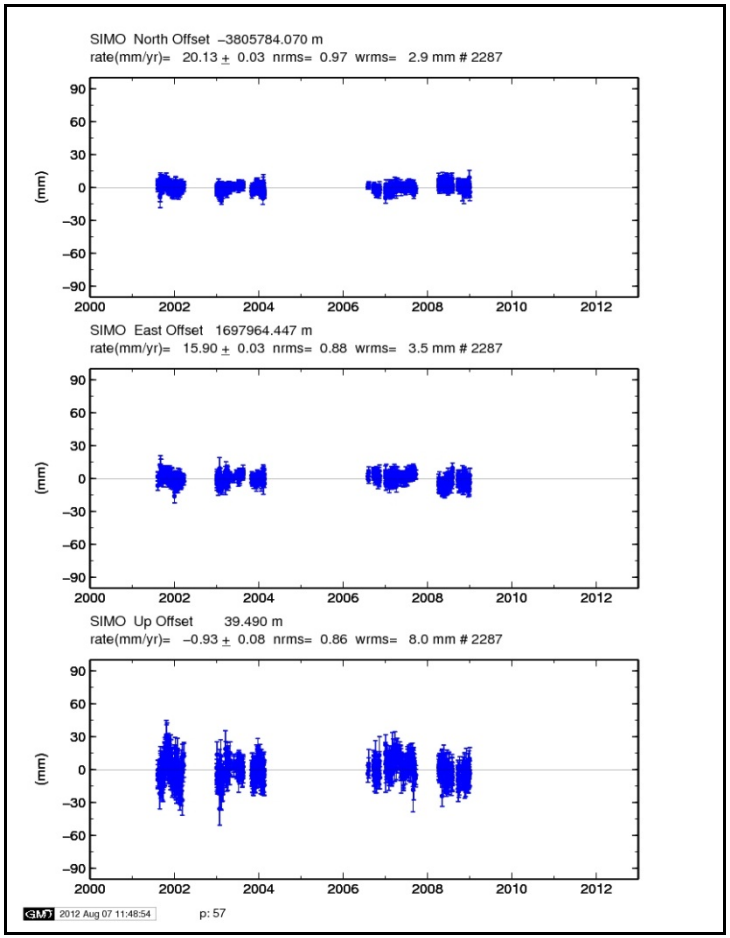


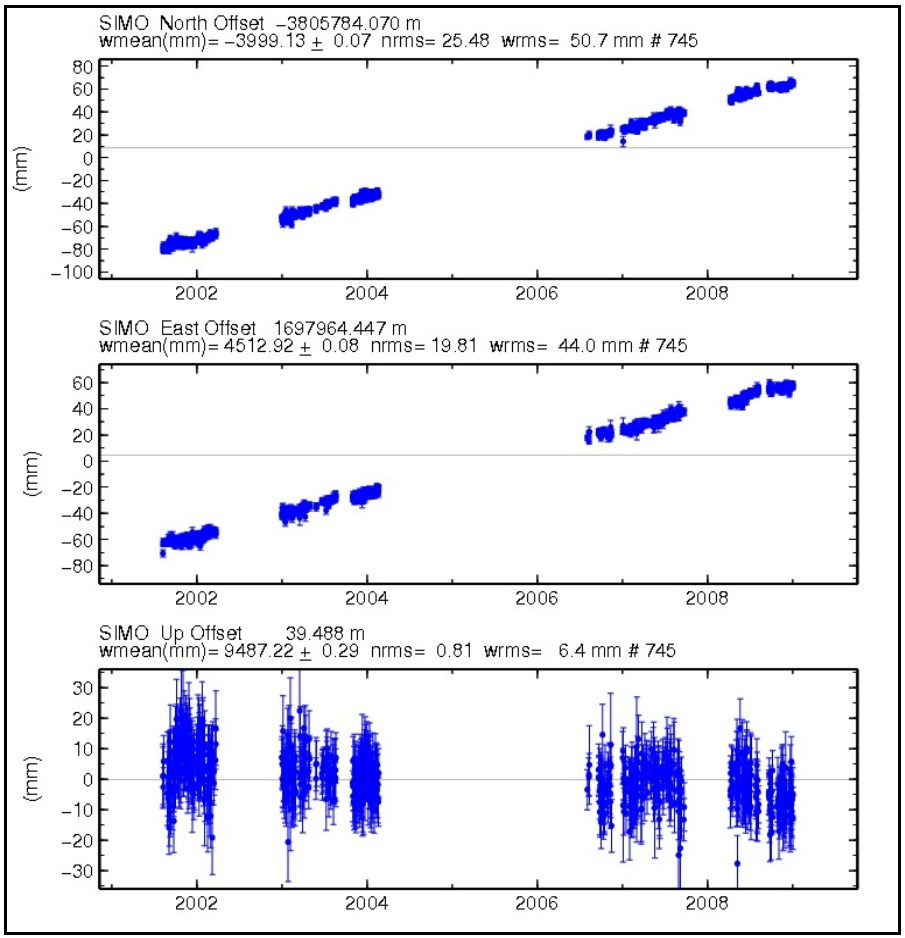


# Simonstown GPS station (SIMO), South Africa

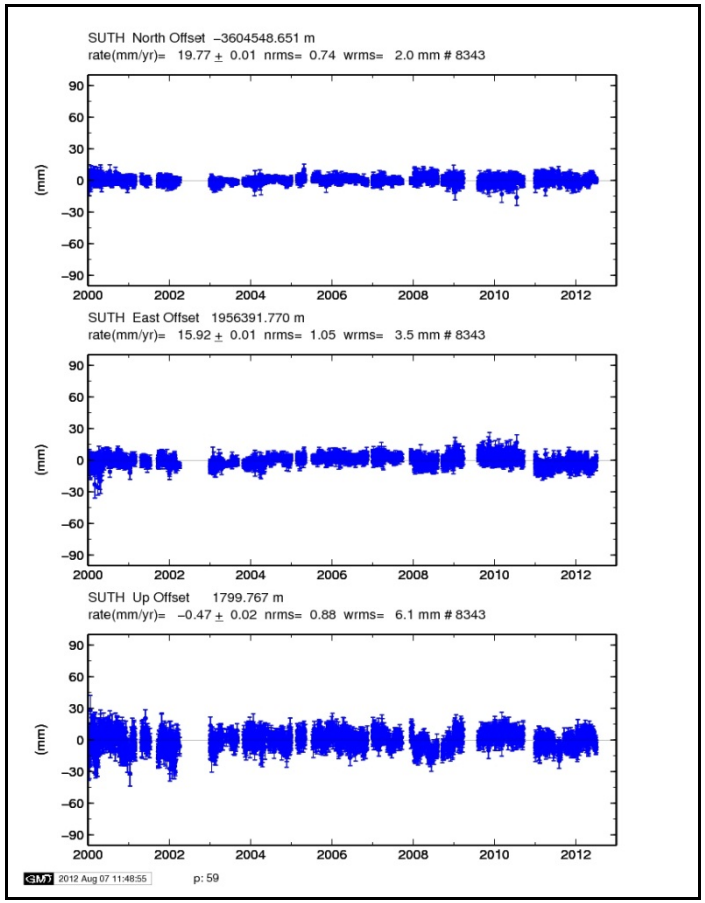


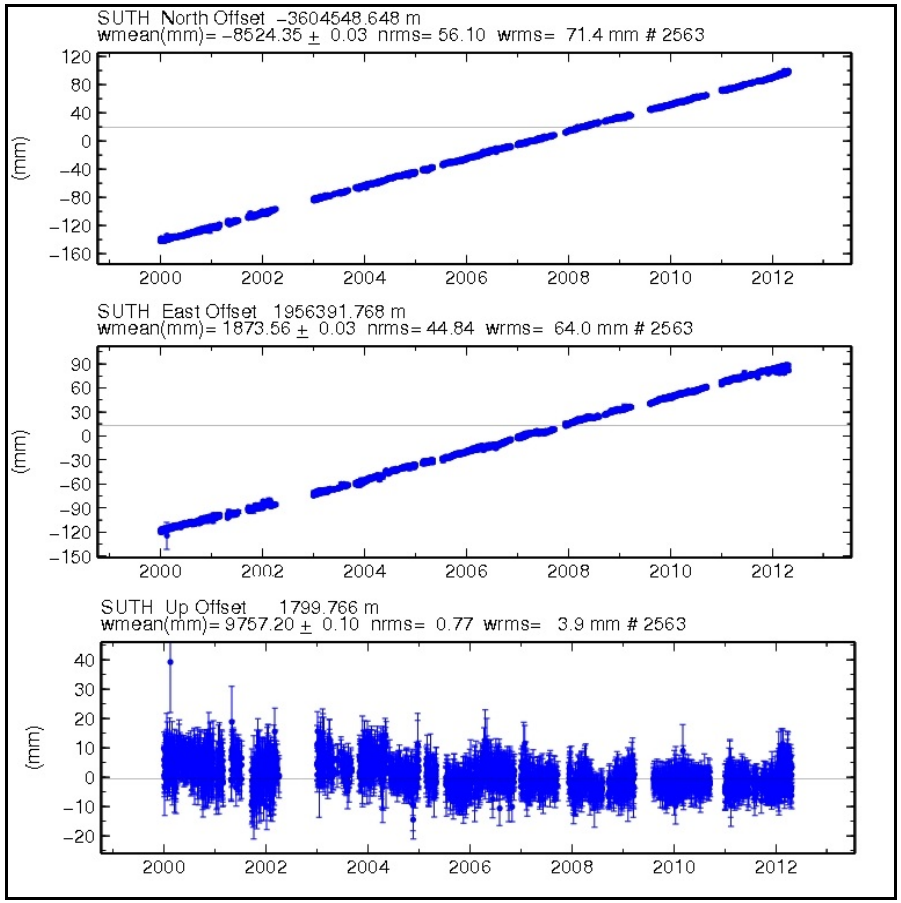


# Sutherland GPS station (SUTH), South Africa

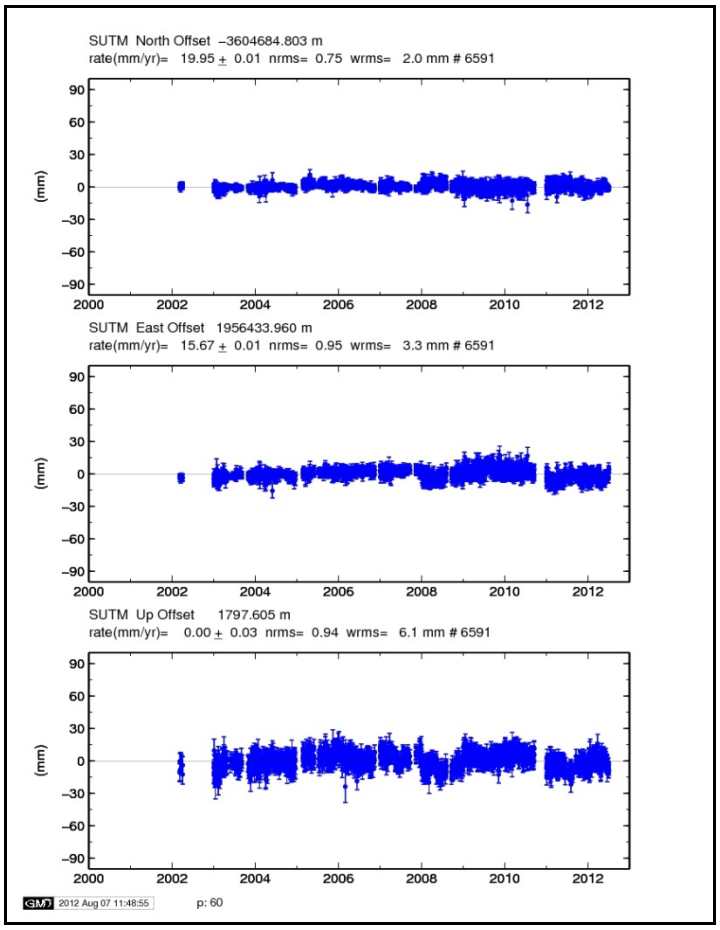


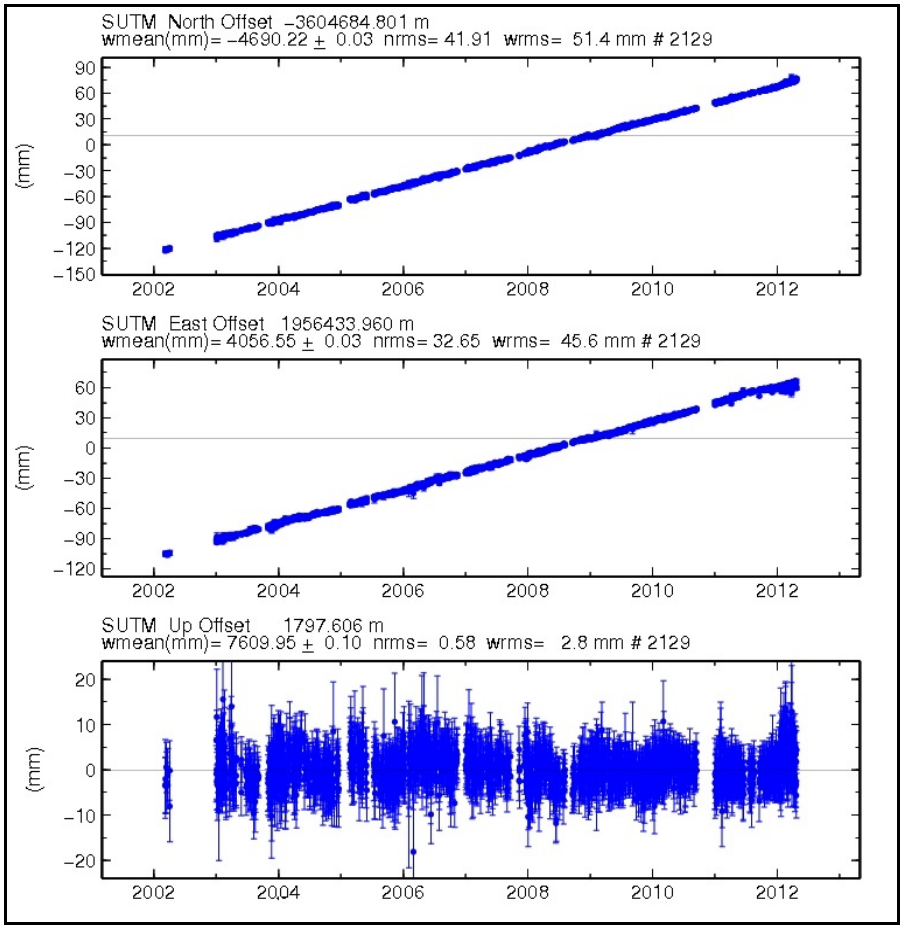


# Sutherland GPS station (SUTM), South Africa

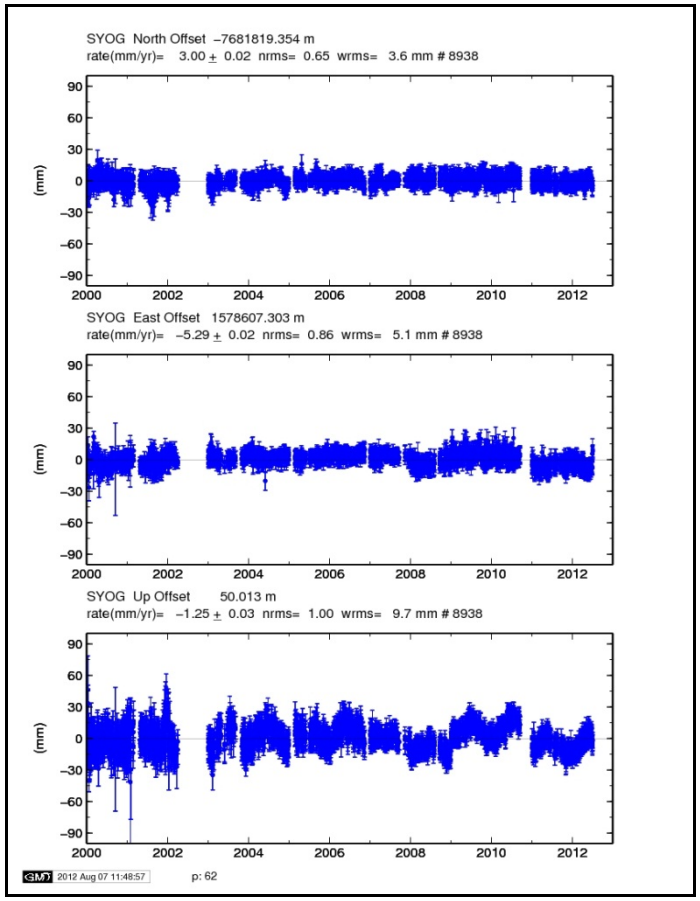


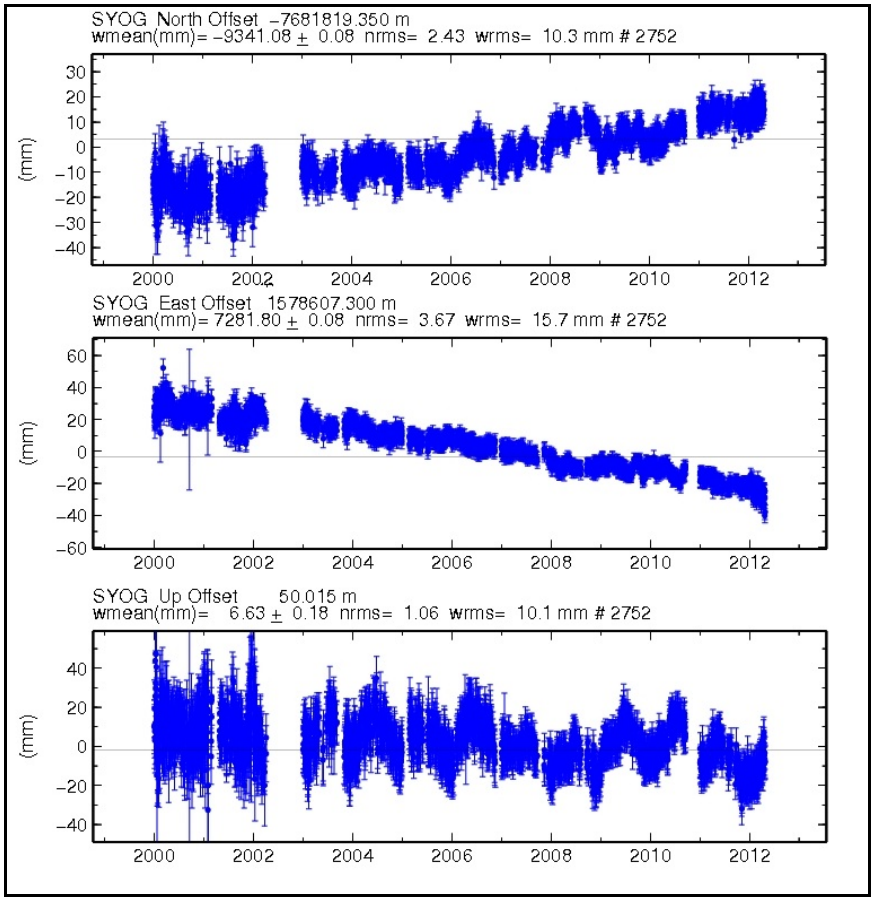


# Syowa GPS station (SYOG), East Obgle Island

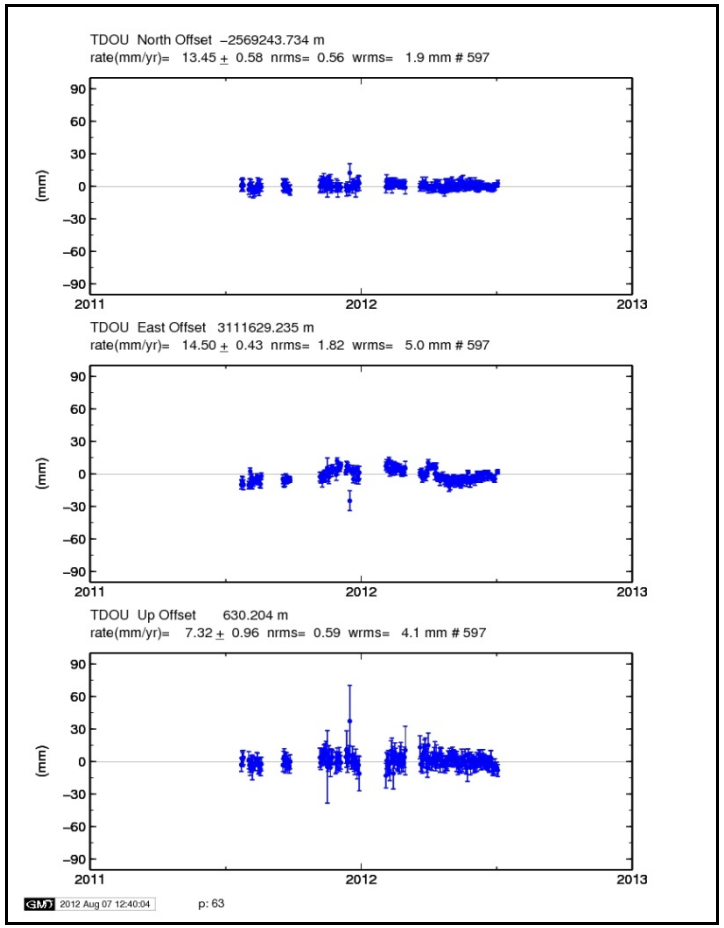


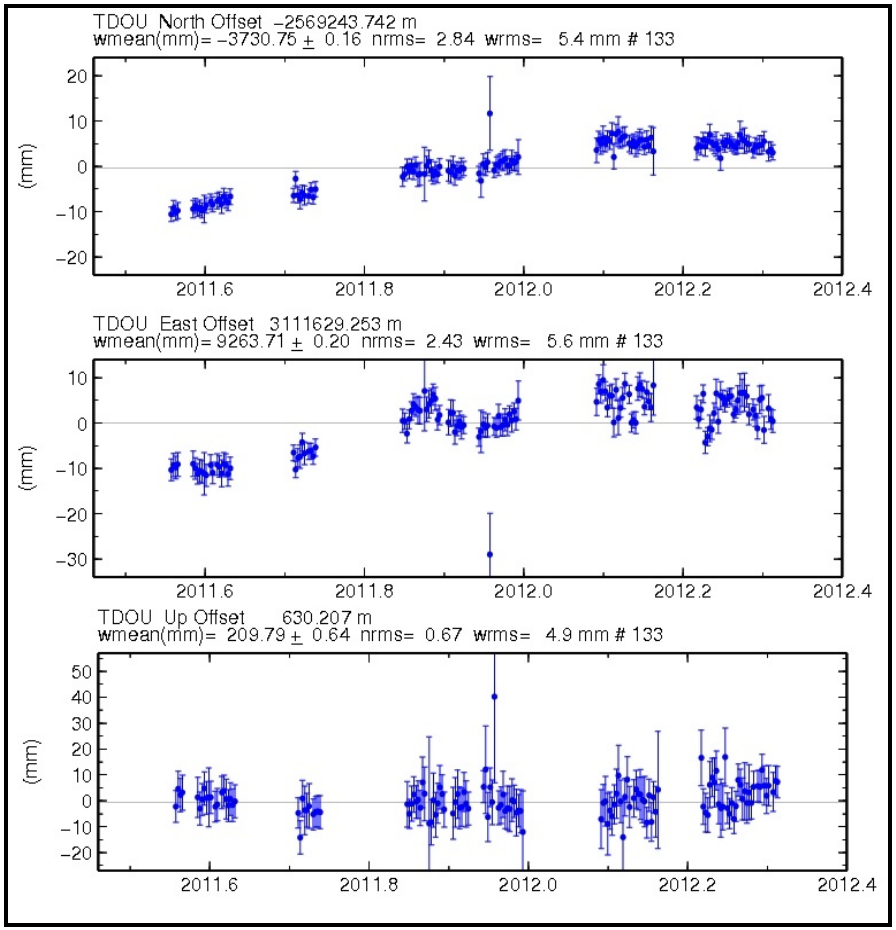


# Thohoyandu GPS station (TDOU), South Africa

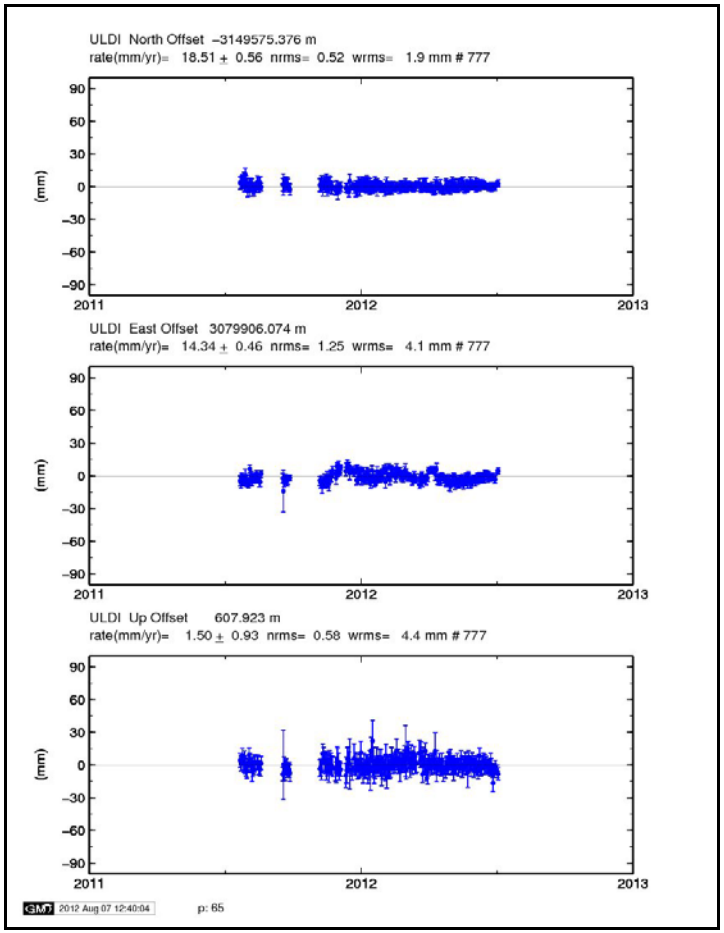


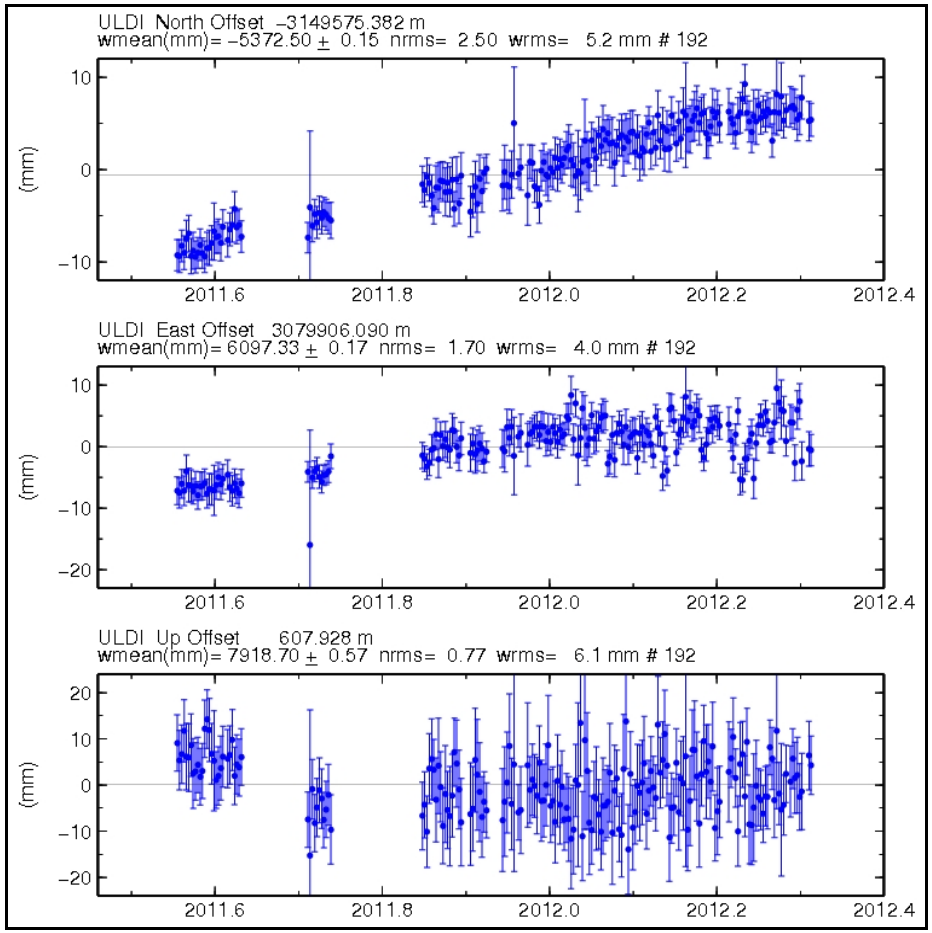


# Ulundi GPS station (ULDI), South Africa

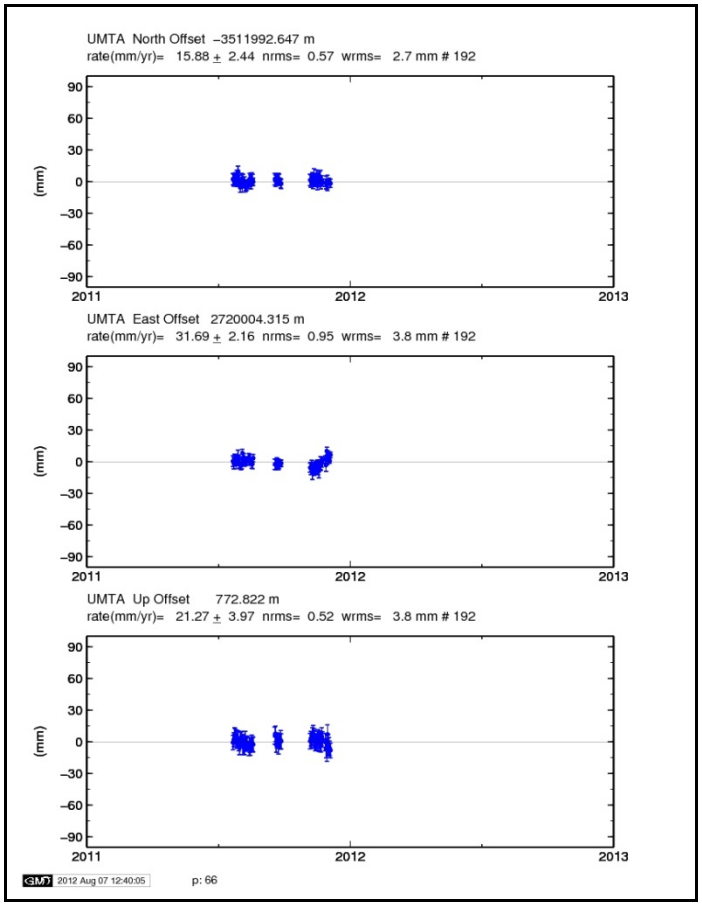


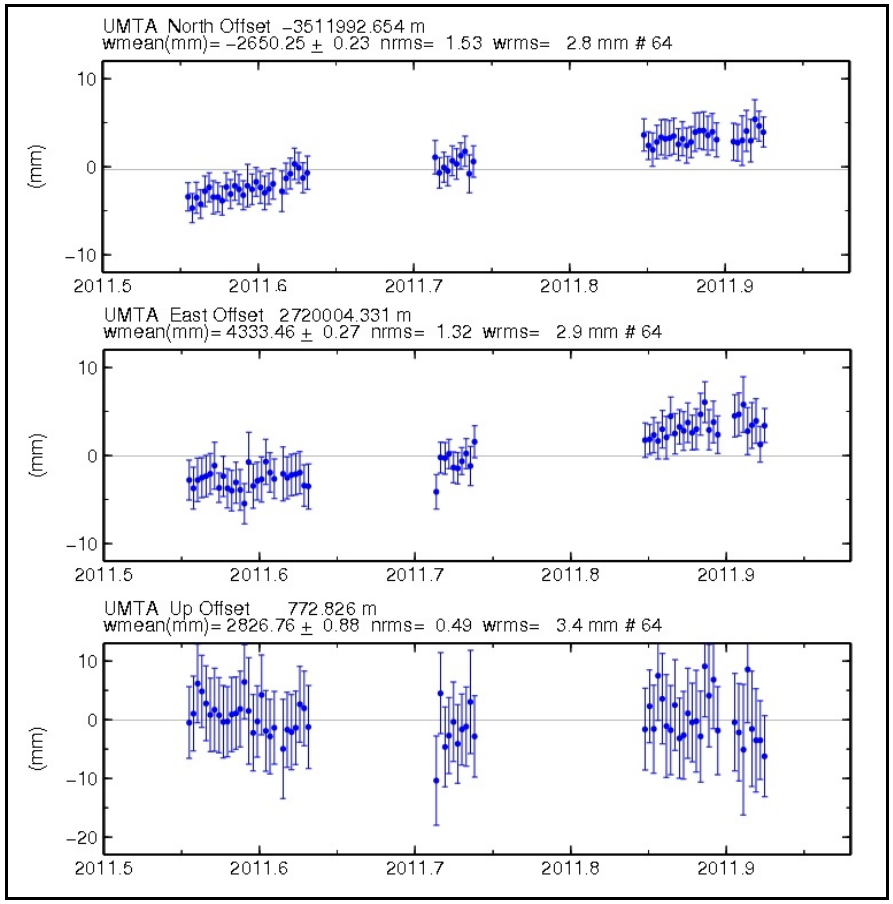


# Umtata GPS station (UMTA), South Africa

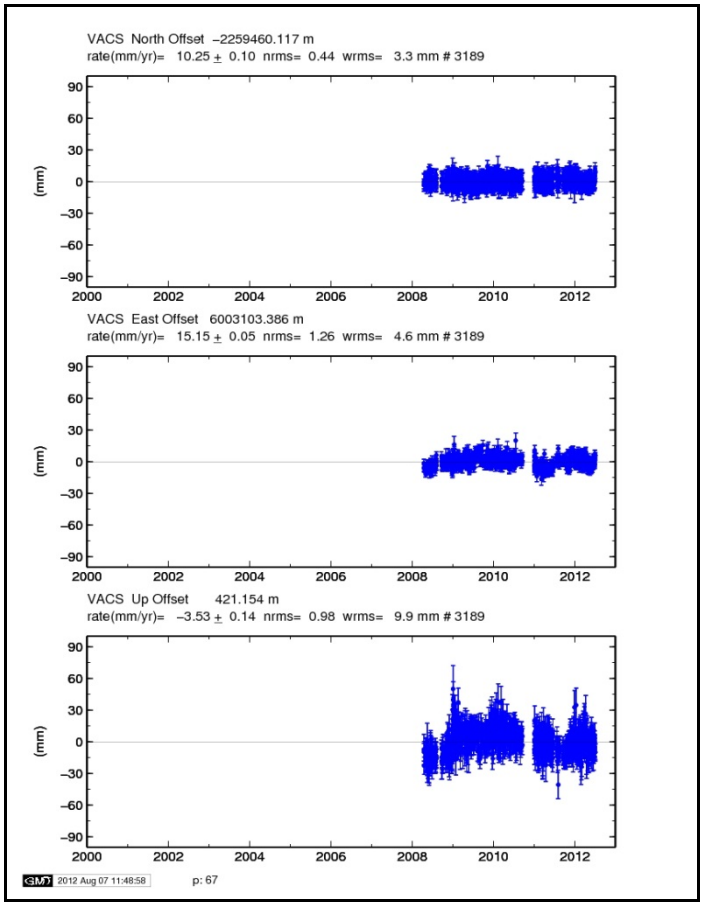


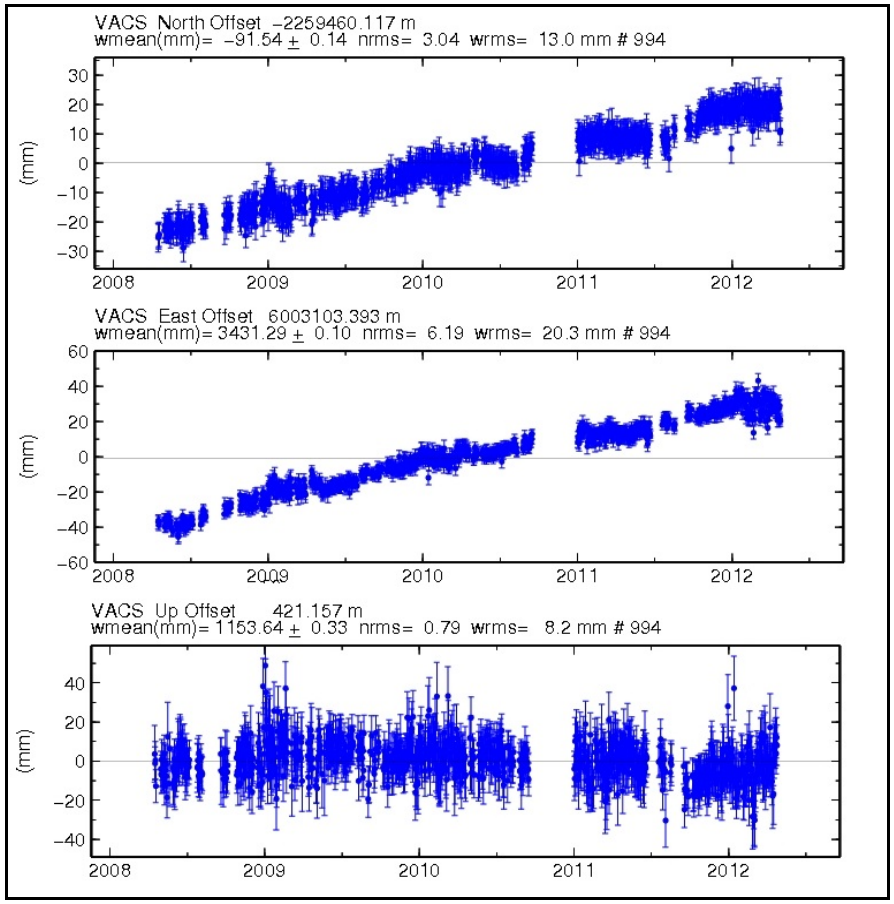


# Vacoas Meteo GPS station (VASC), Mauritius

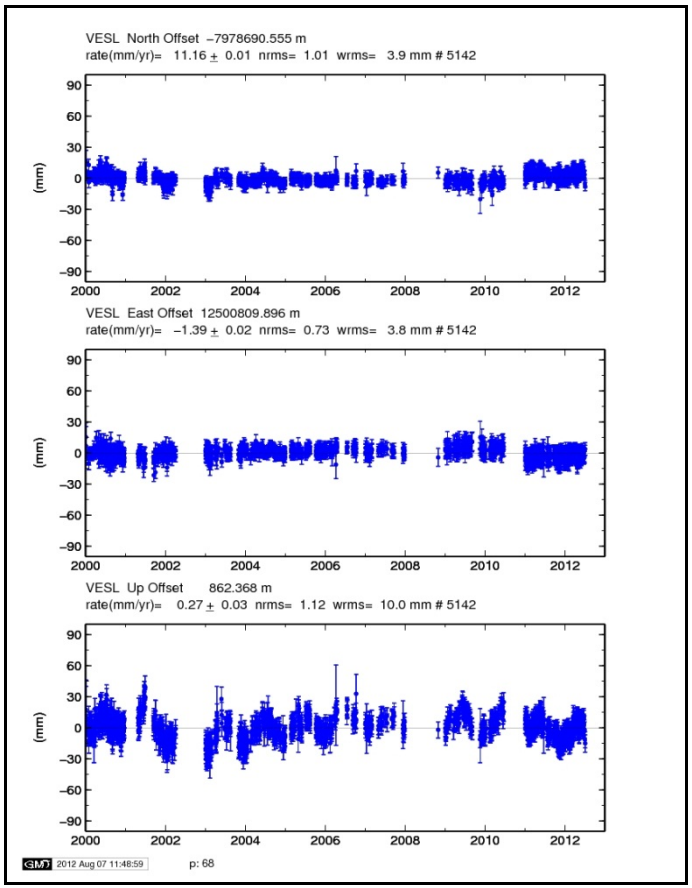


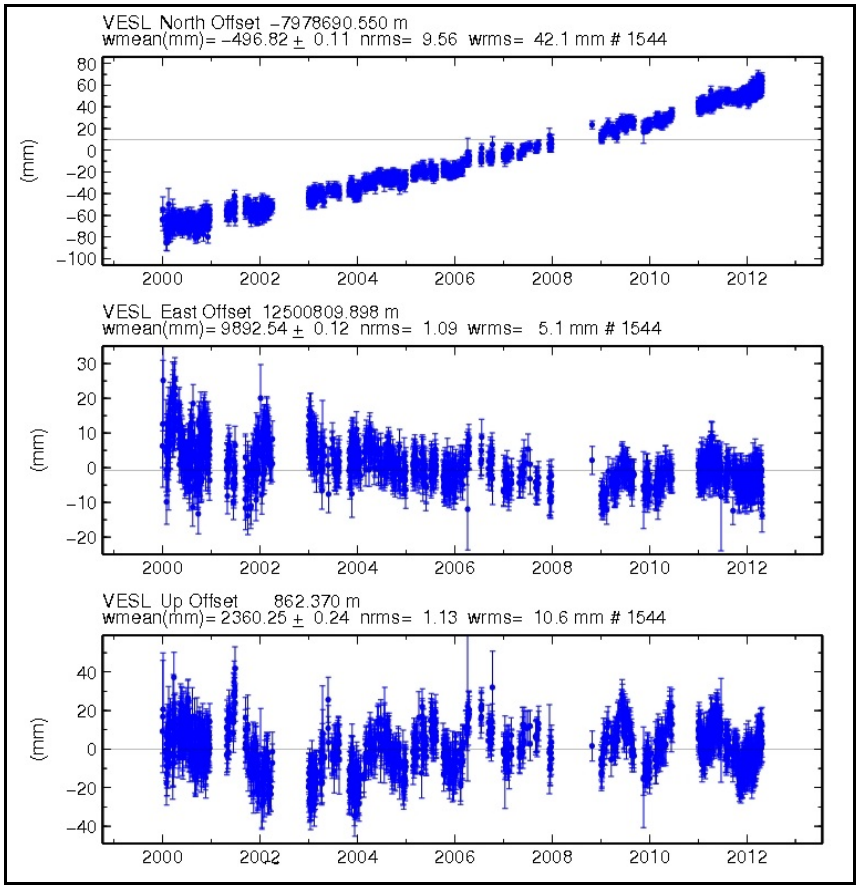


# Vesleskarvet GPS station (VESL), Antarctica

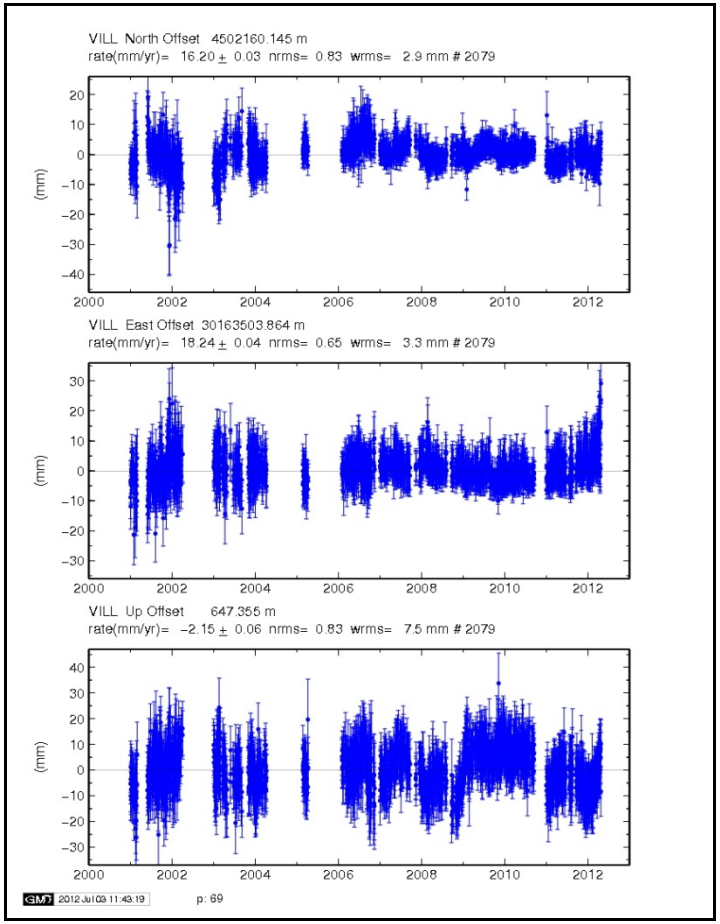


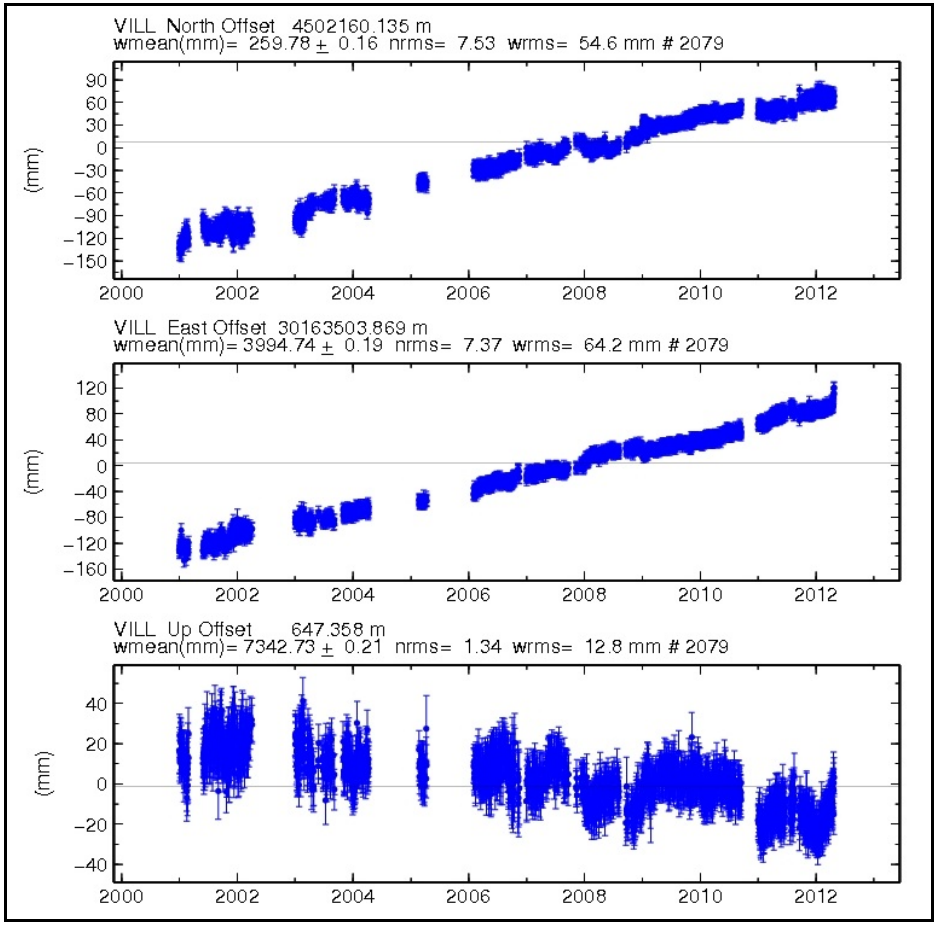


# Villafranca GPS station VILL, Spain

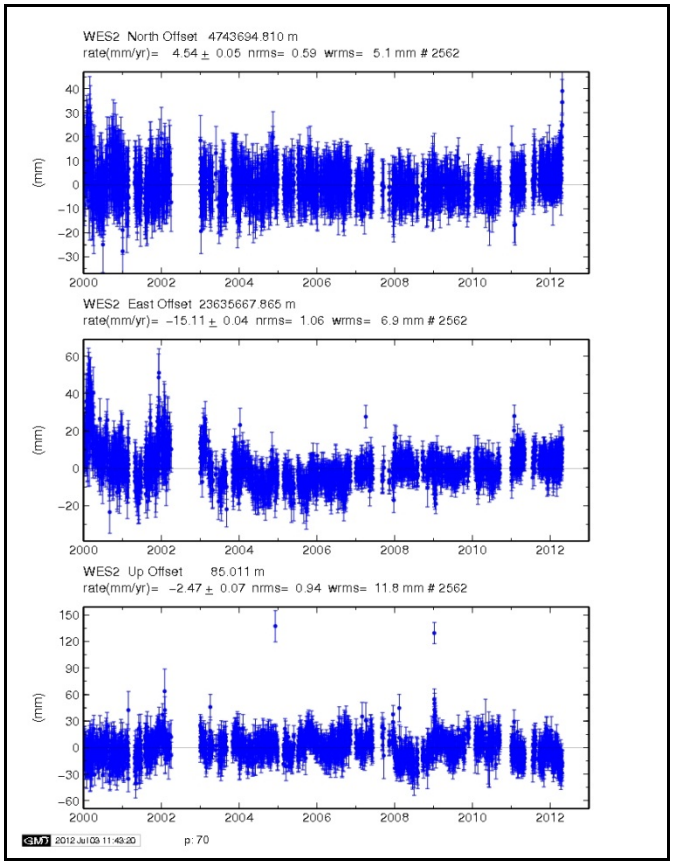


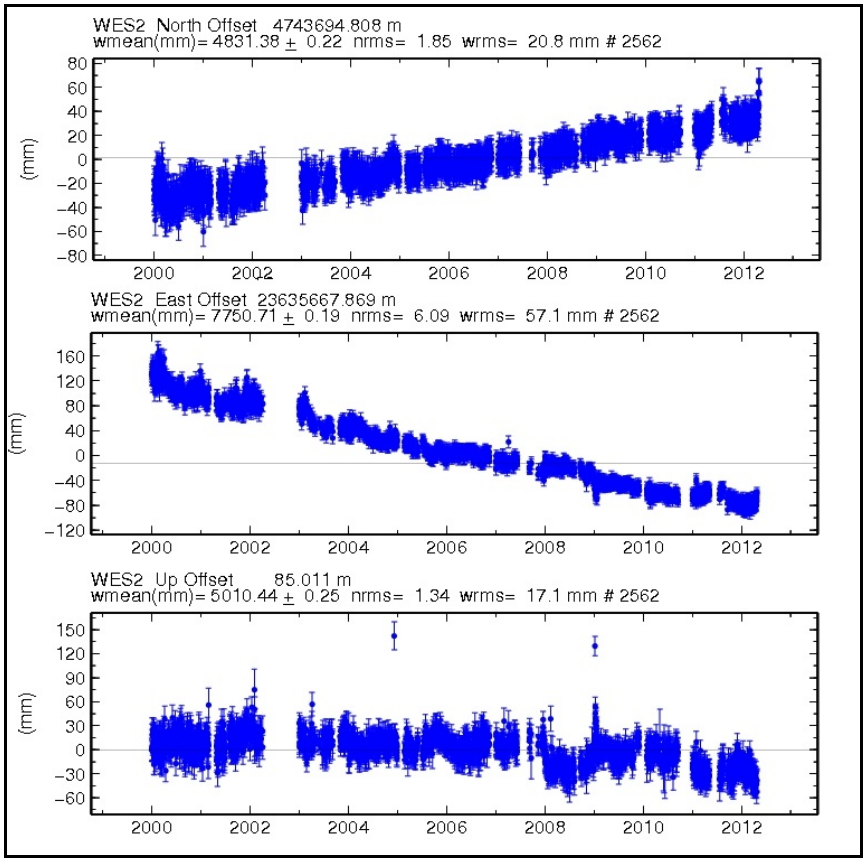


# Westford GPS station (WES2), USA

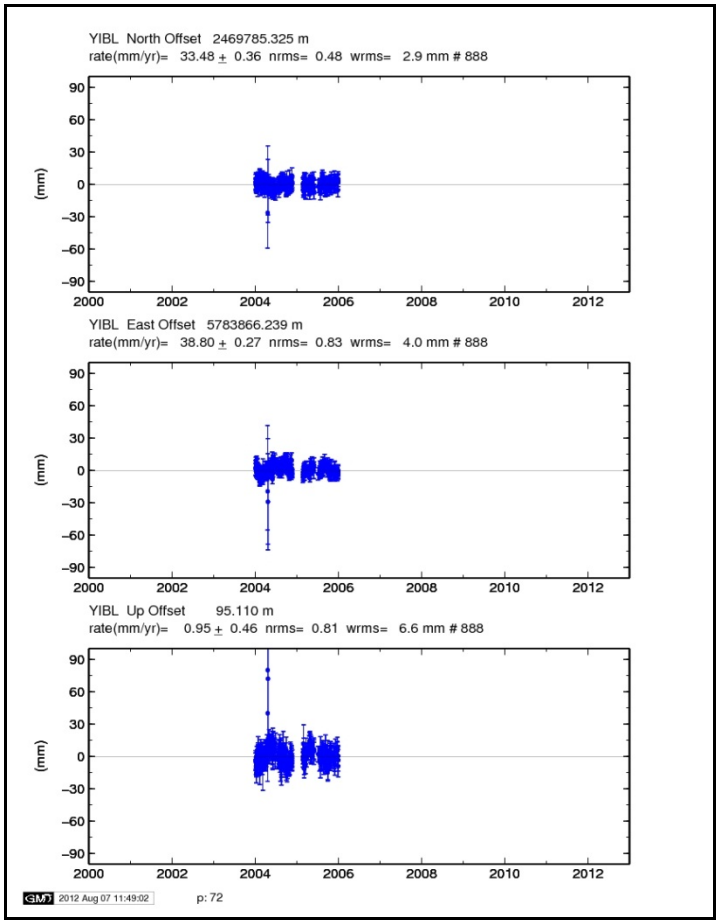


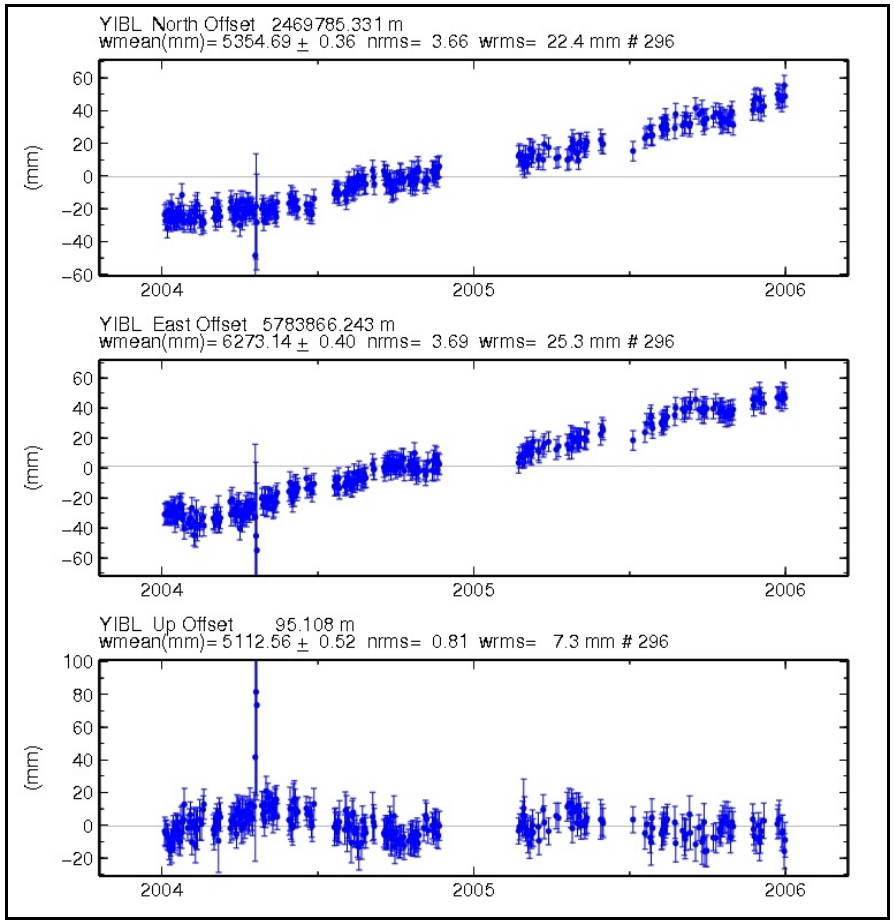


# Yibal Oman GPS station (YIBL), Oman

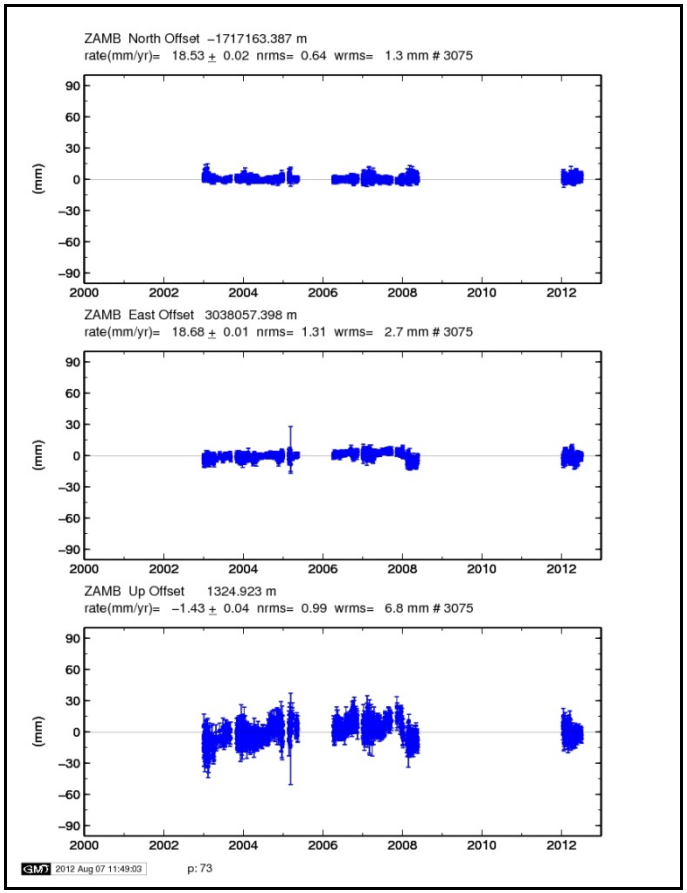


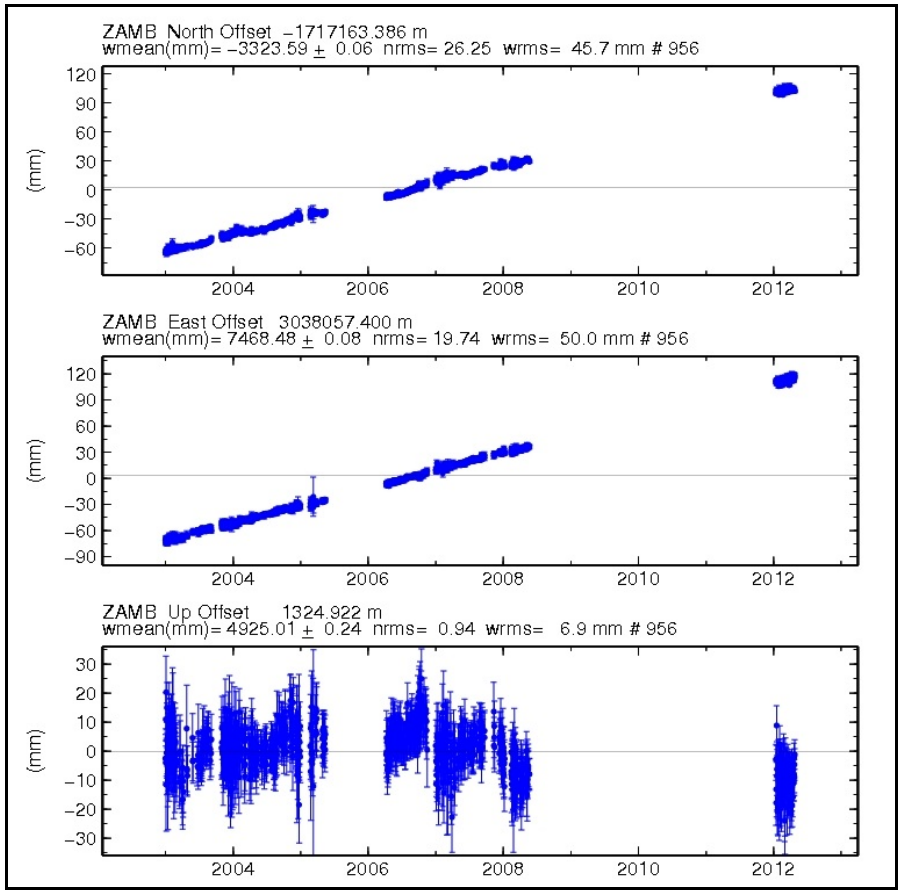


# Zambia GPS station (ZAMB), Zambia